Towards an understanding of the physical and biological controls on the cycling of dimethylsulfide (DMS) in Arctic and Antarctic sea ice

by

Gauthier Carnat

UNIVERSITY OF MANITOBA

A thesis submitted to the Faculty of Graduate Studies of

The University of Manitoba

in partial fulfilment of the requirements of the degree of

DOCTOR OF PHILOSOPHY

Department of Environment and Geography

University of Manitoba

Winnipeg, Manitoba, Canada

Abstract

In the last two decades there has been an increasing interest in the role played by the marine cryosphere in the production and emission of the climate-active gas dimethylsulfide (DMS). This was motivated by observations of high concentrations of the DMS precursor, the intracellular metabolite dimethylsulfoniopropionate (DMSP), in Arctic and Antarctic sea ice. The understanding of the factors driving the cycling of DMS in sea ice is limited. Little is known about the spatio-temporal variability and fate of the sea ice DMS pool. To date, studies have essentially focused on biotic factors, linking the high DMSP concentrations to the high biomass of sympagic communities, and to their physiological adaptations to the low temperatures and high salinities of the brine habitat. In this thesis, an approach integrating both biotic and abiotic factors is presented, and the influence of ice growth processes and brine dynamics on the DMS cycle is investigated. First, the halo-thermodynamic evolution of sea ice and brine dynamics from growth to melt are explored and defined based on a significant data set of ice temperature and salinity collected in the Arctic. A strong desalination phase over a small time window in the spring is identified. Using calculated proxies of permeability (brine volume fraction) and of the intensity of brine convection (Rayleigh number), this phase is shown to correspond to full-depth gravity drainage initiated by restored connectivity of the brine network on warming. This halo-thermodynamic background is then used to investigate the spatio-temporal variability of DMS in Arctic sea ice during a year-round survey in the Amundsen Gulf. The influence of processes such as scavenging and brine convection on the sea ice DMS cycle is shown, and the first combined measurement of DMS, DMSP, and

dimethylsulfoxide (DMSO), a third organosulfur compound acting as both source and sink for DMS through photo-chemical and bacterial processes, is presented. DMSO is shown to largely dominate the dimethylated sulfur pool in surface ice when the snow cover is low. Based on strong relationships with irradiance, it is suggested that this DMSO originates from the photo-chemical oxidation of DMS trapped in impermeable ice. Finally, the spatio-temporal variability of DMS in Antarctic sea ice is investigated during another year-round survey in McMurdo Sound. Platelet crystals growth under the influence of ice shelf waters are shown to favor the incorporation of strong DMSP producers, to increase the environmental stress on the cells in interior ice, and to favor the accumulation of DMS,P by reducing permeability. The increase of permeability on warming is shown to trigger an important release of DMS in the ocean and a vertical redistribution of DMSP concentrations in the ice cover. On the whole, this thesis provides a clear picture of the spatial and seasonal variability of dimethylated sulfur compounds in sea ice, highlighting strong contrasts between both hemispheres, and contributes to a better understanding of some of the biological and physical factors driving the DMS cycle in the polar regions.

Acknowledgments

First and foremost, I would like to acknowledge my thesis supervisor, and friend, Tim Papakyriakou for his unlimited patience, trust, and wisdom. You definitely were the cement of this work and your selfless dedication to both my personal and academic development will stay forever engraved in my memory. I was really touched by your compassion and sensitivity towards other people's problems, a very unique gift. Your contribution towards this thesis extended way beyond scientific guidance. On the same day, we could spend hours building and rebuilding sentences in a manuscript, and hours discussing about politics around a fire where bison meat was roasting. I really hope that our paths will keep crossing in the future.

I would like to extend my gratitude to my thesis committee members, Feiyue Wang, Maurice Levasseur, and Mario Tenuta for their untiring assistance and guidance throughout the years. Mario, thank your for bringing your sagacity and enthusiasm to each of my presentations, and for always finding the right words to take my anxiety away. Fei, thank you for teaching me the fundamentals of aquatic chemistry in such bright and inventive ways. I will always keep a piece of chocolate in my pockets to share with my friends. Maurice, I will never forget the trust you placed in a young scientist at the dawn of his career, giving him unconditional access to your most sensitive equipment. Thanks also for the extreme human kindness I could feel every time I talked to you.

My interest for polar science was sparked when my life path crossed that of Jean-Louis Tison and his colorful and inspirational slides during my undergraduate years. I could not be prouder of my academic roots. Jean-Louis not only planted the seed, but also provided continuous water and nutrient supply to the tree, with

so much energy and generosity that I long thought he had a twin brother. This twin brother could definitely have been Bruno Delille, who was given wings to cross the oceans many times a year but remained always available to provide fruitful comments on my work. I am eternally grateful to the two of you for the memorable times spent sampling sea ice in comfortable Tyvek suits, for your support, your trust, and your teaching. More than great mentors, I always considered you as good friends and I really hope this thesis honors the time you have invested in me.

Field trips to the hostile but magnificent polar regions were the cornerstones of this thesis and will undoubtedly stay in my mind forever. I have tremendous respect for the commitment and professionalism of the talented captains and crews of the CCGS Amundsen and RV Nathaniel B. Palmer, and of the BASC and Scott Base teams. Thanks to these true heroes of polar research who brought me back home safely from these labyrinths of dangers. These field trips lied upon the shoulders of David Barber, Steve Ackley, Hajo Eicken and Tim Haskell, visionary and humble founding fathers who dedicated their life to polar science. I have been fortunate to share endless days and nights of sampling and analyses with great individuals. Thanks to the mercury team, Debbie Armstrong, Alexis Burt, and Monica Pucko for their much appreciated help in the field and in the labs, to my friend Benoît Philippe, the Zinedine Zidane of the poles, to my great sister in science Isabelle Dumont, and to Rodd Laing for the unforgettable times looking for bears in the Alaskan wilderness. I am very grateful to the British Columbia CO_2 contingent, Lisa Miller, Kristina Brown, and the legendary and inexhaustible duo, Keith Johnson and Nes Sutherland, from whom I have learned so much.

This thesis would not have been possible without the incredible work of lab technicians. I would like to thank Art Hildebrand who helped me to diagnose the

many illnesses that can affect the sensitive patients that are gas chromatographs, Emmelia Stainton, Bruce Johnson and Vlad Petrusevich who helped me to order, prepare and ship all the ingredients of a successful scientific trip to the North Pole. I am eternally grateful to Saïda El Amri, the most efficient and dedicated individual I know. Choukrane for the tasty pastries and the teaching of Arabic and astrology; true social oases amid a lonely world of lab instruments. I would also like to acknowledge the staff of CEOS, DSTE and graduate studies for guiding me through the mystifying maze of the university administration, always with a generous smile. Denise Whynot, Gail Yacucha, Linda Chow, David Mosscrop and Claire Lelouchier, you were my Ariadne's thread through this thesis. My thoughts also go to Pat Gutoski who helped me take my first steps as a graduate student, but unfortunately will not see me cross the finish line.

During my thesis, I had the great chance to collaborate with very enthusiastic and skilled scientists from across the world. I have wonderful memories of my time in the lab of Maurice Levasseur in Université Laval, Québec. Martine Lizotte, Myriam Luce, Sarah-Jeanne Royer, Michael Scarratt, and Sonia Michaud, thanks for your hospitality. Many online collaborators generously take their time and energy to help me solve the multifaceted problems of sea ice biogeochemistry, may they all be warmly thanked for their investment. A heartfelt thanks to Martin Vancoppenolle and his sidekick Ivan Grozny for the hours spent computing and interpreting Rayleigh numbers, to Sangeeta Sharma for sharing her secrets on atmospheric DMS sampling, to Janne-Markus Rintala for his detailed observations of the infinitely small world of ice algae, and to Jacqueline Stefels, an indisputable source of inspiration for the DMS community.

This thesis was a long adventure that I was fortunate to share with other graduate and post-graduate students. Thanks to all the CEOS students at UofM for the friendly working atmosphere, and to all my Canadian colleagues for introducing the chocolate eater and soccer addict that I am to the wonderful world of donuts and hockey. Thanks to Alex Hare for sharing his enthusiasm for the mesmerizing Canadian wilderness, to CJ Mundy and Jens Ehn for the fruitful discussions at the beginning of the thesis, to Matthew Asplin for making the tastiest deep dish pizza you will find on Earth, and to Ryan Galley, the living proof that scientific excellence and a great sense of humour are not incompatible. My friend Tao Li, I enjoyed every second of our enriching cultural exchanges, and I sincerely hope to play a game of Yǔmàoqiú with you in Qingdao in the near future. A special thanks to Brent Else, my brother in arms, who impressed a generation of young scientists with his maturity and professionalism. Thanks also to all the DSTE students and staff who perfectly illustrate the legendary warmth and joie de vivre of the Belgian people. Bedankt Frank Pattyn, the Salvador Dalí of science, a true genius with a small grain of healthy madness. Thanks to the modelling team, Reinhard Drews, Lionel Favier, David Docquier, and Alain le Glaciologue for the carefree moments spent in our beloved Sonian forest. Thanks to Marie Dierckx for the biweekly supply of saturated fat and carbohydrates, to Ceri Middleton for the English tips and palatable cakes, to Celia Sapart, François Fripiat, and Véronique Schoemann for their valuable advices and warm encouragements at the end of the thesis, and to Denis Callens, Morgane Philippe, and Brice Van Liefferinge for their perpetual great mood. A special thanks to Jiayun Zhou, whose cleverness and sheer strength of will helped me to move icebergs, and to Gaëlle Gilson, the first student I had the chance to co-supervise, who invested considerable efforts to gather some of the results presented in this thesis. I am particularly grateful to Frédéric Brabant, the

most rigorous and ethical individual I know, for his mentorship and for sharing the load of thousands of DMS measurements, and to Nicolas-Xavier Geilfus, my wingman during most of my polar adventures, for his great enthusiasm, expertise, and dedication in our quest of calcium carbonate crystals. Science was never monotonous thanks to the two of you.

This work was supported by many friendly Manitoban, whose deservedly famous hospitality helped me feel at home in Winnipeg. Thanks to Laura Sims and to my soccer buddies Shadow and Maxie for the long and memorable walks in the Churchill park, always followed by delightful traditional French breakfasts. Thanks to all the feather enthusiasts from UofW and Wildewood badminton clubs, and to all the soccer addicts of the UofM team and Peter Tan's Cooligans team, who greatly contributed to my cultural and social blossoming. Thanks to Robert Gregoire, Paul Browning and Garry Pfeil, who all brought a little bit of magic in my Canadian journey, and to my friend Jenisis Del Monte, for their unswerving support. I am eternally grateful to the families Rush and Athayde who always considered and treated me as their own son. I would never have finished this thesis without your infinite generosity and kindness.

This work was also followed by all my comrades in Belgium who all put the lie to the old saying "far from the eyes, far from the heart". Thanks to my friends from JetPlume, Evere, St-Job and BEC for their warm encouragements and for giving me the opportunity to unwind in time of mental stress. You are all very important to me. A special thanks to my very special best men, Thomas Jadoule Goossens, and Amik Lemaire for providing me with an endless supply of musical delights, peaceful companions during the long sessions of writing and analysis. Thomas, I have the happy feeling our life paths will never meander to far from each other,

despite our tendency to behave as free electrons. As the inspiring Sylvain Tesson said: “As long as there will be huts in the woods, nothing will be completely lost”. My thoughts also go to the Hordies tribe, to their love and support over the years. I will never forget the enthusiastic welcome home committee at the airport after my journeys to the poles, nor will I ever forget that you always spontaneously and generously fill the emotional void I was leaving behind me during these journeys.

This thesis is dedicated to my family, to all the sacrifices they have made so that I could accomplish my dreams. To my grandparents, who left us too soon. To my beloved parents, who fought hard and gave everything they had to raise their children in a carefree and loving environment, by far the hardest and most valuable job in the world. Thanks for instilling within me at a very young age a sense of awe and curiosity about nature, which found a central place in this thesis. But above all, thank your for showing me that true love is immortal as long as you keep a teenager soul. To my beloved sister, who always protected her little brother against the hazards of life, including tanking a car in the middle of a thunderstorm. Thanks for being such an important and enjoyable life companion since I was born, making me smile and dance when others would have cried. My final thanks go to my wonderful wife, Noémie. This thesis, and my whole life, would not have a lot of sense without you. Thanks for always believing in me and supporting all my projects, even if they would sometimes break your heart, for the dignity and courage you have shown during these difficult times when I was not there to hold your hand. You shared the joys and the sorrows of this long selfish trip, digging me out of the hole on so many occasions. I feel so fortunate and honoured to be loved by such a beautiful and true person. Asavakkit.

“We observe a fraction of the process, like hearing the vibration of a single string in an orchestra of supergiants. We know, but cannot grasp, that above and below, beyond the limits of perception or imagination, thousands and millions of simultaneous transformations are at work, interlinked like a musical score by mathematical counterpoint. It has been described as a symphony in geometry, but we lack the ears to hear it”

Solaris, 1961. By Stanislaw Lem

Contents

Abstract I
Acknowledgments III
List of Tables XIII
List of Figures XIV
Chapter 1 Introduction 1
1.1. Motivation 1
1.1.1. Climatic and biogeochemical significance of dimethylsulfide 1
1.1.2. Atmospheric oxidation of DMS and the CLAW hypothesis 1
1.1.3. Criticisms about the CLAW hypothesis 2
1.1.4. Towards a regional climate regulation role for DMS 4
1.2. Background 8
1.2.1. The cycling of DMS in oceanic waters 8
1.2.1.1. DMSP synthesis and physiological functions 8
1.2.1.2. DMSP release from the cell 11
1.2.1.3. Enzymatic cleavage to DMS 14
1.2.1.4. DMS loss pathways 18
1.2.1.5. The particulate DMSO pathway 22
1.2.1.6. Atmospheric oxidation of DMS 23
1.2.2. The cycling of DMS in sea ice 25
1.2.2.1. Defining the sea ice biome 25
1.2.2.2. DMS,P,O concentrations in sea ice 28
1.2.2.3. Sympagic communities 35
1.2.2.4. Influence of sea ice environmental parameters on DMSP synthesis, release, and degradation 42
1.2.2.5. Brine dynamics 49
1.3. Thesis objectives 54
1.4. Thesis outline 55
Chapter 2 Investigations on physical and textural properties of Arctic first-year sea ice in the Amundsen Gulf, Canada, November 2007-June 2008 (IPY-CFL system study) 57
Abstract 58
2.1. Introduction 59
2.2. Material and methods 63
2.2.1. Study area and sampling strategy 63
2.2.2. Sampling and measurements 66

2.3. Results 70
2.3.1. General ice properties and sea ice conditions 70
2.3.2. Sea ice temperature and bulk salinity 72
2.3.3. Sea ice textural properties and water stable isotope ($\delta^{18}O$) 74
2.4. Discussion 79
2.4.1. Halo-thermodynamic evolution of sea ice during the IPY-CFL study 79
2.4.1.1. Sea ice temperature and bulk salinity 79
2.4.1.2. Brine volume fraction and Rayleigh number 81
2.4.2. Spatial variability 91
2.4.3. Sea ice formation and deformation processes during the IPY-CFL study 94
2.4.3.1. Snow ice and superimposed ice 94
2.4.3.2. Frazil accumulation vs thermodynamic congelation growth 95
2.4.3.3. Sandwiched granular ice layers 96
2.4.3.4. Platelet ice layers 98
2.5. Conclusion 99
2.6. Insights gained about the DMS cycling in sea ice 101
Chapter 3 Temporal and vertical variability of DMS,P,O concentrations in Arctic first-year sea ice (Amundsen Gulf, Canada): evidence for photo-chemical oxidation of DMS in surface ice 104
Abstract 105
3.1. Introduction 106
3.2. Methods 111
3.2.1. Study area and sampling strategy 111
3.2.2. Sample collection 115
3.2.3. Analysis 116
3.2.3.1. Background measurements 116
3.2.3.2. DMS,P,O concentrations 116
3.2.3.3. Potential storage artefacts 119
3.3. Results 120
3.4. Discussion 130
3.4.1. Sea ice DMS,P,O ranges 130
3.4.2. Biological and physical controls on the temporal and vertical variability of DMS and DMSP 133
3.4.2.1. Sympagic biomass 134
3.4.2.2. Community composition 135

3.4.2.3. Temperature and salinity 138
3.4.2.4. Sea ice texture 140
3.4.3. Contribution of DMSO to the total dimethylated sulfur pool 143
3.4.4. Brine dynamics and exchanges at the ocean-ice-atmosphere interfaces 151
3.5. Conclusions 156
Chapter 4 Physical and biological controls on DMS,P dynamics in ice shelf-influenced fast ice during a winter-spring and a spring-summer transition 160
Abstract 161
4.1. Introduction 162
4.2. Material and methods 167
4.2.1. Study site and samples collection 167
4.2.2. Analyses 169
4.2.2.1. DMS,P concentrations 169
4.2.2.2. Physical properties 172
4.2.2.3. Biological properties 173
4.3. Results 174
4.3.1. General ice and atmospheric conditions 174
4.3.2. Sea ice growth processes 176
4.3.3. Ice permeability and brine dynamics 178
4.3.4. Biomass and biomass composition 180
4.3.5. DMS,P dynamics 185
4.4. Discussion 189
4.4.1. Importance of DMS,P production in sea ice at Cape Evans 189
4.4.2. Influence of platelet ice formation on DMS,P dynamics in interior ice 193
4.4.3. Influence of ice permeability and brine dynamics on DMS,P dynamics during the spring-summer transition 195
4.4.4. Coupling between DMS,P and chl *a* during the winter-spring transition 200
4.5. Conclusions and perspectives 203
Chapter 5 General conclusions and perspectives 207
References 216

List of Tables

1.1. Summary of available sea ice DMS, DMSP and DMSO data in the literature. The horizontal dashed-line separates Arctic and Antarctic data…….....34

2.1. General ice and surface conditions at the sampling stations. Time is local time (GMT-7). Ice concentrations are given in tenths. The horizontal line separates drift ice stations from fast ice stations. NS: new snow; FF: frost flowers; WS: wind slabs; SU: superimposed ice; MP: melt ponds; nd: not determined……68

2.2. Spatial variability parameters……93

3.1. General ice and surface conditions of the sampling stations. The horizontal line separates drift ice stations from fast ice stations. NS: new snow; FF: frost flowers; WS: wind slabs; SU: superimposed ice; MP: melt ponds; nd: not determined……115

3.2. Statistical parameters of sea ice DMS, DMSP and DMSO concentrations at each station. Nd: not determined……125

3.3. Spearman's rank-order correlation table for dimethylated sulfur compounds and biological (chl *a*) and environmental parameters (T and S) in vertical profiles of sea ice at the IPY-CFL stations (n = 121). TotalS is the total dimethylated sulfur pool (DMS + DMSP + DMSO). When applicable, the level of significance of the coefficient is denoted by * ($p < 0.05$), ** ($p < 0.01$), and *** ($p < 0.001$). Spearman's rank-order correlation was preferred over Pearson's product-moment correlation because of the lack of homoscedasticity shown by the dataset…….……134

4.1. Summary of the snow and ice conditions at the sampling sites……..……176

4.2. Statistical parameters of sea ice DMS and DMSP concentrations at each station……..…186

4.3. Overview of available Antarctic sea ice DMS,P data sets. Note that the resolution of vertical sampling found in the different studies (0.05, 0.10, and 0.20 m) can affect the reported DMS,P concentrations. Because DMS,P is found in discrete bands within sea ice, the signal can be obscured in case of coarse ice core sectioning. In this study, we report values based on a high vertical sampling resolution (0.05 m). If we had chosen a 0.10 to 0.20 m vertical sampling resolution, our maximum DMS,P would have been 20 to 55% lower. Note also that means should not be compared between studies with different sampling strategies. For instance, in DiTullio et al. [1998], only the bottom 5 to 20 cm of ice cores with visible discoloration (and hence important algal biomass) were analyzed, whereas in the other studies referenced in this table, full ice cores were analyzed……191

4.4. Summary of atmospheric DMS measurements. Samples were acquired using Tenax-TA cartridges following the methodology presented in Sharma et al. [1999a]……199

List of Figures

2.1. A. Map of the study area showing the bathymetry and the location of the sampling stations. The dotted lines indicate the extent of fast ice on 5 May 2008. Data for fast ice extent delimitation were obtained from the Canadian Ice Service sea ice charts. B. Air temperature recorded during the IPY-CFL study. The sampling stations icons are plotted on a temperature series of air temperature measured with a Rotronics MP 101A temperature sensor located at ~ 18 m above the ice surface with a resolution of 0.1 °C and an accuracy of ± 0.3 °C……..64

2.2. Vertical profiles of sea ice temperature (T) at the sampling stations……75

2.3. Vertical profiles of sea ice bulk salinity (S_i) at the sampling stations……76

2.4. Sea ice textural properties for a subset of the sampling stations. Representative pictures of the five textural types identified are shown. Granular texture (A) was defined as layers composed of small (millimeter-sized) isometric crystals, columnar texture (B) as layers with long (centimeter-sized) vertically elongated (prismatic) crystals, mixed columnar/granular texture (C) as a transition zones with coexisting granular and columnar textures, draped platelet texture (D) as centimeter-sized crystals with wavy uneven edges, and platelet texture (E) as layers of elongated acicular crystals with no specific orientation. Vertical scale is in centimeters……..78

2.5. A. Water stable isotope ($\delta^{18}O$) vs depth in sea ice for a subset of the sampling stations. B. Evolution of the under-ice water $\delta^{18}O$ (sampling depths 2 to 5 m) during the sampling season. Adapted from Chierici et al. [2011]……..79

2.6. The evolution throughout the sampling season of: A. Daily mean air temperature. B. Mean sea ice temperature. C. Mean sea ice bulk salinity. D. Minimum brine volume fraction and E. Mean Rayleigh number. The vertical dashed line indicates the start of fast ice sampling. In (B) the horizontal dashed line is the ocean freezing temperature (T_f) calculated using $T_f = -AS_w$ where $A = 0.054\,°C.psu^{-1}$ [Assur, 1958]. In (D) the horizontal dashed lines are permeability thresholds (5% and 7%) [Golden et al., 2007]……82

2.7. The linear relationship ($R^2 = 0.87$) between the daily mean air temperature and the mean ice temperature recorded at the IPY-CFL stations. The snow depth (cm) measured at each station is indicated next to the icon of each station……....83

2.8. Vertical profiles of brine volume fraction (V_b/V) at the sampling stations. The vertical dashed lines are permeability thresholds (5% and 7%) [Golden et al., 2007]……89

2.9. Vertical profiles of the Rayleigh number (Ra) at the sampling stations…….90

2.10. Vertical profiles of sea ice temperature (T) and bulk salinity (S_i) for each of the groups defined in section 2.4.2. The curves are drawn through the midpoints of individual sections. Depth scales are normalized to unity……93

3.1. A. Map of the study area showing the bathymetry and the location of the sampling stations. The dotted lines indicate the extent of fast ice on 5 May 2008. Data for fast ice extent delimitation were obtained from the Canadian Ice Service sea ice charts. B. air temperature and photosynthetic active radiation (PAR)

recorded during the IPY-CFL study. The sampling stations icons are plotted on temperature series of air temperature and PAR measured with, a Rotronics MP 101A temperature sensor located at ~ 18 m above the ice surface with a resolution of 0.1°C and an accuracy of ± 0.3°C, and a PARLite™ quantum sensor Kipp and Zonen® located on a tower at the bow of the ship……113

3.2. Vertical profiles of chl *a* (horizontal bars), and percentage of phaeopigments in the ice at the sampling stations. Note the difference in chl *a* scale for station F2. The vertical dashed-lines are set at 50% of phaeopigments……...123

3.3. Vertical profiles of sea ice temperature (T), bulk salinity (S_i), brine volume fraction (V_b/V) and Rayleigh number (Ra) at the sampling stations. The vertical dashed-line is set at 5% of brine volume fraction……..127

3.4. Vertical profiles of DMS (top panel), DMSP (middle panel), and DMSO (bottom panel) concentrations in the ice during the IPY-CFL study. The concentration axis on each plot is in log scale. Superimposed on the DMSO plots is the contribution of each dimethylated sulfur compounds to the total dimethylated sulfur pool. The length of the horizontal bars indicate the percentages of each compound at a given depth……...128

3.5. Triangular plots showing the speciation of dimethylated sulfur compounds in sea ice during the IPY-CFL study in the Canadian Arctic (this study) and during the Arise study in East-Antarctica (Carnat, unpublished results), and in surface waters during various oceanic studies (Simó et al. [1998], Zemmelink et al. [2005], Hatton and Wilson [2007]). Note the dissimilarity in distribution of the dots between the Arctic plot and the two other plots……145

3.6. Percentage of DMSO in the total dimethylated suflur pool in sea ice as a function of estimated irradiance ($W.m^{-2}$) in the 400 to 450 nm wavelength range for stations D33-2, D36NF, D45, and F7-1 above, and D1 and F2 below. Details on the estimation of irradiance at depth in the ice cores, as well as on the choice of the wavelengths are given in section 3.4.3……150

4.1. A. Location of the study site (Cape Evans, 77°38' S, 166°23'E) in the McMurdo Sound. B. Terra MODIS (250 m spatial resolution) satellite image of the study site on the first week of April 2011. C. View of the ice coring site, looking towards Cape Evans……..169

4.2. Evolution of the air temperature (°C) and solar radiation ($MJ.m^{-2}.day^{-1}$) in 2011 and 2012, as recorded by a weather station at Scott Base (25 km away from Cape Evans). Sampling stations are shown as vertical dashed-lines. SF and PF shaded areas are the estimated onset of ice growth and platelet ice growth respectively. SF was estimated from Terra MODIS (250 m spatial resolution) satellite images of the study site. PF was estimated using a freezing degree day (FDD) calculation. First, we calculated the cumulative FDD (θ), following Maykut [1986], using the thickness of columnar ice formed until platelet crystals started to appear in the ice texture. We found θ = 746 in 2011, and 689 in 2012. Then, following Weyprecht [1875] we determined on which days the θ were reached using the mean daily air temperature recorded by a weather station at Scott Base (25 km away from Cape Evans)……175

4.3. Overview of the ice texture observed during the spring-summer transition in 2011 (stations 1 to 3) and the winter-spring transition in 2012 (stations 4 to 8).

Close-ups of the following textural features are also shown: A. Well organized columnar ice with long (cm sized, prismatic) vertically oriented crystals. B. Randomly oriented crystals with ragged edges (arrow pointing at one of the crystals). C. Long triangular crystals (arrow pointing at one very large crystal). Circled in Figure 4.3C is a large refrozen brine tube……177

4.4. Vertical profiles of ice temperature and bulk salinity at A. station 4 (winter-spring), B. station 2 (spring-summer)……179

4.5. Contour plots of brine volume fraction (%) during the spring-summer transition in 2011 (left panel) and the winter-spring transition in 2012 (right panel). Sampling stations are shown as vertical dotted-lines……180

4.6. Vertical profiles of chl *a* (horizontal bars, log scale), and percentage of small cells (0.8 to 10 µm) (black dots) in the ice during the spring-summer transition in 2011 (upper panel) and winter-spring transition in 2012 (lower panel). The vertical dashed-lines are set at 50% of small cells……183

4.7. Biomass composition observed at selected depths of three stations. Note the difference in horizontal scale for the bottom ice layers. DMSP profiles are also shown as grey dots for comparison purposes……...184

4.8. Vertical profiles of DMS concentrations (grey dots) in the ice during the spring-summer transition in 2011 (upper panel) and winter-spring transition in 2012 (lower panel). For comparison purposes, chl *a* concentrations in ice are reported as horizontal bars. Ice texture is reported as vertical colored bars next to the right y-axis, using the same color code as in Figure 4.3. Dark grey is granular ice, light grey is columnar ice, and light blue is mixed columnar/platelet ice……188

4.9. Vertical profiles of DMSP concentrations (grey dots) in the ice during the spring-summer transition in 2011 (upper panel) and winter-spring transition in 2012 (lower panel). For comparison purposes, chl *a* concentrations in ice are reported as horizontal bars. Ice texture is reported as vertical colored bars next to the right y-axis, using the same color code as in Figure 4.3. Dark grey is granular ice, light grey is columnar ice, and light blue is mixed columnar/platelet ice……189

4.10. Evolution of DMS (nM), DMSP (nM), and chl *a* (µg.L^{-1}) concentrations in bottom ice (5 cm) during the spring-summer transition in 2011 (left panel) and winter-spring transition in 2012 (right panel). Each set of dots corresponds to a sampling station, identified by its number (1 to 8)……201

Chapter 1

Introduction

1.1. Motivation

1.1.1. Climatic and biogeochemical significance of dimethylsulfide

The biogenic gas dimethylsulfide (DMS) attracted attention in 1972 when it was found to be ubiquitous in the world oceans, and transferred at a significant rate to the atmosphere [Lovelock et al., 1972]. It was proposed and soon demonstrated that DMS was the missing sulfur species required to enable the steady-state flow of sulfur between oceans and terrestrial regions [Lovelock et al., 1972; Andreae, 1990], and thus a key link in the global sulfur cycle. Oceanic emissions of DMS (about 13 to 37 Tg of S.year^{-1}) contribute to 90% of the total annual flux of biogenic DMS (about 28 to 45 Tg of S.year^{-1}), which represents about half of the total biogenic sulfur emissions, the remaining half originating from volcanoes and vegetation [Bates et al., 1992]. Although anthropogenic emissions largely dominate the sulfur emissions on a global scale (80 to 90%), DMS emissions still represent a significant fraction of the total sulfur emissions in the southern hemisphere and in the tropical latitudes of the northern hemisphere [Bates et al., 1992]. More than an important sulfur carrier, DMS, through its oxidation products in the atmosphere, is believed to be a climate-active gas.

1.1.2. Atmospheric oxidation of DMS and the CLAW hypothesis

After ventilation to the atmosphere, DMS is quickly oxidized to various sulfur-containing compounds such as dimethylsulfoxide (DMSO) and dimethylsulfone ($DMSO_2$), methane sulfonic acid (MSA), and sulfur dioxide (SO_2)

[Andreae, 1990; Turnipseed and Ravishankara, 1992; Kloster et al., 2006]. The SO_2 produced by the oxidation of DMS can further be oxidized to sulfuric acid (H_2SO_4), which can nucleate or condense on existing particles to produce sulfate (SO_4^{2-}) aerosols. These sulfate aerosols alter the atmospheric chemistry (e.g. acidity of precipitation) and hydrological cycle [Charlson and Rodhe, 1982], but also pre-eminently alter the radiative properties of the atmosphere directly by scattering of incoming solar radiation, and indirectly by forming cloud condensation nuclei (CCN) that increase clouds reflectivity [Charlson et al., 1987]. This provided the background for the CLAW hypothesis, DMS-climate feedback [Charlson et al., 1987], which suggests that a homeostatic feedback exists between oceanic phytoplankton and the Earth's climate through DMS production. Basically, an increase in oceanic DMS emissions would result in an increase in aerosol sulfates, CCN, and cloud albedo. This would in turn reduce the amount of solar radiation reaching the ocean surface, changing the speciation and abundance of phytoplankton producing dimethylsulfoniopropionate (DMSP, the biological precursor of DMS), and reducing the oceanic DMS production, establishing the climate feedback loop and maintaining the Earth in homeostasis.

1.1.3. Criticisms about the CLAW hypothesis

Each major assumption of CLAW has been critically weakened by several observational and modelling studies throughout the years [Ayers and Cainey, 2007], leading Quinn and Bates [2011] to recently suggest that it was time to retire the hypothesis. For example, DMS-derived sulfates do not appear to be the only and dominant source of CCN over large parts of unpolluted oceanic areas. Other potential important sources include sea salts, other biogenic chemical species (e.g. iodine and ammonia) and organic aggregates injected to the atmosphere through

bubble bursting [Bigg, 2007; Twohy and Anderson, 2008]. Also, the SO_2 yield of the atmospheric oxidation of DMS, which determines the DMS potential to provide a source of CCN, does not seem to be systematically high. For instance, BrO radicals in the atmosphere of remote oceanic areas can transform a significant fraction of DMS into DMSO, leading to a decrease of the SO_2 yield [Boucher et al., 2003; von Glasow and Crutzen, 2004]. Then, the sensitivity of CCN to changes in DMS emissions appears to be low over large parts of the oceans, as shown by the modelling study of Woodhouse et al. [2010].

This general low sensitivity of CCN to DMS also inevitably weakens the second assumption of CLAW. Furthermore, an increase in CCN does not only increase the cloud albedo but can also decrease the cloud lifetime, reducing the net effect of CCN on the global radiative budget [Wood, 2007; Small et al., 2009]. For example, an increase in CCN concentration in a regime of non-precipitating clouds can lead to faster evaporation rates owing to smaller cloud droplets, which can increase the entrainment of sub saturated air surrounding the cloud and ultimately reduce the cloud fraction.

Finally, some model simulations indicate a small, and sometimes negative, feedback associated with an increase in solar radiation and/or surface temperature on DMS production and emissions [Bopp et al., 2004; Vallina et al., 2007], and conversely a small sensitivity in climate to an increase in oceanic DMS [Gunson, 2006]. For instance, the global DMS ocean surface concentration would increase by only 1% in case of an increase in the solar radiation due to a 50% increase in the atmospheric CO_2 concentration [Vallina et al., 2007]. Similarly, Bopp et al. [2004] simulated the radiative impact resulting from a change in DMS emissions following a doubling of atmospheric CO_2 concentrations. In the low latitudes, DMS

production would be reduced by 10% due to enhanced stratification and reduction in nutrient supply, while in the high latitudes, DMS production would increase by 20% due to a longer growing season. The average global increase would be low, around 1%. The globally averaged annual DMS emissions would increase by 3%, and would result in a radiative impact of 1 $W.m^{-2}$ in the low latitudes, and -1 $W.m^{-2}$ in the Southern Ocean between 40 and 60°S. Globally, the impact would be very small, averaging -0.042 $W.m^{-2}$.

1.1.4. Towards a regional climate regulation role for DMS

If the validity of CLAW on a global scale is strongly called into question, the influence of phytoplankton DMS emissions on the regional climate of remote oceanic areas such as the Southern and Arctic Oceans could still be significant [Lana et al., 2012]. The CCN production per unit mass of DMS emitted seems to vary strongly across oceanic areas (by more than a factor 20) [Woodhouse et al., 2013]. Krüger and Grassl [2011] showed using a synergistic analysis of satellite observations that the phytoplankton related emissions of DMS and isoprene into the atmosphere strongly influence cloud properties in the Southern Ocean during the austral summer. They showed that phytoplankton blooms from 45 to 65°S are associated with an increase in CCN, an increase in cloud droplet effective radius, and an increase in cloud optical thickness of water clouds. Along these lines, Sharma et al. [1999b] suggested that the cloud albedo in the Arctic summer could be strongly influenced by DMS emissions given the very low aerosol concentrations that prevail in this region. This is further supported by recent field observations linking particle formation events, atmospheric DMS concentrations, and oceanic DMS concentrations across the Arctic [Chang et al., 2011; Tunved et al., 2013]. For instance, Chang et al. [2011] showed a good coincidence between

nucleation periods of atmospheric particles and high atmospheric and ocean surface DMS concentrations during a field study conducted in the Canadian Arctic Archipelago in the summer of 2008. During that same study, Rempillo et al. [2011] observed that levels of biogenic SO_2 were sufficiently high to trigger the formation of new aerosols in the early autumn of 2008. The authors suggested that SO_2 resulting from the atmospheric oxidation of DMS could result in new particle formation in the clean air conditions present in the Arctic.

The potential influence of DMS production in the Arctic Ocean on the Arctic climate could somewhat revive the CLAW hypothesis on a regional scale, especially in the recent context of rapid warming observed in the Arctic [Blunden and Arndt, 2013; Levasseur, 2013]. Hence, there is a considerable interest to determine if the ongoing reduction in thickness and area of the sea ice cover [e.g. Cavalieri and Parkinson, 2012; Kwok et al., 2009] will ultimately lead to an increase of marine DMS emissions, and if this increase could partly mitigate the effect of the ice-albedo feedback [Levasseur, 2013]. Arctic DMS models currently indicate an increase of the Arctic DMS emissions in the near future [Gabric et al., 2005; Qu and Gabric, 2010]. Gabric et al. [2005] calculated an increase of 80% of DMS emissions under a CO_2 tripling scenario (by 2080), in response to a strong decrease in sea ice extent (18,5% annually, and 61% in summer-autumn), a 1°C increase of the mean annual sea surface temperature, and an annual 13% decrease of the mixed layer depth. Gabric's model is largely based on the reasonable assumption that DMS emissions will be significantly facilitated by the removal of sea ice, and by the increase in the lead and melt pond fractions [Nilsson et al., 2001; Leck et al., 2002].

However, future DMS emissions will also greatly depend on the future net DMS production by the Arctic marine biota, which is currently not well constrained in the DMS models. This is mainly due to the limited understanding of the complex web of biogeochemical processes that control DMS production in oceanic waters (i.e. the oceanic cycling of DMS, see section 1.2.1). In view of this biogeochemical processes, future DMS production could potentially be strongly influenced by major shifts in phytoplankton abundance and speciation [Arrigo et al., 2008; Merico et al., 2003; Hegseth and Sundfjord, 2008; Galí and Simó, 2010], and by changes in environmental stressors such as light exposure [Taalba et al., 2013] and ocean acidification [Archer et al., 2013], all expected (and already observed) to occur with warming and sea ice loss.

Moreover, the contribution of the sea ice biome itself to today's (and future) DMS emissions is currently not taken into account by model predictions. Sea ice has long been considered to be an impermeable barrier to gas exchange between the ocean and the atmosphere [Tréguer and Pondaven, 2002] and a seasonal ice mask is typically applied over the polar marine regions (Arctic and Antarctic) in the various DMS climatologies and modelling studies of oceanic DMS concentrations and emissions [Kettle et al., 1999; Lana et al., 2011]. However, recent studies showed that sea ice, through liquid brine contained therein, can exchange gases with both the ocean and the atmosphere [e.g. Loose et al., 2011b], and significant DMS fluxes (up to 30 $\mu mol.m^{-2}.day^{-1}$) from sea ice have been detected in the Antarctic [Zemmelink et al., 2008a; Nomura et al., 2012]. Furthermore, sea ice is more than just a mechanical conduit. Rather, sea ice is a biome favorable to substantial DMS production [Kirst et al., 1991; Levasseur et al., 1994]. All these observations suggest that the sea ice biome could significantly and directly

contribute to regional DMS emissions, and should therefore be integrated as a dynamic component in the DMS models. Accurate quantifications of regional sea ice DMS production and emissions and their integrations in models require a good understanding of the cycling of DMS in sea ice, which we currently do not have, and which is the central motivation of this thesis.

In the next section of this introduction, the main biogeochemical processes and pools involved in the biogeochemical cycling of DMS in oceanic waters are briefly introduced. Then, the main findings about these processes and pools in sea ice from studies conducted in the Arctic and Antarctic are summarized, and the critical knowledge gaps that will be addressed in the thesis are highlighted.

1.2. Background

1.2.1. The cycling of DMS in oceanic waters

DMS is part of a complex biogeochemical cycle including multiple sulfur species, all of which are linked by numerous biotic and abiotic processes. A thorough review of the cycle is provided by Yoch [2002] and Stefels et al. [2007]. The classical view of the DMS cycle starts with its biological precursor, dimethylsulfoniopropionate (DMSP).

1.2.1.1. DMSP synthesis and physiological functions

DMSP ($(CH_3)_2S^+CH_2CH_2COO^-$) is an intracellular metabolite synthesized by macro and microalgae, and some species of terrestrial and aquatic vascular plants [Stefels, 2000]. Produced mostly by phytoplankton, DMSP represents the majority of the reduced sulfur pool in the marine ecosystem [Simó et al., 2002]. Since DMSP contains five atoms of carbon, it is also important in the carbon cycle, accounting for 3 to 10% of the global marine primary production [Kiene et al., 2000]. Intracellular DMSP is commonly referred to as particulate DMSP, or $DMSP_p$, which is typically measured as the fraction of DMSP caught on filters such as Whatman GF/F filters (nominal initial retention size of 0.7 µm) [Kiene and Slezak, 2006]. DMSP is synthesized in phytoplankton from the amino acid methionine after the assimilatory uptake of sulfate from the medium [Gage et al., 1997]. DMSP synthesis has the same starting material in phytoplankton and higher plants, but the pathways differ from there. In phytoplankton, DMSP synthesis occurs as follows: methionine transaminated to → 4-methylthio-2-oxobutyrate, reduced to → 4-methylthio-2-hydroxybutyrate, S-Methylation to → 4-dimethylsulfonio-2-hydroxybutyrate, and finally oxidation to DMSP [Gage et al., 1997].

Regarding phytoplankton, the cytosolic levels of DMSP vary considerably from one species to another [Keller et al., 1989]. The typical intracellular DMSP production of the major DMSP producing phytoplankton groups is given by Stefels et al. [2007].

Since cellular DMSP concentrations are rarely measured, the DMSP production capacity of a given algal assemblage is usually approached using DMSP-to-C or DMSP-to-chl *a* ratios. High DMSP producing groups and low DMSP producing groups are typically identified as groups with DMSP-to-chl *a* ratios above 100 $nmol.\mu g^{-1}$ and below 50 $nmol.\mu g^{-1}$ respectively [e.g. Turner et al., 1995]. Haptophytes (mainly coccolithophores), dinoflagellates and chrysophytes are usually acknowledged as major individual DMSP producers, and diatoms as minor individual DMSP producers. Such general classifications should however be considered with caution. Indeed, the variability within groups can be high. Furthermore, the cytosolic level of DMSP is function of the age of the cell [Malin and Kirst, 1997], and of its physiological response to environmental stresses, which we will introduce later in this section. It is also worth noting that the global DMSP production of a species is also function of its ability to form blooms [Stefels et al., 2007]. For instance, some species of haptophytes (such as *Phaeocystis sp.*, and *Emiliania Huxleyi*) are known to produce very high quantities of DMSP during monospecific blooms.

The high variability in cytosolic levels of DMSP between different algal species partially explains why DMSP and indicators of biomass such as chlorophyll *a* (chl *a*) are not better correlated. For instance, Andreae [1990], in a study regrouping over 1000 measurements, showed that chl *a* only explains about 30% of the DMSP variability. Much of this variability also comes from variability in

environmental parameters (e.g. light, nutrients, temperature, and salinity) and their influence on intracellular DMSP production. DMSP is a multifunctional compound, but its exact physiological roles are still unresolved, and it is possible that it serves distinct roles in different species. Because of its high cytosolic concentrations, DMSP could function as an osmoregulator and cryoprotecant [Karsten et al., 1996; Stefels 2000]. In this respect, an exponential increase of intracellular DMSP was observed in *Phaeocystis* cultures upon increasing salinity levels [Stefels, 2000], and both *Emiliana huxleyi* and *Phaeocystis* are known to increase their DMSP production at low temperatures [van Rijssel and Gieskes, 2002; Stefels et al., 2007]. However, mechanisms regulating intracellular DMSP upon short-term salinity and temperature shifts are still obscure. High intracellular DMSP were also observed in algal cultures under oxidative stress, such as *Emiliana huxleyi* cultures under high visible light and ultraviolet radiations [van Rijssel and Gieskes, 2002; van Rijssel and Buma, 2002]. Sunda et al. [2002] developed the hypothesis that DMSP and its breakdown products could serve as antioxidants by scavenging hydroxyl radicals and other reactive oxygen species. Oxidative stresses in the marine environment can typically arise from high ultraviolet radiations but also nutrient limitation [Bucciarelli and Sunda, 2003; Sunda et al., 2007]. In this respect, Bucciarelli et al. [2013] recently observed increased intracellular DMSP in iron-limited assemblages of the diatom *Thalassiosira oceanica*. Furthermore, DMSP could be produced as an alternative to N-containing osmolytes under nitrogen limitation. This hypothesis, although supported by the fact that DMSP has a chemical structure analog to that of the osmolyte glycine betaine [Challenger, 1951], has yet to be demonstrated. Along the same line, DMSP could be synthesized as an overflow mechanism for excess reduced sulfur, carbon, and energy, in cases where nutrient limitation results in unbalanced nitrogen and

carbon metabolic pathways [Stefels and van Leeuwe, 1998]. As a whole, the link between intracellular DMSP and nutrient limitation remains hard to establish since cell size reduction under N or Fe limitation can also cause an apparent increase of the cellular DMSP concentration. Finally, DMSP, through one of its breakdown product acrylate, could serve as a chemical grazing deterrent [Wolfe and Steinke, 1996; Wolfe et al., 1997]. This is supported by a recent study of Fredrickson and Strom [2009] who observed a strong inhibition of grazing rates (28 to 75% decrease) following the addition of DMSP to ciliates and dinoflagellates cultures. On the other hand, DMSP, through its breakdown product DMS, may also act as an attractant (signaling compound) for some zooplankton species [Breckels et al., 2013], and bacteria [Miller et al., 2004]. Steinke et al. [2006] suggested that macrozooplankton could use DMS to detect the grazing of microzooplankton, and that DMSP production may therefore be a strategy of phytoplankton to limit the abundance of small grazers.

1.2.1.2. DMSP release from the cell

Four different pathways of particulate DMSP release from the cell to the medium have been proposed: autolysis, viral infection, zooplankton grazing, and exudation. Autolysis has logically been suggested as one of the most important pathways [Nguyen et al., 1988], since a strong increase in DMSP breakdown products is usually observed during the senescent phase of phytoplankton blooms [e.g. Merzouk et al., 2008], which is characterized by an important cell mortality.

Viral infection, leading to cell mortality, could also be an important pathway. This was initially suggested by the study of Malin et al. [1998] who observed cell lysis and an increase of 400% of DMSP breakdown product (DMS) following the viral infection of a *Phaeocystis pouchetii* culture. However, the authors could not

determine if the measured DMS was directly derived from the cells, or derived from bacterial conversion of DMSP to DMS (see section 1.2.1.3). The Malin et al. [1998] hypothesis is further supported by experiments with infected axenic cultures of *Emiliana huxleyi* [Evans et al., 2007]. Furthermore, viral infection could also favor DMSP release by terminating large blooms (e.g. senescent *Emiliania huxleyi* blooms are typically infected by large viruses [Bratbak et al., 1995; Martinez et al., 2007]). The effect of viruses on senescent *Emiliania huxleyi* blooms and associated DMSP release remains however uncertain. While Stefels et al. [2007] observed an increase of DMS upon virus-induced bloom termination, Wilson et al. [2002] showed that the effect of viral lysis could be negligible compared to that of zooplankton grazing.

Regarding grazing, since feeding strategies of zooplankton directly influence DMSP release, an important distinction needs to be made between small grazers (microzooplankton) and larger grazers (meso- and macrozooplankton). Microzooplankton such as ciliates and heterotrophic dinoflagellates typically engulf their prey by phagotrophy, while meso- macrozooplankton such as krill and copepods can also rip or tear their prey resulting in the physical breakage of the cells (sloppy feeding) [Williams, 1981]. The influence of microzooplankton grazing on DMSP release was first illustrated by Wolfe and Steinke [1996] in a culture study of dinoflagellate predation on *Emiliania huxleyi*. In another culture study with heterotrophic dinoflagellates, Tang and Simó [2003] showed that 32 to 44% of the ingested DMSP remained in the grazer and was mainly used as a carbon and sulfur source for growth. In general, it is assumed that approximately 70% of the DMSP ingested by micrograzers will be released in the medium, either under dissolved DMSP or in fecal pellets [Archer et al., 2001]. During sloppy feeding by

large grazers, an even larger fraction of DMSP could be released since the cellular content is not fully ingested [e.g. Daly and DiTullio, 1996]. However, the few studies on meso- and macrozooplankton grazing on DMSP producing species showed a significant mismatch between the DMSP content of the grazed assemblage and the breakdown products of DMSP measured in the medium. Whether this mismatch is mainly due to an incorporation of DMSP in the grazer's biomass, to a packaging of DMSP into sinking fecal pellets lost to the euphotic zone by deep export, or to bacterial conversion processes of the DMSP breakdown products released in the medium, remains unknown [Kwint and Kramer, 1996; Tang et al., 1999].

Active exudation is the metabolic excretion of DMSP by the cell in response e.g. to changes in environmental factors [Vairavamurthy et al., 1985]. Despite the fact that some suggested functions of DMSP (e.g. antioxidant, osmoregulator) require the algae to be able to regulate their intracellular DMSP concentration, very little is known on the rate of DMSP exudation, and its distribution in gradients surrounding the cells. DMSP cannot effectively permeate through membranes without a specific transporter [Kiene et al., 1998]. This transporter could be for example glycine betaine transmethylase (GBT), as shown by Vila-Costa et al. [2006b] in a culture study of DMSP uptake by diatoms. Laroche et al. [1999], in a modelling study, found that the dinoflagellate *Prorocentrum minimum* was exuding DMSP at a rate of 1% of its DMSP cellular content per day, and that the release was independent of the growth phase. Microalgae exudates typically form diffusion-limited chemical gradients in the boundary layer around the cell, called phycosphere [Bell and Mitchell, 1972]. Fredrickson and Storm [2009] calculated the increase in DMSP in the phycosphere based on a theoretical exudation rate of

0.1% and found that the DMSP concentration was compatible with a signaling function. Using another model integrating diffusion losses in the phycosphere and exudation rates modelled by Laroche et al. [1999], Breckels et al. [2010] found concentrations 10^6-fold lower than those calculated by Fredrickson and Strom [2009], challenging their conclusions. This last result is coherent with the general observation that actively growing healthy phytoplankton assemblages release relatively low amounts of DMSP in the surrounding water [Turner et al., 1988]. As a whole, there is still little evidence for the active exudation of DMSP, and it remains very difficult to distinguish the contribution of all the DMSP release pathways in both natural and culture studies [Stefels et al., 2007].

1.2.1.3. Enzymatic cleavage to DMS

Algae could also regulate their intracellular DMSP concentration by influencing DMSP degradation pathways within cells (catabolic pathway). Breakdown products of DMSP would be more easily transported through cell membranes than DMSP itself. DMSP is enzymatically cleaved to DMS, acrylate, and a proton by a DMSP-lyase enzyme (dimethylpropiothein dethiomethylase) [Cantoni and Anderson, 1956].

Despite being so important for the suggested physiological roles of DMSP in phytoplankton and for the conversion and release of DMS to oceanic waters, the enzymology of DMSP cleavage in cells has not been studied in great details [Stefels et al., 2007]. DMSP-lyase activity is detectable in some but not all phytoplankton species [Niki et al., 2000; Franklin et al., 2010]. High DMSP-lyase activity was observed in two important DMSP producers, *Phaeocystis* and *Emiliania huxleyi* [Steinke et al., 1998], but was absent in the DMSP-producing prasinophyte *Tetraselmis subcordiformis* [Steinke et al., 1996], suggesting that

DMSP synthesis and DMSP cleavage are not necessarily related. The activity would vary strongly among species, and even among strains within species [Steinke et al., 1998]. There is also some uncertainty about the physical location of the enzyme in the cells. Cytosolic DMSP could be physically separated from the DMSP-lyase since healthy phytoplankton assemblages release relatively low amounts of DMS in the surrounding water [Turner et al., 1988]. In some species, DMSP-lyase could be membrane-bound (extacellular) [Steinke et al., 1998], which is compatible with some suggested physiological roles for DMSP (e.g. overflow mechanism for excess reduced compounds) [Stefels, 2000]. This is supported by the acrylate accumulation observed in the mucus layer of some *Phaeocystis* colonies [Noordkamp et al., 2000]. On the other hand, other suggested physiological roles would require an intracellular location of DMSP-lyase, such as in the chloroplast. This is the case for example for the antioxidant hypothesis developed by Sunda et al. [2002] since harmful reactive oxygen species are typically found in the chloroplasts. Although bacterial DMSP-lyase activity (see below) is usually thought to dominate DMS production [Kiene, 1992], some studies suggest that in some cases phytoplankton DMSP-lyase activity could also be important [Niki et al., 2000]. For instance, Steinke et al. [2002], during the sampling of some North Atlantic sites during an *Emiliania huxleyi* bloom, showed that 75 to 80% of the total DMSP-lyase activity could be attributed to dinoflagellates when their biomass rose above that of the coccolitophores. These results should however be considered with caution since it remains very difficult to isolate phytoplankton DMSP-lyase activity from membrane-attached bacterial DMSP-lyase activity [Yoch, 2002; Stefels et al., 2007].

The DMSP fraction that has not been cleaved in the cell or in the phycosphere is released in oceanic waters under the form of dissolved DMSP ($DMSP_d$). Despite its high abiotic stability under natural conditions (half-life > 8 years [Dacey and Blough, 1987]), $DMSP_d$ is generally characterized by a very short turnover time in oceanic waters (a few hours) [Kiene and Linn, 2000]. This is explained by the rapid consumption of $DMSP_d$ by the microbial food web. The microbial consumption of DMSP manifests itself through many different pathways that remain difficult to study, since $DMSP_d$ is technically challenging to quantify [Kiene and Slezak, 2006]. Non-DMSP-producing phytoplankton could uptake and assimilate dissolved DMSP released by high-producing phytoplankton partners, as shown for two species of centric diatoms in a recent incubation study [Vila-Costa et al., 2006b]. This process, which requires further documentation, would confirm the role of DMSP as an important carrier of S and C in the microbial food web. Under certain conditions, this process could be quantitatively significant and similar to bacterial uptake in magnitude, representing 20% of the total DMSP consumption. Bacterial uptake of dissolved DMSP is better documented, notably through the use of the radiolabelled tracer ^{35}S-DMSP and genetic studies [Todd et al., 2007]. A large number of heterotrophic bacteria taxa have been shown to consume DMSP in oceanic waters, including free-living bacteria, bacteria in the phycosphere, bacteria attached to zooplankton or in their guts [Yoch, 2002]. This consumption serves multiple purposes. First, similarly to algae, bacteria could use DMSP as an osmolyte or cryoprotectant. This is supported by several laboratory observations of increased bacterial growth following enhanced DMSP uptake in response to increased osmotic stress [e.g. Diaz et al., 1992]. Second, bacteria could use DMSP as a substrate for growth. Several studies have shown that DMSP could satisfy 1 to 13% of the total bacterial carbon demand, and up to 100% of the

total bacterial sulfur demand [Kiene et al., 2000; Simó et al., 2002]. Sulfur and carbon uptake from DMSP degradation depends on the DMSP degradation pathways used. Bacteria degrade assimilated DMSP following several distinct pathways [Todd et al., 2007]: (1) the cleavage pathways (DMSP-lyase pathway such as in algae and DddD enzyme pathway), (2) the demethylation/demethiolation pathway (DmdA enzyme). The cleavage pathways yield DMS as an end-product and provide carbon to the bacteria. Several bacteria have been found to express DMPS-lyase activity [Stefels and Van Boekel, 1993; Wolfe and Steinke, 1996] but the cleavage pathway would in general represent only 5 to 10% of assimilated DMSP metabolism [Kiene, 1996]. Bacteria preferentially use the demethylation/demethiolation pathway which has a greater potential energy benefit than DMSP-lyase and which in addition to carbon provides active methyl groups and reduced sulfur for incorporation into proteins and amino acids. However, demethylation/demethiolation does not produce DMS. Hence, the DMS yield of DMSP consumption of a given microbial food web strongly depends on the ratio of DMSP degraded following the cleavage pathways to that degraded following the demethylation/demethiolation pathway. Furthermore, Kiene et al. [2000] suggested that this ratio could be governed by the bacterial carbon and sulfur demands, and that bacteria would generally switch from demethylation/demethiolation to DMSP-lyase when their sulfur demand is satisfied. Genes involved in the algal and bacterial DMSP-lyase and bacterial DMSP metabolism (e.g. demethylation/demethiolation pathway) have been the focus of much attention during the last decade (e.g. Todd et al. [2007]; Todd et al. [2012]), but I will not present them in details here. Hence, the reader is referred to the synthesis of Moran et al. [2012] for further information.

1.2.1.4. DMS loss pathways

Once cleaved from DMSP, DMS can be lost from oceanic waters by three processes: abiotic photolysis (photo-chemical oxidation), biological DMS consumption (or BDMSC), and ventilation to the atmosphere. The two first processes can lead to the formation of dissolved dimethylsulfoxide ($DMSO_d$, $(CH_3)_2SO$) [Kieber et al., 1996; del Valle et al., 2007b].

DMS, unlike DMSP, seems to be consumed by a limited number of bacteria taxa (approximately 1/3, according to Vila-Costa et al. [2006a]). BDMSC has been observed in phototrophic bacteria, to which DMS can provide electron donors for carbon dioxide fixation [Zeyer et al., 1987], and in heterotrophic bacteria, to which DMS can provide a source of sulfur and carbon [e.g. Fuse et al., 2000]. A synthesis of the genes involved in BDMSC is provided by Schäfer et al. [2010]. Little is known about the BDMSC rates in oceanic waters. BDMSC seems to increase with DMS production and would therefore maintain the DMS concentration in a narrow range between 0 and 20 $nmolS.L^{-1}$ [Simó, 2004]. The turnover time of DMS due to BDMSC has generally been observed to be rapid (on the order of 1 to 2 days) [Kiene and Bates, 1990]. For instance, DiTullio et al. [2003] observed very high BDMSC during a *Phaeocystis* bloom with high DMS concentrations in the Ross Sea. BDMSC does not systematically lead to DMSO production. Sulfates is another major end-product, that would dominate over DMSO in waters with fast biological DMS turnover, as suggested by experiments conducted in the Ross Sea by del Valle et al. [2009]. The DMSO yield from BDMSC and production rates of $DMSO_d$ have also been assessed by del Valle et al. [2007a] in the oligotrophic Sargasso Sea. In that specific case, $DMSO_d$ production rates from BDMSC were typically slow, indicating long turnover times (15 to 61 days) for the $DMSO_d$ pool.

The same authors also observed the DMSO yield from BDMSC to vary with water depth (72% in the surface mixed layer vs 16% below it) but could not identify the reason of this trend.

Photolysis of DMS in surface waters is also believed to be an important DMS loss pathway [Brimblecombe and Shooter, 1986]. DMS itself does not photo-dissociate outside of the UV range (wavelength longer than 260 nm), but photo-chemical oxidation can occur at visible wavelengths via photosensitizers [Kieber et al., 1996]. In oceanic waters, DMS is mainly photo-chemically oxidized in DMSO by UV-A and visible light, and photolysis rates are usually maximal between 380 and 460 nm [Kieber et al., 1996]. Photo-chemical oxidation by UV-B can also occur, but does not result in DMSO production [Hatton, 2002]. Photo-chemical oxidation of DMS would primarily be mediated by oxidants produced by photoreactions of chromophoric dissolved organic matter (CDOM) [Brugger et al., 1998; Toole et al., 2003]. Toole et al. [2003] also showed that the DMSO yield from DMS photolysis is sensitive to temperature, doubling with an increase of 20°C. Furthermore, Toole et al. [2004] observed very high photo-chemical destruction of DMS during early spring in the Southern Ocean due to high nitrate concentrations, suggesting that nitrate photochemistry could also mediate DMS photolysis. This dependence of photo-chemical oxidation of DMS on CDOM and nitrate was further confirmed by Taalba et al. [2013] in the western Canadian Arctic. The nitrate-induced photolysis of DMS can be further enhanced by the presence of bromide ions and bicarbonate/carbonate ions, as shown by Bouillon and Miller [2005] in a laboratory study.

A very large range of DMS photolysis rates and DMSO yield from photo-chemical oxidation of DMS is typically observed in oceanic waters and is probably

due to variability in location, temperature, light intensity, depth, CDOM and nitrate concentrations. For instance, DMSO yields of 14% were reported by Kieber et al. [1996] in the Equatorial Pacific Ocean, while values between 22 and 99% were reported by Hatton [2002] in the North Sea, and values from 33 to 45% were reported by Toole et al. [2004] in the Southern Ocean. Similarly, photolysis rates comprised between 0.001 and 0.009.day^{-1} were reported from various oceanic areas [Kieber et al., 1996; Brugger et al., 1998; Hatton, 2002; Toole et al., 2004]. In a recent incubation study conducted in the Ross Sea, del Valle et al. [2009] showed an increase in the DMSO yield following exposure of seawater to full spectrum sunlight for 72 h. A same increase was not observed following exposure to photosynthetically active radiation (PAR) only, suggesting that UV radiation may trigger a shift from BDMSC dominated DMSO production to photo-chemically dominated DMSO production.

Since DMS is rapidly oxidized in the atmosphere (see section 1.2.1.6), oceanic waters are always observed to be saturated with DMS relative to the atmosphere. Hence, a strong gradient in concentrations exists and as soon as DMS is produced in seawater, a net flux to the atmosphere is observed.

In gas exchange models, the flux (*F*) of a gas across the air-water interface is typically expressed as:

$$F = k_{gas}.\Delta C \qquad (1.1)$$

where ΔC is the air-water concentration disequilibrium and k_{gas} a kinetic parameter, transfer velocity which quantifies the rate at which the gas crosses the air-sea interface [Liss and Slater, 1974].

k_{gas} is usually parameterized as the waterside transfer velocity (k_w) which is function of wind speed (*U*) and temperature. Many parameterizations for the determination of k_w can be found in the literature for a large range of temperatures and wind speeds. Amongst these, Stefels et al. [2007] recommend to use the Nightingale [2000] parameterization, intermediate between all others, whereas the Liss and Merlivat [1986] and Wanninkhof [1992] are the most commonly used. There is a large uncertainty associated with the determination of k(estimates typically vary by a factor of 2), especially at high wind speeds due to a lack of available measurements.

Given all the uncertainties related to gas exchange models, direct measurements of DMS fluxes should be preferred over calculations. Current measurement techniques include eddy correlation [Huebert et al., 2004], eddy accumulation, and gradient flux technique [Zemmelink et al., 2004]. However, the sophisticated equipment and profound technical knowledge required by these advanced micrometeorological techniques limit their use to only a few research groups.

The global contribution of DMSP originally synthesized by phytoplankton cells synthesis to DMS emissions has to date not been fully constrained. Considering the DMS yield from DMSP consumption, a very wide range of values can be found in the literature, from 1 to 100% [e.g. Simó et al., 2000; Acher et al., 2002]. This wide range reflects the complexity and great regional variability of the biotic and abiotic factors controlling the DMSP release and conversion to DMS. Regarding DMS losses, it is estimated that only 10% of the produced oceanic DMS will ultimately be vented to the atmosphere [Archer et al., 2002]. Ventilation is generally the dominant loss process near the ocean surface (upper meter), while

photoxidation can sometimes dominate in the upper 10 to 20 m. Integrated over the whole water column, BDMSC is largely dominant, removing approximately 50 to 80% of the DMS pool [Archer et al., 2001; Simó, 2004]. These percentages of course strongly depend on the local environmental and meteorological forcing (e.g. cloudiness, storminess, and water mixing conditions) and can therefore not been used as a rule of thumb [Simó and Pedros-Alio, 1999].

1.2.1.5. The particulate DMSO pathway

Similarly to DMSP, $DMSO_p$ (GF/F retained DMSO) can also be biosynthesized by marine microalgae, and then released into the environment as $DMSO_d$ [Simó et al., 1998; Hatton and Wilson, 2007]. The $DMSO_d$ production pathway could be comparable in magnitude to the production from dissolved DMS photo-chemical oxidation, and could exceed DMSO production from BDMSC in surface oceanic waters exposed to sunlight, as suggested in experimental incubations by del Valle et al. [2007b]. In dark or low UV conditions, BDMSC would nevertheless still dominate DMSO production.

DMSO was found in several natural phytoplankton assemblages and cultures (e.g. dinoflagellates such as *Amphidinium carterae*, and coccolitophores such as *Emiliania Huxleyi*), suggesting that its synthesis might be as widespread as that of DMSP [Simó et al., 1998]. $DMSO_p$ concentrations are generally lower than $DMSP_p$ concentrations, with $DMSP_p$-to-$DMSO_p$ ratios typically comprised between 1 and 13 [Simó and Vila-Costa, 2006], although values < 1 have also been reported [Riseman and DiTullio, 2004]. Strong correlations between the two compounds are also observed. This suggests that both compounds have a common origin in the phytoplankton cells and that $DMSP_p$ might be the precursor of $DMSO_p$, following e.g. the intracellular oxidation of DMS [Hatton et al., 2004].

As for DMSP, the exact physiological roles of DMSO are still unresolved, and it is possible that it serves distinct roles in different species. DMSO has been suggested to act as a cryoprotectant and osmoregulator in extreme environments, as an intracellular electrolyte modifier [Lee and de Mora, 1999], and as a free radical scavenger in the Sunda et al. [2002] antioxidant hypothesis. This last role is further supported by the fact that DMSO is able to permeate through intact cell membranes and is well known as an effective radical scavenger [Hatton et al., 2004; Lee and de Mora, 1999; Stefels et al., 2007]. In that respect, Riseman and DiTullio [2004] observed a simultaneous increase in $DMSO_p$ and β-carotene (a known scavenger of reactive oxygen species) under low-iron conditions in a study of the Peruvian upwelling system. Finally, as shown by Spiese et al. [2009], $DMSO_P$ can be recycled back by algae to DMS through its reduction by DMSO reductase enzymes. This reduction process of DMSO was initially thought to be limited to several species of aerobic and anaerobic bacteria [Lee and de Mora, 1999]. But in fact, it would be widespread among phytoplankton groups, even in species with no detectable DMSP, and could therefore act as a significant supplementary source of DMS in oceanic waters [Spiese et al., 2009].

1.2.1.6. Atmospheric oxidation of DMS

Many features of the atmospheric oxidation of DMS are very complex and still poorly understood [von Glasow and Crutzen, 2004]. It is well-known that 95% of the oxidation occurs in the gas phase, and occurs very rapidly, given the very short lifetime of atmospheric DMS (between 20 and 28 h). DMS oxidation is principally promoted by hydroxyl radicals (OH) and by nitrate radicals (NO_3) [Levy, 1971; Koga and Tanaka, 1993]. OH radicals (formed by reaction of water vapor with O (^1D) – a product of ozone photolysis) concentration usually peaks at noon

and is negligible during nighttime, due to the high reactivity of OH. NO_3 radicals (formed by reaction of ozone and NO_2) rapidly photolyze during the day and are thus only active at night. In unpolluted remote oceanic areas, OH radicals are believed to be the major oxidants, leading to a pronounced diel cycle of DMS concentrations [Bandy et al., 1996]. DMS concentration builds up overnight in the absence of OH radicals and declines continuously during daytime. In polluted oceanic areas during the night, NO_3 radicals can become the dominant oxidizers [Wine et al., 1984]. This is also observed at high latitudes where sunlight is strongly limited during the winter [Monks, 2005]. Other free radicals, such as ozone and halogen radicals produced from sea salts aerosols (CLO, IO, and bromine oxide BrO), could also locally be important oxidizers [Monks, 2005; Seinfeld and Pandis, 2006]. The removal of DMS by BrO could for example be significant in the tropical Atlantic and in the Arctic and Southern Oceans [Monks, 2005; Read et al., 2008].

The end-products of DMS oxidation are function of the oxidation pathways followed by the various free radicals.Two major oxidation pathways have been identified [Hynes et al., 1986]. In the addition pathway (direct O-addition), DMS reacts with OH or BrO to form DMSO, which may further transform in $DMSO_2$, methylsulfinic acid (MSIA) and MSA when no clouds are present. In the abstraction pathway (H-atom abstraction), DMS reacts with OH, NO_3 or Cl radicals to form SO_2 and H_2SO_4 via several intermediate reactions. One should note that MSIA may also lead to the production of SO_2 and therefore join the abstraction pathway. DMS oxidation by OH radicals is strongly influenced by atmospheric temperature: the abstraction pathway dominates at high temperatures, and the addition pathway speeds up at low temperatures. Only H_2SO_4 leads to new aerosol particles formation, thereby increasing the amount of CCN and increasing the albedo. Other

end and intermediate products condense on and enlarge existing particles, thereby increasing the size and hygroscopicity of CCN and decreasing the albedo [von Glasow and Crutzen, 2004].

1.2.2. The cycling of DMS in sea ice

Sea ice represents a very distinct biome governed by its own biogeochemical dynamics. Hence, the processes presented in the previous section need to be reevaluated before they can be integrated in models of sea ice DMS production and emissions. To my knowledge, there is no comprehensive review of the processes controlling the production and transport of DMS, DMSP and DMSO in the sea ice biome (the review of Levasseur [2013] is centered on the Arctic only). Hence, this section is drawn from a compilation of information found in the relatively limited sea ice DMS literature.

1.2.2.1. Defining the sea ice biome

A prerequisite to this section is to define and geographically delimitate the sea ice biome. Sea ice is defined as any form of ice found within the ocean that has originated from the freezing of seawater [WMO, 1985]. Sea ice can be classified as either landfast (or simply fast) ice or pack ice (also known as drift ice). Landfast ice is defined by Weaver [1951] as the coastal ice which, in stationary sheets, builds seaward from the shore of landmasses by being more or less attached to the shore, or by being otherwise confined. Pack ice is formed offshore in the open ocean and remains mobile throughout the year. Pack ice and landfast ice can be further classified based on their age and thickness [WMO, 1985]. Non-consolidated ice that just formed and which is thinner than 10 cm is classified as new ice. When the ice thickness reaches 10 cm, the ice is named young ice, and when it reaches 30 cm, first-year ice. First-year ice can further be categorized in

thin (30 to 70 cm), medium (70 to 120 cm), and thick (> 120 cm) ice. First-year ice that survives one summer melt season is then named multi-year ice.

Sea ice growth usually occurs through several formation stages which differ based on ice growth conditions (agitated or calm) [Petrich and Eicken, 2010]. In both calm and agitated conditions, the first stage of new ice is the formation of frazil ice, fine spicules or orbicular crystals floating freely in the ocean. In agitated conditions (ice growth in a wave field), frazil crystals coagulate in grease ice and consolidate into pancakes, a nearly circular piece of ice with raised rims. In calm conditions (ice growth through quiescent bottom freezing, such as in small leads for example), frazil crystals aggregate into a thin elastic crust called nilas and consolidate into young ice (grey ice 10 to 15 cm, and grey-white ice 15 to 30 cm).

Sea ice is primarily found in the oceanic Arctic and Antarctic regions. If both polar regions share common features, there are also fundamental differences between their oceanic and sea ice properties. Considering common features, both polar regions undergo strong seasonal changes, ranging from 24 of light and above freezing temperatures in the summer to complete darkness and subfreezing temperatures in the winter. These changes not only affect the ocean properties by i.e. the growth and melt of seasonal sea ice but also strongly affect the polar food web (see sections 1.2.2.3 and 1.2.2.4). The most striking oceanic difference between the Arctic and Antarctic is found in their respective geography. The Arctic is a closed basin surrounded by continental land masses with only one deep passage through which water can be readily exchanged with the other oceans, whereas the Antarctic or Southern Ocean is directly connected to the Pacific, Atlantic, and Indian oceans [Dieckmann and Hellmer, 2003]. Shallow continental shelves cover about one-third of the Arctic region whereas the Antarctic is

characterized by either narrow or very deep continental shelves [Wadhams, 2000]. Terrestrial inputs represent another strong contrast [Anderson, 2001]. In the Arctic, terrestrial inputs are an important feature through significant river discharge, whereas in the Antarctic, river discharge is a minor process. In the Antarctic, sediments transport is exclusively made by ice, and freshwater inputs solely provided by precipitation or melt. There are also 5 major differences in the thermodynamic and dynamic conditions of ice growth between the two polar regions [Thomas and Dieckmann, 2010]. Sea ice develops over a larger latitudinal range in the Arctic (44°N to 90°N) than in the Antarctic (55°S to 75°S)). The snow cover, playing the role of a strong insulator, is generally thicker in Antarctica. Sea ice is generally older in the Arctic since sea ice stays longer in the Arctic basin and thickens through accumulation of pressure ridges. The ocean heat flux is typically stronger in the Antarctic due to a lesser stratification of the ocean due to the absence of riverine influence. Sea ice drift is mainly converging in the Arctic and diverging in the Antarctic due to the topography of both regions [Haas, 2003]

All these fundamental dissimilarities account for the critical differences observed in the ecological and physical properties and dynamics of sea ice in these regions (see section 1.2.2.3) [Haas, 2003]. Hence, one could expect the cycling of DMS in sea ice to differ between the two polar regions, and maybe strongly so. To my knowledge, this important regional contrast has never been tackled. In the following sections and in the body of the thesis, a clear distinction between the two regions will always be made when observations and biogeochemical processes will be discussed.

1.2.2.2. DMS,P,O concentrations in sea ice

This section synthesizes the observations of DMS,P,O concentrations in sea ice. DMS,P,O can be observed in various oceanic polar habitats as described by Levasseur [2013]. These include: open water or partially ice-covered water, under-ice water, polynya, leads, melt ponds, snow, and the various sea ice stages described in section 1.2.2.1. Here, the focus will be on the sea ice biome itself, under-ice water, snow, and melt ponds. Under-ice water, strongly influenced by sea ice inputs, has properties different than surface waters and needs to be considered independently. Melt ponds are ponds of water that form on the surface of sea ice when surface melt occurs [Eicken et al., 2002]. Melt ponds are a significant feature in the Arctic and an insignificant feature in the Antarctic, due to a colder and dryer atmosphere in the Antarctic that cools the ice surface even in summer [Andreas and Ackley, 1981]. The reader is referred to the synthesis of Levasseur [2013] for concentrations in Arctic oceanic waters.

As mentioned in section 1.1.4, observations of sea ice DMS,P,O concentrations are relatively scarce (a summary of available data is presented in Table 1.1). Furthermore, most of the available measurements are limited to total DMSP ($DMSP_p$+$DMSP_d$) or total DMSP+DMS concentrations. Indeed, until recently, accurate separate measurements of DMS, DMSP and DMSO were not possible. Previous analytical methods typically involved the melting of samples, leading to unavoidable salinity stress on sympagic algal cells. Such salinity stress, known to trigger strong physiological responses of the cells such as cell lysis and active exudation of intracellular compounds, were shown to lead to artificial conversion of dimethylated sulfur compounds (i.e. enzymatic cleavage of DMSP in DMS) [Brabant et al., 2011; Stefels et al., 2012]. DMSP is particularly vulnerable

to conversion given the presence of DMSP-lyase enzymes in the cell or in the phycosphere (see section 1.2.1.3).

In the framework of this thesis (see research paper in Appendix B, Stefels et al. [2012]), two new methods to accurately measure DMS,P,O concentrations in sea ice samples were developed and tested. In the first method, called the dry-crushing method, DMS is first extracted from sea ice by crushing a small ice cuboid in a precooled gas-tight stainless-steel container by repeated impacts with stainless-steel marbles. The released gas phase is analysed with a traditional purge and trap-gas chromatograph system. DMSP and DMSO in pulverized ice are then converted to DMS following hydrolysis with a strong base and conversion by a reductase enzyme respectively [Brabant et al., 2011]. The dry-crushing method was shown to accurately reproduce DMS,P,O concentration profiles in sea ice, even in ice cores stored for a long period of time (up to several months). A current limitation of the dry-crushing method is that the particulate and dissolved phases of DMSP and DMSO cannot be discriminated. Hence, only the total DMSP and DMSO concentrations can be evaluated. This has also long remained challenging in seawater samples, in which some classical filtration protocols were observed to trigger the artificial release of DMSP from cells [Kiene and Slezak, 2006]. In the second method presented by Stefels et al. [2012] (see Appendix B), the conversion of dimethylated sulfur compounds is monitored during melting of the samples by adding differently deuterated isotopes of DMS and DMSP (D3-DMS, D6-DMS, D6-DMSP). This promising method allows to reconstruct the dissolved and particulate fractions of all dimethylated sulfur compounds, and is also suitable for the determination of process rates within the DMS cycle. However, since the method requires the samples to be analysed immediately with a mass

spectrometer, it might not always be suitable for field measurements in the remote polar regions.

To my knowledge, there are only two studies that specifically targeted DMS compounds in Arctic sea ice [Levasseur et al., 1994; Lee et al., 2001], and a few additional others that reported occasional opportunistic measurements [Uzuka 2003; Levasseur, 2013]. In the most comprehensive study to date, Levasseur et al. [1994] presented vertical profiles of $DMSP_p$ concentrations in spring first-year pack ice from the Resolute Passage and showed concentrations ranging from 0 to an astonishing 5995 nmolS.L^{-1} (the initial value presented in the study of Levasseur et al. [1994] was 12000 nmolS.L^{-1}, but it has been since corrected to 5995 nmolS.L^{-1} [Levasseur, pers. comm.]). Uzuka [2003] found even higher concentrations of total DMSP (up to 16000 nmolS.L^{-1}) in spring first-year landfast ice in the Chukchi Sea near the coast of Barrow, Alaska. In both studies, the vertical distribution of the concentrations showed a small peak in surface ice, no DMSP or lower concentrations in interior ice, and highest concentrations in bottom ice. Uzuka [2003] also observed that the concentrations were increasing from close to detection limit in March, to maximum concentrations in the end of April, and were then decreasing again to detection limit in May. Lee et al. [2001] observed the same evolution in pack ice from the North Water, with maximum concentrations found around the April-May transition ($DMSP_p$ as high as 987 nmolS.L^{-1}), and lower concentrations in June. Finally, Gali and Simó [2010] found total DMSP concentrations reaching 90 nmolS.L^{-1} in unidentified bottom ice in the Greenland Sea in summer. High total DMSP concentrations (729 nmolS.L^{-1}) were also surprisingly observed in July in 200 cm thick multiyear ice at the North Pole during a crossing of the Arctic Ocean [Levasseur, 2013]. To date, there is clearly

insufficient data for a comparison between different ice stages and ice categories (section 1.2.2.1), and no information on winter and early spring concentrations. Very few sea ice DMS data are available. High concentrations (29 nmolS.L-1) were measured in brine inclusions at the bottom of multiyear ice in the central Arctic, and in the bottom ice (up to 2000 nmolS.L^{-1}) of the Canadian Archipelago at the end of the algal bloom [Levasseur, 2013]. Measurements of $DMSO_p$ and $DMSO_d$ in sea ice samples are limited to one sampling site, the North Water polynya. Bouillon et al. [2002] reported $DMSO_d$ concentrations between 20 and 116 nmolS.L^{-1} in the bottom 2 cm of the ice, and Lee et al. [2001] $DMSO_p$ concentrations between 1.3 and 102 nmolS.L^{-1}.

In the Antarctic, regardless of the region or season, DMS and DMSP concentrations reported in the literature are high (Table 1.1). Curran et al. [1998] reported total DMSP concentrations between 0 and 193 nmolS.L^{-1} in winter first-year pack ice in the Dumont D'Urville Sea. Many of the available studies focused however on the spring-summer transition showing a temporal evolution similar to the one described by Uzuka [2003], with an increase of concentrations towards the end of the spring and a decrease during the summer. Kirst et al. [1991] observed total DMSP concentrations between 4 and 1664 nmolS.L^{-1} in spring first-year pack ice in the Weddell Sea. Also in spring first-year pack ice, Turner et al. [1995] reported total DMSP between 17 and 546 nmolS.L^{-1} in the Bellingshausen Sea, Curran et al. [1998] reported concentrations between 8 and 725 nmolS.L^{-1} in Prydz Bay, and DiTullio et al. [1998] found concentrations between 5 and 980 nmolS.L^{-1} in the Ross Sea. The same authors reported concentrations in landfast ice in the same area between 81 and 219 nmolS.L^{-1},while Gambaro et al. [2004] found concentrations between 4 and 450 nmolS.L^{-1} in the Gerlache inlet landfast ice in

summer. Unlike Arctic sea ice, the vertical distribution of total DMSP concentrations (as well as DMS concentrations) does not follow a characteristic pattern. Maximum concentrations are sometimes found in surface ice [Gambaro et al., 2004], sometimes in interior ice [Trevena et al., 2003], and sometimes in bottom ice [Tison et al., 2010]. A comparison between thin young ice and thicker first-year ice also suggested that concentrations could be higher in the young ice [Trevena and Jones, 2006]. Regarding multi-year ice, Zemmelink et al. [2008a] reported concentrations of total DMSP as high as 11352 nmolS.L^{-1} in the surface layer of a multi-year ice floe in the Weddell Sea in early summer. Only three sea ice DMS measurements have been conducted in the Antarctic. Concentrations were found to reach 75 nmolS.L^{-1} (0.3 to 75 nmolS.L^{-1}) in spring pack/fast ice offshore Prydz Bay [Trevena and Jones, 2006], and 1430 nmolS.L^{-1} (0.5 to 1430 nmolS.L^{-1}) in decaying summer pack ice of the Weddell Sea [Tison et al., 2010]. In sea ice brines from the Ross Sea and Amundsen Sea in the middle of summer, Asher et al. [2011] observed a mean DMS concentration of 33.2 nmolS.L^{-1}, with a maximum of 277 nmolS.L^{-1}. The same authors were also the first and only one so far to report simultaneously DMS, total DMSP (mean = 305 nmolS.L^{-1}, maximum = 2990 nmolS.L^{-1}) and total DMSO (mean = 138 nmolS.L^{-1}, maximum = 471 nmolS.L^{-1}) concentrations. Concentrations of the three sulfur species were generally highest in brines collected near surface ice, and total DMSP and DMSO distribution explained much (66%) of the vertical variability of DMS.

To put these observations in perspective, the mean and median $DMSP_p$ concentration in oceanic waters have been estimated to 43 and 22 nmolS.L^{-1} respectively [Kettle et al., 1999]. Very high concentrations in phytoplankton blooms often reach 1000 nmolS.L^{-1} [van Duyl et al., 1998]. Sea ice is identified as a biome

favorable to substantial DMS, DMSP and DMSO production (from one to two orders of magnitude higher than average seawater concentrations). Strong contrasts in the vertical distribution of the concentrations are observed between the Arctic and the Antarctic, and large spatial, seasonal but also inter-annual variability is found in both polar regions. One should note that comparisons between sea ice data from different studies should however always be considered with caution since the same vertical sampling resolution is not always used (see Chapter 4 of this thesis, Table 4.3).

In both the Arctic and Antarctic, there is a clear seasonal trend in under-ice water DMS and DMSP concentrations. Below winter and spring ice, $DMSP_p$ concentrations are very small (around oceanic background levels, 0.3 $nmolS.L^{-1}$) [Levasseur et al., 1994; Trevena and Jones, 2006]. Below late spring and summer decaying ice, concentrations increase considerably in both polar regions to reach values as high as 130 $nmolS.L^{-1}$ for total DMSP [Usuka, 2003; Tison et al., 2010]. Nomura et al. [2012] observed an increase in under-ice water DMS from 4.4 to 9.5 $nmolS.L^{-1}$ in less than three weeks during summer in Lützow-Holm Bay in Antarctica. Under-ice water concentrations are however sometimes small compared to adjacent surface water concentrations, as shown by Trevena et al. [2006]. It is also worth noting that concentrations are usually higher below thin ice than below thick ice [Leck and Persson, 1996].

Table 1.1: Summary of available sea ice DMS, DMSP and DMSO data in the literature. The horizontal dashed-line separates Arctic and Antarctic data.

Location	Ice Type[a]	Season[b]	DMS,P,O[c]	DMS[d] (nM)	DMSP[d] (nM)	DMSO[d] (nM)	Chla[d] ($\mu g.L^{-1}$)	Reference
			sampling resolution (m)					
Amundsen Gulf	P	Fa/Wi	0.05 (F.C.)	**3.1** (<0.3-95.3)	**31.4** (<0.3-1065.1)	**7.9** (1.5-124.7)	**2.95** (nd-36.92)	This study
Amundsen Gulf	P+F	Sp/Su	0.05 (F.C.)	**13.6** (0.1-769)	**29.8** (1.2-1636.1)	**112.6** (1.9-5427.9)	**22.5** (0.02-655.1)	This study
Resolute Passage	P	Sp	0.02/0.05 (F.C.)	NA	**325**[e] (nd-12000)	NA	**278.5** (1.0-2187.2)	Levasseur et al. [1994]
Baffin Bay	P+F	Sp/Su	0.02 (B.S.)	NA	**126**[e](8.6-987)	**13.7**[f] (1.3-102)	**364.3** (4.01-2000)	Lee et al. [2001]
Ross Sea	P	Sp/Su	0.05/0.20 (B.S.)	NA	**206.5** (4.4-980.0)	NA	**54.4** (1.2-243.3)	DiTullio et al. [1998]
Ross Sea	F	Sp	0.05/0.20 (B.S.)	NA	**150.0** (80.9-218.8)	NA	**103.7** (38.7-138.5)	DiTullio et al. [1998]
Prydz Bay	F	Sp/Su	0.10(F.C.)	NA	**112** (9-1478)	NA	**5.6** (0.03-84.8)	Trevena et al. [2003]
Gerlache inlet	F	Su	0.10 (F.C.)	NA	**nd** (4.4-450)	NA	(nd-160)	Gambaro et al. [2004]
Offshore Prydz Bay	P	Sp	0.10 (F.C.)	NA	**107** (6-787)	NA	**4.9** (0.1-41.5)	Curran and Jones [2000]
Prydz Bay	P	Sp	0.10/0.20 (F.C.)	NA	**144** (8-725)	NA	NA	Trevena et al. [2000]
Bellingshausen Sea	P	Sp/Su	0.15/0.20 (F.C.)	NA	**200** (17-546)	NA	**4.6** (0.2-24)	Turner et al. [1995]
Weddell Sea	P	Sp	0.10(F.C.)	NA	**408.9** (4.1-1663.8)	NA	**24.8** (3.4-155.7)	Kirst et al. [1991]
Dumont D'Urville Sea	P	Wi	0.10/0.20 (F.C.)	NA	**40** (nd-193)	NA	NA	Curran et al. [1998]
McMurdo Sound	F	Wi/Sp	0.05 (F.C.)	**7.5** (<0.3-377)	**76** (<0.3-3865)	NA	**28.4** (0.00-1440.7)	This study
McMurdo Sound	F	Sp/Su	0.05 (F.C.)	**12** (<0.3-369)	**87** (<0.3-683)	NA	**7.6** (0.08-285.4)	This study
Indian sector of SO	P+F	Sp	0.10 (F.C.)	**12** (<0.3-75)	**185**[g] (45-796)	NA	NA	Trevena and Jones [2006]
Western Weddell Sea	P	Su	0.05 (F.C.)	**58** (0.5-1430)	**171** (5-2627)	**33** (6-289)	**5.3** (0.1-28.4)	Tison et al. [2010]
Dumont D'urville Sea	P	Wi/Sp	0.05 (F.C.)	**48.3** (nd-1422.4)	**226.3** (12.2-3313.7)	**78** (6.6-1202.1)	**5.19** (0.02-34.25)	This study

[a]P, pack ice; F, fast ice

[b]Fa, fall; Wi, winter; Sp, spring; Su, summer

[c]F.C., full core; B.S., bottom sample

[d]**Mean** (range); NA, non available; nd, not determined

[e]$DMSP_p$ only

[f]$DMSO_p$ only

[g]Calculated for ice categories with ice thickness <1.20 m, number of cores weighted average

In melt ponds in both polar regions, DMS,P,O concentrations are usually low compared to sea ice concentrations. In the Antarctic, Nomura et al. [2012] reported DMS concentrations always below 3.7 nmolS.L^{-1}, which is very close to the values measured in melt ponds formed in the central Arctic Ocean and Greenland Sea (maximum value of 2.2 nmolS.L^{-1}) [Sharma et al., 1999b; Levasseur, 2013]. Similarly, Trevena et al. [2006] detected no $DMSP_p$ in melt ponds near Prydz Bay, Antarctica. On the other hand, very high DMS (> 250 nmolS.L^{-1}), total DMSP (> 2500 nmolS.L^{-1}) and DMSO (> 400 nmolS.L^{-1}), and $DMSP_d$ (> 125 nmolS.L^{-1}) concentrations were observed in melt ponds in the Ross Sea and Amundsen Area by Asher et al. [2011]. In that study, melt ponds were actually the most productive sea ice related medium.

To my knowledge, particulate DMSP was never detected in the snow layers covering sea ice. However, associated and derived sulfur species have been found in both hemispheres [Gali and Simó, 2010; Larose et al., 2010]. For instance, Gali and Simó [2010] measured total DMSO concentrations ranging between 7.9 and 12.2 nmolS.L^{-1} in snow in the Greenland Sea and Arctic Ocean. Since total DMSP was not detected in the same samples, the authors suggested that this DMSO had an atmospheric origin. In addition, surface layers of Antarctic sea ice cores showing high concentrations of DMS, DMSP, and DMSO could correspond in fact to refrozen snow layers or slush layers [Zemmelink et al., 2008a; Asher et al., 2011; Nomura et al., 2012].

1.2.2.3. Sympagic communities

Algae in the polar regions flourish in sea ice, where they are called ice-algae (forming sympagic communities). The development of sympagic communities is strongly related to sea ice growth processes. The formation of new

ice through frazil crystals accumulation is the first mechanism of incorporation of organisms in sea ice. This mechanism is called scavenging [Garrison and Buck, 1989]. Basically, particles and organisms are scavenged from the water column as the newly-formed frazil crystals rise to the surface. If frazil crystals formation and scavenging can occur at any time of the year in recently opened leads for example (see Chapter 2 of this thesis), the initial stage of ice formation usually begins in the late autumn when there are still algae from the autumnal bloom in the water.

When pancakes fuse together or nilas reach a given thickness, a continuous and stable ice sheet is formed and the ice further develops vertically, forming long elongated crystals called columnar crystals. During sea ice growth, most of the impurities (gases, salts, and organisms) are expelled from the pure ice matrix in the under-ice water at the ice-ocean interface. However, a small fraction (~ 10%) of these impurities remains trapped in the ice matrix under the form of bubbles or brine inclusions, making the ice a porous medium [Eicken, 2003]. During winter and early spring, when cold conditions and sea ice growth prevail, these brine inclusions are usually very cold (sometimes below -20°C) and very salty (sometimes over 200 psu) and contain most of the sea ice microbial food web. When the sea ice sheet thickens, the sympagic algae contained in the brine inclusions become progressively isolated from the ice-ocean interface, forming internal communities.

At the interface between columnar crystals (forming the so-called columnar ice) and seawater, a skeletal layer develops [Eicken, 2003]. This lamellar ice-ocean interface, relatively porous, acts as a substrate for algae. Algae developing in this layer at any time of the year form the bottom communities. Under specific conditions (see Chapter 2 of this thesis) (e.g. a lens of fresh water circulating under

coastal sea ice, sea ice under the influence of ice shelf waters), a platelet ice layer develops at the ice-ocean interface through double diffusion (salts and heat) processes [Kipfstuhl, 1991]. This platelet layer is a semi-consolidated layer ranging from a few centimetres to several meters in thickness. Highly porous, it also acts as a substrate for algae.

Following the formation of new ice, snow starts to accumulate through precipitation or wind blowing at the surface of the ice. When this snow cover is heavy enough to depress the sea ice surface below the ocean level, a process called flooding occurs. Seawater containing nutrients and algae infiltrates the snow, forming a slush layer (mix of melting snow, seawater and ice). This process leads to the formation of a surface community. Flooding can also occur during rafting (mechanical deformation of the ice sheet whereby one ice floe overrides another) [Lange et al., 1989], or at the ice edge.

When intense surface melt occurs (primarily in the Arctic, see section 1.2.2.2), melt ponds form at the surface of the ice. The ecology of melt ponds is still poorly documented. However, several studies observed significant melt pond communities, fuelled by seawater infiltration [Gradinger et al., 2005]. Sympagic communities can also survive for many years in multi-year ice, where primary production is usually characterized by short bursts followed by a long season of decomposition and remineralisation [Lizotte, 2003].

Rafting, ridging (mechanical deformation of the ice sheet whereby ice floes are stacked together into ridges [Hopkins, 1994]), ice break-up and deformation can all vertically and horizontally redistribute sympagic communities [Lizotte, 2003]. Also, when sea ice temperature is warm enough (usually > -5°C), brine inclusions become interconnected and form larger brine tubes or brine channels

[Golden et al., 1998], making the ice permeable to fluid transport and increasing the exchanges with the under-ice water. This has a strong influence on the vertical distribution of sympagic communities and solutes (see sections 1.2.2.5).

Considering ice types and regional variability, several important observations can be made. As landfast ice usually forms in more stable surface conditions than pack ice, the frazil ice layer and scavenging mechanism is usually less important in that ice type. On the other hand, since platelet ice formation typically requires low salinity water inputs from the continent (e.g. ice shelf water), platelet communities mainly develop in landfast ice. Large and numerous ice shelves make platelet ice a common feature in the Antarctic, whereas platelet ice is only sporadically found in the Arctic [Gow et al., 1998]. Similarly, due to large differences in snow accumulation, flooding is considered as important in the Antarctic and negligible in the Arctic.

Microalgal biomass in sea ice can cover up to six orders of magnitude, from low values typical of oceanic waters to the highest values recorded for any aquatic environment [Lizotte, 2003]. Using chl *a* and primary production data from the Arctic and Antarctic sea ice literature, Arrigo [2003] made the following observations:

-Antarctic sea ice supports higher algal biomass than Arctic sea ice. This difference would mainly be due to the contribution of the highly productive platelet ice communities. Removing platelet ice brings the estimates to comparable values.

-Amongst the different sympagic communities, platelet communities are by far the most productive, with chl *a* concentrations reaching 6500 $\mu g.L^{-1}$ [Arrigo et al., 1995].

-Landfast ice in both polar regions accumulate more algal biomass than pack ice.

-Bottom ice communities in the Antarctic are usually more productive than surface communities, which are usually more productive than internal communities.

These observations are understandable when looking at the nutrients and light available to the communities. Surface communities benefit from optimal light conditions but low nutrient supply. Nutrient replenishment for these communities can however be provided via flooding [Thomas et al., 1998]. The internal communities survive in extreme conditions of low temperature, high salinity, and low nutrient supply, until connectivity of brine inclusions is restored. Although they receive very little light, bottom communities benefit from stable temperature and salinity conditions, and higher nutrient supply from under-ice water. Furthermore, platelet ice due to its high porosity offers more surface for algal attachment than any other ice texture.

Regarding algal groups and species, sympagic communities resulting from passive incorporation (e.g. scavenging and flooding) initially have the same species composition as nearby seawater communities. In older ice, lower diversity suggests that only a few species are able to adapt to and survive in the sea ice biome [Gleitz et al., 1998]. In permeable ice (interconnected brine inclusions), species might actively or passively colonize internal ice layers. Horner [1992] and Lizotte [2003] described the major groups and species found in Arctic and Antarctic sea ice. On the whole, sea ice communities are typically dominated by sea ice diatoms. However, a major difference is observed between the two polar regions. If flagellates are commonly found in both Arctic and Antarctic sea ice, dinoflagellates and haptophytes, commonly found in the Antarctic, are very scarce in the Arctic.

General trends in the vertical variability of sea ice $DMSP_p$ concentrations are usually well explained by the biomass distribution. This is clearly seen by plotting $DMSP_p$ and chl *a* with respect to depth. $DMSP_p$ profiles generally mimick chl *a* profiles with major $DMSP_p$ peaks matching chl *a* maxima [Trevena et al., 2003; Gambaro et al., 2004]. However, the relationship is sometimes weaker, and $DMSP_p$ and chl *a* maxima are observed at different depths [Levasseur et al., 1994; Tison et al., 2010]. This is particularly true for internal and surface ice concentrations, whereas bottom ice concentrations generally match pretty well. This mismatch between chl *a* and $DMSP_p$ concentrations could be explained by differences in communities composition and variability in environmental parameters (e.g. light, nutrients, temperature, and salinity) as observed in oceanic waters (see section 1.2.1.1). Also, Trevena et al. [2003] suggested that the mismatch could originate from a difference in the timing of degradation of $DMSP_p$ and chl *a*.

DMSP-to-chl *a* ratios have been reported for a few sympagic communities. On one hand, sea ice haptophytes and dinoflagellates show equivalent or higher ratios than their pelagic counterparts. For instance, Trevena et al. [2000;2003] observed ratios as high as 3200 $nmol.\mu g^{-1}$. On the other hand, diatoms dominated communities seem to have comparable or lower ratios than their pelagic counterparts. For example, Gambaro et al. [2004] reported ratios between 1.5 and 7.6 $nmol.\mu g^{-1}$ in Antarctic sea ice, and Bouillon et al. [2002] ratios between 0.02 and 14.8 $nmol.\mu g^{-1}$ in Arctic sea ice. Trevena et al. [2003] also observed higher (> 500 $nmol.\mu g^{-1}$) ratios in internal communities than in bottom and surface communities (< 500 $nmol.\mu g^{-1}$), and attributed this difference to an increase of

$DMSP_p$ production by the internal communities as a physiological response to the extreme and changing environmental conditions of interior ice.

Using DMSP-to-chl *a* ratios to compare different sympagic communities can be misleading since algae adjust their photosynthetic pigment content in response to light intensity [Gosselin et al., 1990], which vary strongly with depth in sea ice [Lizotte and Sullivan, 1991]. Another way to estimate cytosolic DMSP levels, is to divide the $DMSP_p$ concentration by the corresponding total algal concentration (number of cells) [Levasseur et al., 1994]. If the algal community is mono specific, the typical cytosolic DMSP level of a given species/group in given environmental conditions can be determined. In Arctic sea ice, Levasseur et al. [1994] reported $DMSP_p$ quotas of cells ranging from 0.001 to 1.17 $pg.cell^{-1}$ for a pennate diatom dominated assemblage. These quotas are significantly lower than the maximum value reported for pennate diatoms in culture studies [Keller et al., 1989]. In Antarctic sea ice, DiTullio et al. [1998] and Kirst et al. [1991] found quotas of about 6 $pg.cell^{-1}$ and 7.9 $pg.cell^{-1}$ for diatoms and haptophytes communities respectively, which are this time higher than the maximum values reported by Keller et al. [1989]. Finally, several authors tried to correlate $DMSP_p$ concentrations with specific photosynthetic pigments. For instance, Trevena et al. [2000] observed good correlations between $DMSP_p$ and 19'-hexanoyloxyfucoxanthin (HEX), peridin (PER), and fucoxanthin (FUC), pigments characteristic of the algal groups haptophytes, dinoflagellates, and diatoms respectively. Based on this, the authors suggested that all the three groups could be associated with $DMSP_p$ production in sea ice. All these observations lead to the conclusion that haptophytes and dinoflagellates are high $DMSP_p$ producers due to high cytosolic levels, and diatoms are high $DMSP_p$ producers due to their high biomass.

1.2.2.4. Influence of sea ice environmental parameters on DMSP synthesis, release, and degradation

In this section, the main findings and hypotheses on the influence of sea ice environmental parameters on DMSP synthesis, release, and degradation are summarized. This is done assuming the physiological functions of DMSP are the same as those suggested in oceanic waters (1.2.1.1).

In sea ice, important vertical and temporal variability in salinity, together with subfreezing and variable temperatures, are observed. For example, brine salinity can range from hypersaline in the winter (over 100) to hyposaline in early summer (under 5), and temperatures can switch from < -30°C in winter surface ice to the freezing point of seawater at the ice-ocean interface. High salinities and low temperatures have been suggested to be responsible for the high cytosolic levels of DMSP found in sympagic algae and pelagic algae from polar regions [Matrai and Vernet, 1997]. In Antarctic sea ice, Trevena et al. [2003] observed a strong positive correlation between bulk ice salinity and $DMSP_p$, but not between salinity and chl *a*. Similarly, Delille et al. [2007] observed a drastic increase in DMS production in brine channels, inversely related to a decrease in brine salinity, and suggested a release of $DMSP_p$ by healthy cells in response to rapidly decreasing osmotic conditions. This would also support active exudation in sympagic algae. As mentioned by Delille et al. [2007], sympagic algae also experience a strong shift in salinity upon release in the under-ice water following brine drainage or melting, that could lead to active exudation of $DMSP_p$ and cleavage to DMS.

Light and nutrients are both recognized as strong controlling factors of algal growth. In the polar regions, light is a key parameter since it reduces the algal growth season to a few months. Additionally, strong vertical gradients in light

intensity and nutrients are observed in sea ice [Lizotte, 2003] (see section 1.2.2.3). In Arctic sea ice, Levasseur et al. [1994] suggested a light control of the $DMSP_p$ quotas observed, based only on a lack of correlation with other potential controlling factors. Recently, some authors (Galindo and Levasseur, personal communication) suggested that the high DMS and DMSP concentrations observed along the ice edge could result from a physiological response of sympagic algae and under-ice algae to the increase in light intensity resulting from ice break-up, following the antioxidant hypothesis of Sunda et al. [2002]. $DMSP_p$ is generally not correlated with any nutrient in sea ice [Levasseur et al., 1994; Trevena et al., 2000; Trevena et al., 2003]. Curran et al. [1998] did observe significant correlations with nitrates (both positive and negative) but could not verify the hypothesis of glycine betaine replacement in osmoregulation [Challenger, 1951].

Sea ice is known to accumulate iron during the winter and spring (iron concentration would be 10 to 100 times higher in sea ice than in under-ice water), and to deliver up to 70% of the daily iron supply to oceanic waters in the polar regions upon melting. According to budget estimates in East-Antarctica [Lannuzel et al., 2007], iron in sea ice would mainly derived from incorporation of under-ice water particles rather than from atmospheric inputs from the continent. In summer, iron release from sea ice would drive the phytoplankton blooms observed at the ice edge and could therefore explain the high $DMSP_p$ concentrations measured in these regions [Sedwick and DiTullio, 1997].

Delille et al. [2007], in a concurrent study of DMS and CO_2/O_2 dynamics in brine channels in the coastal area of Adelié Land, Antarctica, observed a net increase of the DMS concentration following a drastic CO_2 drawdown and O_2 increase linked to the sea ice bloom development. The authors suggested that this

observation could support the antioxidant role of $DMSP_p$ in sympagic algae in hyperoxic conditions.

Grazing might also be an important process in the cycling of DMS in polar waters and sea ice. Indeed, strong grazing activity has been frequently reported on under-ice communities. In the Southern Ocean, Turner et al. [1995] observed a small increase in DMS and $DMSP_p$ concentrations, and a large increase in $DMSP_d$ concentrations associated with high macrozooplankton density. Grazing should however play a small role in winter and early spring sympagic communities when small and disconnected brine inclusions limit the vertical mobility of grazers. Grazing could logically become more important with warming and widening of the brine channels later in the season, as suggested by Delille et al. [2007]. The function of $DMSP_p$ as a grazing-activated chemical defence precursor [Breckels et al., 2010] could also be significant upon melting, when the grazing pressure on freshly released sympagic algae strongly increases.

Very little is known about the degradation processes of DMS in sea ice (photo-chemical oxidation and biological consumption (BDMSC)). High light regimes at the surface of the ice in spring and summer could be favorable to the photo-chemical oxidation of DMS, but also to the production of DMSO following the antioxidant cascade as suggested by Asher et al. [2011]. There is however still no evidence for this. Furthermore, photo-chemical oxidation could be facilitated by the high levels of CDOM sometimes measured in sea ice samples. These levels could significantly increase in the near future in the Arctic, since melting of the Arctic permafrost may increase the input of terrestrial CDOM to oceanic waters [Stedmon et al., 2011]. The high bacterial abundance usually observed in Arctic and Antarctic sea ice [Krembs and Engel, 2001; Thomas et al., 2001] could be

favorable to BDMSC. Similarly to photo-chemical oxidation, there is still no evidence for this. BDMSC could be strongly depth and season dependent in sea ice given the vertical (similar to that of salinity) and seasonal (decreasing from autumn to winter, and increasing from winter to summer) variability of bacterial abundance. Degradation of DMS to DMSO (both photo-chemical and bacterial) could represent an important removal pathway in sea ice, especially when the ice is cold and impermeable and no flux to the atmosphere can occur.

DMS ventilation to the atmosphere from ice covered regions can occur through openings in the ice during all seasons (cracks, leads and polynya), and through melt ponds during summer surface melt. The DMS produced by sympagic communities can also be transferred to open water or partially ice-covered water through advection of under-ice water at the ice margin during ice melt or brine drainage, or through ice break-up [Levasseur et al., 1994]. These can all be considered as indirect fluxes from sea ice. Trevena and Jones [2012] provided some estimates of these indirect fluxes in the sea ice zone of East-Antarctica. They estimated that melting of 0.4 m of ice in October, 0.6 m of ice in November and December, and 1.0 to 1.2 m of ice in December, could result in oceanic DMS hot spots of 20 to 50 nmolS.L^{-1}, 150 to 270 nmolS.L^{-1}, and 100 nmolS.L^{-1} respectively. From October to December, these hot spots would result in strong DMS fluxes, and these fluxes would be higher in the pack ice zone (1 to 325 µmol.m^{-2}.day^{-1}), than in the fast ice zone (10 to 50 µmol.m^{-2}.day^{-1}), than at the ice edge (1.2 to 26 µmol.m^{-2}.day^{-1}). Fluxes from tidal cracks in fast ice were also estimated to be high (6 to 81 µmol.m^{-2}.day^{-1}), and slightly higher than the lead fluxes estimated by Zemmelink et al. [2005] (0.1 to 20 µmol.m^{-2}.day^{-1}) in the Weddell Sea. In contrast, fluxes from fast ice melt ponds would be low (0.5 to 7 µmol.m^{-2}.day^{-1}). It is worth

noting that all these estimates were calculated using parameterizations typically developed for oceanic waters (see section 1.2.1.4). However, these parameterizations could not be fully suitable to smaller bodies of water such as ponds and leads. Wave-breaking strongly influences the relationship between k_w and wind velocity, and is a function of wind velocity and fetch (the distance over which a wind of nearly constant direction has blown over water). Very small fetches characterize leads and melt ponds, and the influence of breaking waves on the relationship between k_w and wind velocity should be reduced. In the only study reporting direct measurements (accumulation chamber coupled to a mass spectrometer) of DMS fluxes above ice cracks and melt ponds, Nomura et al. [2012] reported much lower values (0.12 to 5.30 $\mu mol.m^{-2}.day^{-1}$ for the ice cracks, and 0.08 to 0.11 $\mu mol.m^{-2}.day^{-1}$ for the melt ponds) for comparable DMS concentrations. In the Resolute Passage (Arctic), Levasseur et al. [1994] calculated that the rapid release of DMS from sea ice during ice break-up could generate a DMS pulse of 22 $\mu mol.m^{-2}.day^{-1}$.

In recent years, there has been a growing body of evidence that gas exchange directly occurs through sea ice. This has been shown in lab experiments with tracers such as SF_6 [Loose et al., 2011a] and in field studies for various gases such as CO_2 [e.g. Geilfus et al., 2012]. Calculations and measurements of direct sea ice DMS fluxes in the Antarctic are very scarce, and inexistent in the Arctic. Trevena and Jones [2012] calculated the direct flux of DMS from pack and fast ice in East-Antarctica using the Liss and Merlivat [1986] parameterization and a DMS concentration estimated via a total DMSP:DMS conversion ratio. These fluxes are relatively high, averaging 54 $\mu mol.m^{-2}.day^{-1}$ for pack ice and 16 $\mu mol.m^{-2}.day^{-1}$ for fast ice (in which DMS concentrations were lower). This approach assumes that

the ice-atmosphere interface is analogous to the ocean-atmosphere interface. This is based on the observation that warm ice is highly porous (volume of voids range from 2 to 40% of the total ice volume) and that the voids are filled with brine and gas. As acknowledged by the authors, this approach may not be very accurate since the seawater k_w values may not describe molecular processes occurring at the ice-atmosphere interface very well. These estimates are comparable to the upper range of DMS fluxes (20 to 30 $\mu mol.m^{-2}.day^{-1}$) measured by Zemmelink et al. [2008a] over multi-year ice in the Weddell Sea using relaxed eddy accumulation. Since these fluxes were measured above a very productive slush community, one could assume that the Trevena and Jones [2012] fluxes are overestimated. In another study in the Lützow-Holm Bay, Antarctica, Nomura et al. [2012] reported direct measurements (accumulation chamber) of DMS fluxes above a slush layer. Their values are significantly lower (0.1 to 0.3 $\mu mol.m^{-2}.day^{-1}$) than the ones reported by Zemmelink et al. [2008a], despite comparable DMS concentrations. Nomura et al. [2012] developed the hypothesis that the difference could originate from the formation of superimposed ice over the slush layer. Superimposed ice, which forms when snow meltwater percolates and refreezes at depth in the snow cover or at the snow-ice interface, has been shown to considerably impede CO_2 fluxes [Nomura et al., 2010]. After removal of the superimposed ice layer in the Nomura et al. [2012] study, fluxes increased to 5.3 $\mu mol.m^{-2}.day^{-1}$, which is still much lower than the estimates of Trevena and Jones [2012] and Zemmelink et al. [2008a].

Considering particulate DMSO, low temperatures and light limitation in sea ice could favor the synthesis of DMSO by algae as a cryoprotectant and light harvester. Both hypotheses were tested by Lee et al. [2001] in the North Water

polynya. The authors observed lower $DMSO_p$-to-chl *a* ratios in sympagic communities (0.01 to 6.28 nmol.µg^{-1}) than in pelagic communities which seems to contradict the cryoprotectant hypothesis. Furthermore, they suggested that the DMSO cellular content (roughly estimated to at most a few tens to hundreds of mmol.L^{-1}) in sympagic algae were not large enough to significantly depress the freezing point of the intracellular fluid. Regarding the light harvesting function, no significant relationship was observed between $DMSO_p$-to-chl *a* ratios and irradiance or photosynthetic rates. It is worth noting however that the authors only sampled the bottom 2 cm of the ice where the temperature remains close to the freezing point of seawater. Higher $DMSO_p$-to-chl *a* ratios could be expected in other ice layers. In isotope tracers experiments with brine samples in the Antarctic, Asher et al. [2011] showed that $DMSO_p$ reduction can be a major pathway of DMS production in sea ice when $DMSO_p$ concentrations are high. The authors further suggested that this reduction could be part of a rapid redox cycling between DMS and DMSO in response to oxidative stress, following, again, the Sunda et al. [2002] hypothesis.

Asher et al. [2011] also provided the first and only available estimates of the rates of production and degradation of DMS,P,O in sea ice. They observed very high rates in brine samples (higher than in adjacent oceanic waters), indicating an intense cycling of DMS,P,O. In one experiment using their isotope tracers and mass balance calculations, they observed a net DMS production rate of 17 ± 3.5 nmol.L^{-1}.day^{-1}, and a gross DMS consumption rate (bacterial and photo-chemical) of 88 ± 20 nmol.L^{-1}.day^{-1}. This yielded a gross DMS production rate of 105 ± 24 nmol.L^{-1}.day^{-1}. 25 ± 6.9 nmol.L^{-1}.day^{-1} of DMS was produced from DMSP cleavage, and 96 ± 26 nmol.L^{-1}.day^{-1} was produced from DMSO reduction. In

another experiment, they showed that an exact mass balance could only be reached by including an important direct DMS release from algal cells (> 50 nmol.L^{-1}.day^{-1}). It was not assessed by the authors whether this release was caused by cell lysis or active exudation in response to change in environmental parameters.

1.2.2.5. Brine dynamics

When sea ice grows, most of seawater impurities (i.e. algae, gases) and major ions are rejected ahead the advancing freezing front. This is because voids in the ice crystal lattice are strongly reduced upon freezing. Yet, the rejection is never complete, and a small fraction of the impurities and salts remain trapped in the ice matrix, contributing to maintain a significant liquid fraction in the form of brine inclusions [Cox and Weeks, 1983]. Since liquid (brine) and solid (pure ice) phases have very different attributes, most sea ice properties are influenced by the amount, size and shape distribution of brine in the ice (i.e. the microstructure of sea ice). The influence of the microstructure of sea ice on sea ice permeability is probably the most remarkable [Freitag and Eicken, 2003]. When sea ice grows, brine inclusions are displaced from the warm ice-ocean interface causing freezing around the inclusions walls and concentration of the impurities and salts in the remaining liquid. In cold ice, brine inclusions are isolated from each other and the ice is considered as impermeable to fluid transport. When sea ice warms up, brine inclusion walls start to melt and the size of the inclusions considerably increases. Inclusions eventually become interconnected and form brine channels, which can further coalesce into wider brine tubes connected to the ocean and the atmosphere, making the ice permeable to fluid transport. The control exerted by permeability on the mobility (vertical distribution) and exchanges at the ocean-ice-atmosphere interface of key biogeochemical variables is highlighted in many

studies. This is the case, for example, for sympagic biomass [Krembs et al., 2000] and nutrients [Fritsen et al., 1994], for contaminants such as mercury [Chaulk et al., 2011] and for climate- active gases such as CO_2 [Geilfus et al., 2012].

Brine salinity (S_b) and brine volume fraction (defined as the fraction of brine relative to the bulk sea ice volume, $\frac{V_b}{V}$) are logically tightly linked to sea ice temperature and salinity. This link is illustrated by the following equations:

$$\frac{V_b}{V} = (1 - \frac{V_a}{V}) \frac{\rho S_i}{F_1(T) - \rho S_i F_2(T)} \quad (1.2)$$

$$S_b = \left(1 - \frac{54.11}{T}\right)^{-1} 1000 \quad (1.3)$$

where $\frac{V_a}{V}$ is the gas volume fraction, ρ is the pure ice density, F_1 and $F_2$are empirical polynomial functions reading $F_i(T) = a_i + b_i T + c_i T^2 + d_i T^3$. Cox and Weeks [1983] coefficients are typically used for T < -2°C, and Leppäranta and Manninen [1988] coefficients for T ≥ -2°C. The gas volume fraction is usually negligible compared with the brine volume fraction in cold ice [Petrich and Eicken, 2010]. However, for warmer sea ice (> -5°C), the gas volume fraction can represent a significant fraction of the total volume, usually from 0 to 2% [Tison et al., 2002; Rysgaard and Glud, 2004] although extreme values of 13% have been reported [Rysgaard and Glud, 2004]. Since S_i and T are relatively easy to measure, one can always calculate the brine volume fraction and brine salinity of a given ice sample. Golden et al. [1998], following their percolation theory, showed that brine inclusions typically become interconnected (and hence the ice becomes permeable) above a critical threshold in brine volume fraction. This threshold in well aligned columnar ice is 5%, which roughly corresponds to an ice temperature of -5°C for an ice with a salinity of 5. Permeability has a strong dependence on the ice texture, which is

currently not perfectly known. For more complicated ice textures the threshold is presumably higher [e.g. Golden et al., 2007]. For instance, the formation and incorporation of platelet crystals (elongated acicular crystals with no specific orientation) in the ice cover can strongly modify the connectivity of brine inclusions and constrain the development of large vertical brine tubes. Furthermore, sea ice formation, growth and decay processes also strongly influence the vertical distribution of solutes and organisms (e.g. scavenging of organisms by frazil crystals, see section 1.2.2.3). Hence, a good knowledge of the sea ice texture (shape, size, and orientation of the ice crystals) is required to fully understand the cycling of DMS in sea ice.

Strong exchanges of solutes (e.g. salts) with the under-ice water have been shown to occur following processes called gravity drainage (or brine convection) and flushing. Gravity drainage is the convective overturning of brine in connected brine inclusions (permeable ice) [Cox and Weeks, 1975; Notz and Worster, 2008]. Gravity drainage is governed by the ice thickness, the permeability and the brine density gradient [Wettlaufer et al., 1997, 2000]. These relationships have been approached analytically in the mushy-layer theory [Worster, 1992; Wettlaufer et al., 1997] using a porous-medium Rayleigh number. At a depth z (0 at the ice base, positive upwards), it reads:

$$Ra = \frac{\Delta z g \beta (S_b(z) - S_{OC}) \Pi \left(\frac{V_b}{V_{\min}}\right)}{\kappa \eta} \quad (1.4)$$

where g = 9.81 m.s^{-2} is the acceleration due to gravity, $\beta(S_b(z) - S_{OC})$ is the density difference between brine density at a level z and that of seawater at the ice-ocean interface, $S_b(z)$ is the salinity of brine at a depth z diagnosed from temperature (assuming thermal equilibrium), S_{OC} is the salinity of seawater, β = 0.78 kg m^{-3} ppt^{-}

[1] is the haline expansion coefficient of seawater at 0 ℃ [Fofonoff, 1985], Π ($\frac{V_b}{V_{\min}}$)is the effective sea ice permeability (m^2), and η and κ are the dynamic viscosity and thermal diffusivity of brine, respectively. Based on experimental studies, Notz and Worster [2009] suggested that for convection to occur at a given ice depth, the Rayleigh number must exceed a critical value, typically 10 (the critical value might be lower in natural ice given e.g. the loss of salts during sampling [Zhou et al., 2013]). Physically, this means that convection only occurs once buoyancy forces due to the vertical brine density gradient expressed in the numerator of *Ra* overcome dissipation (the product between dynamic viscosity and thermal diffusivity of the brine) as expressed by the denominator. In growing cold ice, gravity drainage is limited to the permeable ice layer at the interface with the ocean. In warming permeable ice, full-depth gravity drainage can develop, which results in strong exchanges of brine and solutes with the ocean. Flushing is typically triggered by summer melting [Eicken et al., 2004; Notz and Worster, 2009]. In this process, the hydraulic head created by the snow and surface ice meltwater flushes downwards the existing brine network, resulting in another important release of solutes to the under-ice water.

To date, sea ice DMS studies have essentially compared the temporal and spatial variability of the DMS,P,O concentrations to biological parameters (e.g. algal abundance, nutrients, bacterial abundance). Hence, very little is known about the influence of sea ice permeability and brine dynamics (referred in this thesis as physical or thermodynamical controls) on the cycling of DMS. In summer decaying sea ice in the Antarctic Western Weddell Sea, Tison et al. [2010] suggested that drastic temporal brine volume and brine salinity changes with seasonal warming directly impacted the migration of DMS and DMSP through the brine network. The

authors observed two stages of brine dynamics. During the first half of their study, sea ice was characterized by a regime of active brine convection. Sea ice was permeable at all depths and the brine network was unstable (a gradient in brine density was observed from the top towards the bottom of the ice). Active brine convection during this period corresponded to a vertical redistribution of DMS and DMSP concentrations. The authors also observed a strong increase in the under-ice water DMS burden simultaneous to a strong decrease in the ice DMS burden. This seemed to suggest that strong DMS release to the under-ice water occurred following gravity drainage. The release of salts during the first stage of brine dynamics contributed to stabilize the brine network, leading to the second regime. During the second half of their study, the brine network showed indeed homogeneous brine density at all depths, and hence the potential for brine convection drastically reduced. The migration of DMS and DMSP became limited to diffusion and sedimentation, and fewer changes in the concentrations profiles were observed. The study of Tison et al. [2010] clearly demonstrated the influence of brine dynamics on the cycling of DMS in warm and permeable Antarctic summer sea ice. However, we still have no information on the thermodynamical controls on the cycling of DMS during other seasonal episodes (autumn, winter, and spring), nor do we have information about thermodynamical controls in the Arctic or in other Antarctic regions, where local conditions could lead to different sea ice growth mechanisms and ice textures, and hence different brine dynamics. It is these fundamental gaps in our understanding of the DMS cycling in the marine cryosphere that provide the motivation for this thesis and direct the research objectives presented below.

1.3. Thesis objectives

The underlying focus of this thesis is the DMS cycling in sea ice. Insight gained into DMS dynamics is based largely on two major time series studies that were conducted as part of large multidisciplinary studies in the Arctic and Antarctic. Measurements were made in the Amundsen Gulf at the western terminus of the Northwest Passage in the Canadian Arctic as part of the International Circumpolar Flaw Lead System Study, IPY-CFL (2007-2008) [Barber et al., 2010], and at Cape Evans, in the McMurdo Sound, in the Antarctic, as part of the 2011-2012 Year Round Survey of Ocean Sea Ice Air Exchanges study (YROSIAE). The overarching objectives of the thesis are to:

1. Characterize the seasonal evolution of brine dynamics in natural ice, with a specific focus on gravity drainage events during the spring-summer transition. This is a crucial step if we are to understand how brine dynamics affect the vertical and seasonal distribution of DMS,P,O in sea ice and how the DMS pool is ultimately transferred to the ocean and the atmosphere.

2. Document DMS,P,O concentrations in seasonal sea ice, and show how the concentrations of the respective sulfur compounds vary within sea ice at a location, with time over the seasonal transition, and spatially between polar regions.

3. Assess the influence of biological factors (biomass and community composition), sea ice growth, and brine dynamics, on this spatial and temporal variability.

Objective 1 provides the framework necessary for a physical interpretation of DMS,P,O dynamics in sea ice, thereby linking objectives 2 and 3. Collectively the work presents the opportunity to discuss how differences in sea ice properties between the Arctic and the Antarctic can affect the DMS cycle.

1.4. Thesis outline

This thesis is comprised of three research papers, each of which makes up an individual chapter. The first paper (Chapter 2) characterizes the brine dynamics and sea ice growth processes of Arctic sea ice in the Amundsen Gulf during the IPY-CFL study in 2007-2008 from growth to melt, and uses proxies of sea ice permeability and of the intensity of brine convection to identify gravity drainage events. This paper addresses objective 1, and it has been peer-reviewed and published in *Journal of Glaciology*.

Carnat, G., Papakyriakou, T., Geilfus, N.-X., Brabant, F., Delille, B., Vancoppenolle, M., Gilson, G., Zhou, J., and Tison, J.-L. (2013). Investigations on physical and textural properties of Arctic first-year sea ice in the Amundsen Gulf, Canada, November 2007-June 2008 (IPY-CFL system study). *Journal of Glaciology*, 59 (217), 819-837, doi: 10.3189/2013JoG12J148

The second paper (Chapter 3) presents the first simultaneous measurement of DMS,P,O concentrations in Arctic sea ice, and describes the seasonal and vertical variability of the compounds from samples collected from growth to melt in the Amundsen Gulf during the IPY-CFL study in 2007-2008. Controlling factors of the concentrations are identified using ancillary biological and physical parameters, including brine dynamics and sea ice growth processes described in Chapter 2. This paper addresses objectives 2 and 3, and it is currently undergoing review by co-authors before submission to *Journal of Geophysical Research – Oceans*.

Carnat, G., Tison, J.-L., Gilson, G., Delille, B., Brabant, F., Levasseur, M., Geilfus, N.-X., and Papakyriakou, T. Temporal and vertical variability of DMS,P,O concentrations in Arctic first-year sea ice (Amundsen Gulf, Canada): evidence for photo-chemical oxidation of DMS in surface ice. In preparation for submission to *Journal of Geophysical Research – Oceans*.

The final paper (Chapter 4) reports the seasonal and vertical variability of DMS and DMSP in Antarctic fast ice during a winter-spring and a spring-summer transition from samples collected at Cape Evans, McMurdo Sound, during the YROSIAE study in 2011-2012. Trends in concentrations are compared to the seasonal evolution of the ice algal biomass and of the physical properties of the ice cover, with emphasis on platelet ice formation and brine dynamics. This paper addresses objectives 2 and 3, and it has been peer-reviewed and published in *Journal of Geophysical Research – Oceans*.

Carnat, G., Zhou, J., Papakyriakou, T., Delille, B., Goossens, T., Haskell, T., Schoemann, V., Tison, J.-L., Fripiat, F., and Rintala, J.-M. (2014) Physical and biological controls on DMS,P dynamics in ice shelf-influenced fast ice during a winter-spring and a spring-summer transition. *Journal of Geophysical Research – Oceans*, 119, doi: 10.1002/2013JC009381

In Chapter 5, the results of Chapters 2-4 are summarized, highlighting potential differences between the Arctic and Antarctic sea ice DMS cycling, and concluding remarks and recommendations for future work are presented.

Chapter 2

Investigations on physical and textural properties of Arctic first-year sea ice in the Amundsen Gulf, Canada, November 2007-June 2008 (IPY-CFL system study)

Journal of Glaciology, 59 (217), 819-837

doi: 10.3189/2013JoG12J148

Gauthier Carnat[1], Timothy Papakyriakou[1], Nicolas-Xavier Geilfus[1], Frédéric Brabant[2], Bruno Delille[3], Martin Vancoppenolle[4], Gaelle Gilson[2], Jiayun Zhou[2], and Jean-Louis Tison[2]

[1]Centre for Earth Observation Science, Department of Environment and Geography, University of Manitoba, Winnipeg, Manitoba, Canada

[2]Université Libre de Bruxelles, Laboratoire de Glaciologie, 50 Av. F.D. Roosevelt, 1050 Bruxelles, Belgium

[3]Unité d'Océanographie Chimique, Université de Liège, Liège, Belgium

[4]Laboratoire d'Océanographie et du Climat, CNRS, Paris, France

Abstract

We report sea ice temperature and bulk salinity measurements as well as textural analysis from 33 first-year drift and fast ice stations sampled between November 2007 and June 2008 in the southern Beaufort Sea-Amundsen Gulf, Canadian Arctic, during the International Polar Year Circumpolar Flaw Lead (IPY-CFL) system study. We use this significant dataset to investigate the halo-thermodynamic evolution of sea ice from growth to melt. A strong desalination phase is observed over a small time window in the spring. Using calculated proxies of sea ice permeability (brine volume fraction) and of the intensity of brine convection (Rayleigh number) we demonstrate that this phase corresponds to full-depth gravity drainage initiated by a restored connectivity of the brine network with warming in the spring. Most stations had a textural sequence typical of Arctic first-year ice, with granular ice overlying columnar ice. Unusual textural features were observed sporadically: sandwiched granular ice, platelet ice and draped platelet ice. We suggest that turbulence in leads and double diffusion in strong brine plumes following the refreeze of cracks are plausible mechanisms for the formation of these textures. As a whole, this study provides a thorough characterization of the physical environment in which sea ice DMS,P,O concentrations will evolve. It strongly defines the timing of processes important for the vertical and seasonal distribution of DMS and related compounds (e.g. restored permeability of the ice cover allowing the mobility of solutes within the brine network, incorporation of sympagic organisms via scavenging by granular ice), and for the exchanges of these compounds with the ocean and the atmosphere. Of particular interest is the timing of occurrence of the full-depth gravity drainage episodes which have the potential to release a significant fraction of the DMS pool to the under-ice water.

2.1. Introduction

Arctic sea ice, on track towards a thinner seasonal ice cover [e.g. Kwok et al., 2009], is an important component of the Earth system. Sea ice is known to influence, among others, global climate and oceanic circulation [Aagaard, 1981; Curry et al., 1995], major biogeochemical cycles [e.g. Thomas et al., 2010] and the transport and fate of contaminants [e.g. Pfirman et al., 1995]. An understanding of the roles played by Arctic sea ice in the Earth system requires a good knowledge of its physical (temperature and bulk ice salinity) and textural (size, shape and orientation of ice crystals) properties. The conventional approach is to consider the relationships between sea ice temperature and bulk salinity and the fraction volume and salinity of the brine entrapped in the ice [Cox and Weeks, 1983]. As liquid (brine) and solid (pure ice) phases have very different attributes, most sea ice properties are influenced by the amount, size and shape distribution of brine in the ice (referred to as ice microstructure). This is the case, for example, for the strength and mechanical behavior of the ice [Timco and Frederking, 1990] and shortwave radiation scattering in the ice [Perovich et al., 1998]. The influence on sea ice permeability is probably the most remarkable [Freitag and Eicken, 2003]. Above a critical threshold in brine volume fraction, brine inclusions become interconnected and the ice is considered permeable to fluid transport [Eide and Martin, 1975; Golden et al., 1998].The control exerted by permeability on the mobility and exchanges at the ocean-ice-atmosphere interface of key biogeochemical variables is highlighted in many studies. This is the case, for example, for algal biomass [Krembs et al., 2000] and nutrients [Fritsen et al., 1994], for contaminants such as mercury [Chaulk et al., 2011] and for climate-active gases such as CO_2 [Geilfus et al., 2012] and dimethylsulfide [Tison et al., 2010].

Textural properties provide information on sea ice formation, growth and decay processes and are therefore also connected to sea ice halo-thermodynamic evolution. Formation and growth processes define, for example, how solutes (including salts) are initially incorporated in sea ice, as shown for algal biomass by Ackley and Sullivan [1994]. For all these reasons, detailed physical and textural analyses constitute the basis for many other investigations of the sea ice system.

Numerous investigations of the sea ice system were conducted during the International Polar Year Circumpolar Flaw Lead (IPY-CFL) system study in the southern Beaufort Sea-Amundsen Gulf, Canadian Arctic (Figure 2.1), aboard the icebreaker CCGS Amundsen from 18 October 2007 until 7 August 2008. Over 350 participants, organized in 12 teams [for details see Barber et al., 2010], tried to answer a wide range of key scientific questions related to the different roles played by Arctic sea ice in the Earth system. The initial objective of the present study was to provide a common interpretative framework of physical (temperature and bulk ice salinity) and textural properties to the IPY-CFL community and especially for investigations based on ice coring, which is often carried out for a wide range of multidisciplinary projects [e.g. Lewis et al., 2011]. The same framework should also be of some interest for future experiments in the Amundsen Gulf. We therefore measured sea ice temperature and bulk ice salinity from ice cores collected throughout the sampling season. We also regularly made textural analysis based on thin-section pictures. We ended up with a large dataset covering a complete cycle from growth to the start of melt (i.e. 28 November 2007 to 18 June 2008).

Measurements of sea ice temperature and bulk ice salinity extending over such a long time period are very scarce. Field observations are usually limited to the spring and summer seasons due to technical difficulties inherent to winter

sampling. Hence, our dataset represented a unique opportunity to investigate the halo-thermodynamic evolution of sea ice over a long period. The annual cycle of sea ice temperature has been well described by Perovich and Elder [2001]. Sea ice temperatures in first-year Arctic sea ice are generally driven by the surface heat balance and buffered by the snow cover, the oceanic heat flux typically being small in most regions of the Arctic [Steele and Flato, 2000]. The annual cycle of sea ice bulk salinity is governed by sea ice desalination processes. Sea ice desalination is critical as it directly influences ocean circulation [e.g. Aagaard, 1981]. Some early time series of sea ice bulk salinity showed salinity profiles typically C-shaped in winter cores and Z-shaped when surface melting occurs [Malmgren, 1927].

In another time series study, Nakawo and Sinha [1981] investigated the effect of growth rate on salinity. They showed that from a few days after ice formation until warming in spring the salinity of an ice layer remains stable. Untersteiner [1968] suggested several potential sea ice desalination mechanisms. Two of these mechanisms (brine diffusion and brine expulsion) only lead to salt redistribution within sea ice but do not contribute to any measurable sea ice desalination [Notz and Worster, 2009]. On the contrary, it is generally agreed that flushing results in an important and net salt loss during the melt season [Eicken et al., 2004; Notz and Worster, 2009]. The hydraulic head created by the snow and surface ice meltwater flushes downwards the existing brine network. Before the melt season and during ice growth, it was generally assumed that salt loss was governed by segregation of salts at the ice-ocean interface [Cox and Weeks, 1988]. Segregation of salts was considered to be a function of ice growth rate, with higher salinities obtained at higher growth rates. In the past two decades, several studies suggested that the salt loss observed during ice growth and warming was

uniquely the result of gravity drainage [e.g. Wettlaufer et al., 1997; Vancoppenolle et al., 2006; Notz and Worster, 2009].

Gravity drainage is the convective overturning of brine in connected brine inclusions [Cox and Weeks, 1975; Notz and Worster, 2008]. With gravity drainage, the net desalination is caused by the salinity difference between the brine leaving the ice and the brine entering the ice. Gravity drainage is governed by the ice thickness, the permeability and the brine density gradient [Wettlaufer et al., 1997, 2000]. These relationships have been approached analytically in the mushy-layer theory [Worster, 1992; Wettlaufer et al., 1997] using a porous-medium Rayleigh number. For gravity drainage to occur, the Rayleigh number must exceed a critical value. Based on experimental studies, it was estimated to be typically 10 [Wettlaufer et al., 1997; Notz and Worster, 2009]. For a given ice depth, gravity drainage only occurs once the buoyancy forces due to the vertical brine density gradient expressed in the numerator of the Rayleigh number overcome dissipation (the product between dynamic viscosity and thermal diffusivity of the brine), as expressed by the denominator. In growing cold ice, gravity drainage is limited to the permeable ice layer at the interface with the ocean, which gives rise to a quasi-steady-state salinity. In warming permeable ice, full-depth gravity drainage can develop, which results in a net desalination of the ice cover.

The Rayleigh number has had some success as a proxy of sea ice desalination in laboratory experiments. However, it has rarely been applied to field measurements [Wettlaufer et al., 2000; Notz and Worster, 2008; Gough et al., 2012] and certainly not over a complete cycle from growth to start of melt. The large dataset presented in this study provided an opportunity to achieve this. We therefore apply the evolution of the measured mean bulk ice salinity from

November 2007 until June 2008 to the evolution of both calculated brine volume fraction and Rayleigh number. It should be acknowledged here that this study was not initially designed as a real time series study. Hence our dataset also integrates spatial variability, which we also discuss.

Finally, we provide a regional analysis of the sea ice formation and deformation processes based on textural analysis. The Amundsen Gulf is an oceanic area of particular interest since it is characterized by the development of polynya and flaw leads [Barber and Massom, 2007]. Expected to increase in number and to expand in size and duration, such areas could also represent a glimpse of the future sea ice conditions in the Arctic.

2.2. Material and methods

2.2.1. Study area and sampling strategy

The IPY-CFL study was conducted aboard CCGS Amundsen in the southern Beaufort Sea-Amundsen Gulf area between 18 October 2007 and 7 August 2008 (Figure 2.1). The region's sea ice climatology has recently been described by Galley et al. [2008] over 1980-2004. Sea ice in the Amundsen Gulf generally starts to form in October in shallow areas along the coast as fast ice, while a drift ice regime with small leads dominates offshore. In some years, fast ice covers the entire Amundsen Gulf over winter and early spring. Interaction between the fast ice edge that develops between Cape Perry and Banks Island and the perennial mobile pack ice that rotates with the Beaufort Gyre is responsible for the development of the flaw lead [Proshutinsky et al., 2002; Barber and Hanesiak, 2004]. Break-up in the Amundsen Gulf usually occurs in early June and creates the feature known as the Cape Bathurst polynya.

Figure 2.1: A. Map of the study area showing the bathymetry and the location of the sampling stations. The dotted lines indicate the extent of fast ice on 5 May 2008. Data for fast ice extent delimitation were obtained from the Canadian Ice Service sea ice charts. B. Air temperature recorded during the IPY-CFL study. The sampling stations icons are plotted on a temperature series of air temperature measured with a Rotronics MP 101A temperature sensor located at ~ 18 m above the ice surface with a resolution of 0.1 °C and an accuracy of ± 0.3 °C.

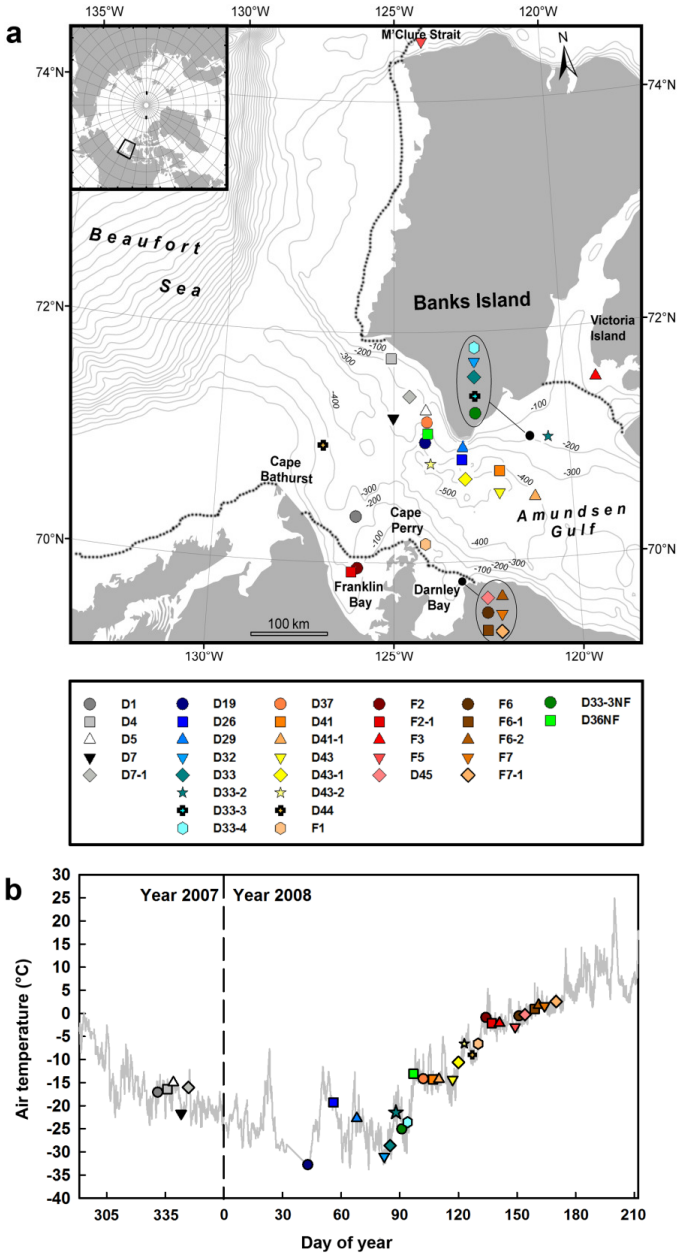

A description of sea ice dynamics in the Amundsen Gulf in 2007 and 2008 is available from Barber et al. [2010]. Sea ice was highly mobile in 2007 and 2008. In 2007, sea ice formation started around the third week of September, and by 26 October freeze-up was complete [Barber et al., 2010]. Strong easterly winds kept the sea ice mobile throughout much of the winter season. Fast ice remained restricted to near-shore locations while a sea ice regime characterized by drifting floes interspersed with small short-lasting leads continued to dominate until ice break-up in the first week of May 2008 [Barber et al., 2010].

Samples analyzed in this study were collected during the IPY-CFL study between 28 November 2007 and 18 June 2008 in approximately area 69-75° N, 119-127° W (Figure 2.1). The IPY-CFL was a multidisciplinary study. Sampling site selection was aimed to satisfy a multitude of research objectives [Barber et al., 2010]. The initial plan was to establish a semi-permanent ice camp along a fast ice edge that usually forms between Banks Island and Cape Perry (Figure 2.1). However, since sea ice was highly mobile in 2007 and 2008 the ship was constantly repositioned for safety and logistical reasons. This resulted in a geographic dispersion of the sampling sites across the Amundsen Gulf. The ship repositioned in numerous drift ice sites south of Banks Island (Figure 2.1) over a period between the end of November and the first week of May and associated ice break-up. Thereafter, the ship moved to near-shore fast ice sites primarily located in two sheltered bays (Franklin and Darnley Bays) (Figure 2.1). One fast ice site in the mouth of M'Clure Strait and one on the west coast of Victoria Island were also visited (Figure 2.1).

Samples from 21 of the sites (15 drift ice and 6 fast ice sites) visited by the ship are analyzed here. The time spent at each of these sites varied between a

few hours and 22 days. Generally, one ice floe was sampled at each site during 1 day. However, for some sites where the ship stayed for a few days, the IPY-CFL teams collected samples on multiple days and each day on a different ice floe. In this study, each of these sampling days is referred to as a station. In total, we report measurements from 33 stations (23 drift ice and 10 fast ice stations) (Table 2.1). The stations were named by a letter (D for drift ice, F for fast ice), a number (ID of the site) and a hyphen followed by a number if there was more than one station per site. On two occasions, NF (newly formed) letters were added to the name of the station to designate sampling of sea ice recently formed in a refrozen lead. The location of the stations is shown in Figure 2.1. Also shown is the extent of fast ice on 5 May 2008 drawn from the Canadian Ice Service sea ice charts. On average, sampling occurred every 5 days over the study period. However, sampling was suspended between 13 December 2007 and 6 February 2008 since no member of our research team was aboard the ship at that time.

2.2.2. Sampling and measurements

Sampling always started with ice floe selection. The criteria used to select a floe included floe size (large floes of a few hundred meters or greater were preferred), and a minimum distance from pressure ridges (> 500 m) was enforced. An area dedicated to the ice coring was delimitated on the ice floe upwind of the ship and access to the area limited to the team members to ensure pristine conditions. Within this area, a small work sub-area (~ 5 m x 5 m) with homogeneous surface conditions was selected to limit spatial variability. On a few occasions, an ice cage lowered from the ship was used for sampling. This occurred over thin ice in November and December and when the ship was navigating in refrozen leads later in the field season (stations D33-3NF and D36NF).

Once on the ice floe, snow cover type and conditions (wetness, hardness and grain size) were characterized by visual observations using the terminology of Massom et al. [2001] and Sturm et al. [2002]. These are reported in Table 2.1.

Snow thickness was measured with a ruler. A maximum of ten sea ice cores were then collected using an electropolished stainless-steel corer (Lichtert Industry®, Belgium) (ID = 7 cm) for various biogeochemical analyses. Only two of these cores from each station were used in this study. The first sea ice core was dedicated to sea ice temperature, bulk salinity and water stable-isotope ($\delta\,^{18}O$) measurements, while the second was dedicated to sea ice texture determination. The distance between the two sea ice cores was always < 20 cm. Core lengths and freeboard were measured with a ruler after extraction. These are also reported in Table 2.1.

Sea ice temperature, T (°C), was measured in situ on the first core extracted at each station. The delay between core extraction and the beginning of the measurement was always very short (< 60 s). A fast-response handheld portable digital thermometer equipped with a calibrated probe (TESTO® 720) was used. The probe was inserted in 2 mm diameter holes drilled to the center of the core at 5 cm intervals. In case the end of a 5 cm interval corresponded to a crack in the core, the measurement was made a few centimeters further. The precision of the probe was ± 0.1°C with an accuracy of ± 0.2°C. The drilling process may have impacted both the accuracy and precision of the sea ice temperature measurements, but it is doubtful that the effect will have been large given the high heat capacity of sea ice [Untersteiner, 1961].

Table 2.1: General ice and surface conditions at the sampling stations. Time is local time (GMT-7). Ice concentrations are given in tenths. The horizontal line separates drift ice stations from fast ice stations. NS: new snow; FF: frost flowers; WS: wind slabs; SU: superimposed ice; MP: melt ponds; nd: not determined.

Station ID	Date	Sampl. Time	Sea ice type	Ice Thickness (cm)	Ice Conc.	Snow (cm)	Freeboard (cm)	Snow cover type
D1	28 Nov 2007	09:00AM	Drift Ice	51	9+	2	3	NS
D4	3 Dec 2007	04:00PM	Drift Ice	33	9	3	3	FF
D5	6 Dec 2007	10:00AM	Drift Ice	36	9	2	3.5	FF
D7	10 Dec 2007	01:00PM	Drift Ice	54	9+	1.5	4.5	NS
D7-1	13 Dec 2007	09:00AM	Drift Ice	60	9+	1.5	5	NS
D19	6 Feb 2008	02:00PM	Drift Ice	58	10	8	3.5	NS 1, WS 7
D26	25 Feb 2008	02:00PM	Drift Ice	123	9	2.5	11	nd
D29	8 Mar 2008	02:00PM	Drift Ice	124	9	3.5	11	WS
D32	22 Mar 2008	01:00PM	Drift Ice	140	nd	10	10	WS
D33	25 Mar 2008	03:00PM	Drift Ice	140	10	nd	nd	nd
D33-2	28 Mar 2008	09:00AM	Drift Ice	140	10	3	10.5	WS
D33-3	31 Mar 2008	08:30AM	Drift Ice	145	10	nd	nd	nd
D33-3NF	31 Mar 2008	02:30PM	Refrozen Lead	55	10	2	5	FF
D33-4	3 Apr 2008	09:00AM	Drift Ice	145	10	nd	nd	WS
D36NF	6 Apr 2008	09:00AM	Refrozen Lead	71	9	1.5	7	FF
D37	11 Apr 2008	nd	Drift Ice	125	9	nd	nd	nd
D41	16 Apr 2008	nd	Drift Ice	125	nd	nd	nd	nd
D41-1	19 Apr 2008	nd	Drift Ice	132	nd	nd	nd	nd
D43	26 Apr 2008	09:00AM	Drift Ice	132	9	6.5	10.5	NS 2, WS 4,5
D43-1	29 Apr 2008	09:00AM	Drift Ice	136	9	4.5	12	WS
D43-2	2 May 2008	08:40AM	Drift Ice	131	9	8	9	WS
D44	6 May 2008	01:00PM	Drift Ice	79	9	2	7	WS
D45	30 May 2008	09:40AM	Drift Ice	86	10	12	9	NS 2, SU 10
F1	9 May 2008	08:40AM	Fast Ice	121	8	3.5	11	WS
F2	13 May 2008	09:40AM	Fast Ice	162	10	18	14	NS 9, WS 9
F2-1	16 May 2008	09:40AM	Fast Ice	97	10	3	11	SU 3
F3	20 May 2008	09:20AM	Fast Ice	127	10	20	8.5	NS 2, WS 8, SU 10
F5	28 May 2008	08:00AM	Fast Ice	180	10	11	13	WS 9, SU 2
F6	2 Jun 2008	09:30AM	Fast Ice	181	10	1	25	SU, MP
F6-1	7 Jun 2008	nd	Fast Ice	141	10	0	11.5	No Snow, MP
F6-2	9 Jun 2008	nd	Fast Ice	133	10	0	9.5	No Snow, MP
F7	12 Jun 2008	nd	Fast Ice	122	10	0	9.5	No Snow, MP
F7-1	18 Jun 2008	09:00AM	Fast Ice	100	10	0	12	No Snow, MP

The same ice core was then immediately cut into sections with a stainless-steel saw using the same vertical resolution as for sea ice temperature. The whole process typically took 5 to 10 min depending on the core length. Ice core sections were stored in sealed plastic containers and melted at room temperature aboard the ship. Sea ice bulk salinity, S_i, of each melted core section was determined through conductivity using a Thermo-Orion® WP-84TPS meter (accuracy of ± 0.1‰). Salinity data are reported using the practical salinity scale.

Water aliquots (10 mL) were also collected in no-head-space vials from the melted core sections for water stable-isotope (δ ^{18}O) measurements. Snow was always carefully scraped off the surface of the ice cores collected, to avoid snow contamination of the samples. Aliquots were analyzed at the G.G. Hatch Isotope Laboratories, University of Ottawa, using a Gasbench + DeltaPlus XP isotope ratio mass spectrometer (ThermoFinnigan®, Germany) and the conventional water-CO_2 equilibration method (accuracy with respect to Vienna Standard Mean Ocean Water (VSMOW) was ± 0.15‰). Water stable-isotope (δ ^{18}O) data are reported as per mil deviation of the $^{18}O/^{16}O$ ratio of the CO_2 equilibrated with the water samples relative to VSMOW:

$$\delta^{18}O = \left\{ \frac{(^{18}O/^{16}O)_{sample}}{(^{18}O/^{16}O)_{VSMOW}} - 1 \right\} 1000‰ \quad (2.1)$$

The second ice core collected was stored in an insulated box filled with ice packs precooled to -30°C and brought back to the ship. The core was stored horizontally at -26°C until processing as suggested by Eicken et al. [1991]. Vertical sections of the ice core were attached to glass plates and planed down to 0.6 to 0.8 mm using a microtome (Leica® SM2400). The thin sections obtained were installed on a light table equipped with cross-polarized sheets, and pictures were

taken with macro setting activated on the camera (Nikon® Coolpix S200, 7.1 megapixels) following the standard procedure presented by Langway [1958]. The size, shape and orientation of the crystals were used to discriminate between the different textural types. Since the differences in crystal properties between the different ice layers were easily identifiable on the pictures, c-axis orientation measurements with a universal stage were not made.

Air temperature was recorded on the ship deck by a Rotronics MP 101A temperature sensor located at ~ 18 m above the ice surface. The sensor had a resolution of 0.1°C and an accuracy of ± 0.3 C. Geographical coordinates and ice conditions (ice type and concentration) of the sampling sites were available from the ship logbook and from the Canadian Ice Service sea ice charts.

2.3. Results

2.3.1. General ice properties and sea ice conditions

The evolution of the air temperature during the sampling season as recorded by the temperature sensor located on the ship's deck is shown in Figure 2.1. An icon was then added to this temporal series at the corresponding sampling date of each station. General ice properties (ice type, thickness and concentration) and snow cover properties (snow type, thickness and freeboard) are reported in Table 2.1. All stations sampled were first-year ice and the freeboard was always positive.

The first sampling period occurred between 28 November 2007 (day 331) and 13 December 2007 (day 347) in the Amundsen Gulf between Cape Perry and Banks Island (Figure 2.1). Air temperature decreased from November to December with the progression towards winter (ranging between -25°C and -15°C). Five

stations were sampled during this period (D1 to D7-1). All stations consisted of thin drift ice (30 to 60 cm thick), and the ice concentrations were always high (9 to 9+ tenths). The snow cover was typically thin (1.5 to 3.0 cm) and consisted of new snow. Frost flowers were observed at stations D4 and D5.

Sampling was then suspended for roughly a month and a half due to a lack of team members aboard the ship. Sampling resumed on 6 February 2008 and was continuous until 18 June 2008. From 6 February 2008 (day 37) until 3 April 2008 (day 94), the air temperature recorded at the stations remained low (< -20°C). During this period, eight stations (D19 to D33-4) were sampled in the Amundsen Gulf just south of Banks Island (Figure 2.1). Most stations consisted of medium and thick drift ice (58 to 145 cm thick) and the ice concentrations were always high (9 to 10 tenths). The snow cover (2.5 to 10.0 cm) consisted either of a thin wind slab layer (cohesive layer of snow formed when wind deposits snow onto sea ice) or of a thin new snow layer over a thicker wind slab layer. One thinner station (D33-3NF on 31 March 2008, 55 cm thick) was clearly identified by observers as a recently refrozen lead and had frost flowers at its surface.

From 3 April 2008 until the end of the sampling season, the air temperature recorded at the stations rose almost continuously. Between 3 April 2008 (day 91) and ice break-up (first week of May), eight additional drift ice stations (D36NF to D44) were sampled. These were located in the Amundsen Gulf, just south of Banks Island and north of Cape Bathurst (Figure 2.1). The stations consisted of medium and thick ice (71 to 136 cm thick), and ice concentrations were high (9 to 10 tenths). Air temperature ranged between -15°C and -5°C. The snow cover varied from a thin wind slab layer (1.5 to 2.0 cm) on the medium ice to a thicker wind slab layer

(4.5 to 8.0 cm) on the thick ice. One refrozen lead station (D36NF) had relic frost flowers buried in snow at its surface.

After ice break-up, the ship visited fast ice stations. The extent of fast ice on 5 May 2008 is shown by dashed lines in Figure 2.1. From 9 May 2008 (day 130) until 28 May 2008 (day 149), five fast ice stations (F1-F5) were sampled in various locations such as Franklin Bay, the mouth of M'Clure Strait and the west coast of Victoria Island (Figure 2.1). The ice cover was thick at all stations (97 to 180 cm thick), and ice concentrations ranged between 8 and 10 tenths. Air temperature was high, ranging between -5°C and 0°C. Signs of surface melting appeared and 2 to 10 cm of superimposed ice was observed at stations F2-1 to F5.

Six more stations were sampled in Darnley Bay (Figure 2.1) after 30 May 2008 (day 151), corresponding to the air temperature rising above 0°C. The first station (D45 on 30 May 2008) consisted of medium drift ice (86 cm thick) with a 10 cm layer of superimposed ice under 2 cm of new snow. The five remaining stations (F6 to F7-1) were on thick fast ice (100 to 181 cm thick), with a very thin layer of superimposed ice at station F6 and no snow at all the other stations. Melt ponds were observed at station F6 (2 June 2008) and at subsequent stations until the end of the field season.

2.3.2. Sea ice temperature and bulk salinity

Depth profiles of sea ice temperature (T) and bulk salinity (S_i) at each sampling station are provided in Figures 2.2 and 2.3. Ice temperature profiles measured during the first sampling period (D1 to D7-1) showed a general linear increase from a cold surface to a warmer ice base held at its melting point. The vertical ice temperature gradient ($\partial T/\partial z$) was calculated as the difference between temperatures at the ice surface and base, divided by the ice thickness (a positive

value indicating a negative heat flux through the ice). The mean gradient during the first sampling period (28 November 2007 to 13 December 2007) was 17°C.m^{-1}. Comparable gradients (averaging 16°C.m^{-1}) were observed at stations between D19 (6 February 2008) and D36NF (6 April 2008) although the actual temperature difference across the ice vertically was larger. From station D37 (11 April 2008) until station D44 (6 May 2008), we observed that the gradients slackened (averaging 5°C.m^{-1}), corresponding to an increase in surface ice temperature. The last drift ice station sampled (D45 on 30 May 2008) had a slightly negative gradient (-1°C.m^{-1}) in its top 20 cm, while deeper ice as near-isothermal. Sea ice was near-isothermal at all the coldest fast ice stations (from F1 on 9 May 2008 until F5 on 28 May 2008) with gradients averaging 1°C.m^{-1}. Some stations (F2, F2-1 and F5) also had a slightly negative gradient in their surface ice sections. Finally, the warmest fast ice stations (from F6 on 2 June 2008 until F7-1 on 18 June 2008) were close to melting at all depths.

Ice salinity profiles (Figure 2.3) were C-shaped from station D1 (28 November 2007) until station D44 (6 May 2008) as typically observed in growing sea ice [e.g. Nakawo and Sinha, 1981; Eicken et al., 1991]. However, the pattern was not always perfectly defined. Some stations had much higher surface ice salinity relative to bottom salinity. These were stations sampled between 3 December 2007 (D4) and 6 February 2008 (D19) as well as station D33-3NF, which corresponded roughly to all the thin-ice stations. The ice salinity profile of the last drift ice station sampled (D45 on 30 May 2008) transitioned to a ?-shape, as previously described by Eicken et al. [1991]. Surface ice became fresher while a bottom maximum in salinity vanished. Fast ice stations had variable salinity profiles. Station F1 and F2 had C-shaped profiles, stations F2-1 and F3 reverse S-

shaped profiles [Eicken et al., 1991; Eicken, 1992], while ?-shaped profiles were observed at all other stations.

2.3.3. Sea ice textural properties and water stable isotope ($\delta^{18}O$)

Samples of ice texture are presented in Figure 2.4. This selection of stations gives a good overview of the ice surveyed during the IPY-CFL study as it covers most of the sampling season and the different ice types (drift ice/fast ice). We identified five different ice textures (granular, columnar, mixed columnar/granular, platelet and draped platelet) in the thin-section pictures based on descriptions found in the literature [Eicken and Lange, 1989, 1991; Jeffries et al., 1993; Tison et al., 1998]. Granular texture was always orbicular rather than polygonal (Figure 2.4a). Some polygonal granular ice, corresponding to superimposed ice, was observed during the study (see Table 2.1) but systematically scraped off the ice surface before sampling. Hence it could not be detected in the thin-section pictures. Three granular orbicular sub-textures, fine grain sizes (< 2 mm across), medium grain sizes (2 to 5 mm across) and coarse grain sizes (> 5 mm across) were observed. Typically, cores had a thin layer of granular orbicular texture underlain by columnar texture (Figure 2.4b). On average, granular texture represented 9% (ranging between 0 and 49%) of the total ice thickness and columnar texture 87% (ranging between 50 and 100%). Thin layers of granular texture (1 to 2 cm) were also occasionally found in interior ice (e.g. D7-1 and D32). Mixed columnar/granular texture (Figure 2.4c) was found at five stations (D29, D33-2, D43-1,D45 and F1) and represented 4 to 17% of the total ice thickness of these stations.

Figure 2.2: Vertical profiles of sea ice temperature (T) at the sampling stations.

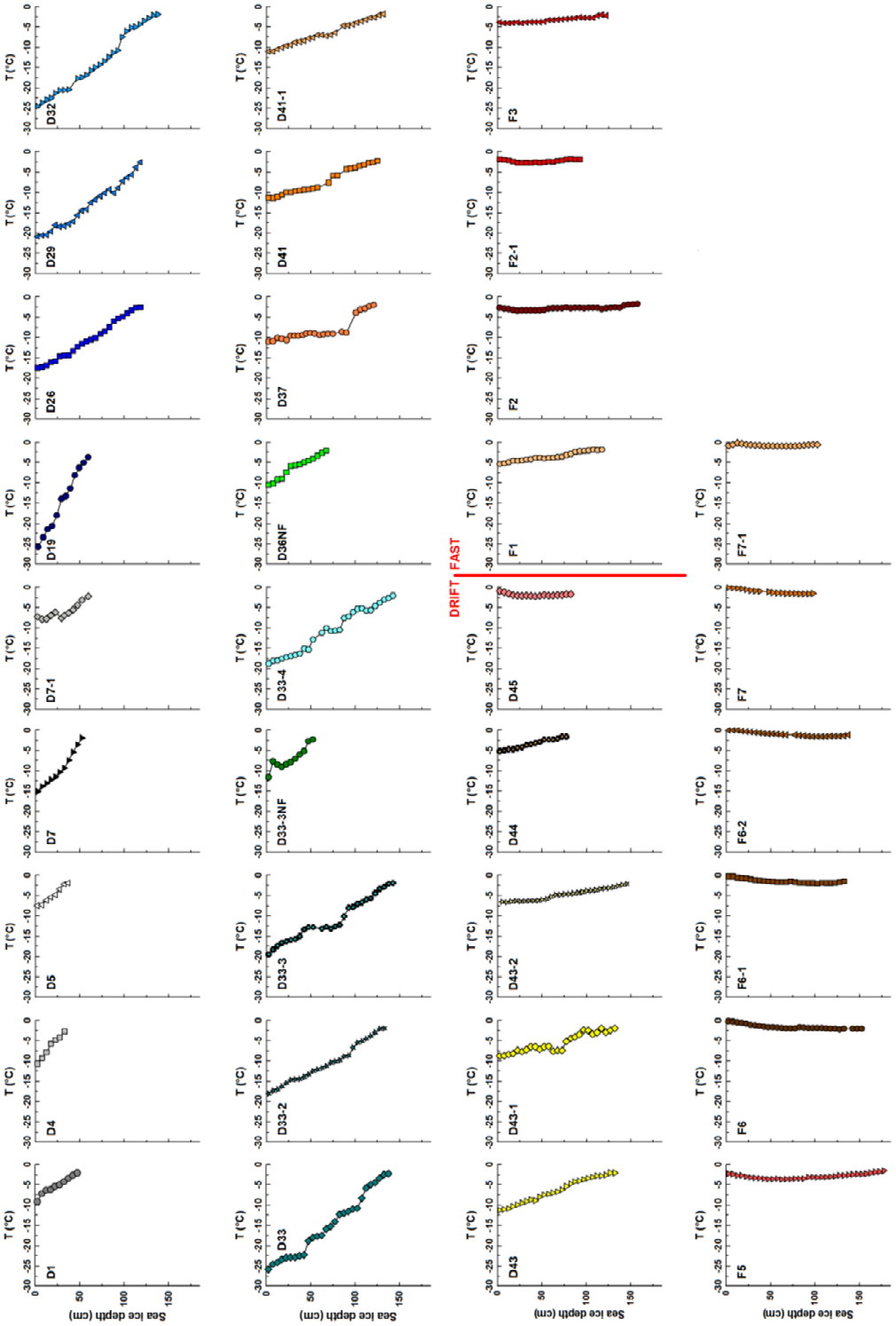

Figure 2.3: Vertical profiles of sea ice bulk salinity (S_i) at the sampling stations.

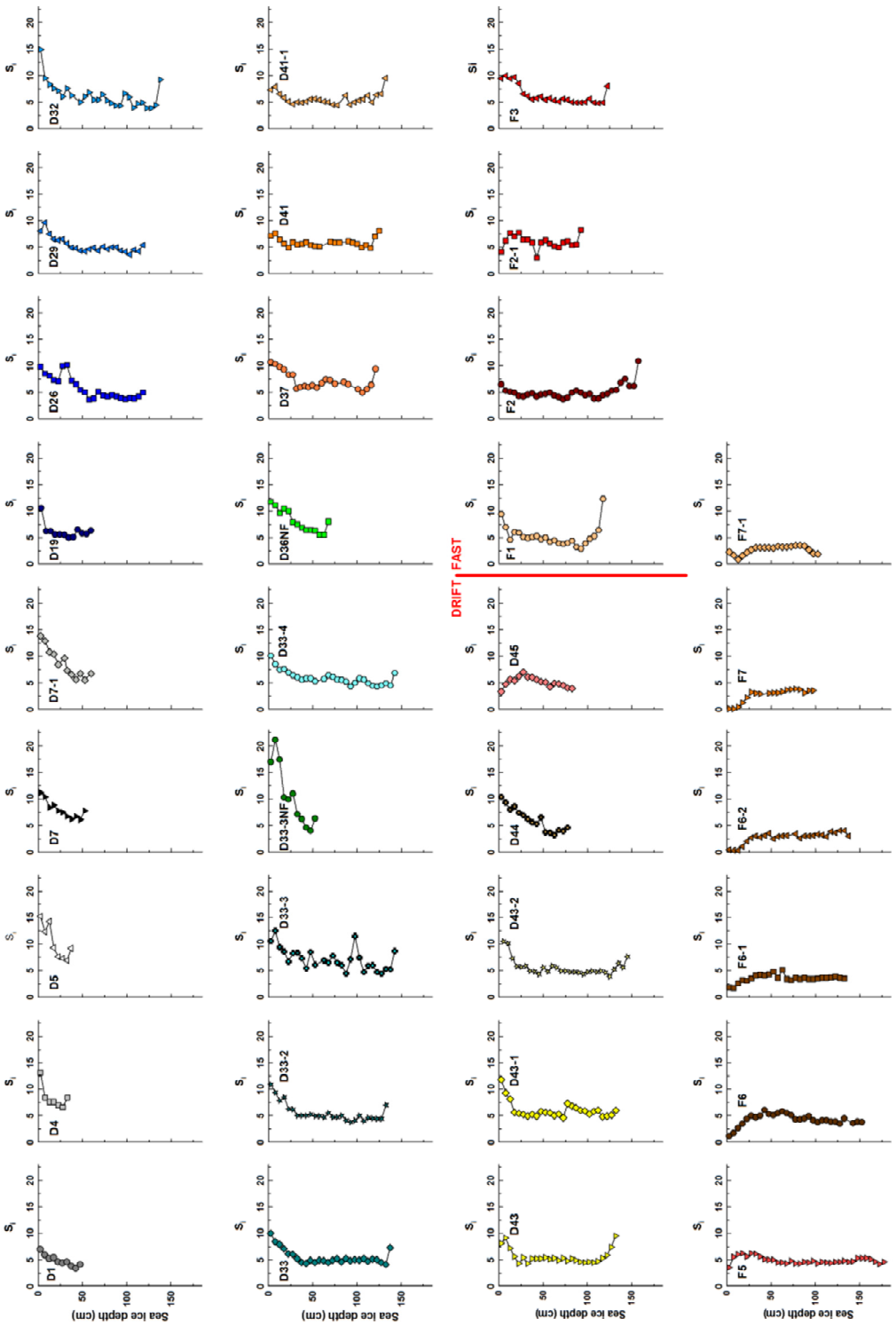

We observed some peculiar textural characteristics in some cores. Station D33-3NF was composed entirely of columnar texture, while station D1 had a thick 23 cm layer of granular texture. Station D29 had the most disturbed texture, with 20 cm of draped platelet texture (Figure 2.4d) (17% of the total ice thickness) at ~ 15 cm depth, 5 cm of platelet texture (Figure 2.4e) at the ice bottom and layers of granular texture incorporated in columnar texture. A thin 5 cm layer of platelet texture was also found at the bottom of station F2, accounting for 2% of its total ice thickness.

Available $\delta^{18}O$ data are shown in Figure 2.5. The ice $\delta^{18}O$ varied between -7.95‰ and 0.23‰ (mean = -1.10‰, SD ± 0.68‰). The most negative value was found in the top 5 cm layer of the fast ice station F6-1. In all other layers of this station and in all other stations, the isotopic composition was considerably more positive (ranging between -2.88‰ and 0.23‰). $\delta^{18}O$ values in the upper 10 cm of the cores (typically corresponding to the granular texture layers) varied between -2.88‰ and -0.67‰, with a mean of -1.49‰. Station D1 showed significantly more negative $\delta^{18}O$ values in these layers relative to all other stations. The $\delta^{18}O$ values increased slightly in the columnar texture layers and remained fairly constant towards the bottom of the cores, ranging between -1.89‰ and 0.23‰, with a mean of -0.95‰. Some large fluctuations were, however, observed. Significantly less negative $\delta^{18}O$ values (up to 0.23‰) were measured from 20 to 60 cm at station F6-1. Some stations also showed local minima (e.g. D26 and D41) and maxima (e.g. D7 and D32) in the interior ice layers (< 1 SD). The evolution of under-ice water $\delta^{18}O$ (sampling depths 2 to 5 m) during the sampling season is also plotted in Figure 2.5. Data have been previously presented by Chierici et al. [2011]. Values ranged between -4.57‰ and -2.11‰ (mean = -3.18‰, SD ± 0.56‰). Snow $\delta^{18}O$

values were measured at stations D37 and D41 (-14.92‰ and -12.80‰). One melt pond analyzed at station F6-1 had an isotopic composition of -9.87‰.

Figure 2.4: Sea ice textural properties for a subset of the sampling stations. Representative pictures of the five textural types identified are shown. Granular texture (A) was defined as layers composed of small (millimeter-sized) isometric crystals, columnar texture (B) as layers with long (centimeter-sized) vertically elongated (prismatic) crystals, mixed columnar/granular texture (C) as a transition zones with coexisting granular and columnar textures, draped platelet texture (D) as centimeter-sized crystals with wavy uneven edges, and platelet texture (E) as layers of elongated acicular crystals with no specific orientation. Vertical scale is in centimeters.

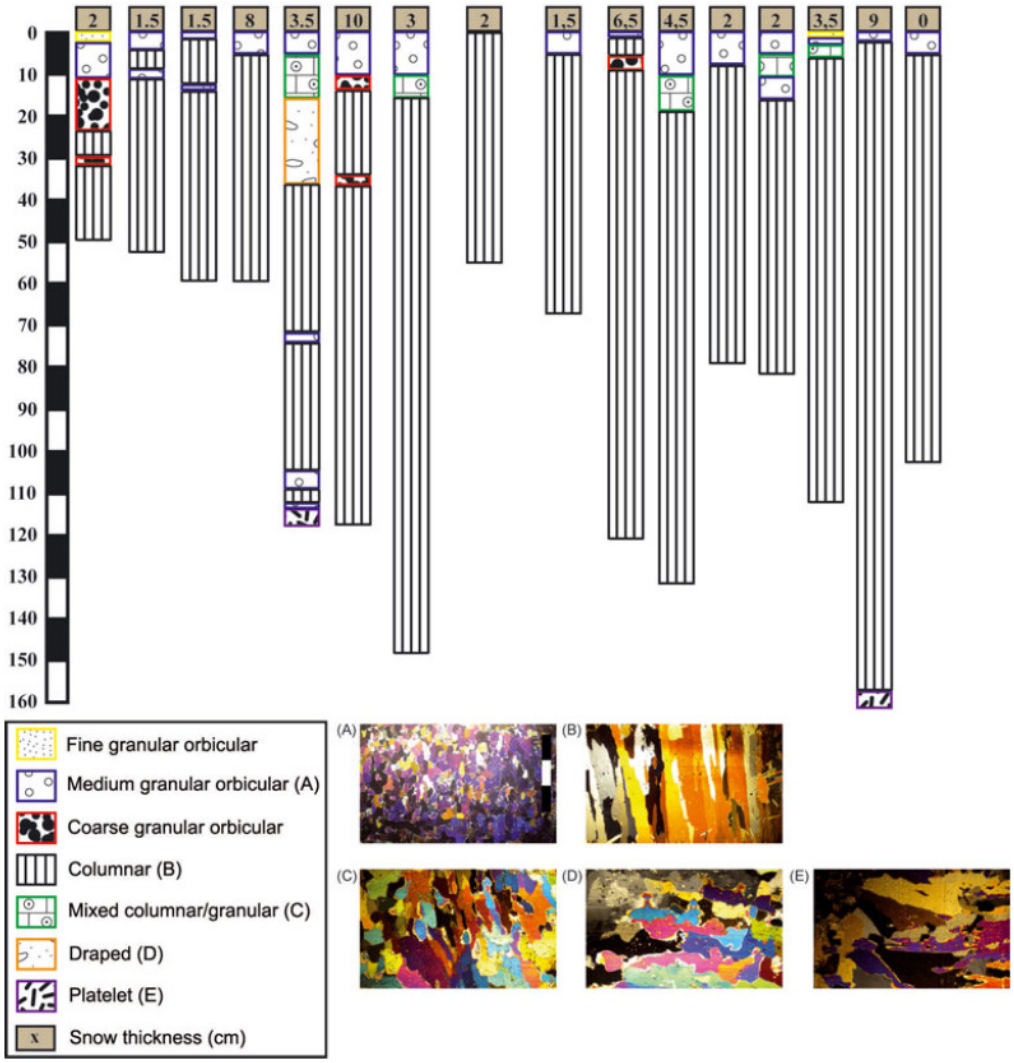

Figure 2.5: A. Water stable isotope (δ ^{18}O) vs depth in sea ice for a subset of the sampling stations. B. Evolution of the under-ice water δ ^{18}O (sampling depths 2 to 5 m) during the sampling season. Adapted from Chierici et al. [2011].

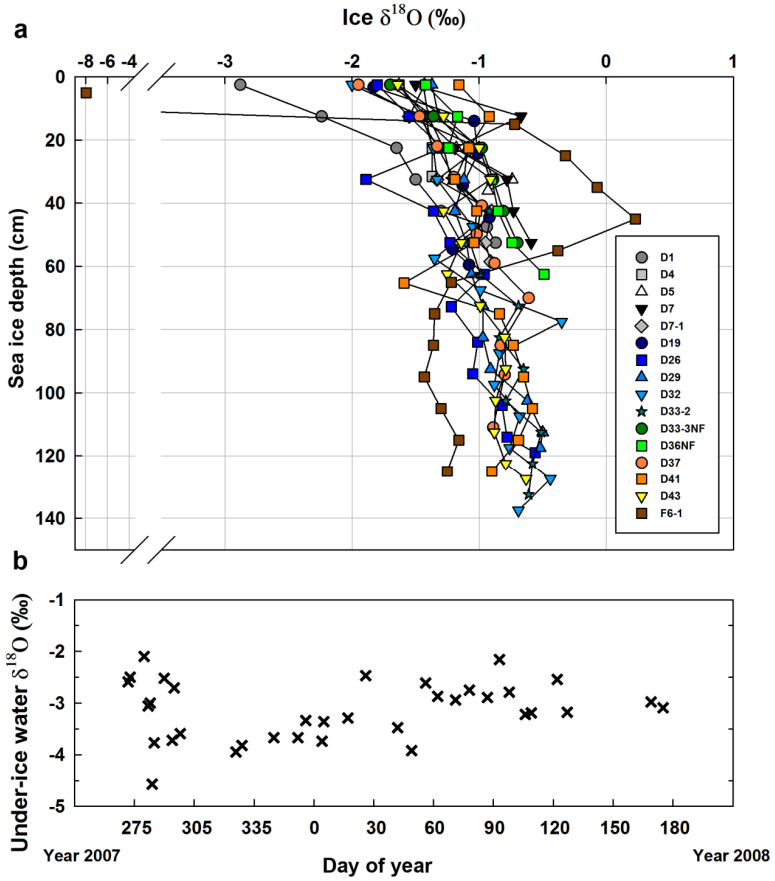

2.4. Discussion

2.4.1. Halo-thermodynamic evolution of sea ice during the IPY-CFL study

2.4.1.1. Sea ice temperature and bulk salinity

The temporal evolution of the mean sea ice temperature (T) and bulk salinity (S_i) is shown in Figures 2.6b and c. Trends were observed in both properties. The temporal changes observed in ice temperature and the ice temperature profiles described in section 2.3.2 are typical of an annual temperature cycle of first-year ice in the Arctic, as described for example by Perovich and Elder

[2001]. From station D1 (28 November 2007) until station D44 (6 May 2008), the profiles were similar to those previously observed in growing ice [e.g. Maykut, 1982; Cottier et al., 1999]. The vertical ice temperature gradient ($\partial T/\partial z$) slackened as air temperature rose at the beginning of April (station D37). Ocean freezing temperature also appears in Figure 2.6b. The ice temperature profiles became near-isothermal as air temperature approached the ocean freezing temperature, which occurred around the first week of May. Further warming brought a negative vertical ice temperature gradient in surface ice of some stations (F2, F2-1 and F5), as previously observed in summer first-year ice [Haas et al., 2001; Tison et al., 2008]. The evolution of the mean sea ice temperature closely followed the evolution of the air temperature recorded during the study (Figures 2.6a and 2.6b). We found a strong linear relationship ($R^2 = 0.87$) between the two variables as shown in Figure 2.7, which suggested that our ice temperature profiles were driven mainly by atmospheric forcing. Ice temperature profiles are generally driven by the surface heat balance, the oceanic heat flux and the properties of the snow cover. The ocean heat flux is typically small in most regions of the Arctic [Steele and Flato, 2000]. The snow cover, which has a lower effective thermal conductivity than that of sea ice [Sturm et al., 1997], can strongly influence sea ice temperature profiles. We indicate the snow thickness of each station next to its icon in Figure 2.7. We observed that deviations from the linear relationship with air temperature were not correlated with the snow thickness ($R^2 = 0.01$). Hence it is unlikely that the snow cover strongly influenced our ice temperature profiles. This is understandable since the snow cover was typically thin and consisted most of the time of wind slab layers, which are known to have higher effective thermal conductivity relative to other snow types [Sturm et al., 1997].

The evolution of the mean sea ice bulk salinity (Figure 2.6c) showed a decrease from 8 to 10 during the first sampling period (28 November 2007 to 13 December 2007, with the exception of station D1) to 6 on 6 February 2008 (station D19). This can be explained by the following process: as the ice grew thicker with the progression into winter, drainage of salts at the ice-ocean interface became more efficient, decreasing the mean bulk ice salinity of the ice.

From 6 February 2008 until 20 May 2008 (station F3), the mean bulk ice salinity did not vary much, fluctuating at about 6, corresponding to the quasi-steady-state salinity described by Nakawo and Sinha [1981]. The mean bulk ice salinity subsequently decreased almost linearly from 20 May 2008 until 9 June 2008 (station F6-2), stabilizing at ~ 2.6 until the end of the sampling season (18 June 2008, station F7-1). We suggest that this desalination trend was caused by an episode of full-depth gravity drainage. In order to discuss this, we introduce in the following subsection two additional physical parameters: brine volume fraction and Rayleigh number.

2.4.1.2. Brine volume fraction and Rayleigh number

The brine volume fraction (V_b/V) is defined as the fraction of brine relative to the bulk sea ice volume. Gravity drainage depends actively on the connectivity of brine inclusions, which is usually simplified to be proportional to the brine volume fraction [Petrich and Eicken, 2010]. In brief, above a brine volume fraction of 5 to 7% (i.e. percolation threshold), discrete brine inclusions start to connect and the ice is considered to be permeable to fluid transport, enabling gravity drainage [Weeks and Ackley, 1986; Cox and Weeks, 1988; Golden et al., 1998].

Figure 2.6: The evolution throughout the sampling season of: A. Daily mean air temperature. B. Mean sea ice temperature. C. Mean sea ice bulk salinity. D. Minimum brine volume fraction and E. Mean Rayleigh number. The vertical dashed line indicates the start of fast ice sampling. In (B) the horizontal dashed line is the ocean freezing temperature (T_f) calculated using $T_f = -AS_w$ where A = 0.054°C.psu^{-1} [Assur, 1958]. In (D) the horizontal dashed lines are permeability thresholds (5% and 7%) [Golden et al., 2007].

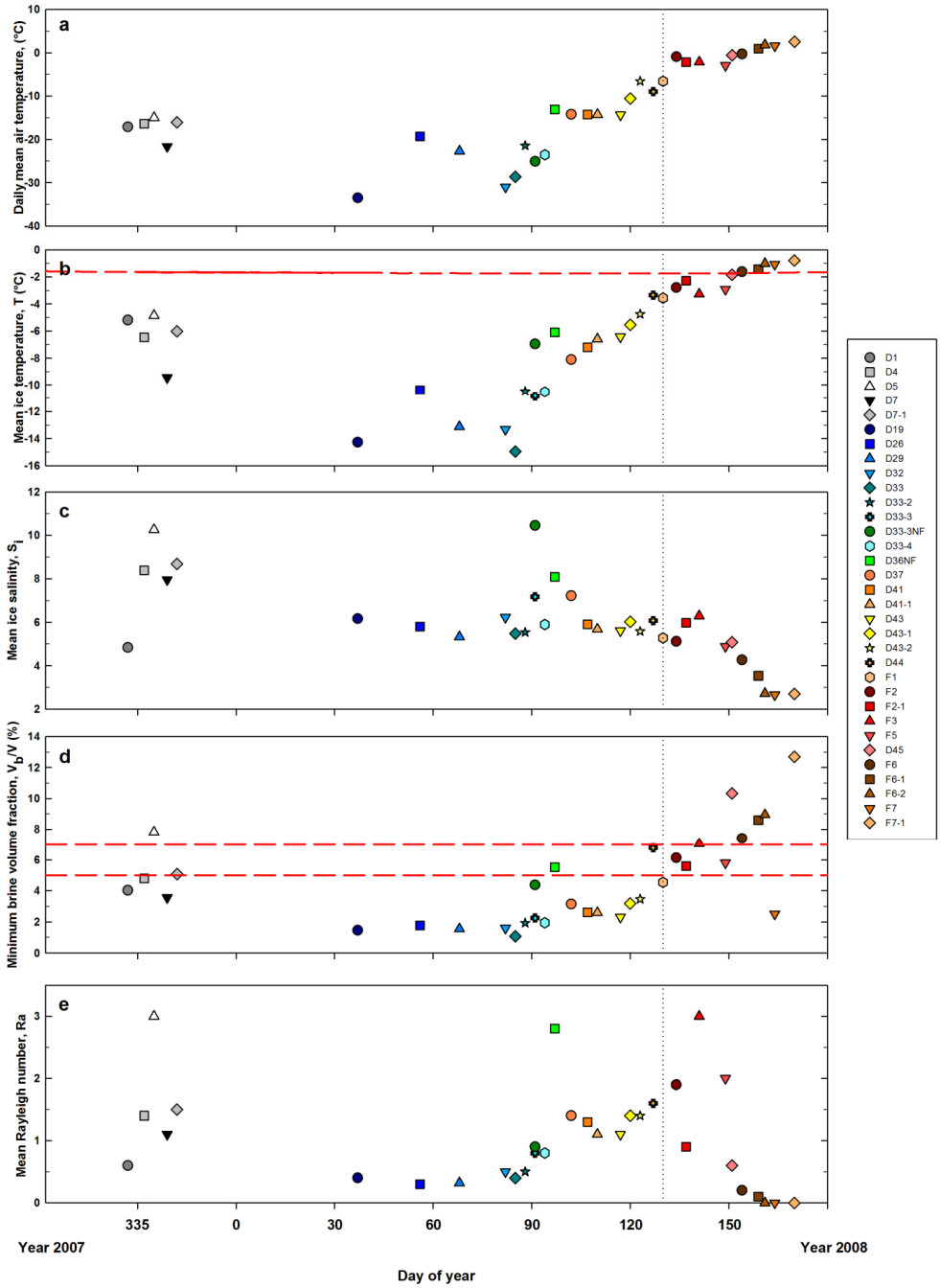

Figure 2.7: The linear relationship (R^2 = 0.87) between the daily mean air temperature and the mean ice temperature recorded at the IPY-CFL stations. The snow depth (cm) measured at each station is indicated next to the icon of each station.

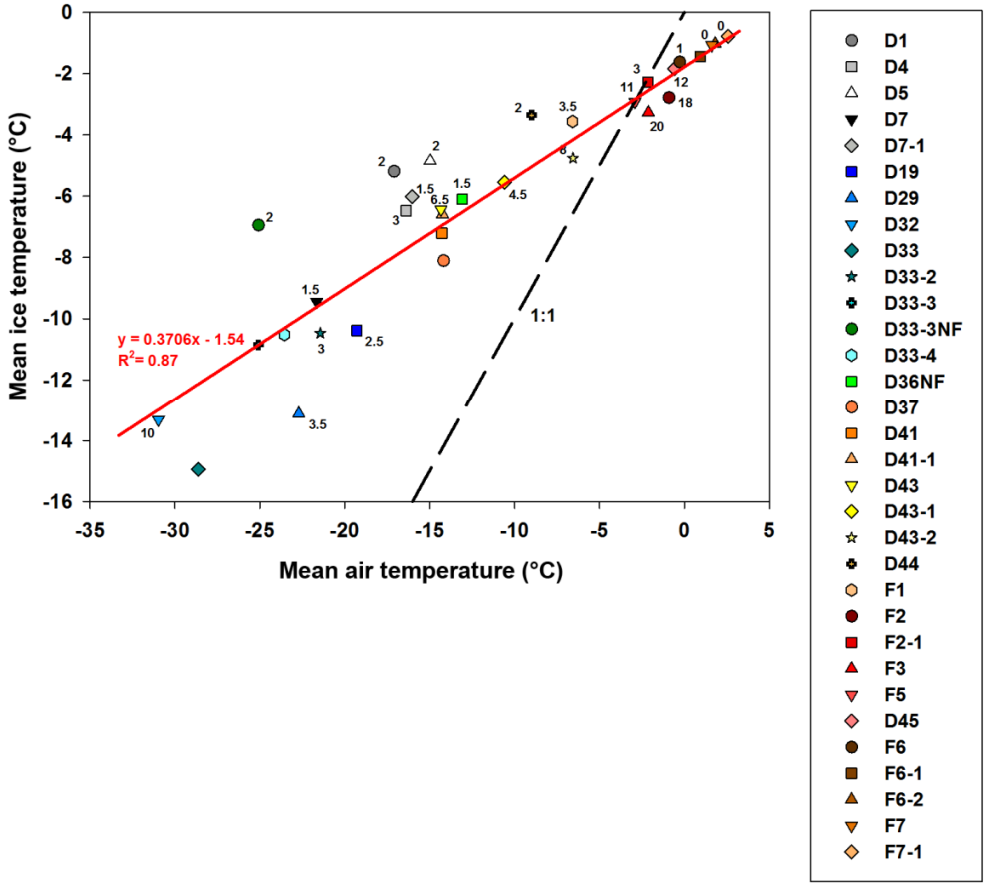

Brine volume fraction was computed from sea ice temperature and bulk salinity using the equations of Cox and Weeks [1983] for ice temperature < -2°C and of Leppäranta and Manninen [1988] for ice temperature ≥ -2°C and assuming thermodynamic equilibrium of the brine with surrounding ice. As sea ice total gas content and sea ice density were not measured, the air volume fraction in the equations was neglected. This approximation is acceptable for the great majority of the stations sampled since the gas volume fraction is usually negligible compared with the brine volume fraction in cold ice [Petrich and Eicken, 2010].

However, for warmer sea ice (ice temperatures > -5°C) the gas volume fraction can represent a significant fraction of the total volume, usually from 0 to 2% [Tison et al., 2002; Rysgaard and Glud, 2004] although extreme values of 13% have been reported [Rysgaard and Glud, 2004]. Hence, the brine volume fractions computed for the warmest stations of this study are probable slight overestimates.

The porous-medium Rayleigh number (Ra) introduced by Notz and Worster [2008] provides a diagnostic criterion for vertical stability within the mushy layer and is used in this study as a proxy for the intensity of brine convection (i.e. gravity drainage). At a depth z (0 at the ice base, positive upwards), it reads:

$$Ra = \frac{\Delta z g \beta (S_b(z) - S_{OC}) \Pi \left(\frac{V_b}{V_{\min}}\right)}{\kappa \eta} \qquad (2.2.)$$

Ra was derived from sea ice temperature and bulk salinity using the following parameters and formulas: g = 9.81 m.s^{-2} is the acceleration due to gravity; $\beta(S_b(z) - S_{OC})$ is the density difference between brine density at a level z and that of seawater at the ice-ocean interface; $S_b(z)$ is the salinity of brine at a depth z diagnosed from temperature, assuming thermal equilibrium using Notz [2005] third-order fit based on the data of Assur [1958]; S_{OC} is the salinity of seawater; β = 0.78 kg.m^{-3}.ppt^{-1} is the haline expansion coefficient of seawater at 0°C [Fofonoff, 1985]; $\Pi \left(\frac{V_b}{V_{\min}}\right)$is the effective sea ice permeability (m^2) computed using the formula of Freitag [1999] as a function of the minimum brine volume fraction (V_b/V_{min}) between the level z and the ice-ocean interface (brine volume fraction is taken from Notz, [2005]); and η = 2.55 x 10^{-3} kg.m.s^{-1} and κ = 1.2 x 10^{-7} m.s^{-2} are, following Notz and Worster [2008], the dynamic viscosity and thermal diffusivity of brine, respectively. Based on experimental studies, Notz and Worster [2009] suggest that for convection to occur, the Rayleigh number must exceed a critical

value, typically 10. Physically, this means that convection only occurs once buoyancy forces due to the vertical brine density gradient expressed in the numerator of Ra overcome dissipation as expressed by the denominator.

We decided to present the depth profiles of brine volume fraction and Rayleigh number (Figures 2.8 and 2.9) since this is, to the best of our knowledge, the first time that both parameters have been computed from ice growth until the start of melt. We added dashed lines representing permeability thresholds of 5% and 7% on each of the brine volume fraction plots (Figure 2.8). The percolation theory was essentially developed for ideal well-aligned columnar ice for which 5% is assumed to be a reasonable permeability threshold [Golden et al., 1998]. Permeability has a strong dependence on the ice microstructure, which is currently not perfectly known. For more complicated ice microstructures the threshold is presumably higher [e.g. Golden et al., 2007]. As revealed by our thin-section pictures analysis (Figure 2.4), most of the ice at the sampled stations was well-aligned columnar ice and a 5% permeability threshold is most probably applicable. However, since we looked at the ice texture and not specifically at the ice microstructure we prefer to consider a range of permeability threshold (5 to 7%) rather than a single value (e.g. 5%). The first sampling period from 28 November 2007 until 13 December 2007 (stations D1 to D7-1) showed brine volume fractions very close to (D1, D4, D7) or just above (D5, D7-1) permeability threshold values, suggesting that some stations were permeable early in the sampling season. As the ice cooled, it became impermeable, with brine volume fractions dropping below 5% at most depths, with the exception of the warmest bottom ice sections (5 to 20 cm). This was observed from 6 February 2008 (station D19) until 11 April 2008 (station D37), with the exception of the recently refrozen lead stations (D33-3NF

and D36NF). The newly formed ice was warmer and more saline. When vertical ice temperature gradients started to slacken on warming, brine volume fractions increased at all depths, exceeding, or being within the range of, permeability threshold values in the bottom half of the ice. This was observed from 16 April 2008 (station D41) until 2 May 2008 (station D43-2). Further warming raised brine volume fractions slightly above 7% at nearly all depths at station D44 (6 May 2008) and well above 7% at all depths at the last drift ice station sampled (D45 on 30 May 2008). Brine volume fractions at the fast ice stations were always above 5%, with the exception of a surface ice layer of station F7 with near-zero salinity. From 9 May 2008 (station F1) until 28 May 2008 (station F5), the brine volume fractions were slightly larger than, or within the range of, permeability threshold values. Brine volume fraction was well above 7% after 2 June 2008 (station F6) and until the end of the sampling season.

Some discussion on the applicability of field-determined Rayleigh number profiles and critical convection thresholds [Notz and Worster, 2009] is required. This became apparent once we realized that our maximum calculated Rayleigh number for this study is 6.1, well below the accepted threshold of 10. Ice coring provides a snapshot of sea ice properties at daily or weekly intervals, while halo-thermodynamic processes can modify the sea ice physical properties within a 24 hour period [Golden et al., 1998; Vancoppenolle et al., 2010]. Vancoppenolle et al. [2010], using their one-dimensional sea ice model, observed that convective instabilities can take several weeks to build, while a critical Rayleigh number can vanish within 2 days. Hence, deriving Rayleigh number from sea ice temperature and bulk salinity using ice cores collected at daily or weekly intervals provides only a glimpse of the actual temporal variations in Rayleigh number. A second sampling

issue relates to the fact that brine is lost through drainage during core extraction, which leads to underestimation of bulk ice salinity [Eicken et al., 1991; Notz et al., 2005]. Based upon comparisons with non-destructive measurements, Notz et al. [2005] found the underestimation in bottom ice salinity to range typically from 1 to 5 (> 20 in some instances). Underestimations in bulk ice salinity of 1 (5) due to ice coring in the lowermost layers lead to differences in Rayleigh number that are > 2 (10). Brine drainage during core extraction is particularly strong in the lower (warm) parts of the cores [Notz et al., 2005] and in high-salinity core sections [Eicken et al., 1991] where brine volume fraction, permeability and hence Rayleigh number are potentially the highest. However, the error in salinity should be of a few tenths at the most when care is taken during sampling (processing cores quickly) and when the ice is colder (e.g. winter). Finally, the Rayleigh number computation relies on several parameters that are not well constrained (e.g. permeability). For all these reasons, the critical convection threshold value of 10 is probably too high when analyzing Rayleigh number profiles obtained from ice core temperature and bulk salinity data. This is confirmed by the low Rayleigh numbers (between 0.1 and 1.9, mean = 0.8, SD ± 0.5) observed in this study in the lowermost layers of growing sea ice where convection is normally expected to occur [e.g. Worster, 1992]. Similar low bottom-ice Rayleigh numbers were reported in field studies in McMurdo Sound, Antarctica, by Gough et al. [2012].

We decided to plot the temporal evolution of the minimum brine volume fraction (V_b/V) and mean Rayleigh number (Ra) in Figure 2.6d and e respectively, and to compare these values with the temporal evolution of the mean bulk ice salinity (Figure 2.6c). Since an impermeable ice layer is enough to prevent full-depth gravity drainage (and hence important desalination), we chose to plot the

minimum brine volume fraction instead of the mean brine volume fraction. Also shown in Figure 2.6d are dashed lines representing permeability thresholds of 5% and 7%. It makes sense to plot both the maximum and mean Rayleigh number; however, since they gave almost exactly the same trends, we chose to plot only the mean. Temporal trends were observed in both parameters, and these trends seem to correspond to the mean bulk ice salinity variations. From station D1 (28 November 2007) until station D43-2 (2 May 2008), the minimum brine volume fraction remained under the permeability threshold and the potential for convection limited to the lowermost layers of the ice. The only trend in the temporal evolution of the mean bulk ice salinity, i.e. the decrease from 13 December 2007 (station D7-1) to 6 February 2008 (station D19), was the result of the increase of the efficiency of drainage at the ice-ocean interface as ice grew thicker (see section 2.4.1.1). As the minimum brine volume fraction increased above 5%, as observed on 6 May 2008 (station D44), the mean Rayleigh number increased significantly, peaking at 3 by 20 May 2008 (station F3). We believe this triggered full-depth gravity drainage, which explains the strong and almost linear decrease in mean bulk ice salinity that we observed from 20 May 2008 (station F3) until 9 June 2008 (station F6-2). Thereafter, desalination stabilized the brine density profiles, decreasing the potential for gravity drainage, as suggested by the decrease in the mean Rayleigh number despite increasing minimum brine volume fraction. Sea ice eventually continued to freshen (bulk salinities approaching 0) through the infiltration of meltwater at the ice surface, as inferred by the $\delta^{18}O$ profile of station F6-1 (Figure 2.5), reducing surface salinities to close to 0. The $\delta^{18}O$ profile of station F6-1 was particularly interesting as it showed the replacement of more negative brine by more positive pure ice melt between 20 and 60 cm depth, a process already described in summer sea ice [Tison et al., 2008].

Figure 2.8: Vertical profiles of brine volume fraction (V_b/V) at the sampling stations. The vertical dashed lines are permeability thresholds (5% and 7%) [Golden et al., 2007].

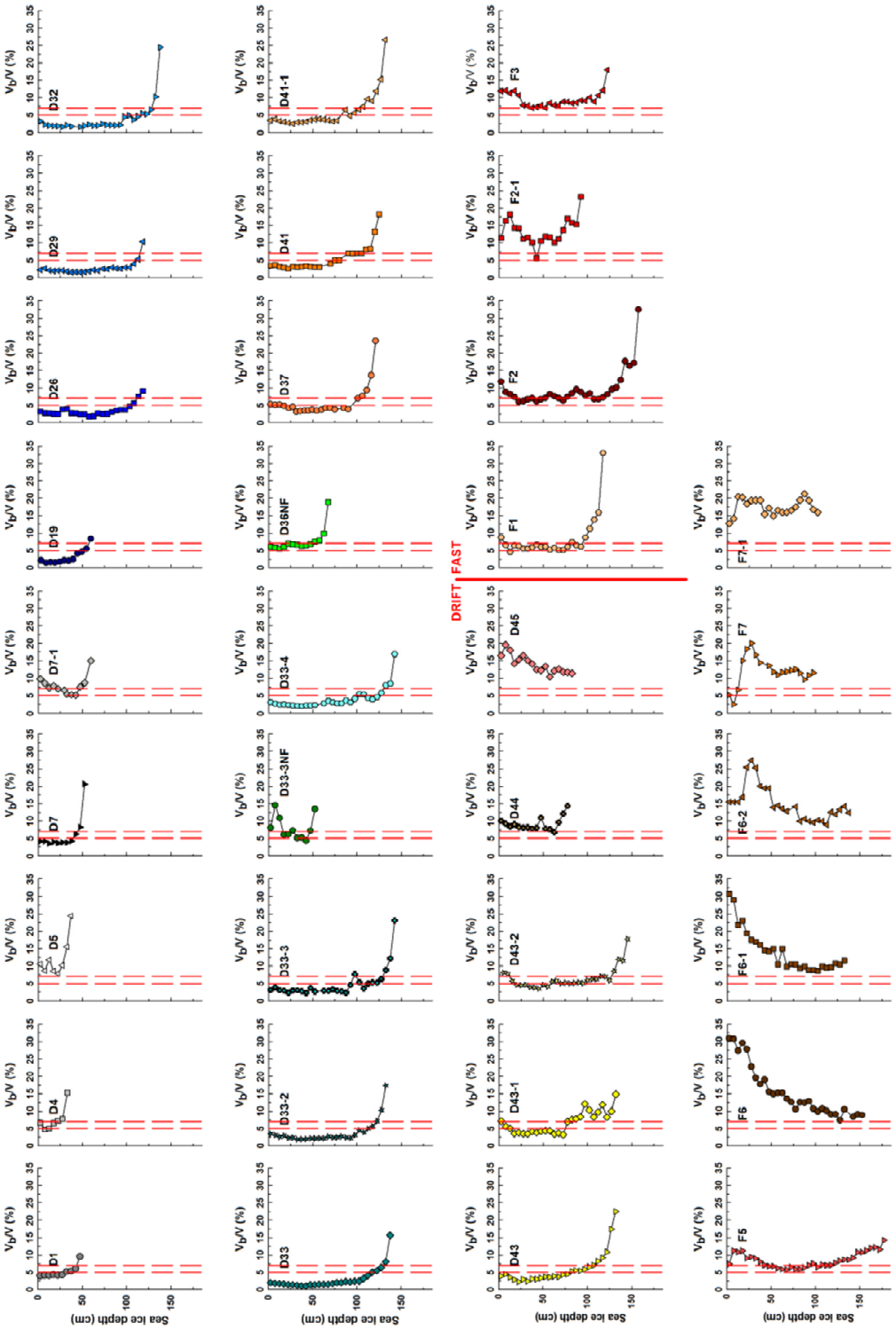

Figure 2.9: Vertical profiles of the Rayleigh number (Ra) at the sampling stations.

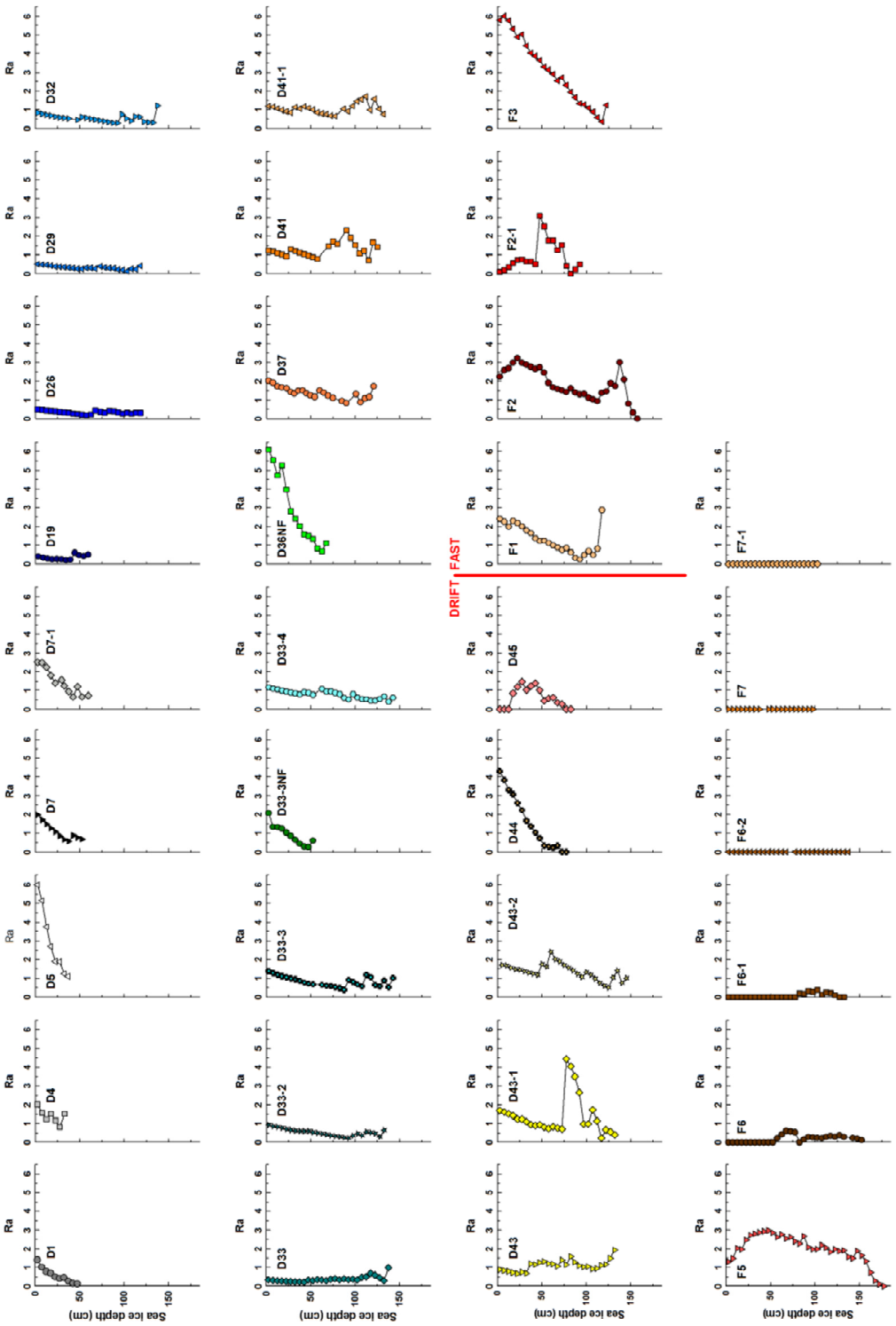

A few stations did not conform to the trends discussed above. Recently refrozen lead stations (D33-3NF and D36NF) had higher mean ice temperatures and bulk ice salinity relative to the other drift ice stations sampled around the same time (April 2008). Sea ice formation in leads at any time of the year is equivalent to restarting an ice growth cycle. Hence, it was not surprising to see that the physical properties of the recently refrozen lead stations were similar to those of the stations sampled in November and December 2007 (D1 to D7-1). Warm ice at stations D5 and D36NF allowed the ice to become permeable early in the season and prone to full-depth gravity drainage (mean Rayleigh number close to 3). Very low mean bulk ice salinity (4.8) was observed at station D1. Coincidentally, the $\delta^{18}O$ values of the upper half section of station D1 (Figure 2.5) were significantly less negative than those of all the other stations. Hence, we suggest that station D1 grew in slightly fresher waters than all the other stations (e.g. waters still influenced by ice melt from the previous melt season or under coastal influence).

2.4.2. Spatial variability

As previously mentioned (section 2.2), this study involved sampling over time within small regions and across great distances, hence the data are subjected to both temporal and spatial variability. We showed in section 2.4.1 (Figure 2.6) that temporal trends in the ice physical properties could easily be identified and linked to atmospheric forcing despite spreading of the stations across the Amundsen Gulf. This suggests that, as long as the ice floes were carefully selected (as was the case during this study; section 2.2.2), the influence of regional spatial variability in the Amundsen Gulf during the IPY-CFL study may be small. That the snow cover thickness showed little variation (Table 2.1) helped to mitigate the effect of spatial variability.

To demonstrate the fact that large-scale (regional) spatial variability was in fact small, we selected three pairs of stations and looked carefully at their ice temperature and bulk ice salinity profiles. The following criteria were used to select the stations: the distance between stations had to be large (a few tens of kilometers), their sampling dates and air temperatures had to be close (within a week and within 2°C) and both fast ice and drift ice stations had to be represented. We ended up with the three groups of data that are presented in Figure 2.10. Depths within the cores were normalized with respect to the total thickness [Eicken et al., 1991]. Criteria used to create the groups are presented in Table 2.2 as well as the standard deviation in mean ice temperature and bulk ice salinity between stations. Standard deviations for both variables were small in all three groups and definitely smaller than the temporal variations described in section 2.4.1. Also, the individual ice temperature and bulk ice salinity profiles are similar between floes (Figure 2.10). Regarding bulk ice salinity, the standard deviation was smaller in group 2 (± 0.1) than in groups 3 (± 0.4) and 1 (± 1.3). This was somewhat expected. Surface seawater properties (as shown by the $\delta^{18}O$ values of under-ice water in Figure 2.5) were likely more variable in the early growth season (group 1). Growth of thick columnar ice and associated drainage limited to the ice-ocean interface (group 2) generates less variability than thin frazil ice growth observed in the first steps of sea ice formation [e.g. Wettlaufer et al., 1997]. It also generates less variability than the strong desalination and surface melting mechanisms occurring later in the season (group 3).

Figure 2.10: Vertical profiles of sea ice temperature (T) and bulk salinity (S_i) for each of the groups defined in section 2.4.2. The curves are drawn through the midpoints of individual sections. Depth scales are normalized to unity.

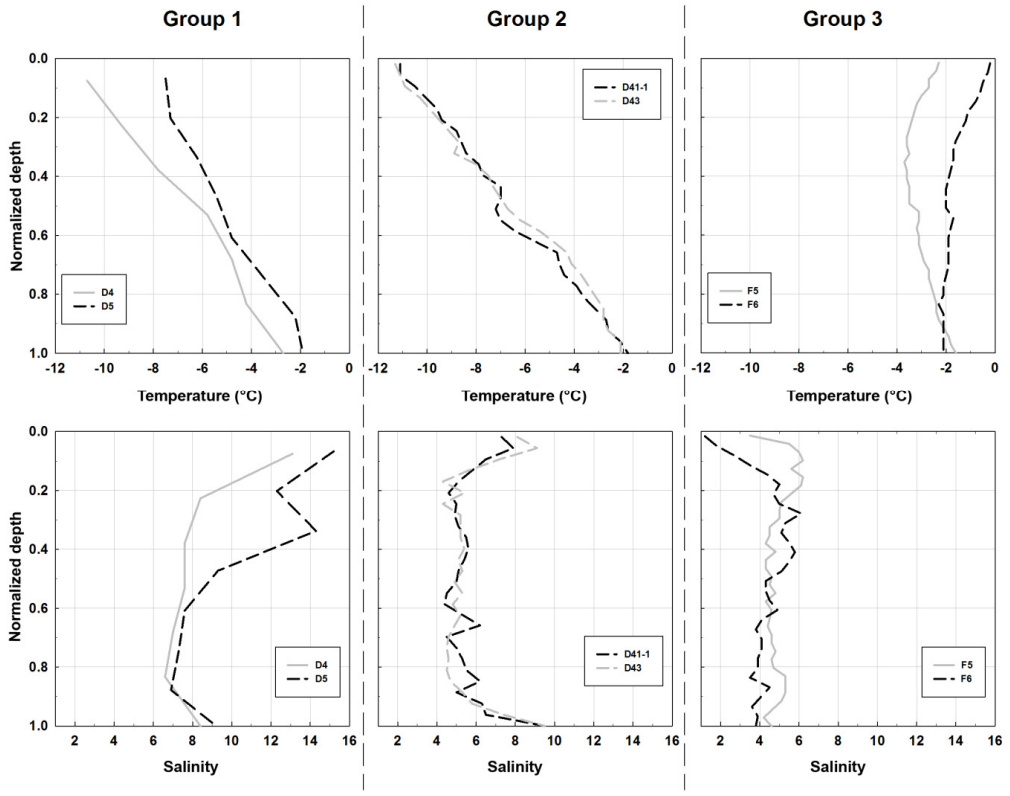

Table 2.2: Spatial variability parameters

	Group 1	Group 2	Group 3
Distance between stations (km)	80	46	690
Air temperature difference between stations (°C)	1.4	0.2	0.2
Elapsed time between stations (days)	3	7	5

	Group 1			Group 2			Group 3		
	St. D4	St. D5	**SD**	St. D41-1	St. D43	**SD**	St. F5	St. F6	**SD**
Mean Ice Temperature T (°C)	-6.5	-4.9	**1.1**	-6.6	-6.4	**0.1**	-2.9	-1.6	**0.9**
Mean Ice Salinity S_i	8.4	10.3	**1.3**	5.7	5.6	**0.1**	4.9	4.3	**0.4**

2.4.3. Sea ice formation and deformation processes during the IPY-CFL study

2.4.3.1. Snow ice and superimposed ice

Most of the stations showed a textural sequence of granular texture overlying columnar texture typical of Arctic first-year ice [Gow and Tucker, 1990]. This sequence usually corresponds to the processes of frazil and congelation ice formation [Weeks and Ackley, 1982]. Granular texture is, however, also associated with the formation of snow ice and superimposed ice. Snow ice forms via the freezing of snow wetted either through flooding or brine wicking and has a fine-grained orbicular granular texture [Massom et al., 1998]. Snow ice can be discriminated from frazil ice through its lower $\delta\,^{18}O$ value [Lange et al., 1990].Very limited (if any) snow ice formed at the IPY-CFL stations, as generally observed in the Arctic where a thin snow cover prevails for much of the year [Petrich and Eicken, 2010]. Conditions favorable to flooding did not develop during the IPY-CFL study since at the maximum the snow cover represented 15% of the ice thickness and the freeboard was always positive (Table 2.1). The $\delta\,^{18}O$ data indicate that only one value (-7.95‰ at station F6-1) was compatible with the formation of snow ice. However, this value was recorded during surface melting and therefore more likely resulted from snow meltwater infiltration. A brine skim could have been present at some stations where frost flowers were observed (D4, D5, D33-3NF and D36NF) since brine skims are known to favor the formation of frost flowers [Perovich and Richter-Menge, 1994]. If so, it only represented a very thin layer most likely scraped off the ice surface prior to coring.

Superimposed ice forms when snow meltwater percolates and refreezes at depth in the snow cover or at the snow-ice interface [Jeffries et al., 1994; Haas et

al., 2001]. As mentioned earlier (section 2.3.3), superimposed ice was removed from the ice surface prior to coring, and its characteristic texture could not be detected in the ice texture analysis. From the snow observations (Table 3.1), we know that superimposed ice formed over a small time window, from station F2-1 (16 May 2008) until station F6 (2 June 2008). This small time window fell between the onset of melting (air temperature close to 0°C at about 9 May 2008; Figure 2.1) and the onset of melt pond formation (station F6, 2 June 2008). However, while being observed over a small time window, superimposed ice layers were occasionally quite thick (1 to 10 cm), representing 18 to 100% (mean = 70%, SD ± 35%) of the total snow cover thickness and 0.5 to 10.0% (mean = 4%, SD ± 4%) of the total ice thickness of the aforementioned stations. These percentages compare well with the percentages measured by Haas et al. [2001] in summer first-year ice in the Weddell Sea, Antarctica.

2.4.3.2. Frazil accumulation vs thermodynamic congelation growth

Based on the preceding discussion, it is reasonable to assume that the great majority of the granular texture in our thin-section pictures was frazil ice. The relative thickness of the granular and columnar texture provides insight into which sea ice formation process (frazil accumulation or thermodynamic congelation growth) dominated at the IPY-CFL stations. We observed congelation growth to have a mean contribution of 95% to the total ice thickness (vs 3% for frazil accumulation) at the three fast ice stations (F1, F2-1 and F7-1). All but two drift ice stations (D1 and D29) showed similar mean percentages (90% vs 7%, excluding the two aforementioned stations). These large contributions of congelation growth compare well with observations from drift ice in the southern Beaufort Sea [Meese, 1989], from fast ice in the Chukchi and Beaufort Seas [Weeks and Gow, 1978] and

from drift ice in the Fram Strait [Tucker et al., 1987]. It is worth noting that in Antarctic platelet ice as much as 75% of the growth of the platelet ice texture can be through congelation [Gough et al., 2012]. Since we could not determine precisely how our platelet and draped platelet texture formed (section 2.4.3.4), we did not add these textures to the congelation growth contribution. Hence, our mean contributions of congelation growth are potentially slightly underestimated.

The amount of frazil ice accumulated before congelation ice starts to grow is a function of the turbulence of surface water. From the mean contributions of congelation and frazil ice, we can deduce that at least three different growth situations occurred during the IPY-CFL study. The great majority of the ice sampled grew in calm surface waters, with congelation ice largely dominating the ice texture. This corresponds well to the low oceanic turbulence and high ice concentration (9 to 10 tenths) observed in the sheltered waters of the Canadian Arctic Archipelago and Amundsen Gulf in winter [Barber et al., 2010]. Some ice grew under extremely calm waters within leads, as illustrated by the 100% congelation ice contribution at station D33-3NF. Finally, some ice grew in more turbulent waters early in the autumn when ice concentrations in the Amundsen Gulf were lower (< 8 tenths) [Barber et al., 2010], as illustrated by the 45% frazil ice contribution at station D1.

2.4.3.3. Sandwiched granular ice layers

Thin layers (1 to 2 cm) of granular ice sandwiched between columnar ice were observed in the near-surface and interior ice of drift ice stations D1, D7, D7-1, D29, D32 and D43. These layers were frazil ice because they consisted of medium to large orbicular granular crystals and their $\delta^{18}O$ values were not overly negative (mean = -1.25‰, SD ± 0.34‰) (Figure 2.5). Frazil ice at depth in the ice

can form through several processes: (1) rafting and ridging, (2) adiabatic supercooling in rising water masses near ice shelves, (3) double diffusion between two water masses of different properties and (4) turbulence in leads [Weeks and Ackley, 1982; Maykut, 1985; Tucker et al., 1987; Lange and Eicken, 1991]. We discount adiabatic supercooling and ridges because we did not sample in the proximity of ice shelves or in areas of ridged ice.

We cannot say for sure that these sandwiched layers did not result from rafting given personal observations of the prevalence of rafting in the study area, as well as documented accounts [e.g. Melling et al., 1993]. However, obvious signs of crystal deformation typical of rafting [Jeffries et al., 1994] were not widely observed. Only station D43 showed a transition from bended or tipped columnar crystals to flattened granular crystals. Also, the physical properties (bulk ice salinity and $\delta\,^{18}O$ signal) of the sandwiched layers did not match those of surface layers, while this usually is the case in rafted ice cores. For example, double C-shaped bulk ice salinity profiles were not observed.

Double diffusion typically takes place in the Arctic in under-ice melt ponds [Eicken, 1994] and in the presence of mixing with river water [Stigebrandt, 1981]. Both processes were unlikely the source of the sandwiched layers since these were observed before melting and no riverine influence (salinity and $\delta\,^{18}O$ signal) was observed in our ice core properties.

The most plausible sources for the sandwiched layers were the leads and cracks regularly observed throughout the sampling season in the Amundsen Gulf [Barber et al., 2010]. Frazil crystals formed within a lead through turbulence could have stirred below adjacent floes or, after the refreeze of the lead, risen back to the bottom of the ice cover with congelation growth resuming after that [Martin,

1981]. Also, double diffusion could have occurred through thermohaline convection around intense brine plumes generated by the refreeze of ice cracks [Martin, 1974].

2.4.3.4. Platelet ice layers

Unusual textural features were observed during this study: (1) a thin layer of platelet ice (Figure 2.4e) at the bottom of stations D29 and F2 and (2) a thick layer of draped platelet ice (Figure 2.4d) in near-surface ice of station D29. Platelet ice forms through unrestrained frazil ice nucleation and growth [Jeffries et al., 1993] and is usually associated with ice shelves and the ice pump mechanism [Lewis and Perkin, 1983]. In the Arctic, where large ice shelves are missing, platelet ice is very scarce and is usually associated with under-ice melt ponds [Eicken, 1994; Jeffries et al., 1995]. Platelet ice in this study was found before the onset of melt pond formation.

According to Jeffries et al. [1995], platelet ice in the Arctic can form through three additional processes: (1) anchor ice formation, (2) double diffusion between two water masses of different properties and (3) a small-scale ice pump involving leads and pressure ridges. We discount anchor ice formation since water depths recorded at the IPY-CFL stations (> 100 m) exceeded depths at which anchor ice forms [Reimnitz et al., 1987] and since no sediments were found in our cores. Double-diffusion processes have already been discussed in section 2.4.3.3 for the sandwiched layers and it is likely that the same processes were also the source of the platelet layers. Alternatively, platelet ice could have formed through a small-scale ice pump that operates as follows. Cold and salty water from the surface of a lead warms as it moves downwards. This water melts a small amount of ice when passing under a ridge, resulting in a layer of water fresher than surrounding waters. This layer, now at its freezing point at depth, rises and eventually becomes

adiabatically supercooled with potential formation of platelet crystals [Jeffries et al., 1995]. Numerous leads and ridges were observed in the Amundsen Gulf throughout the sampling season [Barber et al., 2010]. However, ridges were always located > 500 m from our sampling sites.

Platelet ice was found in only 2 of the 16 cores selected for textural analyses. Hence platelet ice formation was probably not widespread in the Amundsen Gulf during the study, which compares well with previous Arctic first-year ice observations [Jeffries et al., 1995]. However, the mean contribution of platelet ice to the total ice thickness at station D29 (20%) suggested that this formation process was locally significant.

2.5. Conclusion

We have reported sea ice temperature and bulk salinity measurements from 33 stations sampled in the southern Beaufort Sea-Amundsen Gulf from November 2007 until June 2008 during the IPY-CFL study. This represents a significant dataset covering a complete cycle from growth to the start of melt. We provide this dataset in a spreadsheet in the supplementary material (http://www.igsoc.org/hyperlink/12j148/). It represents a useful tool for the IPY-CFL community but also for future experiments in the southern Beaufort Sea-Amundsen Gulf and is a good basis for model validation.

We used this large dataset to investigate the halo-thermodynamic evolution of sea ice. The following trends were observed. There was a strong linear relationship (R^2 = 0.87) between the mean sea ice temperature and the mean air temperature and no correlation (R^2 = 0.01) between the deviations from the linear relationship and the snow thicknesses measured at the stations. This is because

the snow cover was typically thin and consisted most of the time of wind slab layers, which have the highest thermal conductivity of all snow types [Sturm et al., 1997]. The evolution of the mean sea ice bulk salinity showed a strong desalination phase occurring over a very small time window (from 20 May 2008 until 9 June 2008). During this phase, the mean sea ice bulk salinity dropped from 6.0 to 2.6. We suggested this phase corresponded to full-depth gravity drainage initiated by the restored connectivity of the brine network with warming in the spring. We investigated this by calculating a proxy of sea ice permeability, the brine volume fraction, and a proxy of the intensity of brine convection, the Rayleigh number. We observed that the desalination phase started immediately after the minimum brine volume fraction rose above the permeability threshold (5 to 7%) and immediately after the mean Rayleigh number peaked at a value of ~ 3.

This is, to the best of our knowledge, the first time these two proxies have been calculated from field measurements over such a long period of time. Both proxies have been used successfully in controlled ice growth experiments and simulations [e.g. Wettlaufer et al., 1997; Vancoppenolle et al., 2006; Notz et al., 2009]. This study demonstrates their ability to explain sea ice bulk salinity trends in field measurements. Nevertheless, sampling issues related to ice coring force the reconsideration of the critical convection threshold value ($Ra > 10$) proposed by Notz and Worster [2009]. In the lowermost layers of growing sea ice where convection is normally expected to occur frequently, our data suggest looking for a critical Rayleigh number between 0.1 and 1.9 (mean = 0.8, SD ± 0.5). Considering full-depth gravity drainage, we found that a mean Rayleigh number of 3 (and maximum Rayleigh number of 6) preceded a strong desalination phase. While uncertainties certainly remain about the real critical value, we showed that

the Rayleigh number could at least be used as a qualitative indicator of convection. Since we presented the temporal evolution of physical parameters sampled from stations dispersed over the southern Beaufort Sea-Amundsen Gulf, we also briefly discussed spatial variability. We showed that as long as the ice floes were carefully selected, the influence of regional spatial variability in the Amundsen Gulf during the IPY-CFL study was small and therefore did not represent any obstacle to time series studies.

Finally, we investigated sea ice textural properties using thin-section picture analysis. This analysis shed light on the sea ice formation and deformation processes in the southern Beaufort Sea-Amundsen Gulf during the IPY-CFL study. Most stations had a typical Arctic textural sequence of granular (frazil) ice overlying columnar (congelation) ice. Formation of snow ice was not observed. Superimposed ice formed over a small time window between the onset of melting (~ 9 May 2008) and the onset of melt pond formation (2 June 2008) and sometimes had significant thicknesses representing 0.5 to 10.0% of the total ice thickness. The mean relative contribution of congelation and frazil ice (95% vs 3% and 90% vs 7% for fast ice and drift ice, respectively) indicated that sea ice grew mostly in calm conditions. We showed that unusual textural features also could have formed locally. Sandwiched granular ice layers, platelet and draped platelet ice were all observed. We suggested that these unusual textures resulted from turbulence in leads and double diffusion around intense brine plumes generated by the refreeze of ice cracks. However, this needs to be confirmed by further investigations.

2.6. Insights gained about the DMS cycling in sea ice

This thorough characterization of the seasonal evolution of brine dynamics and sea ice growth processes in natural sea ice provides a very useful framework

to investigate the impact of sea ice physics and thermodynamics on the DMS cycle in sea ice. This will be performed in the two next chapters.

Sea ice permeability controls the vertical mobility of solutes within sea ice. Restored connectivity of the brine network allows compounds such as DMS,P,O (either in the dissolved fraction or contained within sympagic organisms) to move away from their initial sites of production. This can be crucial for instance for the migration of DMS produced in productive bottom ice communities towards the surface of the ice where it can potentially be exchanged with the atmosphere. Full-depth gravity drainage events have the potential to release a significant fraction of the sea ice DMS pool to the under-ice water. The timing of these events is crucial to understand the seasonal and vertical variability of DMS,P,O concentrations in sea ice and for the fate of the important sea ice DMS pool.

Through this study, we described the seasonal evolution of sea ice permeability and brine dynamics in sea ice samples that will be compared to the seasonal evolution of DMS,P,O concentrations in the same samples (see Chapter 3). We assessed the timing of the restored connectivity of the brine network and of the occurrence of full-depth gravity drainage events from changes in sea ice temperature and bulk salinity profiles. We validated the use of two proxies (brine volume fraction and Rayleigh number), that can be easily computed in sea ice studies, to track these full-depth gravity drainage events and commented on the critical values that should be considered when using these proxies in natural sea ice. Recommendations on the use of these proxies are very important for future sea ice DMS studies (e.g. Chapter 4).

This study also provides a thorough description of the seasonal evolution of the surface properties of the ice cover (e.g. onset of melt ponds formation,

superimposed ice formation). A good understanding of these properties is crucial if we want to estimate the potential release of DMS from the sea ice biome to the atmosphere (see Chapter 3). Superimposed ice formation has been shown for example to represent an impermeable layer blocking gaseous exchanges with the atmosphere.

Chapter 3

Temporal and vertical variability of DMS,P,O concentrations in Arctic first-year sea ice (Amundsen Gulf, Canada): evidence for photo-chemical oxidation of DMS in surface ice

To be submitted to Journal of Geophysical Research - Oceans

Gauthier Carnat[1], Jean-Louis Tison[2], Gaelle Gilson[2], Bruno Delille[3], Frédéric Brabant[2], Maurice Levasseur[4], Nicolas-Xavier Geilfus[1], and Timothy Papakyriakou[1]

[1]Centre for Earth Observation Science, Department of Environment and Geography, University of Manitoba, Winnipeg, Manitoba, Canada

[2]Université Libre de Bruxelles, Laboratoire de Glaciologie, 50 Av. F.D. Roosevelt, 1050 Bruxelles, Belgium

[3]Unité d'Océanographie Chimique, Université de Liège, Liège, Belgium

[4]Département de biologie, Université Laval, Québec, G1V 0A6, Québec, Canada

Abstract

The cycling of dimethylsulfide (DMS) and its related compounds dimethylsulfoniopropionate (DMSP) and dimethylsulfoxide (DMSO) in sea ice remains poorly understood. This study presents the first combined measurement of the concentration of the three dimethylated compounds in Arctic sea ice samples. We characterize the temporal and vertical variability of the compounds in the Amundsen Gulf during an annual cycle of ice growth (November 2007 - June 2008). Concentrations showed a strong seasonal pattern. Low but non negligible concentrations were found in late-autumn ice. Very high concentrations of DMS (769 nM), DMSP (2174 nM), and DMSO (5427 nM) were observed in spring bottom ice and corresponded to the development of a diatom-dominated bloom (655 µg of chl*a*.L^{-1}). DMSO was shown to dominate the total dimethylated sulfur pool, contrasting with oceanic waters and Antarctic sea ice observations. Depth profiles of the relative proportion of DMSO showed different patterns. During the spring bloom and under a thick snow cover (> 18 cm), highest percentages of DMSO were observed in the bottom half of the ice (70-98%). During the other seasons and when little snow cover prevailed (< 3cm), highest percentages of DMSO were observed in surface ice (66-100%), decreasing with depth. Strong linear relationships (R^2 = 0.4-0.7) between the relative proportion of DMSO and depth-attenuated spectral irradiance (400-450 nm), associated with very low chl *a*, suggested strong photo-chemical oxidation of DMS in surface ice. This process could represent a significant loss pathway of DMS in Arctic sea ice, and should therefore be taken into account in estimates of the contribution of the sea ice biome to regional DMS emissions.

3.1. Introduction

The volatile organic compound dimethylsulfide (DMS) is the dominant biogenic sulfur compound in the oceans [Lovelock et al., 1972] and the main contributor to the global biogenic sulfur flux to the atmosphere [Bates et al., 1992; Kettle and Andreae, 2000]. Oceanic DMS is mainly produced by the enzymatic cleavage of the algal metabolite dimethylsulfoniopropionate (DMSP), which synthesis strongly depends on algal abundance, algal community composition, and various environmental stressors [Keller et al., 1989; Stefels et al., 2007]. Once released in the atmosphere, DMS is oxidized in acidic aerosol sulfates that can potentially cool the climate by scattering and absorbing solar radiation and promoting the formation of cloud condensation nuclei (CCN) [Charlson et al., 1987; Malin, 1997]. If the existence of a significant global scale effect of marine DMS emissions has recently been heavily challenged [Zuidema et al., 2008; Small et al., 2009; Quinn and Bates, 2011], model simulations [Woodhouse et al., 2010] and field observations demonstrated that DMS-derived aerosols could nonetheless exerts a non-negligible influence on local climate in remote oceanic areas, such as the Arctic Ocean [Leck and Person, 1996; Korhonen et al., 2008; Chang et al., 2011].

In regard to the Arctic, the potential cooling effect of marine DMS emissions is particularly relevant in the recent context of rapid warming [Blunden and Arndt, 2013; Levasseur, 2013]. There is a pressing need to determine if the dramatic and ongoing thinning, warming and retreat of the sea ice cover [Kwok et al., 2009] will ultimately lead to an increase of marine DMS emissions which could partly mitigate the effect of the ice-albedo feedback [Levasseur, 2013]. The few Arctic DMS models currently available all point towards an increase of the DMS emissions in

the near future [Gabric et al., 2005; Qu and Gabric, 2010]. These models are largely based on the reasonable assumption that DMS ventilation to the atmosphere will be significantly facilitated by the removal of the sea ice cover, which partially impedes the exchanges between the ocean and the atmosphere, and by the increase in the lead and melt pond fractions [Nilsson et al., 2001; Leck et al., 2002]. However, the magnitude of future DMS emissions will also greatly depend on the future net DMS production by the Arctic microbial food web, which is currently not well constrained in the models [Levasseur, 2013]. Major shifts in algal abundance [Arrigo et al., 2008], community composition [Merico et al., 2003; Hegseth and Sundfjord, 2008; Galí and Simó, 2010], and environmental stressors (e.g. increase in light exposure [Taalba et al., 2013] and ocean acidification [Archer et al., 2013]) are all expected (and sometimes already observed) to occur with warming and sea ice loss. The nature and magnitude of these shifts, as well as their influence on the net DMS production, remain however largely unknown [Levasseur, 2013]. Furthermore, the contribution of the sea ice biome itself to Arctic DMS emissions has yet to be accurately quantified. This quantification requires a good understanding of the DMS cycle in sea ice and a good understanding of the dynamics of DMS,P exchanges at the atmosphere-ice-ocean interfaces.

The DMS cycle in sea ice, consisting of a complex web of biochemical processes [Yoch, 2002; Stefels et al., 2007], remains poorly constrained. We know that the high DMSP concentrations observed in Arctic sea ice [Levasseur et al., 1994; Lee et al., 2001] probably result from a combination of high algal biomass and intense environmental stresses in the sea ice habitat, notably very low temperatures and high salinities. Indeed, acknowledged physiological functions of DMSP include cryoprotection [Karsten et al., 1996] and osmoregulation [Dickson

and Kirst, 1986]. We also suspect that a fraction of intracellular DMSP (particulate $DMSP_p$) is transformed to extracellular DMSP (dissolved $DMSP_d$) and subsequently to DMS in brine, with sometimes very short turnover times, as observed by Asher et al. [2011] in the Antarctic. Whether the transformation of $DMSP_p$ to $DMSP_d$ in brine is mainly the result of active exudation or cell lysis during senescence, grazing or viral attack has yet to be assessed. Certainly the opening and widening of brine channels on warming, increasing the grazing activity, and the decrease in salinity on melting provide favorable conditions for the release of intracellular DMSP [Trevena and Jones, 2006; Delille et al., 2007]. Similarly to DMSP, DMS is present in high concentrations in Arctic sea ice [Levasseur, 2013], but the proportion of $DMSP_d$ cleaved, as well as the respective contribution of algal and bacterial DMSP-lyases remain undetermined. Furthermore, very little is known about the DMS loss pathways in sea ice. Bacterial oxidation to dissolved dimethylsulfoxide ($DMSO_d$) [Kieber et al., 1996; del Valle et al., 2009] could be significant because of the important bacterial biomass generally observed in the sea ice habitat. Also, photo-chemical oxidation to $DMSO_d$ [Brimblecombe and Shooter, 1986] could be strongly stimulated by the high light levels in surface ice during the spring/summer seasons. Meanwhile, bacterial DMSO reduction to DMS has been identified as a major pathway of DMS production in Antarctic sea ice brine [Asher et al., 2011], and high concentrations of $DMSO_p$ (particulate DMSO) have been found in Arctic ice algal communities [Lee et al., 2001]. $DMSO_p$ has been hypothesized to exert several physiological functions similar to those of $DMSP_p$ [Lee and de Mora, 1999], yet its primary function in ice algal cells remains unresolved [Lee et al., 2001]. One very stimulating hypothesis suggests that DMSP, DMS and DMSO could be involved in an oxidation cascade that would scavenge hydroxyl radicals and other reactive oxygen species, thereby preventing

oxidative stress in cells [Sunda et al., 2002]. Strong oxidative stresses in ice algal cells could for example arise in response to high light levels in surface ice and very high oxygen concentrations in blooming conditions [Delille et al., 2007].

The first step to test the validity of the various hypotheses described above is to track the temporal evolution of the three dimethylated compounds (DMS, DMSP, DMSO) in natural sea ice. Unfortunately, accurate and simultaneous quantification of DMS, DMSP and DMSO has long remained impossible in sea ice samples. The hypo-osmotic shock undergone by organisms during the melting of ice samples can lead to strong modifications of the cells physiology and even to cell lysis [Garrison and Buck, 1986], triggering artificial release of $DMSP_p$ and artificial conversion of $DMSP_d$ to DMS by exoenzymes [Stefels et al., 2012]. Hence, in pioneer studies of the sea ice DMS cycle [Levasseur et al., 1994; Bouillon et al., 2002], concentrations are typically reported as total DMS + DMSP. Fortunately, various reliable procedures have recently been developed to circumvent melting biases [Trevena and Jones, 2006; Tison et al., 2010; Stefels et al., 2012]. Thawing in acidic conditions has helped to prevent the artificial conversion of $DMSP_d$ to DMS [Trevena and Jones, 2006] but not the artificial release of $DMSP_p$ [Kiene et al., 2007]. Thawing with addition of differently deuterated isotopes of DMS and DMSP has given an opportunity to monitor the potential transformation of the dimethylated compounds [Stefels et al., 2012]. Fast and simple, the dry-crushing technique, in which a frozen ice sample is reduced to powder by impacts with stainless-steel marbles in a gas-tight container, has allowed to extract DMS directly from the ice matrix without melting [Tison et al., 2010; Stefels et al., 2012]. Comprehensive field studies taking advantage of these methodological developments remain unfortunately very scarce and were exclusively conducted

in Antarctic [Trevena and Jones, 2006; Tison et al., 2010]. Similar studies in the Arctic are definitely required. Indeed, since there are many ecological and environmental differences between Arctic and Antarctic sea ice, one could expect the DMS cycle to be substantially different in the two biomes.

The dynamics of DMS,P exchanges at the atmosphere-ice-ocean interfaces also require further attention. We know that ice algae and dissolved sulfur compounds can be released to oceanic waters during melting and ice break-up, and we suspect that these releases considerably boost the DMS concentration in ice edge waters [Levasseur et al., 1994; Elliott et al., 2012]. The magnitude and timing of these releases, as well as their impact on DMS emissions, are currently poorly estimated. Levasseur et al. [1994] calculated a tenfold increase of Arctic DMS emissions upon ice break-up. However, as acknowledged by the authors, this calculation was based on several approximations. For example, the DMS concentration in sea ice was not measured but fixed to 20% of the total DMS + DMSP pool, and the release of DMS was assumed to occur in only one single step. We also learned from Antarctic observations in recent years that ice algae and dissolved sulfur compounds could be released to oceanic waters before melting through brine drainage [Tison et al., 2010; Carnat et al., in revision]. Furthermore, DMS could be directly emitted from the ice surface to the atmosphere [Zemmelink et al., 2008a; Nomura et al., 2012]. Little is known about these two processes in the Arctic. A parallel measurement of the temporal evolution of sea ice halo-thermodynamic properties and DMS,P concentrations could definitely improve our understanding [Tison et al., 2010]. Indeed, the migration of sulfur compounds across and within sea ice is dictated by its permeability [Tison et al., 2010]. This permeability is controlled by the connectivity of brine inclusions which strongly

varies seasonally with ice temperature and salinity [Eide and Martin, 1975; Golden et al., 1998].

In this study, we present the first combined measurement of DMS, DMSP and DMSO (DMS,P,O) concentrations in first-year Arctic sea ice. Using the dry-crushing technique, we analyze 4 drift ice cores and 2 fast ice cores collected aboard the icebreaker CCGS Amundsen in the Amundsen Gulf (Canadian Arctic), in the framework of the large and multidisciplinary International Polar Year Circumpolar Flaw Lead (IPY-CFL) System Study [Barber et al., 2010]. We provide a picture of the vertical variability of the sea ice dimethylated sulfur pool across seasons, from growth (November 2007) to the start of melt (June 2008). We address the trends observed in the general biological and environmental context of the IPY-CFL study to identify drivers of the Arctic sea ice DMS cycle.

3.2. Methods

3.2.1. Study area and sampling strategy

The collection of samples was conducted aboard CCGS Amundsen in the Amundsen Gulf (Figure 3.1) between 28 November 2007 and 18 June 2008, as part of the International Polar Year Circumpolar Flaw Lead (IPY-CFL) System Study [Barber et al., 2010]. The goal of the IPY-CFL study was to organize a multi-disciplinary sampling program overwintering in the Amundsen Gulf. The Amundsen Gulf is a relatively deep (50 to 500 m depth) coastal shelf region that connects the Beaufort Sea to the Canadian Arctic Archipelago. Sea ice climatology in the Amundsen Gulf is highly variable [Galley et al., 2008]. Typically, seasonal ice begins to form in mid-October in shallow near-shore areas as fast ice, while a drift ice regime with transient leads dominates offshore. In some years, the whole ice cover becomes fast ice in most of the Amundsen Gulf later in the winter, and a

fast ice edge develops between Cape Perry and Banks Island (Figure 3.1). A large area of open water, known as the flaw lead system, is maintained until break-up, between the fast ice edge and the mobile Beaufort Sea pack ice which rotates with the Beaufort Gyre [Galley et al., 2008]. Sea ice retreat usually begins in early June, progressing eastwards and forming the feature known as the Cape Bathurst polynya. The initial plan of the IPY-CFL study was to establish a semi-permanent ice camp along the fast ice edge, and to conduct transects with the ship in the flaw lead system [Barber et al., 2010]. However, in 2007-2008, strong easterly winds kept the ice cover mobile in the Amundsen Gulf throughout the winter and spring and the sampling strategy had to be adjusted. From 26 October 2007, date of the ice freeze-up, until ice break-up during the first week of May 2008 [Barber et al., 2010], the ship was constantly repositioned in the Gulf for safety and logistical reasons. Typically, the ship was either stationing in large drifting ice floes south of Banks Island (Figure 3.1) or transiting through small short lasting leads. Right after ice break-up in the central Amundsen Gulf, the ship successively visited two fast ice areas located in two sheltered bays: Franklin Bay and Darnley Bay (Figure 3.1). The extent of these fast ice areas on 5 May 2008, drawn from the Canadian Ice Service sea ice charts, is shown in Figure 3.1. Sea ice sampling was stopped on 18 June 2008, a few days before the ice break-up in the Bays [Hop et al., 2011].

Figure 3.1: A. Map of the study area showing the bathymetry and the location of the sampling stations. The dotted lines indicate the extent of fast ice on 5 May 2008. Data for fast ice extent delimitation were obtained from the Canadian Ice Service sea ice charts. B. Air temperature and photosynthetic active radiation (PAR) recorded during the IPY-CFL study. The sampling stations icons are plotted on temperature series of air temperature and PAR measured with, a Rotronics MP 101A temperature sensor located at ~ 18 m above the ice surface with a resolution of 0.1°C and an accuracy of ± 0.3°C, and a PARLite™ quantum sensor Kipp and Zonen® located on a tower at the bow of the ship.

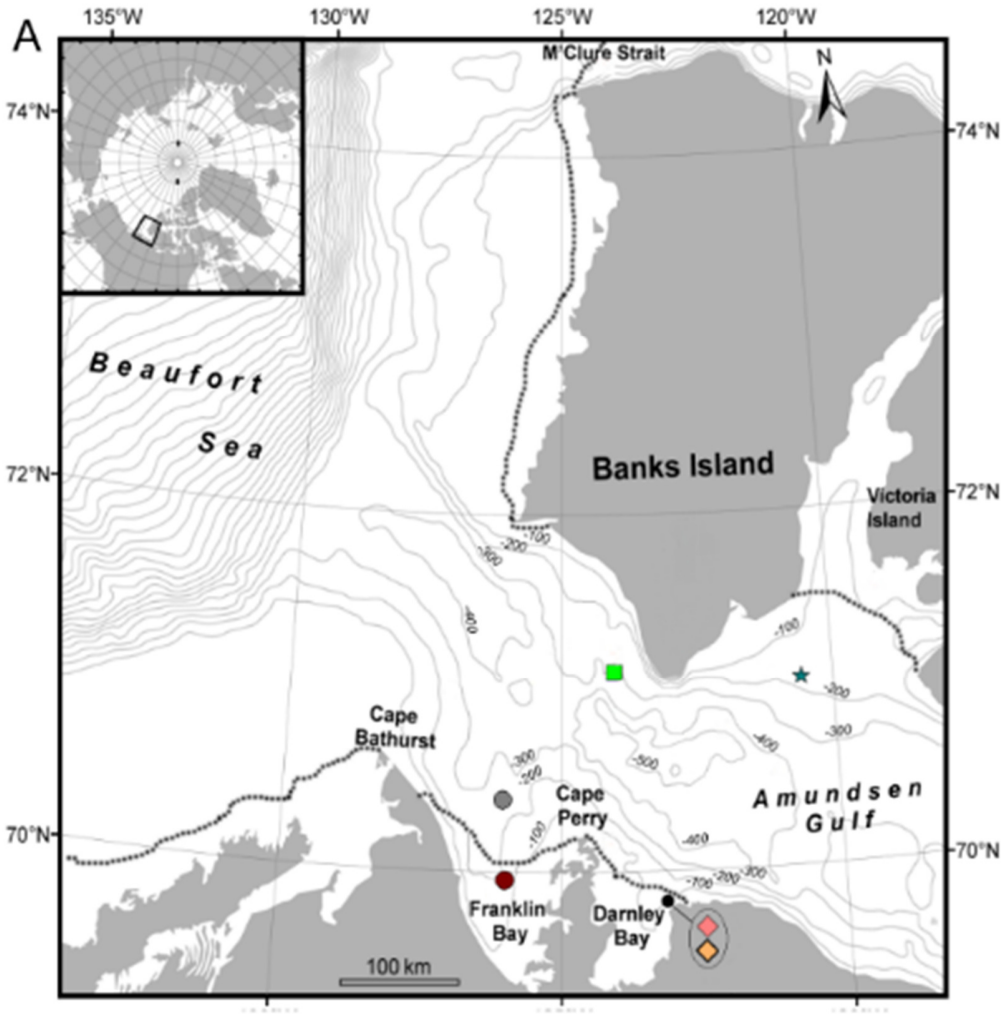

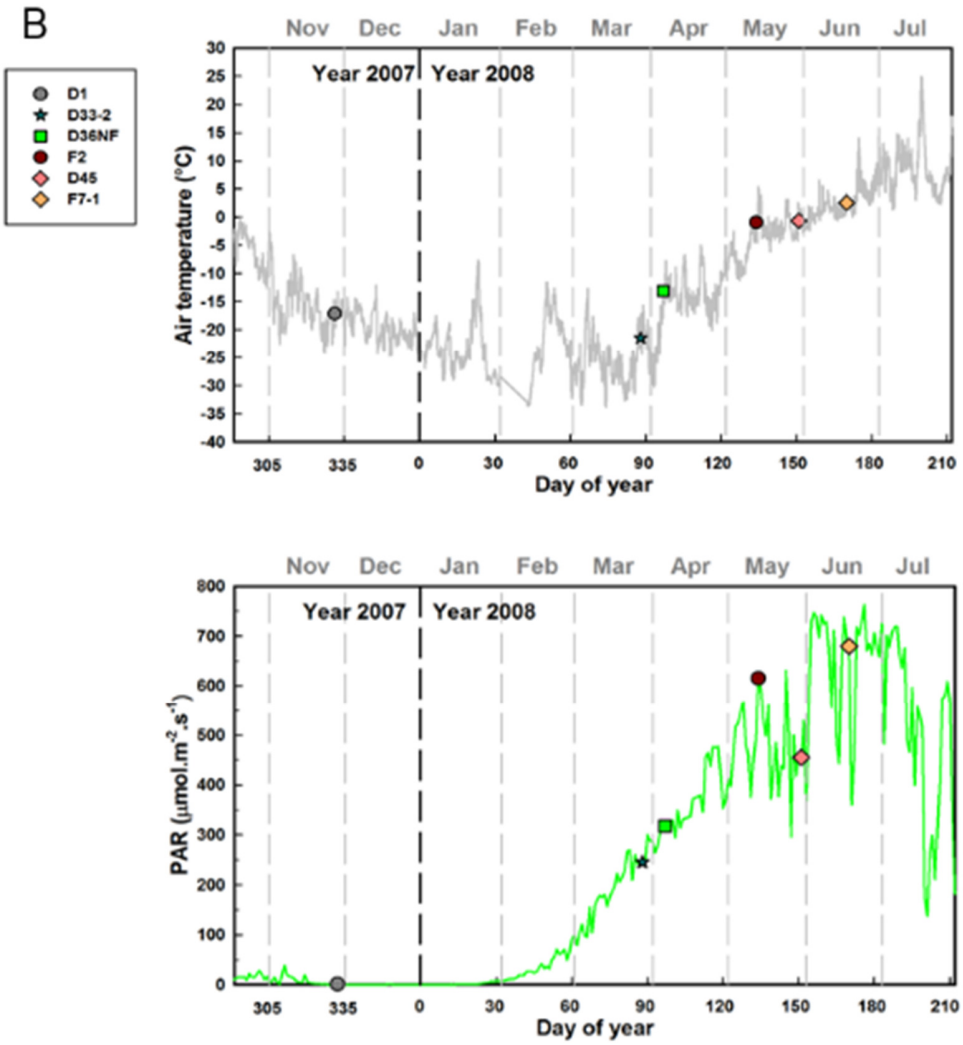

During the IPY-CFL study, we collected samples at 4 drift ice sites and 2 fast ice sites. Each of these sampling sites is referred to as a station in this study. We sampled one single ice floe at each station during one day. The location of these stations is shown in Figure 3.1. Stations are identified in the IPY-CFL community by a letter (D for drift ice, F for fast ice) and a number (ID of the site). One of the drift ice stations consisted of sea ice that had recently formed in a refrozen lead. In that case, NF (newly formed) letters were added to the ID of the station (D36NF). The general ice and surface conditions of the sampling stations

is reported in Table 3.1. All the stations sampled were first-year sea ice. Since the stations were sometimes separated by tens, or even hundreds of kilometers (Figure 3.1), one should bear in mind that the results presented hereafter integrate both temporal and spatial variability.

Table 3.1: General ice and surface conditions of the sampling stations. The horizontal line separates drift ice stations from fast ice stations. NS: new snow; FF: frost flowers; WS: wind slabs; SU: superimposed ice; MP: melt ponds; nd: not determined.

Station ID	Date	Sea ice type	Ice Thickness (cm)	Snow Cover (cm)	Freeboard (cm)
D1	28 Nov 2007	Drift Ice	51	2 (NS)	3
D33-2	28 Mar 2008	Drift Ice	150	3 (WS)	10.5
D36NF	6 Apr 2008	Refrozen Lead	68	1.5 (FF)	7
D45	30 May 2008	Drift Ice	82	12 (NS 2, SU 10)	9
F2	13 May 2008	Fast Ice	160	18 (NS 9, WS 9)	14
F7-1	18 Jun 2008	Fast Ice	103	0 (MP)	12

3.2.2. Sample collection

On each ice floe visited, flags were used to delimitate a pristine sampling area of approximately 25 m^2. The sampling area was always located as far away, and upwind, from the ship as possible to avoid any contamination from the smoke stack, or from other activities conducted on the research vessel. Particular attention was paid to select an area with a homogeneous snow cover. Within the pristine sampling area, a set of ice cores was collected using an electropolished stainless-steel corer (Lichtert Industry®, Belgium) (ID = 7 cm) for various biogeochemical analyses. Cores were immediately wrapped in polyethylene bags, and stored horizontally in an insulated box pre-filled with cold packs frozen at -30°C to limit artificial brine drainage and gas diffusion [Cox and Weeks, 1986], and to limit the physiological activity of ice algae. Cores were brought back to the cold

storage room of the ship (-26°C) directly after sampling, which generally lasted less than two hours.

3.2.3. Analysis

3.2.3.1. Background measurements

Two of the ice cores collected at each station were analyzed for halo-thermodynamical (sea ice temperature, bulk salinity, brine volume fraction and Rayleigh number) and textural properties. Details on the methodology can be found in a companion paper [Carnat et al., 2013]. One ice core was dedicated to chlorophyll *a* (chl *a*) measurements. The ice core was sliced into 5 cm thick sections and melted in the dark at 4°C on the day of extraction. The ice was melted in filtered seawater (0.2 µm, 1:4 volume ratio) to minimize the osmotic stress on the cells, following Garrison and Buck [1986]. Melted ice samples were gently vacuum filtered on Whatman GF/F filters (0.7 µm), and filters placed in 10 mL of acetone (90% volume ratio) over 16 hours in the dark at 4°C for pigment extraction [Parsons et al., 1984]. Chl *a* was then quantified fluorometrically following Yentsch and Menzel [1963] using a 10AU Turner Designs fluorometer.

3.2.3.2. DMS,P,O concentrations

DMS,P,O concentrations were measured on a fourth ice core (DMS ice core), following the dry-crushing technique developed by Stefels et al. [2012]. From November 2007 (station D1) until April 2008 (station D36NF), DMS,P measurements were performed aboard the ship within 48 hours of sample collection. In brief, each core was sliced in the cold laboratory of the ship (-26°C) into 5 cm thick sections. A small ice cuboid of approximately 20 g was taken from the center part of each section and inserted with two stainless-steel marbles into a gas-tight stainless-steel container. The container was hermetically closed with a

Viton® O-ring seal and bolted to an homemade crushing device operated with an electric motor (15 Hz, amplitude: 2.5 cm). The container was subjected to fast up and down movements which resulted in the crushing of the ice cuboid into a fine ice powder by repeated impacts with the stainless-steel marbles. 4 cycles of shaking (45 seconds each) were necessary to ensure that all gas bubbles and brine inclusions were released from the ice matrix. The container was then hooked up to a traditional purge-and-trap system via Swagelok® quick-connect fittings. DMS was purged from the headspace of the container using UHP (99.999%) helium at a constant flow rate of 50 $mL.min^{-1}$ for 30 minutes, and concentrated by cryogenic trapping (PTFE sampling loop in liquid nitrogen, -196°C). After 30 min, DMS was thermally desorbed by plunging the sampling loop in boiling water and injected in a Varian CP-3800 gas chromatograph equipped with a pulse flame photometric detector (PFPD) for quantification. Melting of the sample was prevented during the purge and trap step by placing the container in a Dewar® flask and cooling it down with liquid nitrogen vapor. At the end of the DMS analysis, the container was brought back to the cold laboratory, and the fine ice powder resulting from the crushing weighted and divided in four 20 mL glass vials with butyl/PTFE septa. The first two vials were used on the ship as samples for duplicate DMSP analyzes. The two other vials were stored at -26°C in the dark for further DMSO analyses in a land-based laboratory. DMSP was analyzed as DMS following its hydrolysis with a strong base [Dacey and Blough, 1987]. Two NaOH pellets were added to the vial which was stored to melt in the dark at 4° overnight. The vial was then hooked up to the purge and trap system using PTFE tubing and needles and purged during 15 min with UHP helium at a constant flow rate of 50 $mL.min^{-1}$. A water trap ($CaCl_2$) was added downstream the sample vial in order to remove water vapor from the gas stream. The gas chromatograph was calibrated

with a DMS standard (Kin-Tek Laboratories Inc.) diffusing at a constant rate from a certified permeation tube at 40°C and diluted with UHP helium. DMPS was always measured as total DMSP (particulate $DMSP_p$ + dissolved $DMSP_d$).

The DMS ice cores collected in May and June 2008 (Table 3.1) were kept in the dark in the cold storage room of the ship until the end of the study. During the demobilization of the ship in October 2008, the cores were transferred to the University of Laval (Québec) and analyzed for DMS and DMSP using the same equipment and methodology as described above.

All the DMSO samples (20 mL glass vials) were shipped back frozen to the Université Libre de Bruxelles (Belgium) and analyzed during the summer of 2009. We used the enzyme-linked method developed by Hatton et al. [1994] and recently adapted for sea ice samples by Brabant et al. [2011]. As recently demonstrated by Brinkley [2008], the enzyme-linked method yields the same total DMSO results as the method using the reducing agent $TiCl_3$ as long as the samples are not treated with alkali prior to the reduction step. In brief, DMSO was reduced to DMS using a solution of 50 µl DMSO reductase enzyme ($DMSO_R$), 10 mL of ethylenediaminetetraacetic acid (EDTA), and 10 mL of flavine mononucleotide (FMN), per 80 mL of milliQ water. The DMSO sample was first melted in the dark at 4°. Then, the melted sample was purged during 10 min with UHP helium at a constant flow rate of 25 $mL.min^{-1}$ to remove interfering DMS [Brabant et al., 2011]. The reducing solution (2 mL) was added to the sample, which was placed under incandescent light bulbs (60 watts) to initiate the formation of radicals by EDTA [Hatton et al., 1994]. EDTA radicals reduce FMN to $FMNH_2$, which further acts as an electron donor to $DMSO_R$ catalyzing the reduction of DMSO to DMS. After the reduction step, the vial was hooked up to a traditional purge-and-trap and purged

during 30 min with UHP helium at a constant flow rate of 25 mL.min^{-1}. DMSO was analyzed as DMS using an Interscience (Thermo Finnigan) Trace GC gas chromatograph equipped with a flame photometric detector (FPD). The gas chromatograph was calibrated with dilutions of pure DMSO (> 99.7%) for gas chromatography (Merck®) in ultra-pure water, which were reduced to DMS [Hatton et al., 1994]. As for DMSP, DMSO was always measured as total DMSO (particulate $DMSO_p$ + dissolved $DMSO_d$).

3.2.3.3. Potential storage artefacts

Sea ice DMS,P samples collected in May and June 2008, as well as all DMSO samples, were analyzed after several months of storage. This inevitably raises the question of whether the concentrations measured in the land-based laboratories (Québec and Brussels) were representative of the field situation.

The effects of long-term storage on sea ice DMS,P samples were recently assessed by Stefels et al. [2012]. The authors compared the DMS,P concentration profiles of twin ice cores analyzed right after extraction aboard a ship and in a land-based laboratory after two years of storage (similar conditions as in this study i.e. -30°C and in the dark). They showed that the main vertical features of the DMS,P profiles as well as the DMSP pool were well preserved, and that no conversion of DMSP to DMS and no production of DMSP had occurred during storage. We reasonably assumed that this was also the case for our samples. On the other hand, the authors also observed that land-based DMS concentrations were significantly lower (48.2% on average) than ship-based DMS concentrations, but they could not determine if the difference was due to a lower crushing efficiency of the land-based crusher, or to storage losses by diffusion due to the high volatility of DMS. When we compared DMS profiles of twin ice cores from two IPY-CFL

stations (D33-2, D36NF), we also observed that land-based DMS concentrations (after 18 months of storage) were significantly, and systematically, lower than ship-based DMS concentrations (42.0% on average, n = 35). Given that we used the same crushing device for all of our analysis (ship-based and land-based), we concluded that substantial amounts of DMS are indeed lost during long-term storage. Hence, the DMS concentrations of the IPY-CFL stations sampled in May and June 2008 (Table 3.1) presented in this study should be seen as lower-bound estimates of the pre-storage concentrations, and asymmetric error bars (42%) were added to the corresponding DMS plots.

Very little is known about the effects of long-term storage on sea ice DMSO samples. The general assumption is that frozen DMSO samples, like DMSP samples, are relatively stable and can be analyzed after months of storage [Lee et al., 2001; Brabant et al., 2011]. This is a reasonable assumption since DMSO is not volatile, and since photo-chemical oxidation and cells physiology are greatly reduced in very cold and dark conditions.

3.3. Results

The six stations sampled in this study illustrate the seasonal and ice type variability (drift ice, fast ice, and recently refrozen lead ice) of the IPY-CFL study. Here the physical and environmental settings of the stations are only briefly summarized. A companion paper [Carnat et al., 2013] provides a more thorough analysis of the halo-thermodynamical evolution of the ice cover during the whole IPY-CFL study as well as textural analyses. All stations were unflooded (positive freeboards) first-year sea ice floes (Table 3.1).

Station D1 was sampled in the Amundsen Gulf (Figure 3.1) at the end of November 2007 and was typically a late-autumn station. The ice cover was thin (51 cm) and made up of roughly 45% frazil ice and 55% congelation ice, suggesting that the ice probably grew in turbulent waters. This is consistent with the low ice concentrations observed earlier in the autumn in the Amundsen Gulf [Barber et al., 2010]. Also consistent with turbulent waters, a small frazil ice layer was observed sandwiched between two layers of congelation ice at 30 cm depth. The snow cover was typically thin (2 cm) and consisted of new snow. The air temperature (Figure 3.1) recorded on the ship deck during the month of November was cold (-15.8°C at Station D1) and decreasing with the progression towards winter. The daily average photosynthetically active radiation (PAR) (Figure 3.1), also recorded on the ship deck (PARLite® quantum sensor, Kipp and Zonen®), had already decreased to the detection limit of the instrument (1 $\mu mol.m^{-2}.s^{-1}$) on 17 November 2007. As expected during this cold dark period, the sea ice chl *a* concentrations were extremely low (0.02 to 0.15 $\mu g.L^{-1}$) and increasing towards the bottom of the ice (Figure 3.2). The algal assemblages were already heavily degraded as indicated by the ratio of phaeopigments (phaeo *a*) to the sum of phaeo *a* and chl *a,* which was near or just above 0.5 at all depths (Figure 3.2). An overview of the physical properties of the ice cover is provided in Figure 3.3. Both the ice temperature (linear decrease from a cold surface to a warmer ice base held at its melting point) and bulk salinity profiles (C-shaped) were typical of growing first-year sea ice [Eicken et al., 1991]. The brine volume fractions were below the permeability threshold of 5% [Golden et al., 2007] at all depths except for the warmest bottom ice layers, indicating that the ice cover was mostly impermeable to fluid transport. Low Rayleigh numbers (Ra) were also logically observed, indicating that the potential for brine gravity drainage was low [Wettlaufer et al.,

1997; Notz and Worster, 2008; Carnat et al., 2013]. Vertical profiles of DMS DMSP and DMSO concentrations in ice are shown in Figure 3.4. Statistical parameters for each station are provided in Table 3.2. DMS concentrations at station D1 were below detection limit (< 0.3 nM) at all depths. DMSP concentrations averaged 2.4 nM, ranging from below detection limit in the upper half of the ice, to 13.2 nM in bottom ice. A secondary DMSP maximum (3.1 nM) was observed at 30 cm depth in a layer of frazil ice sandwiched between congelation ice layers. The mean DMSO concentration (2.3 nM) was similar to that of DMSP but the DMSO values were more homogeneously distributed with depth (SD 0.7 nM), ranging from 1.5 nM in interior ice to 4.0 nM at the ice-ocean interface.

Stations D33-2 and D36NF were sampled in the Amundsen Gulf (Figure 3.1) during the early bloom period in the spring, which lasted approximately from 18 March until 19 April 2008 [Alou-Font et al., 2013]. The two stations showed contrasting ice thicknesses, reflecting different growth histories. The ice cover at station D33-2 was 150 cm thick and had started to grow in the early winter, while the ice cover at station D36NF was considerably thinner (68 cm) and had formed more recently in a refrozen lead. The ice texture at both stations was typical of Arctic first-year ice [Meese, 1989], showing a thin layer of frazil ice underlain by congelation ice. This is consistent with the low oceanic turbulence and high ice concentration observed in the Amundsen Gulf in the winter and early spring [Barber et al., 2010].

Figure 3.2: Vertical profiles of chl *a* (horizontal bars), and percentage of phaeopigments in the ice at the sampling stations. Note the difference in chl *a* scale for station F2. The vertical dashed-lines are set at 50% of phaeopigments.

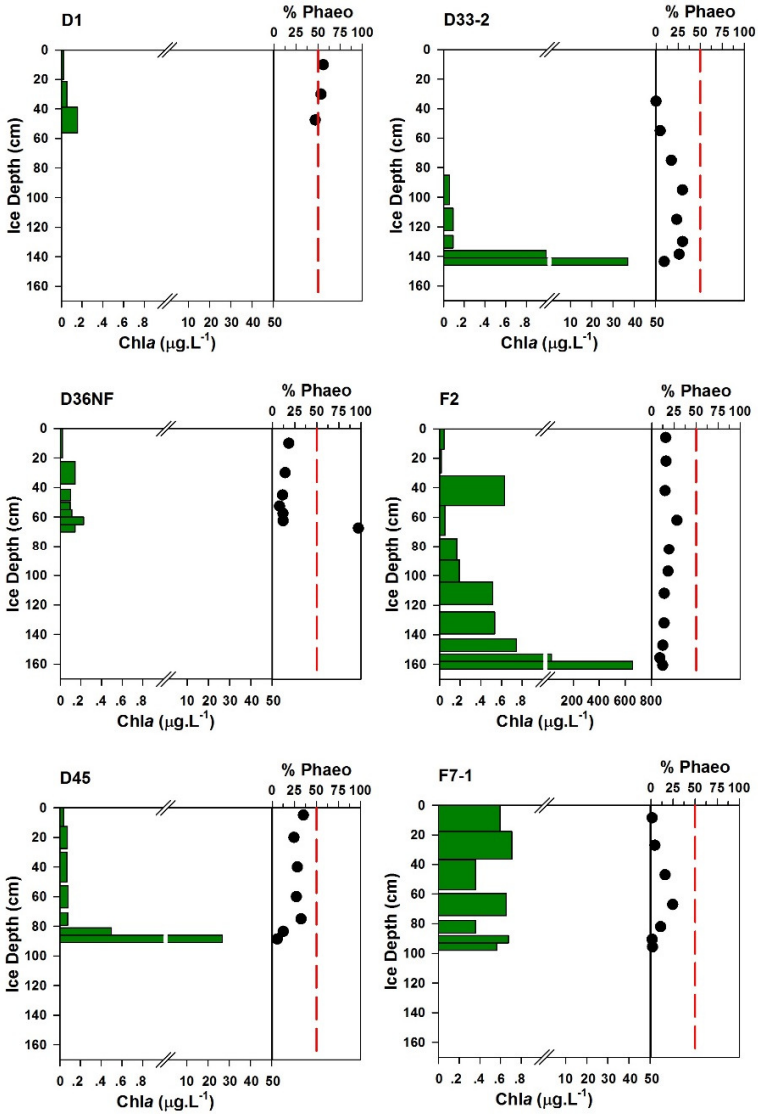

The snow cover consisted of a thin (3 cm) wind slab (cohesive layer of snow formed when wind deposits snow onto sea ice) at station D33-2 and of relic frost flowers buried in snow at station D36NF. Frost flowers, centimeter-scale fern-like ice crystals, composed of atmospheric hoar and liquid derived from sea ice brine, typically form at the surface of newly formed sea ice [Alvarez-Aviles et al., 2008]. The air temperature remained low until early April (-23.7°C at station D33-2, and -

14.4℃ at station D36NF), and then rose almost continuously until the end of the sampling season (Figure 3.1). The daily average PAR started to increase in early February and reached 245 µmol.m^{-2}.s^{-1} at station D33-2, and 318 µmol.m^{-2}.s^{-1} at station D36NF (Figure 3.1). These values are well above the minimum values reported to be required for the initiation of autotrophic production in the Arctic seas (2-9 µmol.m^{-2}.s^{-1}, Horner and Shrader [1982]). Despite similar snow cover thicknesses and similar incident irradiance values, the chl *a* concentration profiles of the two stations were radically different (Figure 3.2). Station D36NF had very low chl *a* concentrations (0.02 to 0.23 µg.L^{-1}) distributed almost homogeneously through the whole ice thickness. On the contrary, station D33-2 showed an increase in chl *a* concentrations with depth (L-shape), from concentrations under the detection limit in the upper half of the ice to typical early bloom concentrations in bottom ice (36.92 µg.L^{-1}). This difference was very likely due to the younger age of station D36NF (less time for algal colonization and growth), combined to a potential error in chl *a* measurement in the bottom ice sample at station D36NF (as suggested by the very high and unusual phaeopigments ratio, close to 100%). Phaeopigments ratios at both stations were < 0.5 suggesting that the algal communities were not heavily degraded (Figure 3.2). Differences were also observed in the physical properties of the two stations (Figure 3.3). The ice cover at station D33-2 was very cold and mostly impermeable, while it was warmer, fully permeable, and prone to brine gravity drainage at station D36NF. The high brine volume fractions and Ra calculated at station D36NF resulted mostly from high bulk salinities. These high salinities are consistent with sea ice that grew quickly in a lead under very cold atmospheric conditions, desalination being a function of ice growth rate [Cox and Weeks, 1988].

Table 3.2: Statistical parameters of sea ice DMS, DMSP and DMSO concentrations at each station. Nd: not determined.

DMS

	D1	D33-2	D36NF	F2	D45	F7-1	Overall
Mean	nd	4.1	0.7	31.1	4.3	1.4	10.1
Min	nd	nd	nd	nd	0.2	0.2	nd
Max	nd	95.3	4.6	769.0	34.6	7.9	769.0
Median	nd	nd	0.2	0.3	0.6	0.4	0.3

DMSP

	D1	D33-2	D36NF	F2	D45	F7-1	Overall
Mean	2.4	41.2	7.4	58.7	15.9	9.3	30.4
Min	nd	nd	1.3	2.2	3.7	1.2	nd
Max	13.2	1065.1	60.2	1636.1	48.1	83.9	1636.1
Median	nd	2.4	2.3	5.0	10.4	3.8	3.7

DMSO

	D1	D33-2	D36NF	F2	D45	F7-1	Overall
Mean	2.3	9.8	4.8	274.2	9.8	6.4	78.0
Min	1.5	2.1	2.0	2.9	2.6	3.1	1.5
Max	4.1	124.7	17.1	5427.8	30.0	15.1	5427.8
Median	2.4	3.5	3.5	22.0	5.9	6.0	4.0

DMS concentrations (Figure 3.4) were higher at station D33-2 (mean = 4.1, range < 0.3 to 95.3 nM) than at station D36NF (mean = 0.7, range < 0.3 to 4.6 nM). At both stations, the highest DMS value was observed in bottom ice. Station D36NF had a small local maximum located in subsurface ice, and station D33-2 multiple small peaks in interior ice (Figure 3.4). DMSP concentrations were approximately ten times higher than DMS concentrations, averaging 41.2 nM (< 0.3 nM to 1061.1 nM) at station D33-2, and 7.3 nM (1.3 to 60.2 nM) at station D36NF. Aside from the bottom ice maxima, the vertical profiles of both stations were radically different, with multiple small peaks in interior ice at station D33-2, and homogeneous concentrations (fluctuating around 2.3 nM, SD 0.7 nM) at station D36NF (Figure 3.4). DMSO concentrations were intermediate between DMS and DMSP

concentrations, averaging 9.8 nM (2.1 to 124.7 nM) at station D33-2, and 4.8 nM (2.0 to 17.1 nM) at station D36NF. Vertical profiles were both approximately C-shaped, with isolated secondary maxima in interior ice (Figure 3.4).

Station F2 was sampled in Franklin Bay (Figure 3.1) during the peak-bloom period in the spring, which lasted approximately from the 26 April until 16 May [Alou-Font et al., 2013]. The ice cover was thick fast ice (160 cm) and the ice texture showed a thin 5 cm layer of platelet ice (elongated acicular crystals with no specific orientation) underneath a more typical succession of frazil and congelation ice. The exact origin of the platelet crystals remains unknown but it is likely they formed through double-diffusion processes at the ice-ocean interface following the incursion of coastal freshwater [Carnat et al., 2013]. The snow cover consisted of 9 cm of new snow covering a 9 cm wind slab. Despite air temperatures approaching 0°C (Figure 3.1) and a near isothermal ice temperature profile (Figure 3.3), signs of surface melting were not yet observed and the bulk ice salinity profile remained C-shaped (Figure 3.3). The chl *a* concentrations profile had again a L-shape, with very high values typical of a peak-bloom measured in bottom ice (655.14 $\mu g.L^{-1}$). High chl *a* concentrations were favored by an elevated daily average PAR (615 $\mu mol.m^{-2}.s^{-1}$) and by an enhanced under-ice water nutrient availability in the Bays due to wind-driven upwelling events [Mundy et al., 2009; Tremblay et al., 2011]. High brine volume fractions (sea ice was permeable at all depths) and high Ra (high potential for brine gravity drainage) (Figure 3.3) at station F2 also probably facilitated nutrient replenishment and algal colonization of the ice cover. Algal assemblages were not heavily degraded at all depths (degradation ratios < 0.5). DMS, DMSP, DMSO concentrations were the highest measured throughout the study, with means of 31.1 nM (up to 52.2 nM if we

consider a storage loss of 42%), 58.7 nM and 274.2 nM respectively. Compared to the previous stations where DMSP dominated, DMSO largely dominated the dimethylated sulfur pool at station F2. Regarding maximum values, DMS reached 769.0 nM (up to 1322 nM if storage loss of 42%), DMSP 1636.1 nM and DMSO 5427.8 nM. These maxima were observed in bottom ice and corresponded to the highly productive platelet ice layer. DMS and DMSP vertical profiles were very similar, showing smaller local maxima in surface ice and interior ice (Figure 3.4). The DMSO vertical profile was radically different, with a remarkable contrast between the upper half (< 10 nM) and the bottom half (> 50 nM) of the ice cover.

Figure 3.3: Vertical profiles of sea ice temperature (T), bulk salinity (S_i), brine volume fraction (V_b/V) and Rayleigh number (Ra) at the sampling stations. The vertical dashed-line is set at 5% of brine volume fraction.

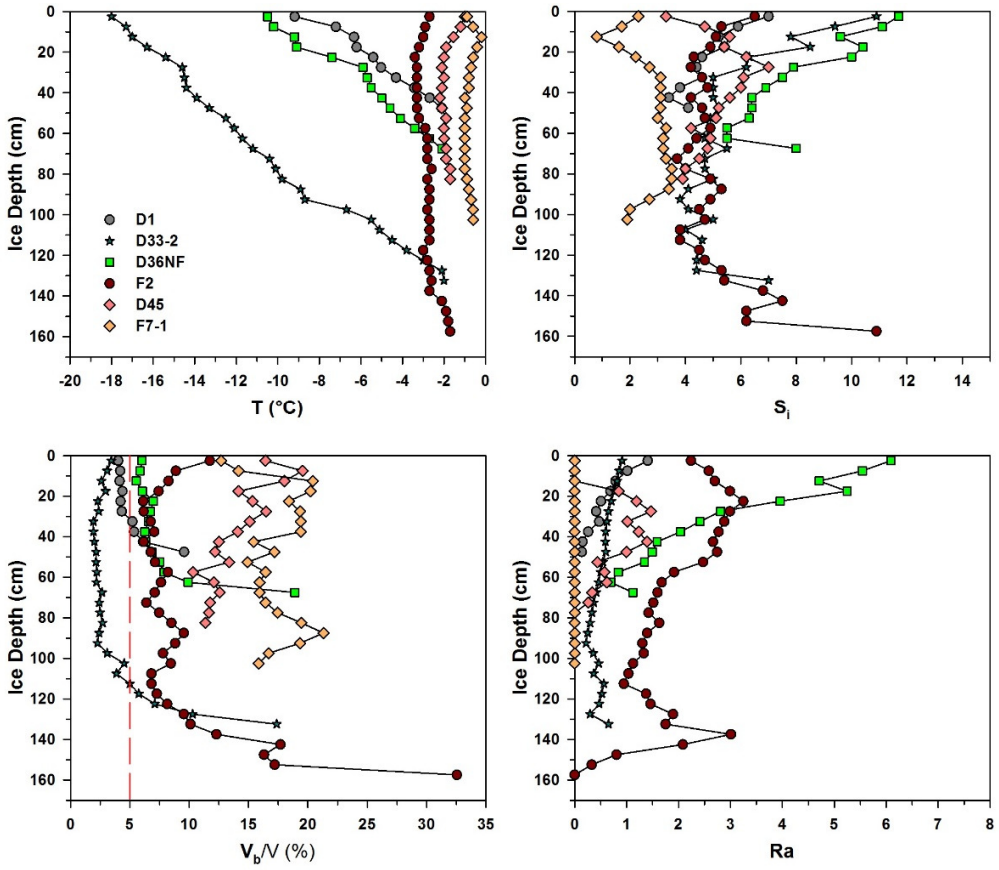

Figure 3.4: Vertical profiles of DMS (top panel), DMSP (middle panel), and DMSO (bottom panel) concentrations in the ice during the IPY-CFL study. The concentration axis on each plot is in log scale. Superimposed on the DMSO plots is the contribution of each dimethylated sulfur compounds to the total dimethylated sulfur pool. The length of the horizontal bars indicate the percentages of each compound at a given depth.

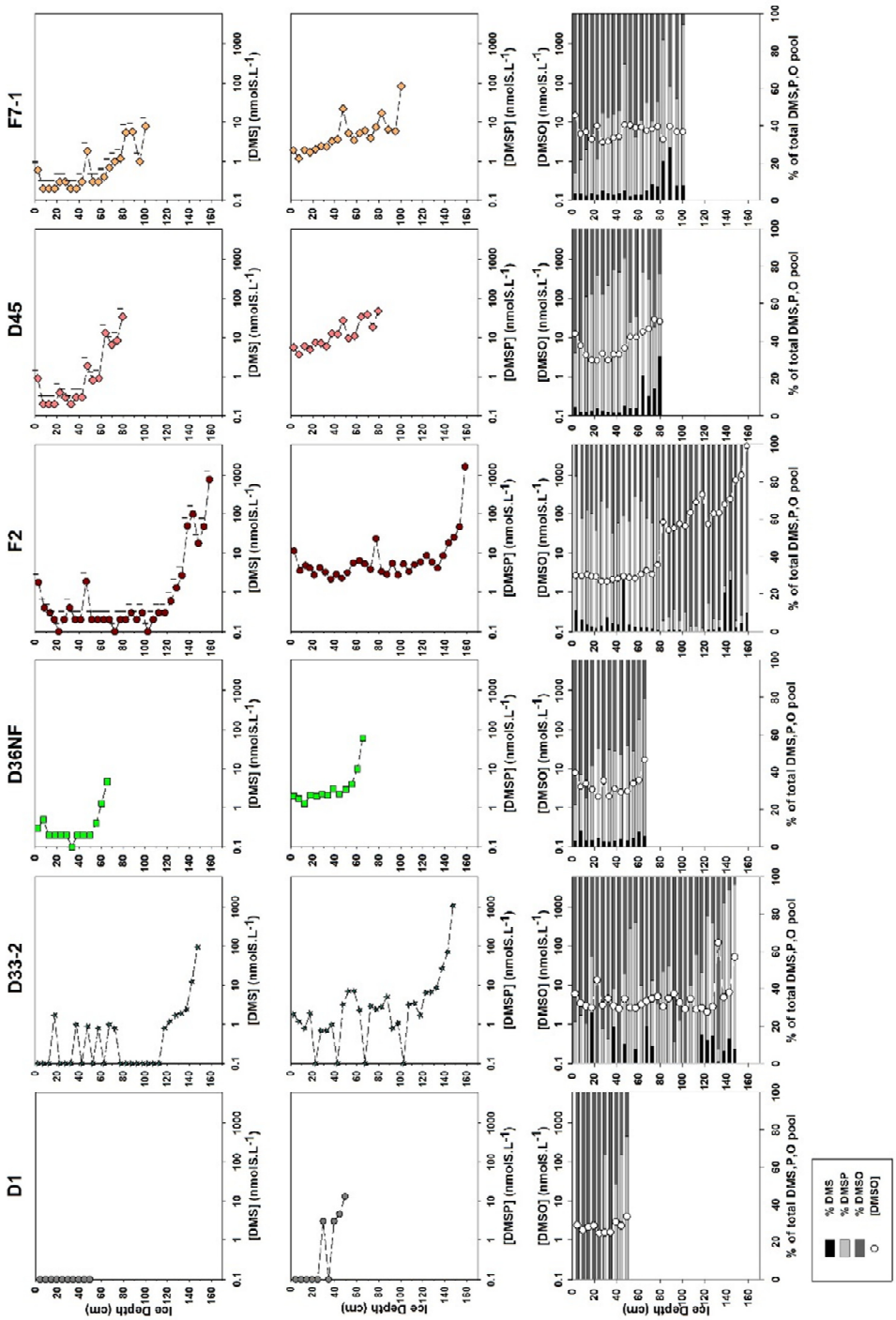

Station D45 and F7-1 were sampled in Darnley Bay (Figure 3.1) during the post-bloom period that took place in the second half of May and in June [Alou-Font et al., 2013]. Both stations were similar in sea ice thickness (82 and 103 cm respectively) and in ice texture (thin layer of frazil ice underlain by congelation ice). Air temperatures rose above 0°C (Figure 3.1) which drastically modified the ice cover. Some surface melting was observed at station D45 (10 cm of superimposed ice). Superimposed ice typically forms in early summer when surface snow melts, percolates, and refreezes at the snow/ice interface [Jeffries et al., 1994]. Surface melting was more advanced at station F7-1 as indicated by the presence of multiple melt ponds. Warming also impacted the sea ice physical and biological properties of both stations. Bulk ice salinity profiles transitioned to a ?-shape, as previously described by Eicken et al. [1991], with the freshening of surface ice and the vanishing of the bottom maximum in salinity (Figure 3.3). Both stations were almost isothermal and fully permeable (V_b/V > 5%), and the potential for brine gravity drainage was small at station D45, and nil at station F7-1 due to very low bulk salinities. The chl *a* concentrations profile of station D45 was very similar to that of station D33-2, with the maximum (26.67 µg.L^{-1}) observed in bottom ice (Figure 3.2). In contrast, station F7-1 had very low chl *a* concentrations at all depths (0.36 to 0.71 µg.L^{-1}), suggesting that ice algae had already been washed out from bottom ice, consistent with the observations of Hop et al. [2011] in Darnley Bay in 2008. Degradation ratios were < 0.5 at all depths at both stations. Post-bloom DMSP concentrations were below early bloom concentrations (Table 3.2) with a mean of 15.9 nM (3.7 to 41.8 nM) at station D45, and a mean of 9.3 nM (1.2 to 83.9 nM) at station F7-1.

DMS and DMSO concentrations were comparable to early bloom concentrations at station D45 averaging 4.3 nM (up to 7.3 nM if storage loss of 42%) and 9.8 nM (2.6 to 30.0 nM) respectively, and slightly lower than early bloom concentrations at station F7-1, averaging 1.4 nM (up to 2.4 nM if storage loss of 42%) and 6.4 nM (3.1 to 15.1 nM). DMS and DMSP vertical profiles (Figure 3.4) were very similar between both stations, with a small local maximum in surface ice, two local maxima in interior ice, and highest concentrations at the ice-ocean interface. The DMSO profile was C-shaped at station D45, and atypical at station F7-1 with relatively homogeneous concentrations at all depths but surface ice, where the maximum concentration was observed.

3.4. Discussion

3.4.1. Sea ice DMS,P,O ranges

Very little data is available on DMS,P,O concentrations in Arctic sea ice, and no data exists for the Amundsen Gulf. The concentrations reported in Table 3.2 are generally in line with those reported by previous Arctic studies, although some important differences can be observed.

DMS in Arctic sea ice has only been reported once, in the Canadian Arctic Archipelago northwest of Resolute Bay [Levasseur, 2013]. Profiles were, as in this study, L-shaped, and maximum concentrations reached 2000 nM in bottom ice at the end of the spring bloom, which is considerably higher than the maximum DMS concentration reported here (peak-bloom concentration of 769 nM, 1322 nM if storage loss of 42%). Since no information is available regarding the environmental conditions in which the DMS production occurred in the study of Levasseur [2013], we cannot further comment on the difference observed between the two studies.

Considering DMSP, the late-autumn (station D1) and early spring concentrations (stations D33-2 and D36NF) presented here are the first to be reported for Arctic sea ice. Concentrations had, until now, essentially been measured during late spring and summer. The shape of peak-bloom DMSP profiles reported by Uzuka [2003] in fast ice from Barrow (Alaska) is very close from the shape of station F2 profile (Figure 3.4), showing highest concentrations in bottom ice decreasing towards the top with a local maximum in surface ice. However, the range of concentrations observed by Uzuka [2003] in bottom ice (500 to 15000 nM) largely exceeds the range of concentrations observed during IPY-CFL in the spring (48 to 1636 nM), despite similar chl *a* values (600 $\mu g.L^{-1}$ vs 655 $\mu g.L^{-1}$). Closer, but still considerably higher, DMSP values were measured by Levasseur et al. [1994] in the Resolute Passage (up to 6014 nM, L-shaped profiles), and slightly smaller values by Lee et al. [2001] in Northern Baffin Bay (up to 1096 nM), despite this time higher chl *a* (up to 2000 $\mu g.L^{-1}$). In summer ice in the Greenland Sea, Galí and Simó [2010] observed a bottom ice DMSP concentration (90 nM) very close to values measured at station D45 (48 nM) and F7-1 (83 nM).

Comparison of DMSO concentrations measured in this study with other studies is limited to the work of Lee et al. [2001] in Northern Baffin Bay. These authors reported DMSO values (1.3 to 102 nM, mean = 13.7 nM, particulate DMSO only) in the bottom 2 cm of spring ice (from March until June, including peak-bloom conditions) that are very close to the values detected in early spring at station D33-2 (124.7 nM) and station D36NF (17.1 nM), but considerably lower than the maximum value observed during peak-bloom (5427.8 nM at station F2). Unfortunately, the authors did not report vertical profiles of the concentrations.

From the above comparisons, it is clear that Arctic sea ice DMS studies (including this one) converge towards a common picture in which sea ice shows considerable DMS,P,O production. It is also clear that the studies generally agree on the order of magnitude of the concentrations (2 to 4 orders of magnitude higher than typical oceanic water concentrations [Kettle et al., 1999]), on the general shape of the profiles (L-shape for DMS and DMSP), as well as on some seasonal trends (e.g. highest concentrations during the spring-bloom, then early spring, summer, and winter).

However, strong regional variability in concentrations can be observed, especially in the highly productive bottom ice layers during spring-bloom. This regional bottom ice variability is puzzling, especially for DMSP, since the main factors thought to drive DMSP production in sea ice (biomass, community composition) show little variability between studies [Levasseur et al., 1994; Lee et al., 2001; Uzuka, 2003]. For instance, in the Canadian Arctic (studies of Levasseur et al. [1994], Lee et al. [2001], as well as this study) spring blooms are typically dominated by a few species of the pennate and centric diatom groups (generally low individual DMSP producers), with little contribution of high DMSP producing groups such as dinoflagellates [Poulin et al., 2011]. Community composition in bottom ice during the IPY-CFL study peak-bloom showed a dominance of *Nitzschia Frigida*, *Fossula Arctica*, *Navicula sp.*, *Nitzschia promare*, and *Entomoneis sp.* [Różańska et al., 2009; Mundy et al., 2011; Alou-Font et al., 2013], which is nearly identical to the community composition reported by Lee et al. [2001] in the Northern Baffin bay (*Nitzschia Frigida*, *Fossula Arctica*, and *Navicula pelagica*).

There is always a chance that some of the variability originates from methodological biases (e.g. modification of cell physiology and cell lysis upon

melting vs dry crushing). Also, concentrations reported in the different studies strongly depend on the vertical sampling resolution selected (e.g. 2 cm in Uzuka [2003] vs 5 cm in this study), since DMSP is found in very discrete bands in sea ice. Most of the biomass (and DMSP) of bottom ice communities is located directly at the interface with the ocean, and concentrations show strong gradients over short distances (< 5 cm) (e.g. Figure 3.4). This is a fundamental difference with oceanic studies which typically report well mixed surface ocean concentrations. Similarly, the horizontal patchy distribution of ice algae in bottom ice could explain some of the variability, especially large differences in DMSP-to-chl *a* ratios, since chl *a* and DMSP cannot be measured on the same ice sample. Variability could finally be explained by differences in environmental factors influencing DMSP synthesis (the very dynamic and permeable bottom ice layer is prone to e.g. grazing, fast nutrient and salt exchanges,…), as well as by differences in the degradation processes of DMSP, such as bacterial DMSP-lyase activity, which remain poorly understood in sea ice.

3.4.2. Biological and physical controls on the temporal and vertical variability of DMS and DMSP

In this section, we discuss which biological (biomass and community composition), environmental (T and S) and physical (sea ice texture) factors could have best explained the temporal and vertical variability in DMS and DMSP concentrations observed during the IPY-CFL study (Figure 3.4). To support the discussion, we computed Spearman's rank-order correlation (R_s) between DMS, DMSP and chl *a*, used here as first-order estimate of biomass (Table 3.3). We also computed the correlation between T and S and DMSP-to-chl *a* ratios to assess the influence of environmental parameters.

Table 3.3: Spearman's rank-order correlation table for dimethylated sulfur compounds and biological (chl *a*) and environmental parameters (T and S) in vertical profiles of sea ice at the IPY-CFL stations (n = 121). TotalS is the total dimethylated sulfur pool (DMS + DMSP + DMSO). When applicable, the level of significance of the coefficient is denoted by * ($p < 0.05$), ** ($p < 0.01$), and *** ($p < 0.001$). Spearman's rank-order correlation was preferred over Pearson's product-moment correlation because of the lack of homoscedasticity shown by the dataset.

	DMS	**DMSP**	**DMSO**	**TotalS**
Chl*a*	0.5**	0.73***	0.59***	0.87***
DMS		0.65***	0.51***	
DMSP	0.65***		0.45***	
DMSO	0.51***	0.45***		

	DMSP/Chl*a*	**DMSO/Chl*a***	**TotalS/Chl*a***
T	-0.29*	-0.5***	-0.4**
S	0.11	0.26*	0.22

3.4.2.1. Sympagic biomass

As typically observed in previous Arctic studies [Levasseur et al., 1994; Lee et al., 2001], maximum DMS and DMSP concentrations were always found in bottom ice, and mean and maximum concentrations were observed to increase from the late-autumn (station D1) through the spring (station D33-2), peaking during the bloom (station F2), and decreasing towards the summer (stations D45, F7-1) (Table 3.2). These trends could have been well explained by the vertical distribution and seasonal evolution of the sympagic biomass (Figure 3.2). Significant positive correlations were observed between chl *a* and DMSP (R_s = 0.73, $p < 0.001$), and even between chl *a* and DMS (R_s = 0.50, $p < 0.01$) (Table 3.3).

A similar coupling between DMS,P and chl *a* has been previously observed in Arctic sea ice [Levasseur et al., 1994; Uzuka, 2003] and in Antarctic sea ice [Trevena and Jones, 2012]. However, weaker relationships have also been reported in other sea ice studies, essentially in the Antarctic [e.g. Trevena et al.,

2003; Tison et al., 2010]. These weak relationships were suspected to originate primarily from differences in communities composition, since the ability to synthesize DMSP is limited to a reduced number of species and since the cytosolic levels of DMSP vary considerably from one species to another [Keller et al., 1989]. In that respect, the fact that the community composition during most of the duration of the IPY-CFL study showed moderate variability (dominance of pennate and centric diatoms, > 40% in bottom ice) [Alou-Font et al., 2013] probably explain the very good correlation observed between DMS,P and chl *a* (Table 3.3).

3.4.2.2. Community composition

To investigate if the moderate variability in the IPY-CFL sympagic community composition could have nonetheless explained some of the variability in the DMSP concentrations observed, we compared the calculated DMSP-to-chl *a* ratios at each station to the seasonal evolution of the sympagic community composition described in the IPY-CFL literature [Różańska et al., 2009; Mundy et al., 2011; Alou-Font et al., 2013]. One should bear in mind that we did not make a distinction between particulate and dissolved DMSP when calculating the ratios. Hence, the ratios discussed here are probably overestimates of the real ratios.

The DMSP-to-chl *a* ratio can be used to evaluate communities as high (DMSP-to-chl *a* > 100 nmol.µg^{-1}) and low (DMSP-to-chl *a* < 50 nmol.µg^{-1}) producers [Trevena et al., 2003]. We more specifically looked at the bottom ice community (for which taxonomic composition was available) and compared the relative contribution of diatoms, usually acknowledged as low individual DMSP producers, to that of dinoflagellates, prasinophytes and prymnesiophytes, usually acknowledged as high individual DMSP producers [Keller et al., 1989].

In late-autumn ice (station D1), the taxonomic composition consisted of unidentified flagellates (32%), prasinophytes (16%), prymnesiophytes (11%), dinoflagellates (11%), with small contribution of centric and pennate diatoms (20%) [Różańska et al., 2008]. DMSP-to-chl *a* ratio was intermediate (58 nmol.µg^{-1}), close to typical oceanic values of prasinophytes and prymnesiophytes assemblages [Stefels et al., 2007]. Throughout the winter [Niemi et al., 2011], diatoms became the predominant group, reaching 40 to 90% during the early spring (station D33-2), followed by cryptophytes (2 to 37%), prasinophytes (2 to 29%), and dinoflagellates (1 to 12%) [Alou-Font et al., 2013]. The DMSP-to-chl *a* ratio of station D33-2 (28 nmol.µg^{-1}) was smaller than that of station D1, but still in the range of oceanic prasinophytes assemblages. DMSP-to-chl *a* ratio at station D36NF was much higher (419 nmol.µg^{-1}), but the taxonomic composition of that station was unfortunately not determined. Given the timing and specific growth conditions (recently refrozen lead) of station D36NF, it is likely that its composition was different than that of station D33-2. D36NF could have for example incorporated a greater proportion of dinoflagellates which were observed to dominate the under-ice water assemblage during the winter [Niemi et al., 2011]. Besides, the very high ratio could also originate from an error in chl *a* measurement in that sample, as mentioned previously, given the very high (unusual) phaeopigment value measured (close to 100%).

The contribution of diatoms further increased during peak-bloom, reaching 87 to 100%, with minor contributions of cryptophytes (1 to 8%), dinoflagellates (1 to 4%), and prasinophystes (< 2%) [Alou-Font et al., 2013]. Interestingly, the DMSP-to-chl *a* ratio dropped to a very low value of 2 nmol.µg^{-1}, very close to the value generally measured in oceanic diatom assemblages (4 nmol.µg^{-1}) [Stefels et

al., 2007]. This provides further evidence that diatoms are important DMSP producers in sea ice because of their large biomass, rather than because of intracellular adaptations of DMSP content to environmental stressors such as the low temperatures and high salinities of the brine habitat [Levasseur et al., 1994; DiTullio et al., 1998; Tison et al., 2010].

During the post-bloom period (stations D45 and F7-1), the community composition became more variable with stations showing > 60% of pennate diatoms (D45), and stations showing < 20% of pennate diatoms (F7-1) with strong contributions of chlorophytes and cryptophytes [Alou-Font et al., 2013]. Interestingly, the DMSP-to-chl *a* ratios of the two post-bloom stations were also radically different, reaching 2 nmol.μg^{-1} at station D45 and a relatively high value of 148 nmol.μg^{-1} at station F7-1.

If the above observations strongly suggest that DMSP concentrations were influenced by community composition in bottom ice during the IPY-CFL study, one should bear in mind that the DMSP-to-chl *a* ratio is not an ideal indicator of the individual DMSP production of sympagic algal cells. Indeed, the sea ice biome is characterized by strong vertical and seasonal gradients (Figure 3.1) in irradiance which cause unquantified changes in the pigment content of algal cells. Furthermore, DMSP and chl *a* could have different degradation rates in sea ice, leading to a temporal mismatch of the concentrations measured. These two artefacts may have explained some of the variability observed in the DMSP-to-chl *a* ratios [Trevena et al., 2003]. Hence, the above observations need to be confirmed by more robust analyses such as cell enumeration.

3.4.2.3. Temperature and salinity

The DMSP temporal and vertical variability observed in sea ice during the IPY-CFL study could have also been driven by environmental parameters. Here we focus on temperature and salinity.

Suggested physiological functions for DMSP include cryoprotection and osmoregulation [van Rijssel and Gieskes, 2002; Stefels et al., 2007]. In that respect, Kirst et al. [1991] hypothesized that the low temperature and high salinities of the sea ice habitat could boost the DMSP production of sympagic communities. This was recently supported by a laboratory study by Lyon et al. [2011]. The authors observed an 85% increase in intracellular DMSP of the sea ice diatom *Fragilariopsis cylindrus* in response to a salinity shift from 35 to 70 (equivalent to the difference between seawater salinity and a moderate sea ice brine salinity). Since sea ice temperature and brine salinities show strong seasonal and vertical variability, one could expect the DMSP-to-chl *a* ratios to vary accordingly. This was observed in the Weddell Sea, Antarctica, by Tison et al. [2010]. The authors found a strong positive correlation ($R^2 = 0.7$) between computed brine salinity and DMSP-to-chl *a* ratio in the upper 12.5 cm of the ice cover. Such relationship has never been tested in the Arctic.

We found a moderate negative correlation ($R_s = -0.29$, $p < 0.05$) between the DMSP-to-chl *a* ratios and sea ice temperature in all our samples (Table 3.3). This would correspond to a moderate positive correlation of the same magnitude with brine salinity ($R_s = 0.29$) given the inverse relationship between the two variables (assuming thermodynamic equilibrium of the brine, brine salinity is solely determined by sea ice temperature and can be calculated following the equation of Cox and Weeks [1983]). This moderate correlation suggests that environmental

parameters could have explained less variability (vertical and temporal) in DMSP concentration than biomass (and probably community composition) in our study.

However, the influence of temperature and salinity on DMSP concentrations could have been stronger than biomass at specific ice depths and during the coldest seasons, as suggested by Tison et al. [2010]. This was investigated by comparing the DMSP-to-chl *a* ratios of our sympagic communities to the typical ratios observed in oceanic communities [Stefels et al., 2007]. If DMSP was produced as a cryoprotectant or osmoregulator in our samples, then it is reasonable to expect that sympagic algae would have had much higher DMSP-to-chl *a* ratios than their pelagic counterparts. Naturally, this assumption only works if the sympagic algae are located away from the ice-ocean interface where strong exchanges with the under-ice water occur. Indeed, in bottom ice communities, where the ice temperature and brine salinity remained very close to under-ice water conditions for much of the year (Figure 3.3.) as always observed in natural sea ice, ratios were systematically comparable to, or lower than, typical ratios of oceanic communities with similar taxonomic composition (see section 3.4.2.2). Even if we consider that our sympagic algae contained more chl *a* per unit cell volume than pelagic algae, due to lower irradiance values in sea ice [Belzile et al., 2000], the difference between ratios would still have remained small.

By contrast, in interior ice during the early spring (station D33-2), when ice temperatures were as low as -12°C and calculated brine salinities as high as 180 (Figure 3.3), very high DMSP-to-chl *a* ratios were observed (448 to 1249 nmol.µg^{-1}), which could indicate that DMSP synthesis was boosted by the strong freezing and osmotic stresses. These ratios are comparable to, or even higher, than ratios measured during blooms of strong DMSP producers, keeping in mind that they

were calculated using total DMSP [Stefels et al., 2007]. For instance, Scarratt et al. [2002] reported ratios of 790 nmol.µg^{-1} in the North Atlantic.

More surprisingly, high ratios (> 200 nmol.µg^{-1}) were also observed in the surface and interior ice layers of the late spring (station F2) and summer stations (stations D45 and F7-1). These high ratios could not be attributed to freezing or osmotic stresses since the sea ice temperature profiles were nearly isothermal at the considered stations (Figure 3.3). Whether these high ratios were the result of other environmental stresses, of the presence of strong individual DMSP producers, of a difference in the timing of degradation of DMSP and chl *a*, or of an important proportion of dissolved DMSP in the total DMSP pool due to the highly degraded state of the ice and communities in post-bloom conditions (stations D45 and F7-1) could not be assessed.

If salinity and temperature could have partially driven trends in DMSP concentrations in some surface and interior ice layers during the cold seasons in our study, their influence on the total DMSP production by the sea ice biome during IPY-CFL would have however remained limited since these layers were always characterized by both very low biomasses and low DMSP concentrations (Figures 3.4 and 3.5).

3.4.2.4. Sea ice texture

Sea ice texture (size, shape and orientation of the ice crystals) could also have controlled the DMS,P profiles, especially the vertical distribution of the concentrations. This has been little investigated in sea ice DMS,P studies [Tison et al., 2010; Carnat et al., submitted], especially in the Arctic.

Sea ice texture can influence the initial vertical distribution of DMS,P during ice growth. Frazil ice is known to incorporate higher concentrations of solutes (e.g. salts, biomass, DMS,P) from the water column than congelation ice during sea ice growth [Ackley and Sullivan, 1994]. Also, scavenging by frazil ice crystals leads to a random and non-selective entrapment of algae in sea ice [Ackley, 1982; Garrison et al., 1983] while congelation ice formation results on the contrary to a selective incorporation favoring large algae. Providing that the community composition of under-ice water is not significantly modified during the different steps of sea ice formation, a contrast in the taxonomic composition (and hence in the potential for DMSP synthesis) of frazil and congelation ice could be expected.

Our data set provides some evidence of a textural control of DMSP vertical distribution during the IPY-CFL study. With the exception of station D1, all stations showed a decrease in DMSP concentrations from surface ice to sub-surface ice (Figure 3.4) corresponding to a textural transition from frazil to congelation ice [Carnat et al., 2013]. Frazil ice can also accumulate or grow at depth under an existing congelation ice cover leading to sandwiched frazil ice layers. These layers can form through several processes such as rafting, double diffusion between two water masses of different properties, and turbulence in leads [Weeks and Ackley, 1982; Maykut, 1985; Tucker et al., 1987]. The sea ice texture during the IPY-CFL study did not vary much [Carnat et al., 2013], with most stations showing a typical Arctic sequence of surface frazil ice (0 to 10 cm) followed by undisturbed congelation ice. However, a small number of stations showed sandwiched frazil ice layers that were most likely originating from turbulence in leads and double diffusion around intense brine plumes generated by the refreeze of ice cracks [Carnat et al., 2013]. This was the case for example for station D1, where a

sandwiched frazil ice layer developed at 30 cm depth. Interestingly, a local DMSP maximum (3 nM, 25% of the bottom ice maximum) was also observed in this layer (Figure 3.4).

Sea ice texture can also influence the vertical transport of DMS,P within the brine network and the transfer of DMS from the ice surface to the atmosphere [Tison et al., 2010; Nomura et al., 2012; Carnat et al., submitted].

Sea ice texture has been shown to influence sea ice permeability and hence the transport of solutes. Frazil ice (granular texture) and congelation ice (columnar texture) presumably have different permeability threshold for fluid and gas transport [Golden et al., 2007]. Connectivity of brine inclusions should be harder to restore in frazil ice (random distribution of granular crystals) than in congelation ice (well vertically aligned columnar crystals). Hence, sandwiched frazil ice layers could represent some local constriction of the brine network and could reduce for example the potential for brine drainage of DMS,P, and diffusion of DMS, leading to local accumulations of the two compounds [Tison et al., 2010; Carnat et al., submitted]. Such processes probably did not impact the vertical variability of DMS,P during the IPY-CFL study since the sea ice texture at the sampled stations was almost exclusively composed of well aligned columnar crystals [Carnat et al., 2013].

Sea ice texture is also known to strongly influence the transfer of gas from the ice surface to the atmosphere through the development of superimposed ice (formed when snow meltwater percolates and refreezes at depth in the snow cover or at the snow-ice interface). This has been clearly demonstrated for CO_2 during the IPY-CFL study [Geilfus et al., 2012], and for DMS in the Antarctic [Nomura et al., 2012]. If DMS transfer to the atmosphere is hampered, one should expect the

DMS produced in surface ice (or slowly accumulated following diffusion from the bottom ice communities) to remain trapped in surface ice. The DMS profiles of the warm and permeable stations D45 and F7-1 (Figure 3.3), showing a local DMS maximum in surface ice (Figure 3.4) under a layer of superimposed ice (Table 3.1), suggest that this could have been the case during the IPY-CFL study.

3.4.3. Contribution of DMSO to the total dimethylated sulfur pool

The most striking result of this study was the overwhelming predominance of DMSO in the sea ice total dimethylated sulfur pool in some sea ice sections. This is illustrated by triangular plots in Figure 3.5. Approximately one half of the sections sampled had over 50% of their dimethylated sulfur pool in the form of DMSO. This contrasts strongly with the percentages typically observed in oceanic waters samples [Zemmelink et al., 2005; Hatton and Wilson, 2007], in which DMSP usually largely dominates, and in which DMSO contribution is rarely above 50%. This contrasts also with observations made in East-Antarctica sea ice samples (Carnat, unpublished results), in which percentages were very close to those of oceanic waters samples. In fact, DMSO contributions largely over 50% have only been reported once, in the study of de Mora et al. [1996] looking at the biogeochemistry of sulfur in glacial meltwater ponds on the McMurdo Ice Shelf in Antarctica.

In this section, we investigate which process could have led to these high DMSO percentages. If high DMSO percentages were observed at all stations, the vertical distribution of these percentages within the cores showed two very distinct patterns (Figure 3.4). This suggests that at least two different processes could have occurred. At station F2, high DMSO percentages were exclusively observed in the bottom half of the core, while at all other stations, high DMSO percentages

were observed in the upper half of the core, showing a general decrease from surface ice to interior ice at stations D33-2, D36NF, D45 and F7-1.

DMSO in oceanic waters has three potential sources. DMSO can be directly synthesized by algae, presumably playing similar physiological roles to that of DMSP, e.a. cryo-osmoregulator, free radical scavenger, and intracellular electrolyte modifier [Lee and de Mora, 1999]. DMSO can also be produced by the bacterial (BDMSC, bacterial DMS consumption) and photo-chemical oxidation (abiotic photolysis) of DMS [Kieber et al., 1996]. In sea ice, DMSO could also come from atmospheric deposition in snow, as suggested by Galí and Simó [2010].

We first focused on the first pattern, the general decrease in DMSO percentages from surface ice to interior ice observed at stations D33-2, D36NF, D45 and F7-1. This depth-dependency of the DMSO percentages prompted us to look for a depth-dependent process that could have affected DMSO concentrations. Atmospheric deposition in snow was quickly discarded for a number of reasons. The snow cover was typically low at most IPY-CFL stations (Table 3.1) [Carnat et al., 2013] (little deposited DMSO available) and the transfer of significant concentrations of DMSO (several nM) to depth in the ice cover would have required a large amount of meltwater percolation, which was not supported by physical and textural observations [Carnat et al., 2013]. Sea ice temperature is a depth-dependent variable in sea ice and we observed a fairly good negative correlation between sea ice temperature and DMSO-to-chl *a* ratios (R_s = -0.50, $p < 0.001$) (Table 3.3), suggesting that sea ice temperature could have explained the trend observed.

Figure 3.5: Triangular plots showing the speciation of dimethylated sulfur compounds in sea ice during the IPY-CFL study in the Canadian Arctic (this study) and during the Arise study in East-Antarctica (Carnat, unpublished results), and in surface waters during various oceanic studies (Simó et al. [1998], Zemmelink et al. [2005], Hatton and Wilson [2007]). Note the dissimilarity in distribution of the dots between the Arctic plot and the two other plots.

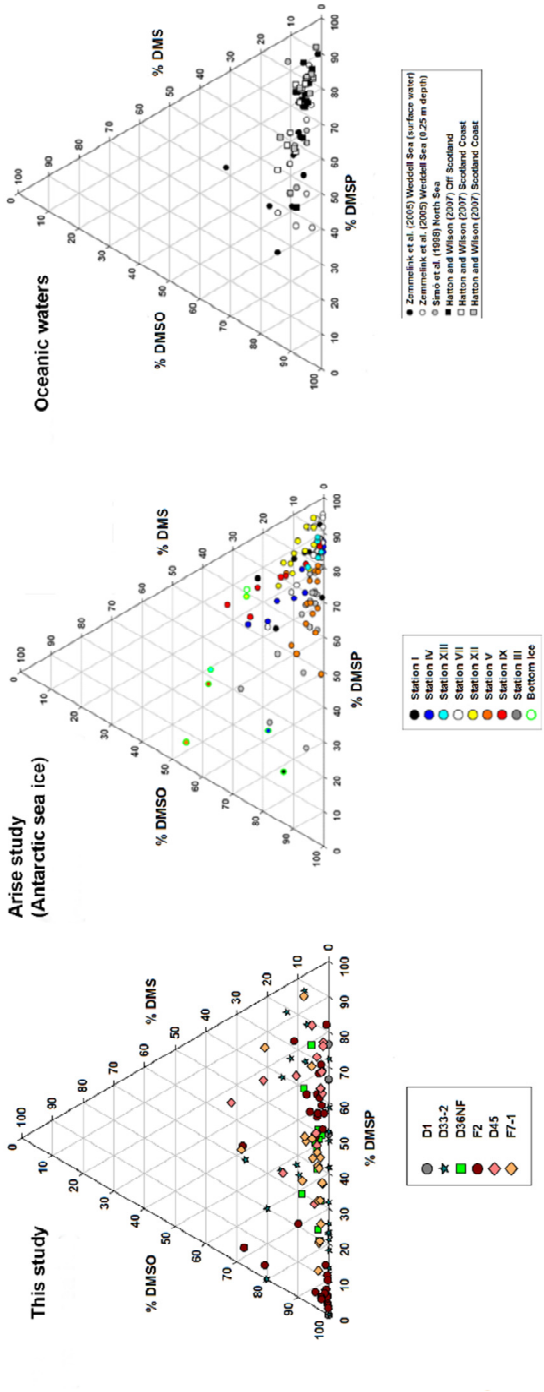

However, the depth-dependency of DMSO percentages was also observed in warm stations (D45, F7-1) showing nearly isothermal sea ice temperature profiles (Figure 3.3). Furthermore, the cryoprotectant function of DMSO in Arctic sea ice has strongly been disputed by Lee et al. [2001] who showed that intracellular concentrations of DMSO reported in sea ice were too low to significantly depress the freezing point of intracellular fluids.

Following the hypothesis made by Asher et al. [2011] to explain high DMSO concentrations observed in brine samples collected in surface ice from the Ross Sea Polynya in Antarctica, we considered light as a strong candidate to explain the depth-dependency of DMSO percentages in surface ice. Light intensity is indeed clearly a depth-dependent variable in sea ice at any time of the year [Lizotte, 2003]. The snow cover measured at the different stations was also supportive of a light control. Snow can significantly reduce the transmission of light through the ice surface. For instance, snow albedos are almost two times larger than sea ice albedos [Grenfell and Maykut, 1977]. The lowest DMSO percentages in surface ice were observed at station F2 which showed a thick snow cover of 18 cm (Table 3.1). The best depth-dependency of DMSO percentages were on the other hand observed for stations that had the lowest snow cover. Station D36NF was only partially covered by frost flowers, and station F7-1 was covered by melt ponds which are known to increase light transmittance at the ice surface [Nicolaus et al., 2012].

Light intensity might have controlled DMSO production in surface ice through two pathways. First, DMSO might have been produced from the photo-chemical oxidation of DMS accumulated in surface ice. Second, high light levels in surface ice (UV) could have led to strong oxidative stress on sympagic cells,

triggering the production of intracellular DMSO following the anti-oxidant cascade hypothesized by Sunda et al. [2002]. The role of DMS oxidation to DMSO in cellular photo-protection has not yet received strong observational support and it remains unclear that DMSO would be the final and dominant dimethylated sulfur compound of an anti-oxidant cascade [Asher et al., 2011]. Furthermore, the very low chl *a* observed in surface ice (< 0.4 $\mu g.L^{-1}$) suggested that little biomass was available for intracellular DMSO production (Figure 3.3). This was particularly striking for station D33-2 where chl *a* was under the detection limit in surface ice. By contrast, as suggested in section 3.4.2.4., DMS produced by bottom and interior ice communities might have diffused towards the ice surface, and might have accumulated in impermeable cold ice or under superimposed ice (Figure 3.4), providing a significant and stable source for photo-chemical oxidation.

Close to nothing is known about DMS photo-chemical oxidation in sea ice. In oceanic waters, DMS is mainly photo-chemically oxidized in DMSO by UV-A and visible light, and photolysis rates are usually maximal at 380 to 460 nm [Kieber et al., 1996]. Photo-chemical oxidation by UV-B can also occur, but does not result in DMSO production [Hatton, 2002]. Outside of the UV range, photo-chemical oxidation is mediated by photosensitizers [Kieber et al., 1996], primarily by oxidants produced by photoreactions of chromophoric dissolved organic matter (CDOM) [Brugger et al., 1998; Toole et al., 2003]. In that respect, photo-chemical reactions could have been promoted in sea ice during this study by the presence of elevated levels of CDOM, as previously observed in Arctic sea ice in Northern Baffin Bay [Belzile et al., 2000].

We investigated the photo-chemical oxidation pathway by comparing the DMSO percentages at each sampling depth with a calculated irradiance intensity

at the corresponding depths (Figure 3.6). Irradiance intensity for a given wavelength (λ) (spectral irradiance) at a given ice depth (*z*) was estimated using Bouguer-Lambert's law [Perovich and Govoni, 1991; Perovich, 1996]:

$$I\ (z,\lambda) = I(0,\lambda)e^{-\kappa z} \qquad (3.1)$$

We decided to work only with a wavelength (λ) range from 400 to 450 nm, for several reasons. First, photolysis rates are usually maximal at 380 to 460 nm [Kieber et al., 1996]. Second, sea ice and snow reduce the transmission of UV more than they reduce the transmission of PAR [Perovich, 2001]. Third, the 400 to 450 nm range of wavelengths has some of the lowest spectral extinction coefficients of the PAR spectrum [Perovich, 1994]. Spectral extinction coefficients (κ) for 400 to 450 nm were taken from Perovich [1996]. We used a mean κ value of 1.2 m^{-1} corresponding to extinction coefficients estimated for the interior of pure white ice [Grenfell and Maykut, 1977]. The surface spectral irradiance at each station was taken as the mean daily spectral irradiance. We observed fairly strong positive linear relationship for stations with a very thin snow cover (R^2 = 0.7, for stations D36NF and F7-1), and moderate-to-low relationships for stations with a slightly thicker snow cover (Table 3.1) (R^2 = 0.4 for station D33-2, and 0.1 for station D45). No linear relationship was obviously observed for station D1 sampled during the dark late-autumn, neither for station F2 with a thick snow cover. If these relationships strongly suggest that DMSO concentrations in surface ice were driven by photo-chemical oxidation during the IPY-CFL study when the snow cover was thin or absent, one should bear in mind that the approach used here is relatively simple. The photo-chemical oxidation hypothesis should be further confirmed in the future by more robust measurements of spectral irradiance attenuation.

Only brief comments and hypotheses can be made for the very high DMSO percentages observed at stations D1 and F2 (Figure 3.4). Given the very low levels of algal metabolism expected in surface ice in cold and dark conditions (station D1), it would not be surprising to see the DMS cycle dominated by bacterial degradation processes (e.g. BDMSC) in these layers, with DMSO as a dominant end-product of these processes.

Interestingly, high DMSO percentages in bottom ice were only observed at station F2, during peak-bloom (655 $\mu g.L^{-1}$) (Figure 3.4). Sympagic communities in blooming conditions might be exposed to very high concentrations of dissolved oxygen (oxygen oversaturation up to 200%) [Rysgaard et al., 2001; Delille et al., 2007], leading to strong oxidative stresses on the cells and a potential reduction of productivity. In that respect, McMinn et al. [2005] observed a strong reduction in the growth, maximum quantum yield, and photosynthetic efficiency of Arctic sea ice *Nitzschia frigida* communities following an increase in oxygen concentrations equivalent to four times air saturation. Peak-bloom at station F2 was precisely dominated by *Nitzschia frigida* [Alou-Font et al., 2013]. Hence, DMSO might have been produced by the bottom ice communities to scavenge the excess active oxygen radicals, following again the anti-oxidant cascade hypothesized by Sunda et al. [2002]. Such an adaptive strategy had already been suggested by Delille et al. [2007] in Antarctic sea ice brines, and definitely warrants further investigation. Strong brine convection at station F2, as suggested by high Ra numbers and high brine volume fractions (Figure 3.3) [Carnat et al., 2013], could have then transferred the DMSO produced in bottom ice through the upper ice layers.

Figure 3.6: Percentage of DMSO in the total dimethylated sulfur pool in sea ice as a function of estimated irradiance ($W.m^{-2}$) in the 400 to 450 nm wavelength range for stations D33-2, D36NF, D45, and F7-1 above, and D1 and F2 below. Details on the estimation of irradiance at depth in the ice cores, as well as on the choice of the wavelengths are given in section 3.4.3.

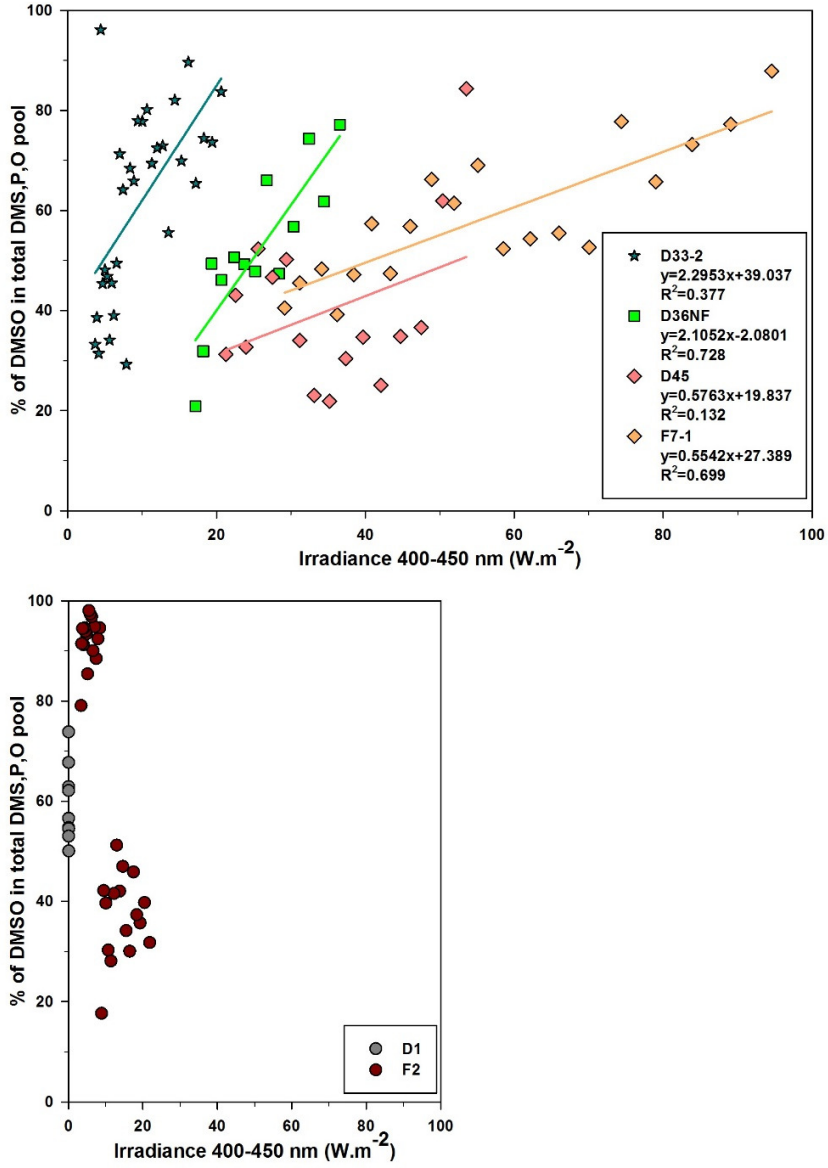

In light of these investigations and hypotheses, the difference in triangular plots (Figure 3.5) between this study and previous Antarctic and oceanic studies are more easily understandable. The Arise stations in East-Antarctica were characterized by a thick snow cover, which could not only have promoted the

formation of DMSP in surface ice via the development of a snow ice surface community [Lannuzel et al., 2006], but could also presumably have limited the photo-chemical oxidation of DMS. DMSO could also have been reduced to DMS as shown by Asher et al. [2011] in brines from the Ross Sea Polynya. The spatial decoupling between the depth of major DMSP production (bottom ice) and the depth of major DMS removal through photolysis (surface ice) during this study could explain the difference observed with oceanic studies where production and removal processes occur at the same depth.

3.4.4. Brine dynamics and exchanges at the ocean-ice-atmosphere interfaces

The comparison of our DMS,P data set with the halo-thermodynamic evolution of the sea ice cover during the IPY-CFL study described by Carnat et al. [2013] gives us an opportunity to comment on the magnitude and timing of DMS release from the sea ice cover. The sea ice DMS pool can be vented to the atmosphere through several pathways, such as openings (leads and cracks) in the ice during the entire season, advection of sedimented ice algae to open waters during ice melt, and during ice break-up over large areas [Levasseur et al., 1994]. Sea ice DMS can also be transferred to and released from melt ponds [Sharma et al., 1999b], and directly emitted from the ice surface [Zemmelink et al., 2008a; Nomura et al., 2012].

The focus of this study was on the sea ice medium and little information was collected on water bodies. Hence, we can only provide limited comments on some of the DMS venting pathways. For instance, we did not sample leads. Only three melt ponds were sampled at station F7-1 ($n = 6$), and all samples showed DMS concentrations below detection limit (< 0.3 nM). This could indicate that melt

ponds played a marginal role in DMS emissions during the end of the IPY-CFL study. This is coherent with the results of Sharma et al. [1999b] who observed very low DMS concentrations (0.1 to 2.2 nM, n = 11) in central Arctic melt ponds during summer, and with the results of Trevena and Jones [2012] whose calculated fluxes from melt ponds in eastern Antarctica were low (0.5 to 7 $\mu mol.m^{-2}.day^{-1}$). However, no general conclusion on melt ponds can be drawn from these limited observations. Indeed, DMS has probably very short turnover times in melt ponds due to rapid venting, and could therefore be hard to detect, especially if DMS is emitted in short pulses. Furthermore, high DMS concentrations could be produced in melt ponds following for example the development of a surface ice community fueled by seawater infiltration [Gradinger et al., 2005]. In that respect, Asher et al. [2011] reported very high DMS concentrations (> 250 nM) in summer melt ponds from the Ross Sea in Antarctica associated with important surface/slush communities. These communities are nevertheless very scarce in the Arctic and were not observed during the IPY-CFL study (Figure 3.2).

Direct DMS emissions from the ice surface have never been measured in the Arctic, despite observations of significant fluxes in the Antarctic associated with surface/slush communities [Zemmelink et al., 2008a; Nomura et al., 2012]. Although we did not directly measure DMS fluxes from the sea ice surface, our observations suggest that direct DMS emissions from the ice surface during the IPY-CFL study should not have been important. First, highest DMS concentrations were measured in bottom ice and no surface/slush communities were observed (Figures 3.2 and 3.4). As discussed in the previous section, a significant fraction of the DMS diffusing to the ice surface was also probably photo-chemically oxidized. Second, the time window during which emissions could have occurred

was very small. Gas transfer at the ice surface should be dominated by diffusive processes, controlled by the porosity of sea ice [Fanning and Torres, 1991; Loose et al., 2011a]. Porosity, which can be approximated by the brine volume fraction (Figure 3.3), is expected to change seasonally. Above a given brine volume fraction (permeability threshold of 5%, corresponding to a temperature of -5°C for a bulk ice salinity of 5), columnar sea ice is permeable to liquid transport. Recent works suggest that gas transfer could require warmer sea ice temperatures and higher brine volume fractions than liquid transport, as the tortuosity of the brine network could for example be more restrictive for gas bubbles migration than liquid migration. In a laboratory study with tracers (SF6), Loose et al. [2011a] showed gas diffusion through sea ice for brine volume fractions slightly above the liquid permeability threshold, between 6.1 and 7.9%. In a field study looking at argon transport in sea ice, Zhou et al. [2013] suggested to look for a gas permeability threshold between 7.5 and 10% of brine volume fraction. Brine volume fraction in surface ice during the IPY-CFL study rose above 7.5% in early May, and in some recently refrozen leads in March and April [Carnat et al., 2013]. Gas transfer at the ice surface can also strongly be impeded by the formation of superimposed ice (formed when snow meltwater percolates and refreezes at depth in the snow cover or at the snow-ice interface), as shown for CO_2 during the IPY-CFL study [Geilfus et al., 2012], and for DMS in the Antarctic [Nomura et al., 2012]. Superimposed ice during the IPY-CFL study started to form in mid-May and was observed at all stations until melt ponds formation [Carnat et al., 2013]. Hence, we believe that direct DMS emissions from surface ice during the IPY-CFL study was restricted to the two first weeks of May (station F2), and occasionally in recently refrozen leads earlier in the season (station D36NF).

Sea ice could have released larger amounts of DMS during ice melt and ice break-up, as already suggested by Levasseur et al. [1994], or during strong brine drainage events as previously reported in Antarctic sea ice [Tison et al., 2010; Carnat et al., submitted].

A strong desalination phase was observed during the IPY-CFL study over a very small time window in the spring, during the two last weeks of May [Carnat et al., 2013]. A net increase in brine volume fraction (above the fluid permeability threshold of 5%) and Rayleigh number (proxy of the intensity of brine convection, [Notz and Worster, 2009]) suggested this desalination phase was the result of full-depth gravity drainage initiated by a restored connectivity of the brine network with warming in the spring. Interestingly, this full-depth gravity drainage episode would have occurred right after peak-bloom (station F2), when bottom ice DMS concentrations were the highest (769 nM), and could have therefore released a significant fraction of the sea ice DMS,P pool to the under-ice water. In that respect, we observed a moderate increase in under-ice water (sampled at the ice-ocean interface with a Cole Palmer, Masterflex® - Environmental sampler) DMS (from < 0.3 to 6 nM) and DMSP (from 4 to 21 nM) during the last two weeks of May. Release of DMS,P through brine drainage could also have occurred earlier in the season in refreezing leads, as suggested by the high Rayleigh numbers observed at these stations [Carnat et al., 2013]. This process could have been spatially significant for the Amundsen Gulf given the fact that roughly 28% of the sea ice extent in March and April consisted of new ice [Forest et al., 2011], indicating a very dynamic ice cover with new exposed leads frequently refreezing. Unfortunately, the magnitude of this release could not be assessed since under-ice water was not sampled during these months. The contribution of this brine

released DMS to regional DMS emissions will strongly depend on the fate of DMS in under-ice water (transportation to depth, bacterial consumption, or advection to open water in leads or at the retreating ice edge) which remains largely unknown.

Regarding DMS release during ice break-up, Levasseur et al. [1994] calculated a DMS pulse of 0.18 to 0.66 $mgS.m^{-2}.day^{-1}$ for the Canadian Arctic Archipelago. However, as acknowledged by the authors, this calculation was based on several approximations. First, the DMS concentration in sea ice was not measured but fixed to 20% of the total DMS + DMSP pool. Second, the total DMS+DMSP pool used in the calculations was measured in late May, and might therefore not have been representative of the sea ice pool at the time of break-up. The results gathered during this study gave us the opportunity to refine the estimates of Levasseur et al. [1994]. First, we could use direct measurements of sea ice DMS concentrations. Using these measurements, we observed that DMS during peak bloom (769 nM) represented 32% of the total DMS + DMSP pool (769 + 1636 nM) suggesting that the estimate used by Levasseur et al. [1994] (20%) could have been slightly conservative. Then, we had the chance to sample two stations (D45 and F7-1) a few days before ice break-up, which gave us a fairly good estimation of the sea ice DMS pool available at the time of break-up. This one would have been considerably lower than the sea ice DMS pool measured in May during peak-bloom (station F2). Using sea ice concentrations measured at station D45 and F7-1 (< 0.3 to 34 nM), and following the methodology of Levasseur et al. [1994], we calculated a DMS pulse comprised between 0.04 and 0.11 $mgS.m^{-2}.day^{-1}$ (0.08 to 0.19 $mgS.m^{-2}.day^{-1}$ if DMS loss of 42%). These values are in the lower range of values calculated by Levasseur et al. [1994], but still approximately twice as high as the estimated Arctic summer ocean-atmosphere flux (0.067

$mgS.m^{-2}.day^{-1}$) [Bates et al., 1987], and estimated autumn ocean-atmosphere flux in the Canadian Arctic Archipelago [Rempillo et al., 2011].

Despite the fact that we improved Levasseur et al. [1994] approach, our calculated fluxes still represent first-order estimates that would need to be confirmed in the future by flux measurements. Indeed, we assumed here that 100% of the DMS released from sea ice would be vented to the atmosphere, whereas it is generally admitted that only 10% of the oceanic DMS makes its way to the atmosphere [Simó and Pedros-Alio, 1999; Archer et al., 2002]. Also, we did not consider sea ice DMSP as a potential source of DMS for surface waters following break-up. The release of ice algae to surface waters might have exposed the cells to strong and rapid shifts in e.g. irradiance, grazing pressure, and salinity, leading to potential cell lysis, anti-oxidant cascades, or exudation of DMSP, which could all have significantly modified the DMS pool.

3.5. Conclusions

This study was the first effort to simultaneously quantify all the compounds of the dimethylated sulfur pool (DMS,P,O) in Arctic sea ice. This effort was performed on 4 drift ice stations and 2 fast ice stations in the Amundsen Gulf (Canadian Arctic), in the framework of the IPY-CFL study. The vertical and temporal variability of the DMS,P,O concentrations were described based on high resolution vertical profiles from ice cores collected from growth (November 2007) to the start of melt (June 2008).

This study confirmed previous observations that Arctic sea ice is a biome favorable to substantial DMS,P,O production, with bottom ice spring peak-bloom concentrations reaching 769 nM, 1636 nM and 5427 nM respectively. This study

also confirmed the strong vertical and temporal variability of the DMS,P concentrations, with profiles typically displaying a general L-shape. Smaller local maxima were nonetheless observed in surface and interior ice. Low but still significant concentrations were for the first time reported in late-autumn (up to 13 nM of DMSP) and early spring ice, as well as in recently refrozen leads.

Concentrations were compared to a set of ancillary biological and physical variables to identify the main driving factors of the sea ice DMS cycle in the Amundsen Gulf. Sympagic biomass and community composition clearly explained much of the vertical and temporal variability in DMS,P concentrations. In that respect, much of the DMSP production was dominated by pennate diatoms within bottom ice during the seasonal sea ice bloom. As already reported, strong DMSP production for that sympagic group was only related to its important biomass and not to intracellular adaptations of DMSP content to the environmental stressors of the sea ice habitat (DMSP-to-chl *a* ratios reaching only 2 nmol.μg^{-1}). This also seemed to be the case for other sympagic groups dominating the late-autumn, early spring and summer bottom ice assemblages (prasinophytes, prymnesiophytes, and dinoflagellates), which all showed DMSP-to-chl *a* ratios comparable to typical oceanic ratios.

Some vertical and temporal trends could however not be explained by biomass or community composition. Moderate correlations between DMSP-to-chl *a* ratios and sea ice temperature and brine salinity suggested that environmental parameters could have explained some of the variability, but the influence of these variables would have been limited to the surface and interior assemblages of cold early spring ice. Similarly, scavenging in frazil ice and superimposed ice formation blocking the exchange of DMS with the atmosphere were both presented as two

plausible processes driving the local maxima in DMS and DMSP observed in surface ice.

Clearly, biomass and community composition could not have explained the trends observed in DMSO concentrations. We reported for the first time the contribution of each dimethylated sulfur compound to the total dimethylated sulfur pool in Arctic sea ice, and observed a distribution different than previous Antarctic sea ice and oceanic waters distributions, with DMSO largely dominating (> 50%) in most ice layers. Good correlations (R^2 = 0.4 to 0.7) were observed between DMSO percentages and calculated attenuated irradiances (400-450 nm) in surface ice for stations with a thin snow cover. This suggested a light control of the DMSO concentrations through photo-chemical oxidation of DMS accumulated in impermeable surface ice. This could represent a new potential important loss pathway for DMS in Arctic surface ice given the prevalence of thin snow covers and would represent a significant difference with Antarctic sea ice where thick snow covers are more widespread.

This study finally reevaluated some aspects of the timing and magnitude of DMS release from the Arctic sea ice cover based on a comparison with the halo-thermodynamic evolution of the ice. The contribution of direct DMS emissions from the ice surface to regional DMS emissions would probably be very small given the small DMS,P production in that layer, the potential strong photo-chemical oxidation of the DMS diffusing from bottom ice communities, and the very small time frame during which the ice is both permeable to gas exchange and not covered by impermeable superimposed ice. Strong DMS release might occur during full-depth gravity drainage events, under recently refrozen leads or during a small time frame in late-spring. Further work should definitely look at the fate of this DMS in under-

ice water once released from the ice cover. Finally, this study refined the calculation of the DMS pulse generated during ice break-up and showed that it could be significantly lower than previously expected, between 0.04 and 0.19 $mgS.m^{-2}.day^{-1}$. These hypotheses and estimates should be further supported by future DMS flux measurements (e.g. accumulation chambers, eddy accumulation), which are clearly missing for Arctic sea ice at the moment.

Chapter 4

Physical and biological controls on DMS,P dynamics in ice shelf-influenced fast ice during a winter-spring and a spring-summer transition

Journal of Geophysical Research – Oceans, 119

doi:10.1002/2013JC009381

Gauthier Carnat[1], Jiayun Zhou[2,3], Timothy Papakyriakou[1], Bruno Delille[3], Thomas Goossens[2], Tim Haskell[4], Véronique Schoemann[2,5], François Fripiat[6], Janne-Markus Rintala[7], and Jean-Louis Tison[2]

[1]Centre for Earth Observation Science, Department of Environment and Geography, University of Manitoba, Winnipeg, Manitoba, Canada

[2]Laboratoire de Glaciologie, D.S.T.E., Université Libre de Bruxelles, Bruxelles,1050, Belgium

[3]Unité d'Océanographie Chimique, Université de Liège, Liège, 4000, Belgium

[4]Callaghan Innovation Research Ltd, Wellington, New Zealand

[5]Department of Biological Oceanography, Royal Netherlands Institute for Sea Research, Texel, Netherlands

[6]Earth System Sciences and Analytical, Environmental and Geo-Chemistry, Vrije Universiteit Brussel, Belgium

[7]Department of Environmental Science, University of Helsinki, Finland

Abstract

We report the seasonal and vertical variations of dimethylsulfide (DMS) and its precursor dimethylsulfoniopropionate (DMSP) in fast ice at Cape Evans, McMurdo Sound (Antarctica) during the spring-summer transition in 2011 and winter-spring transition in 2012. We compare the variations of DMS,P observed to the seasonal evolution of the ice algal biomass and of the physical properties of the ice cover, with emphasis on the ice texture and brine dynamics. Isolated DMS and DMSP maxima were found during both seasonal episodes in interior ice and corresponded to the occurrence of platelet crystals in the ice texture. We show that platelet crystals formation corresponded in time and depth to the incorporation of dinoflagellates (strong DMSP producers) in the ice cover. We also show that platelet crystals could modify the environmental stresses on algal cells and perturb the vertical redistribution of DMS,P concentrations. We show that during the winter-spring transition in 2012, the DMS,P profiles were strongly influenced by the development and decline of a diatom-dominated bloom in the bottom ice, with DMSP variations remarkably following chl *a* variations. During the spring-summer transition in 2011, the increase in brine volume fraction (influencing ice permeability) on warming was shown to trigger (1) an important release of DMS to the under-ice water through brine convection and (2) a vertical redistribution of DMSP across the ice.

4.1. Introduction

Dimethylsulfide (DMS) is the dominant volatile biogenic sulfur compound in the oceans [Lovelock et al., 1972]. Surface ocean waters are found to be supersaturated in DMS, generating a net flux to the atmosphere where DMS is quickly oxidized to acidic sulfate aerosols [Malin, 1997]. These oxidation products increase the acidity of precipitation, alter the hydrological cycle, but also pre-eminently alter the radiative budget of the atmosphere [Charlson et al., 1987; Savoie and Prospero, 1989; Andrea et al., 1995], both directly by backscattering part of the incoming solar radiation and indirectly by acting as cloud condensation nuclei and by modifying cloud properties. DMS is part of a complex biogeochemical cycle including other sulfur compounds, all of which are linked by numerous biotic and abiotic processes [Stefels et al., 2007]. DMS is mainly produced by the enzymatic conversion of dimethylsulfoniopropionate (DMSP), an intracellular compound synthesized by a few classes of marine algae. The physiological roles played by DMSP in the cells are not yet fully constrained. DMSP could act as a compatible solute playing the role of cryoprotectant [Karsten et al., 1996]; an active osmolyte [Dickson and Kirst, 1986]; a grazing-activated chemical defense precursor [Wolfe et al., 1997]; the initial compound in a cascade of oxidations that prevent oxidative stress in cells [Sunda et al., 2002]; a methyl donor in metabolic reactions [Kiene et al., 1999]; an overflow mechanism for excess reduced compounds and energy excess [Stefels, 2000]. DMSP is released from algal cells either by active exudation or cellular lysis, caused by senescence [Stefels and Van Boeckel,1993], viral attack [Hill et al., 1998], or grazing [Wolfe and Steinke, 1996]. Following its release in the ambient medium, DMSP can be enzymatically cleaved into DMS and acrylate by algal and bacterial DMSP-lyases. DMS loss pathways

include not only emission to the atmosphere but also bacterial and photo-chemical oxidation to a third dimethylated sulfur compound, dissolved dimethylsulfoxide ($DMSO_d$) [Hatton et al., 2005]. On the other hand, dissolved DMSO can also be reduced by bacteria in DMS, and particulate $DMSO_p$ synthesized directly by marine algae, probably playing similar physiological roles to that of DMSP, e.g. cryo-osmoregulator, free radical scavenger, and intracellular electrolyte modifier [Lee and de Mora, 1999].

DMS, DMSP and DMSO are ubiquitous in the world oceans but their concentrations, since they are driven by numerous biotic and abiotic factors [Stefels et al., 2007], show large seasonal and regional variability [Lana et al., 2011]. Hence, in order to provide accurate estimates of the global DMS flux across the ocean-atmosphere interface and assess the exact influence of DMS on the Earth's climate, a good understanding of the DMS,P,O distribution and dynamics across different ocean environments is needed. Key areas are the complex and very dynamic polar marine regions, where the DMS,P,O cycle is further complicated by the presence of sea ice. Sea ice has long been considered to be an impermeable barrier to gas exchange between the ocean and the atmosphere [Tréguer and Pondaven, 2002]. Hence, a seasonal sea ice mask is typically applied over the polar marine regions in the various climatology of surface DMS concentrations and emission fluxes [Kettle et al., 1999; Lana et al., 2011], conceivably underestimating the real flux. Recent studies have shown that sea ice, through its liquid brine microstructure, can exchange gases with both the ocean and the atmosphere [Loose et al., 2011b], and significant DMS fluxes (up to 11 $\mu mol.m^{-2}.day^{-1}$) from sea ice have been detected in the Antarctic [Zemmelink et al., 2008a; Nomura et al., 2012]. More than just a mechanical conduct between the

ocean and the atmosphere, sea ice is a distinct biome favorable to substantial production of DMS,P,O. Brine inclusions in sea ice host important algal communities, and hence many potential producers [e.g. Ackley and Sullivan, 1994]. These communities are exposed to various stress factors [e.g. Dieckmann et al., 2005; Mock and Thomas, 2005], including extremely low temperatures, high salinities, nutrient limitations and hyperoxic conditions, all of which require physiological adaptations from the cells. Concentrations of DMSP up to 3 orders of magnitude higher than typical oceanic values were reported in Antarctic and Arctic first-year bulk sea ice samples (sea ice matrix + brine) in the early 1990 [Kirst et al., 1991; Levasseur et al., 1994]. Since then, a dozen studies in the different Antarctic sectors have confirmed these observations [e.g. Turner et al., 1995; DiTullio et al., 1998; Trevena et al., 2003]. Similarly, DMSO was found in high concentrations in Arctic bulk sea ice samples [Lee et al., 2001] and in Antarctic brine samples [Asher et al., 2011]. High DMS concentrations in bulk sea ice and brine samples have also been measured, but published data sets remain very scarce with only a few studies in the Antarctic [Trevena and Jones, 2006; Delille et al., 2007; Tison et al., 2010; Asher et al., 2011] and none in the Arctic.

To date, sea ice studies have essentially compared the temporal and spatial variability of the DMS,P,O concentrations to biological parameters (e.g. algal abundance, nutrients, and bacterial abundance). Trends are usually well explained by the distribution and evolution of the ice algal biomass. Depth profiles of bulk sea ice DMSP generally mimic depth profiles of chl *a* [Trevena et al., 2003; Gambaro et al., 2004]. However, weaker relationships between DMSP and chl *a* have also been reported [Levasseur et al., 1994; Tison et al., 2010]. DMSP production is also strongly species-specific [Keller et al., 1989]. DMSP production

by individual cells in sea ice has been investigated via DMSP-to-chl *a* ratios [Trevena et al., 2000; Gambaro et al., 2004], DMSP quotas of cells [Kirst et al., 1991; Levasseur et al., 1994; DiTullio et al., 1998], and photosynthetic pigments [Trevena et al., 2000]. Amongst the most common ice algal groups in the Antarctic, haptophytes and dinoflagellates are considered as strong producers because of their high intracellular DMSP contents. A suggested explanation for these high intracellular DMSP contents is a physiological response to the high salinities and low temperatures of the sea ice habitat [Kirst et al., 1991; Tison et al., 2010]. Sea ice diatoms do not exhibit higher intracellular DMSP contents than their pelagic counterparts (probably because they are often located in bottom ice where environmental conditions are close to those of under-ice water), but are important contributors to the sea ice DMSP pool due to their high biomass [Levasseur et al., 1994; Trevena et al., 2000; 2003]. In Antarctic sea ice brine samples, conversion of DMSP to DMS has been shown to occur with sometimes very short turnover times, and bacterial DMSO reduction to DMS has been identified as a major pathway of DMS production [Asher et al., 2011].

The influence of the physical properties of sea ice (e.g. ice thermodynamics and ice growth processes) on the DMS cycle in the polar regions is poorly understood. A few studies suggested that sea ice melting in the summer, and subsequent DMS,P release, largely contributes to the DMS hot spots observed in the surface waters of marginal ice zones [Kirst et al., 1991; Trevena and Jones, 2006; Tison et al., 2010]. Some suggest that DMS release associated with these hot spots may significantly contribute to annual DMS emission totals from polar marine regions [Levasseur et al., 1994; Tison et al., 2010]. In like fashion, a significant amount of DMS,P could also be exchanged with the under-ice water

before melting through brine convection, provided the ice is permeable to fluid transport [Tison et al., 2010]. Similarly, brine transport would also strongly influence the vertical distribution of DMS,P,O in sea ice. There has been very little discussion on the influence of sea ice growth processes on DMS,P,O dynamics, although they are widely recognized as important drivers of sea ice biogeochemistry [Garrison et al., 1990; Horner et al., 1992; Arrigo et al., 1995]. Of particular interest is the effect of platelet ice formation associated with supercooled ice shelf waters [Hellmer, 2004] which may significantly contribute to the sulfur budget of Antarctic coastal waters. First, platelet ice formation is known to incorporate substantial amounts of biomass [e.g. Arrigo et al., 1995] suggesting a high potential for DMS,P,O production. Second, platelet ice, through its lattice of large randomly oriented crystals, modifies the connectivity of brine inclusions and has therefore a direct impact on ice permeability and brine dynamics [e.g. Gough et al., 2012]. This may considerably influence DMS,P,O dynamics by (1) modifying environmental stresses (e.g. salinity) and (2) modifying the vertical redistribution and exchanges at the ice-ocean interface of DMS,P,O. The processes described above may be quite common given the fact platelet ice is observed in proximity to ice shelves, and they exist around 44% of the Antarctic coastline [Drewry et al., 1982].

The seasonal and inter-seasonal response of DMS,P,O dynamics in sea ice associated with both biological and physical controls has rarely been measured during months-long time series studies. Most of the existing seasonal measurements integrate spatial variability (sampling on multiple ice floes), which can be large and difficult to constrain in sea ice environments. Hence, there is

uncertainty in our understanding on many issues related to the DMS,P,O production and transmission within and between the ocean-ice system.

In this study, we report high vertical resolution (5 cm) DMS,P concentration profiles in ice shelf-influenced fast ice at Cape Evans, McMurdo Sound (Antarctica) from bulk sea ice samples. We report 8 profiles from two contrasting seasonal episodes, the spring-summer transition in 2011 and the winter-spring transition in 2012. These profiles, in conjunction with ancillary information on physical (ice texture, ice temperature and bulk salinity, and brine volume fraction) and biological (chl *a*, phaeopigments, and biomass composition) properties of sea ice and under-ice water, provide us with the opportunity to critically examine the influences of (1) platelet ice formation (2) ice permeability and brine dynamics, and (3) biomass seasonal evolution on DMS,P dynamics during two seasonal episodes in a coupled sea ice and ocean system, thereby addressing some critical knowledge gaps that we highlight above.

4.2. Material and methods

4.2.1. Study site and samples collection

Sampling took place at Cape Evans (77°38' S, 166°23'E), located on the eastern side of McMurdo Sound, under the western slopes of Mt Erebus, Ross Island, Antarctica (Figure 4.1A,B). A smooth and flat fast ice cover (Figure 4.1C) develops each year under quiescent conditions and typically reaches thicknesses between 150 and 250 cm. The seafloor is shallow (86 m at the location of the sampling site) and dominated by moderately sloping boulder and cobble fields interspersed with gravel and sand [Sutherland, 2008]. Sampling occurred in two phases: from 28 November 2011 to 8 December 2011 and from 19 September 2012 to 1 November 2012. During the first phase, an ice coring site was delimitated

with flags approximately 400 m away from the shore (Figure 4.1C). The exact same location was visited during the second phase but, obviously, with a renewed ice cover. Ice break-up occurred in early February 2011 (approximately two months after the end of the first sampling phase). Cape Evans remained ice-free until the beginning of April in 2012, and at the start of the second sampling phase (19 September 2012), the ice thickness had reached 147 cm.

The ice coring site was visited three times during phase 1 (stations 1 to 3) and five times during phase 2 (stations 4 to 8). Each time the site was visited, a small sampling square zone (10 m^2) was delimitated. Although the ice was of uniform consolidation, these sampling zones were kept fairly close to each other to minimize the potential for spatial variability. Sampling always started with a basic description of the snow cover. Ice cores were then taken using an electropolished stainless-steel ice corer (14 cm ID). Ice cores were immediately wrapped in polyethylene bags and kept at < -30°C horizontally in the dark to prevent brine drainage from the cores [Cox and Weeks, 1986] and limit the physiological activity of ice algae. In the field, this was achieved by placing the cores in an insulated box pre-filled with cold packs frozen at -30°C. Under-ice water was also sampled, using a peristaltic pump (Cole Palmer, Masterflex® - Environmental sampler) with Tygon® tubing. Under-ice water was collected at three depths (ice-ocean interface, 1 m and 20/30 m) through the core hole associated with the extraction of the first core. For each depth, two 20 mL glass vials were filled to the top and crimp sealed with a cap with a butyl/PTFE septum.

4.2.2. Analyses

4.2.2.1. DMS,P concentrations

Processing and analysis of the samples (under-ice water and bulk sea ice samples) started right after sampling. Analysis systematically started with the determination of DMS concentration in under-ice water samples which took always less than 2 hours. Then, bulk sea ice DMS concentrations were determined on an ice core stored at -30°C in the insulated box in the field. This step typically took between 20 and 48 hours, depending on the number of samples and the number of replicates. This timing of analysis is perfectly in line with the literature and is considered as acceptable regarding the amount of DMS lost through diffusion during storage [Stefels et al., 2012].

Figure 4.1: A. Location of the study site (Cape Evans, 77°38' S, 166°23'E) in the McMurdo Sound. B. Terra MODIS (250 m spatial resolution) satellite image of the study site on the first week of April 2011. C. View of the ice coring site, looking towards Cape Evans.

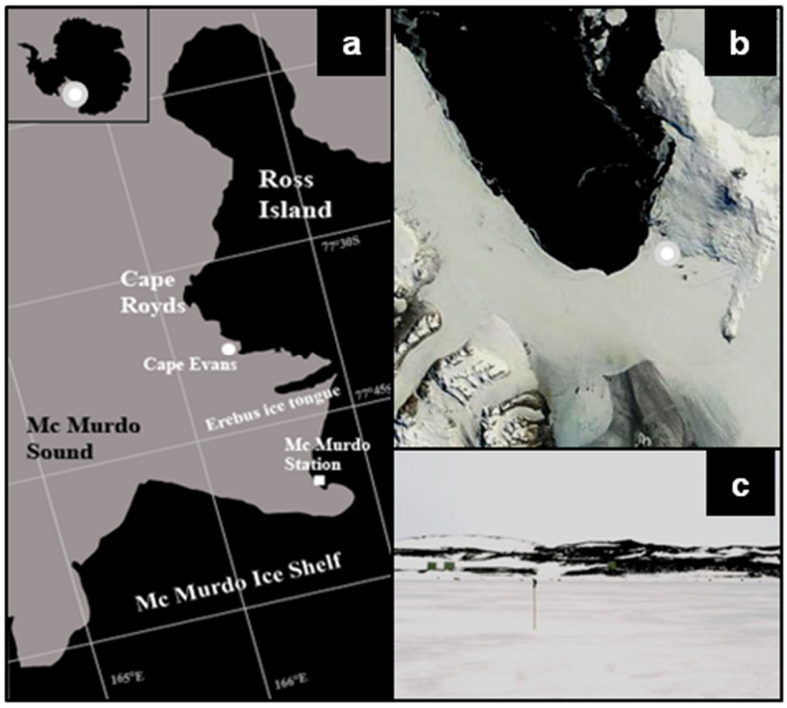

The ice core was sectioned into 5 cm depth sections using a clean band saw installed in a -25°C cold room. The center part of each section was then cut into smaller rectangular cuboids (l = ± 3 cm, w = ± 1.5 cm, h = ± 5 cm), and DMS extracted from the ice cuboids using the dry-crushing technique in the cold room [Stefels et al., 2012]. In brief, an ice cuboid was weighted and inserted with two stainless-steel marbles into a stainless-steel vessel. The vessel is an air-tight container (internal volume = 198 cm^3) specifically designed for DMS analysis in ice. It has Swagelok® quick-connect inlet and outlet and is sealed with a Viton® O-ring seal. The vessel was hermetically closed and installed on a homemade crushing device operated with an electric motor. The vessel was then mechanically shaken by fast up and down movements of the crushing device (15 Hz; amplitude: 2.5 cm) during four cycles of 45 seconds. The crushing phase reduced the ice cuboid into a fine ice powder, ensuring a complete release of gas bubbles and brine inclusions from the ice matrix (bulk sea ice measurement). The vessel was removed from the cold room, kept at < -30°C in a Dewar® flask, and hooked up to a purge-and-trap gas chromatograph system. DMS was purged from the headspace of the container using UHP grade (99.999%) helium at a constant flow rate of 50 $mL.min^{-1}$ for 30 minutes, and concentrated by cryogenic trapping in a PTFE loop (1/8'' OD) immersed in liquid nitrogen (-196°C). The flow of helium was controlled at any time by an electronic flow controller (Aalborg® GFC Mass Flow Controller-17). After 30 minutes, the PTFE loop was immersed in boiling water, DMS thermally desorbed and injected for quantification into a gas chromatograph (GC) through a six-port pneumatic valve.

The GC was an Agilent® 7890A equipped with a Dual flame photometric detector (FPD) and a sulfur-specific Agilent J&W® DB-1 capillary column (30 m x

0.32 mm ID). The FPD was equipped with both a sulfur filter (wavelength = 393 nm) and a phosphorus filter (wavelength = 525 nm) allowing the quantification of a large range of DMS concentrations, as usually found in ice samples [Tison et al., 2010; Stefels et al., 2012]. The temperature of the FPD detector was set at 250°C and gas flows at 50 mL.min^{-1} for H2, 60 mL.min^{-1} for dry air, and 60 mL.min^{-1} for make-up gas N_2. The temperature of the GC oven was programmed as follows: it started at 60°C, rose to 150°C at a rate of 30°C.min^{-1}, stayed at 150°C for 3 min – during which the DMS peak resolved (around 4 min) – and then returned to 60°C. The GC was calibrated using standards prepared from dilutions of pure (> 99%) DMS (Merck) in Milli-Q water. Typically, 10 different standards (from 0.003 to 3 nmol in 10 mL) in triplicate were analyzed to make calibration curves. Linear regressions were obtained from the square root of peak areas, with correlation coefficients always > 0.996.

DMSP was measured as DMS after cold alkali cleavage of DMSP into DMS (1:1 stoichiometry) following Dacey and Blough [1987]. At the end of the DMS analysis, the vessel was brought back to the cold room. The fine ice powder resulting from the crushing was weighted and transferred in a 20 mL glass vial in which two NaOH pellets were added. The vial was then hermetically crimp sealed with a butyl/PTFE septum cap and stored to melt at 4°C in the dark for 24 hours. The vial was hooked up to the purge-and-trap gas chromatograph system described above using PTFE tubing and needles as described by Stefels [2009]. DMS from the DMSP cleavage was purged from the vial using UHP grade (99.999%) helium at a constant flow rate of 50 mL.min^{-1} for 15 minutes, and concentrated by cryogenic trapping in a PTFE loop (1/8'' OD) immersed in liquid nitrogen (-196°C). A -30°C cold bath (ethanol/liquid nitrogen mixture) was installed

downstream the sample vial in order to remove water vapor from the gas stream [Andreae and Barnard, 1983]. After 15 minutes, the PTFE loop was immersed in boiling water, DMS thermally desorbed and injected for quantification into the GC. Triplicate measurements of DMS and DMSP in ice samples gave relative standard deviations < 12%. DMSP values presented in this study are total DMSP (particulate $DMSP_p$ + dissolved $DMSP_d$).

For under-ice water samples, a few milliliters of liquid (typically 5 mL) were transferred from the sampling vial through the septum into a clean pre-sealed 20 ml glass vial. DMS and DMSP concentrations were then measured using the same purge-and-trap GC system and cold alkali treatment as described above. Triplicate measurements of DMS and DMSP in aqueous samples gave relative standard deviations < 7%.

4.2.2.2. Physical properties

The second half of the core used for the DMS,P analysis was used to determine the ice texture, providing information on sea ice growth processes. Thick vertical sections of the core were cut with a band saw and attached to glass plates by freezing milliQ water along the edges of the sections. The thick sections were planed down to thin sections of 600 to 700 µm using a Leica® SM2400 microtome. These thin sections were then installed on a light table equipped with cross-polarized sheets [Langway, 1958]. Textural types were identified based on visual observation of the size, shape, and orientation of the ice crystals and compared to descriptions found in the literature [Eicken and Lange, 1991; Tison et al., 1998].

Ice temperature (T) was measured on site, on a different ice core than the one used for DMS,P and texture, using a fast response handheld portable digital thermometer equipped with a TESTO®720 calibrated probe (precision ± 0.1°C,

accuracy ± 0.2°C). The probe was inserted in 4 mm diameter holes freshly drilled along the core every 5 cm. In case the end of a 5 cm interval corresponded to a crack in the core, the measurement was made a few centimeters further. Bulk ice salinity (S) was measured using the same vertical resolution as for ice temperature. In the cold room, the core was sectioned (5 cm increments) using a band saw. The sections were then allowed to melt at room temperature in sealed plastic containers, a process taking approximately 12 hours. Bulk ice salinity was determined through conductivity by inserting the probe of a Thermo-Orion® WP-84TPS conductimeter in each melted ice section (accuracy of ± 0.1‰). Further details about basic physical measurements can be found in Carnat et al. [2013].

4.2.2.3. Biological properties

Chlorophyll *a* (chl *a*) and phaeophytin *a* (phaeo *a*) measurements were performed on a third ice core. The core was cut in vertical sections of 10 cm with a band saw, in the cold lab (< -30°C) on the day of extraction. Core sections were melted at 4°C in the dark, in seawater (1:4 volume ratio) pre-filtered through 0.2 µm Sartobran 300 cartridges (Sartorius®) to attenuate osmotic stress on the algae. Melted ice was then gently vacuum filtrated successively on 10 and 0.8 µm Nuclepore® polycarbonate filters, under low light conditions. Filters were stored frozen in cryovials until analysis. Filters were extracted in 10 mL of acetone (90% volume ratio) at 4°C for 16h. Extraction was improved by the use of a vortex and of a sonicator, followed by centrifugation. Chl *a* and phaeo *a* (after acidification, 1.2 M HCl) were quantified, following Yentsch and Menzel [1963], with a Turner Design TD700 fluorometer equipped with a 10-040R* Chl *a* optical kit. Total chl *a* and phaeo *a* contents were calculated as the sum of concentrations measured on the

10 and 0.8 µm filters. The same procedure as described here above was used to measure chl *a* in under-ice water samples.

Biomass composition was determined for three stations (1, 5, and 7) through light microscopic cell enumeration in 200 mL aliquots of melted sea ice (same ice core as for chl *a*) stored in brown glass bottles, and preserved with acid Lugol's solution. The bottles were stored in the dark until the cells were settled from a 50 mL, 10 mL, 2 mL or 1 mL volume for up to 24 hours according to Ütermöhl [1958]. Then, the settled cells were visualized (measured and enumerated) using a Leica Leitz DM IL inverted light microscope equipped with 10x and 40x objectives and 10x and 12.5x oculars (maximum magnification of 500x) with an attached digital camera (Leica DC300F) for documentation. Species identification was based on Meddlin and Priddle [1990], Thomas [1997], and Scott and Marchant [2005].

4.3. Results

4.3.1. General ice and atmospheric conditions

The evolution of the air temperature and solar radiation in 2011-2012, as recorded by a weather station at Scott Base (25 km away from Cape Evans), is shown in Figure 4.2. The first sampling phase (stations 1 to 3) occurred during the spring-summer transition in 2011, and the second sampling phase (stations 4 to 8) occurred during the winter-spring transition in 2012. These seasonal episodes will be referred to throughout the paper. Atmospheric conditions during the study varied from very cold air temperature (-35°C) and low light at the end of winter in 2012 (station 4), to air temperature approaching 0°C and high light at the end of spring 2011 (station 3). Snow and ice thickness conditions observed at the stations are summarized in Table 4.1. Terra MODIS (250 m spatial resolution) satellite

images (http://modis.gsfc.nasa.gov/) revealed that fast ice in 2011 and 2012 formed around the beginning of April and broke up in early February. In both years, the snow cover was typically thin (always < 4 cm) and consisted of wind slabs and fresh blown snow. The ice cover was highly homogeneous (small SD in thickness, see Table 4.1) and not flooded (positive freeboards) at any station.

Figure 4.2: Evolution of the air temperature (°C) and solar radiation ($MJ.m^{-2}.day^{-1}$) in 2011 and 2012, as recorded by a weather station at Scott Base (25 km away from Cape Evans). Sampling stations are shown as vertical dashed-lines. SF and PF shaded areas are the estimated onset of ice growth and platelet ice growth respectively. SF was estimated from Terra MODIS (250 m spatial resolution) satellite images of the study site. PF was estimated using a freezing degree day (FDD) calculation. First, we calculated the cumulative FDD (θ), following Maykut [1986], using the thickness of columnar ice formed until platelet crystals started to appear in the ice texture. We found θ = 746 in 2011, and 689 in 2012. Then, following Weyprecht [1875] we determined on which days the θ were reached using the mean daily air temperature recorded by a weather station at Scott Base (25 km away from Cape Evans).

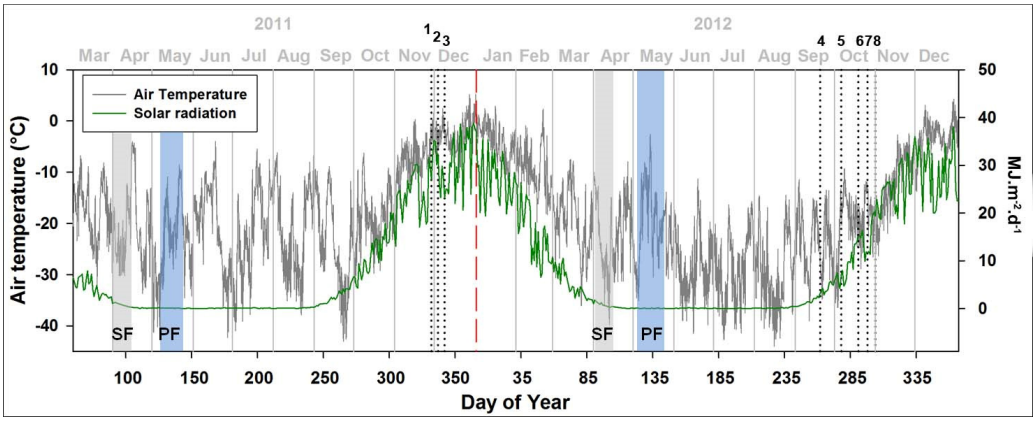

Table 4.1: Summary of the snow and ice conditions at the sampling sites.

	Spring-summer 2011	Winter-spring 2012
Station	1 ; 2 ; 3	4 ; 5 ; 6 ; 7 ; 8
Date (Day of Year)	332 ; 337 ; 342	263 ; 279 ; 292 ; 299 ; 306
Mean snow thickness (cm)	2.5 ; 1.6 ; 0.9	1.2 ; 1.5 ; 0.8 ; 0.8 ; 0.6
Mean ice thickness (cm)	157.1±1.2 ; 153.4±2.1 ; 152.6±1.4	147.2±2.2 ; 160.8±1.3 ; 166.9±0.9 ; 169±1.1 ; 170.7±1.1
Granular ice (%)	0.6 ; 0.6 ; 0.6	6 ; 6 ; 6 ; 5 ; 5
Columnar ice (%)	62 ; 62 ; 63	54 ; 62 ; 64 ; 65 ; 56
Mixed columnar/platelet ice (%)	37 ; 37 ; 36	40 ; 32 ; 30 ; 30 ; 39

The mean ice thickness increased linearly with time during the winter-spring transition in 2012 (ANOVA $p < 0.05$) indicating a growing state, and showed no significant trend during the spring-summer transition in 2011, suggesting a steady-state condition.

4.3.2. Sea ice growth processes

An overview of the ice texture observed during the winter-spring transition in 2012 and spring-summer transition in 2011 is shown in Figure 4.3. Close-ups of vertical thin sections pictures on a light table under cross-polarized filters are also shown for station 1. The ice texture showed little variation between stations. Typically, a thin layer of granular ice (~ 2 cm), composed of small (mm sized) crystals with an orbicular shape, was observed at the surface of each station. This layer corresponded to frazil ice accumulation. The granular ice was followed by a well organized columnar ice with long (cm sized, prismatic) vertically oriented crystals (Figure 4.3A) corresponding to undisturbed congelation growth. Thin layers of frazil ice (~ 3 to 6 cm) were found around 20 cm depth during the winter-spring transition in 2012, sandwiched between columnar ice layers. A more disturbed ice texture started to develop around ~ 80 cm (spring-summer stations

of 2011 + station 4) and ~ 120 cm (winter-spring stations of 2012) depth. A mix of strongly tilted columnar crystals, randomly oriented crystals with ragged edges (Figure 4.3B) and long triangular crystals (Figure 4.3C) was observed at almost all depths in the bottom half of the ice. We classified these layers as mixed columnar/platelet ice.

The relative contribution of the different textural types to the total ice thickness is reported in Table 4.1. Mixed columnar/platelet ice accounted for 34.2% (SD 4.9) and 36.6% (SD 0.5) of the total ice thickness during the winter-spring transition in 2012 and spring-summer transition in 2011, respectively.

Figure 4.3: Overview of the ice texture observed during the spring-summer transition in 2011 (stations 1 to 3) and the winter-spring transition in 2012 (stations 4 to 8). Close-ups of the following textural features are also shown: A. Well organized columnar ice with long (cm sized, prismatic) vertically oriented crystals. B. Randomly oriented crystals with ragged edges (arrow pointing at one of the crystals). C. Long triangular crystals (arrow pointing at one very large crystal). Circled in Figure 4.3C is a large refrozen brine tube.

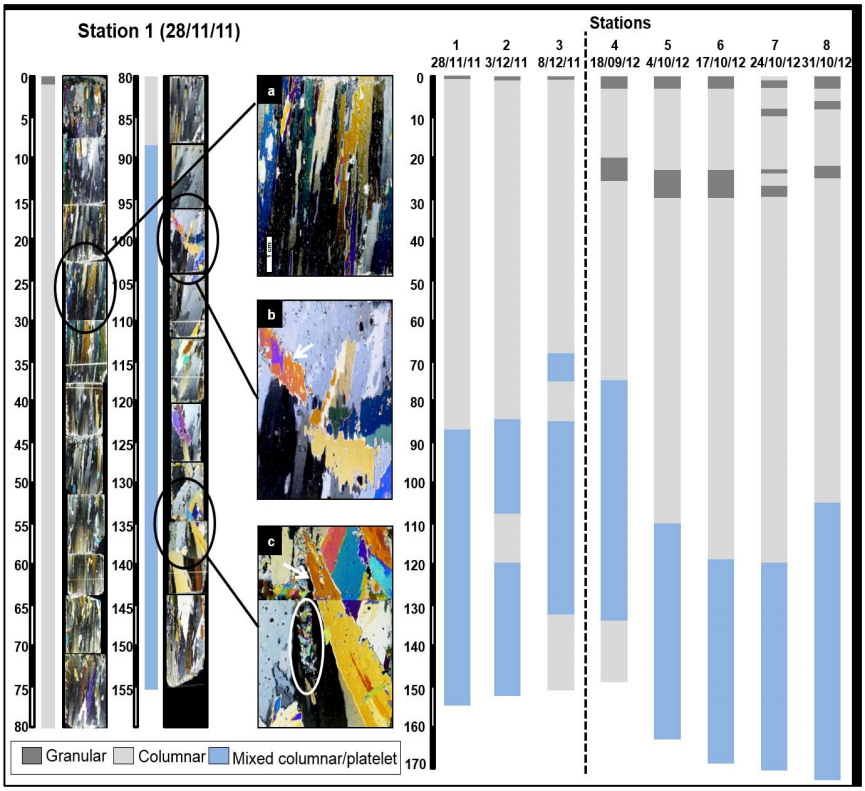

Porosity features such as pores and holes were detected in the thin section pictures taken during the spring-summer transition in 2011. These were particularly numerous in the surface ice layers and in some of the mixed columnar/platelet ice layers. Also, large refrozen brine tubes were seen in some of the interior ice and bottom ice sections (Figure 4.3C).

4.3.3. Ice permeability and brine dynamics

Vertical profiles of ice temperature during the winter-spring transition in 2012 showed a linear decrease from a cold surface to a warmer ice base (Figure 4A). Mean ice temperature increased from station 4 (-11.3°C) to 8 (-6.9°C). Profiles were much warmer during the spring-summer transition in 2011, ranging from -1.8 to -2.9°C, and were almost isothermal (SD < 0.4) (Figure 4B). Vertical profiles of sea ice bulk salinity during the winter-spring transition in 2012 initially showed some resemblance of a double C-shape with a local maximum in interior ice (Figure 4A). From station 6 to 8, the local maximum vanished and the profiles became C-shaped, as typically observed in growing first-year ice [e.g. Weeks and Ackley, 1986]. During the spring-summer transition in 2011, profiles transitioned from a C-shape profile to a near-isohaline profile, with a freshening of surface ice (Figure 4B), typical of summer ice [e.g. Tison et al., 2008]. In general, our ice temperature and bulk salinity profiles were very similar to those reported by Remy et al. [2008] from 1999 to 2003 in first-year ice near Cape Evans.

Ice permeability and brine dynamics were approached in this study by calculating the brine volume fraction. Brine volume fraction, defined as brine volume/bulk ice volume (%), was computed from ice temperature and bulk salinity data using the equations of Cox and Weeks [1983] for ice temperature < -2°C, and of Lepparänta and Manninen [1988] for ice temperature ≥ -2°C, assuming

thermodynamic equilibrium of the brine with surrounding ice and air volume fraction of 1%. Above a critical threshold in brine volume fraction, brine inclusions become interconnected and the ice is considered as permeable to fluid transport [Cox and Weeks, 1988].

Figure 4.4: Vertical profiles of ice temperature and bulk salinity at A. station 4 (winter-spring), B. station 2 (spring-summer).

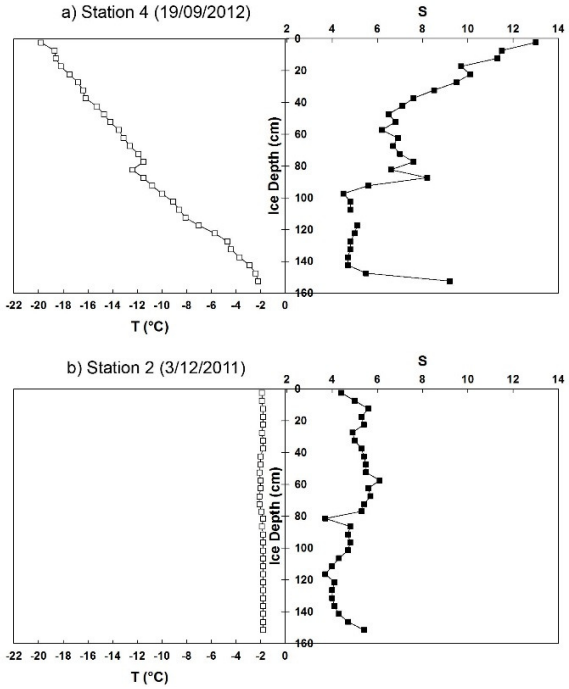

According to the percolation theory, developed for an ideal well aligned columnar ice, a brine volume fraction of 5% is a reasonable permeability threshold [Golden et al., 1998]. However, for more complicated ice textures, as observed in this study (e.g. platelet ice), the threshold is presumably higher (~ 7%) [Golden et al., 2007; Gough et al., 2012]. Contour plots of brine volume fraction during the winter-spring transition in 2012 and spring-summer transition in 2011 are shown in Figure 4.5. A strong contrast between the two seasonal episodes was observed. During the winter-spring transition in 2012, brine volume fraction was initially below 5% at all depths with the exception of the warmest bottom ice sections (bottom 5 to 20 cm),

suggesting that the ice was impermeable. Values then started to increase in interior ice from station 6 to 8 on seasonal warming, reaching 5 to 7%. During the spring-summer transition in 2011, high values (> 8%) were found throughout the profiles, suggesting that the ice was permeable at all times and all depths. Permeable ice is prone to brine convection provided the brine network is unstable, i.e. brine salinity (density) decreasing towards the ice-ocean interface and above the under-ice water salinity (density). Brine salinity was calculated from ice temperature according to Cox and Weeks [1983] and Lepparänta and Manninen [1988]. With the exception of station 2 where brine salinity approached the under-ice water salinity (34.3 to 34.5) at all depths, all stations showed an unstable brine network.

Figure 4.5: Contour plots of brine volume fraction (%) during the spring-summer transition in 2011 (left panel) and the winter-spring transition in 2012 (right panel). Sampling stations are shown as vertical dotted-lines.

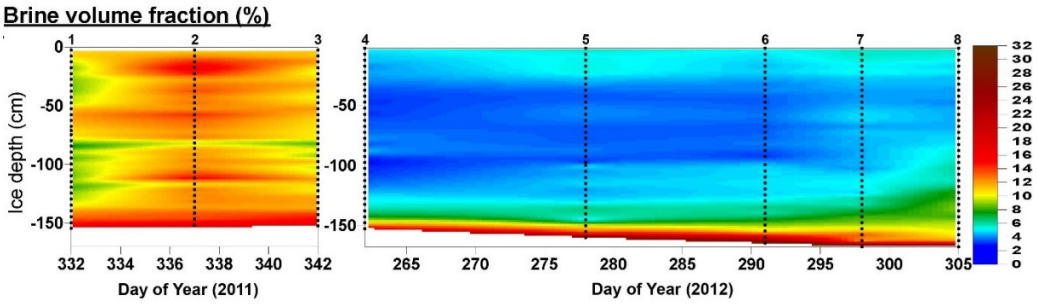

4.3.4. Biomass and biomass composition

Vertical profiles of chl *a* in ice during the winter-spring transition in 2012 and spring-summer transition in 2011 are shown in Figure 4.6. Chl *a* concentrations spanned a wide range: from < 0.1 to 1440.7 µg.L-1 during the winter-spring transition in 2012, and from 0.1 to 285.4 µg.L^{-1} during the spring-summer transition in 2011. Ice algal biomass was predominantly located in the bottom 10 cm of the cores. These layers had a strong discoloration. Chains and filaments of algae were also seen protruding from the ice bottom, corresponding

to a stranded community. The bottom 10 cm biomass represented on average 87% (SD 13) of the total ice algal biomass. During the winter-spring transition in 2012, bottom ice chl *a* increased consistently from station 4 (13.2 $\mu g.L^{-1}$) to station 7 (1440.7 $\mu g.L^{-1}$), illustrating the dark-light transition from winter to spring (Figure 4.2). The very high chl *a* measured at station 7 (130 mg chl $a.m^{-2}$) matched the observations of Ryan et al. [2006] at Cape Evans during peak-bloom in early November 1999 (bottom ice chl a of 173 mg chl $a.m^{-2}$). The productivity of bottom ice algae in McMurdo Sound is essentially limited by light availability until the spring bloom [Bunt and Lee, 1970; Grossi et al., 1987]. In that respect, the snow cover observed during the study was not thick enough (< 4 cm, Table 4.1) to considerably affect photosynthetic activity [Mundy et al., 2005; Juhl and Krembs, 2010]. Similarly, low under-ice water currents at Cape Evans usually provide stable growth conditions for bottom ice communities (no ablation) [Ryan et al., 2006]. After the peak-bloom (station 7), chl *a* decreased to 501.7 $\mu g.L^{-1}$ at station 8. During the spring-summer transition in 2012, bottom ice chl *a* strongly decreased from station 1 (285.4 $\mu g.L^{-1}$) to station 2 (22.6 $\mu g.L^{-1}$), and stabilized from station 2 to 3 (24.8 $\mu g.L^{-1}$). In the other ice layers, chl *a* concentrations were two to five orders of magnitude lower than bottom ice concentrations, with values < 2.5 $\mu g.L^{-1}$ measured throughout the whole study. Small local maxima were observed at ~ 80 to 90 cm depth at stations 2 and 3, at ~ 100 to 120 cm depth at stations 4, 5 and 8, and at ~ 20 cm at station 7.

The successive filtration of the chl *a* samples on 10 and 0.8 µm filters allowed the separation of ice algae in two groups based on cell size (small 0.8-10 µm, large > 10 µm) (Figure 4.6). The bottom 10 cm of the ice, where the maxima in chl *a* were always recorded, was largely (> 90%) dominated by large cells at all

stations. Over 50% of large cells were observed in most of the ice layers during the winter-spring transition in 2012, with the exception of some interior ice layers at stations 6, 7, and 8 (Figure 4.6). During the spring-summer transition in 2011, a marked contrast at stations 1 and 2 was observed between the upper (> 50% of small cells) and bottom (< 50% of small cells) half of the ice. This was not observed at station 3 where large cells dominated in all but one layer.

The ratio of phaeo *a* to the sum of phaeo *a* and chl *a* for the 0.8 to 10 µm and > 10 µm cell sizes was also calculated (data not shown). This ratio indicates whether degraded cell pigments dominate over active cell pigments in a distinct algal assemblage [Jeffrey et al., 1997]. A ratio > 0.5 corresponds to a highly degraded assemblage while a low ratio (near 0) corresponds to a low-degraded assemblage. Throughout the study, the ratio remained low (< 0.3) in the bottom 10 cm of the ice cover for both small and large cells.

In under-ice water (data not shown), low chl *a* was observed at all sampling depths (0 to 30 m) throughout the study, ranging from < 0.1 to 2.5 $\mu g.L^{-1}$ (overall average = 0.2 $\mu g.L^{-1}$). From station 4 to station 8 during the winter-spring transition in 2012, chl *a* was always < 0.1 $\mu g.L^{-1}$, with a slight increase observed at the ice-ocean interface from station 5 to station 7. From station 1 to station 3 during the spring-summer transition in 2011, chl *a* remained < 0.5 $\mu g.L^{-1}$ at 1 and 30 m depth, while at the ice-ocean interface they increased from 0.1 to 2.5 $\mu g.L^{-1}$. Under-ice algal assemblages were dominated by large cells with the exception of the ice ocean interface at stations 2, 4, and 6. During the winter-spring transition in 2012, both the small and large cells assemblages were initially highly degraded (stations 4 to 5). Assemblages became less degraded at stations 6 and 7.

The biomass composition observed in the different ice layers of stations 1, 5, and 7 is shown in Figure 4.7. We identified three main groups: diatoms, dinoflagellates, and other flagellates. The composition only slightly differs between the winter-spring stations 5 and 7. The upper-half of the ice was largely (71 to 99%) dominated by flagellates (other than dinoflagellates) at both stations.

Figure 4.6: Vertical profiles of chl *a* (horizontal bars, log scale), and percentage of small cells (0.8 to 10 µm) (black dots) in the ice during the spring-summer transition in 2011 (upper panel) and winter-spring transition in 2012 (lower panel). The vertical dashed-lines are set at 50% of small cells.

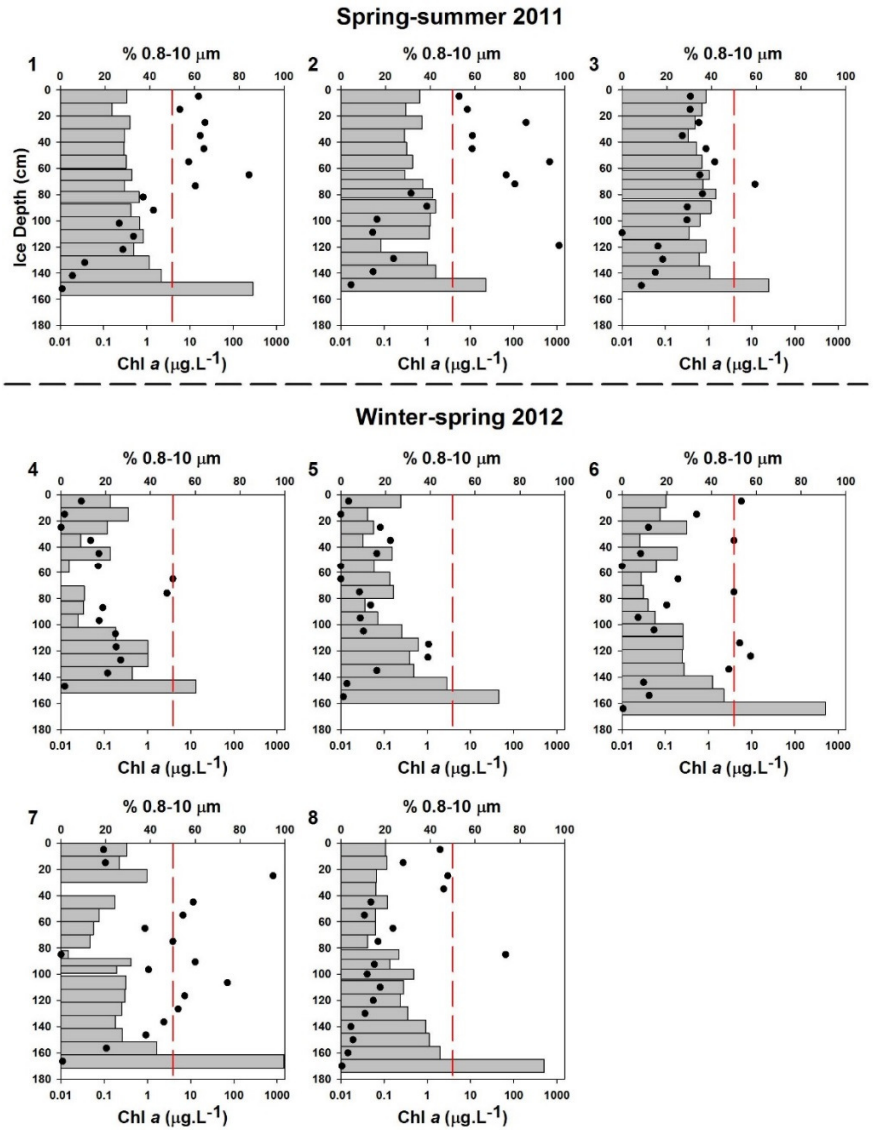

The bottom ice assemblages were also relatively similar in composition, with 68 to 71% of diatoms, 2% of dinoflagellates, and 27 to 29% of other flagellates. The lower interior ice layers were dominated by dinoflagellates (33 to 94%) and other flagellates (2 to 55%) at station 5, and by other flagellates (52 to 67%) at station 7.

Figure 4.7: Biomass composition observed at selected depths of three stations. Note the difference in horizontal scale for the bottom ice layers. DMSP profiles are also shown as grey dots for comparison purposes.

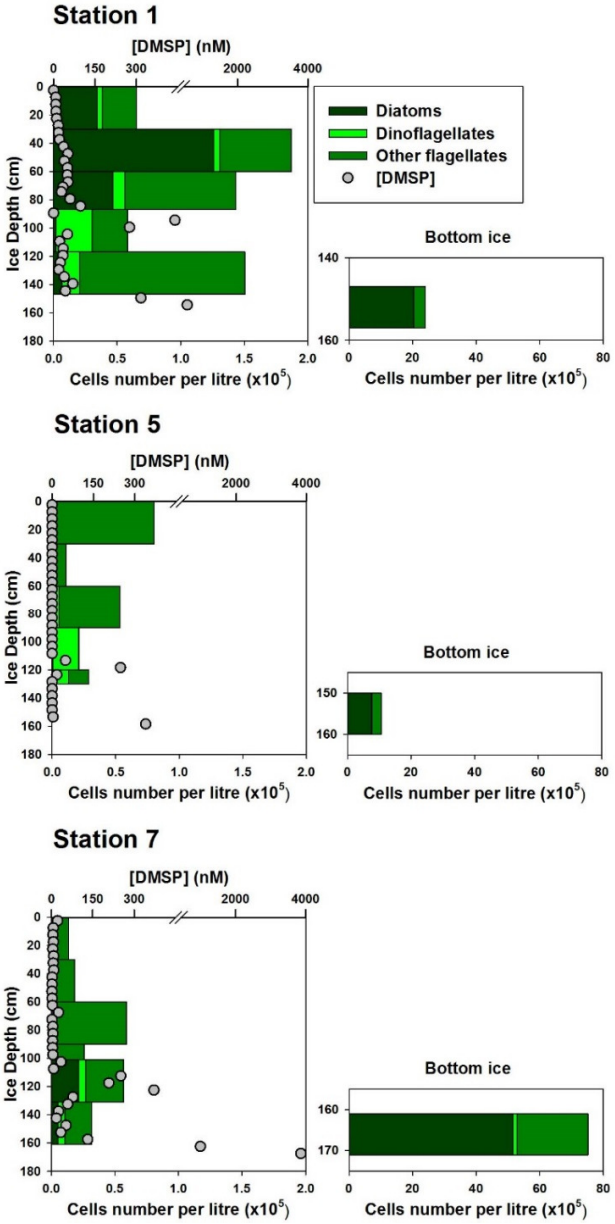

The bottom and lower interior ice composition of the spring-summer station 1 resembled that of station 5, except for the very high percentage of dinoflagellates found around 90 and 120 cm depth at station 5. The upper-half assemblage of station 1 was relatively well mixed compared to the winter-spring stations, with diatoms and flagellates dominating over dinoflagellates. Our observations are in good agreement with previous observations of the vertical distribution of ice algal biomass at Cape Evans, showing a few species of diatoms – *Nitzschia stellata*, *Nitzschia lecointei*, and *Entomoneis kjellmanii* – typically dominating the bottom assemblages [McMinn et al., 2000; Ryan et al., 2006; Remy et al., 2008; Sutherland, 2008].

4.3.5. DMS,P dynamics

Vertical profiles of DMS and DMSP concentrations in sea ice during both seasonal episodes are shown in Figures 4.8 and 4.9 respectively. Statistical parameters (geometric mean, median and standard deviation) of the concentrations are provided in Table 4.2.

During the winter-spring transition in 2012 (stations 4 to 8), DMS in ice ranged from below detection limit (< 0.3 nM) to 377.0 nM. DMSP was consistently higher, ranging from below detection limit (< 0.3 nM) to 3865 nM. DMS was found at only one depth (100 cm) at station 4, reaching a concentration of 9 nM. No DMS was detected at station 5. High DMS concentration was observed in bottom ice later in the season, increasing from 231 to 377 nM between station 6 and station 7. A second peak in concentration was detected in interior ice after station 6, at ~ 110 to 120 cm depth. Concentration at that depth increased from 33 to 45 nM between station 7 and station 8. At all the other depths, DMS remained close to detection limit throughout the winter-spring transition in 2012. DMSP was found at

two depths at station 4, at ~ 70 cm depth (143 nM) and ~ 100 cm depth (41 nM). A strong peak in DMSP concentration started to develop in bottom ice at station 5 (339 nM), reached 3865 nM at station 7, and then dropped to 1334 nM at station 8. Similarly to DMS, a second peak in concentration was detected in interior ice at ~ 110 to 120 cm depth between station 5 and station 8, fluctuating around a mean value of 250 nM.

Table 4.2: Statistical parameters of sea ice DMS and DMSP concentrations at each station.

		$[DMS]_{ICE}$ (nM)		
	Station	Mean (Geo.)	Median	STDEV
Spring-summer	1	2,1	2,9	46,8
	2	2,6	4,6	64,7
	3	1,3	1,9	5,4
	Overall	**2,2**	**2,7**	**46,2**
Winter-spring	4	0,3	0,3	1,7
	5	<0.3	<0.3	<0.1
	6	0,9	0,7	39,3
	7	1,5	0,5	31,1
	8	1,5	0,6	64,5
	Overall	**0,8**	**0,3**	**37,3**

		$[DMSP]_{ICE}$ (nM)		
	Station	Mean (Geo.)	Median	STDEV
Spring-summer	1	30,4	35,5	130,3
	2	44,7	43,7	130,2
	3	55,2	46,7	139,8
	Overall	**42,2**	**42,2**	**132,2**
Winter-spring	4	0,6	0,3	27,1
	5	0,7	0,3	73
	6	12,2	9	371,5
	7	18,5	8,7	675,2
	8	14,5	10,3	235,7
	Overall	**4,5**	**5,2**	**369,6**

During the spring-summer transition in 2011 (stations 1 to 3), DMS in ice ranged from below detection limit (< 0.3 nM) to 369 nM (Figure 4.8). DMSP was again consistently higher than DMS, ranging from below detection limit (< 0.3 nM) to 683 nM (Figure 4.9). Some common features in the DMS profiles were observed at the stations sampled during the spring-summer transition in 2011. Concentrations were below detection limit (< 0.3 nM) throughout the upper 50 cm of the ice cover. The highest concentrations were always found in bottom ice. Similarly to the winter-spring profiles of 2012, a second peak in concentration was observed in interior ice, at ~ 100 cm depth, decreasing from 27 to 11 nM between

station 1 and station 3. An important change in the profiles with time was the remarkable decrease in bottom ice concentration from 369 to 23 nM between station 2 and station 3. DMSP profiles somewhat mimicked DMS profiles at stations 1 and 2, as indicated by the coefficients of determination of the linear relationship between DMS and DMSP at these stations (0.60 and 0.78 respectively). Low but non negligible concentrations (few tens of nM) were observed in the upper 50 cm ice, highest concentrations were observed in bottom ice, and a second peak in concentration was found at ~ 100 cm depth. Similarly to DMS, the greatest fluctuations in DMSP were seen between station 2 and station 3. The second peak at ~ 100 cm depth vanished and concentrations markedly increased in near-surface ice (from subnanomolar levels to 77 nM), while concentrations remained high in bottom ice.

DMS and DMSP in under-ice water were below detection limit (< 0.3 nM) at all sampling depths (0, 1, and 30 m) during the winter-spring transition in 2012 (data not shown). During the spring-summer transition in 2011, DMS ranged from below detection limit (< 0.3 nM) to 24 nM. DMSP was slightly higher, ranging from below detection limit (< 0.3 nM) to 38 nM. At station 1, both DMS and DMSP were very low (subnanomolar). DMS increased about 2 orders of magnitude at all sampled depths from station 1 to station 2, with the maximum concentration found at the ice-ocean interface (6 nM).

Figure 4.8: Vertical profiles of DMS concentrations (grey dots) in the ice during the spring-summer transition in 2011 (upper panel) and winter-spring transition in 2012 (lower panel). For comparison purposes, chl *a* concentrations in ice are reported as horizontal bars. Ice texture is reported as vertical colored bars next to the right y-axis, using the same color code as in Figure 4.3. Dark grey is granular ice, light grey is columnar ice, and light blue is mixed columnar/platelet ice.

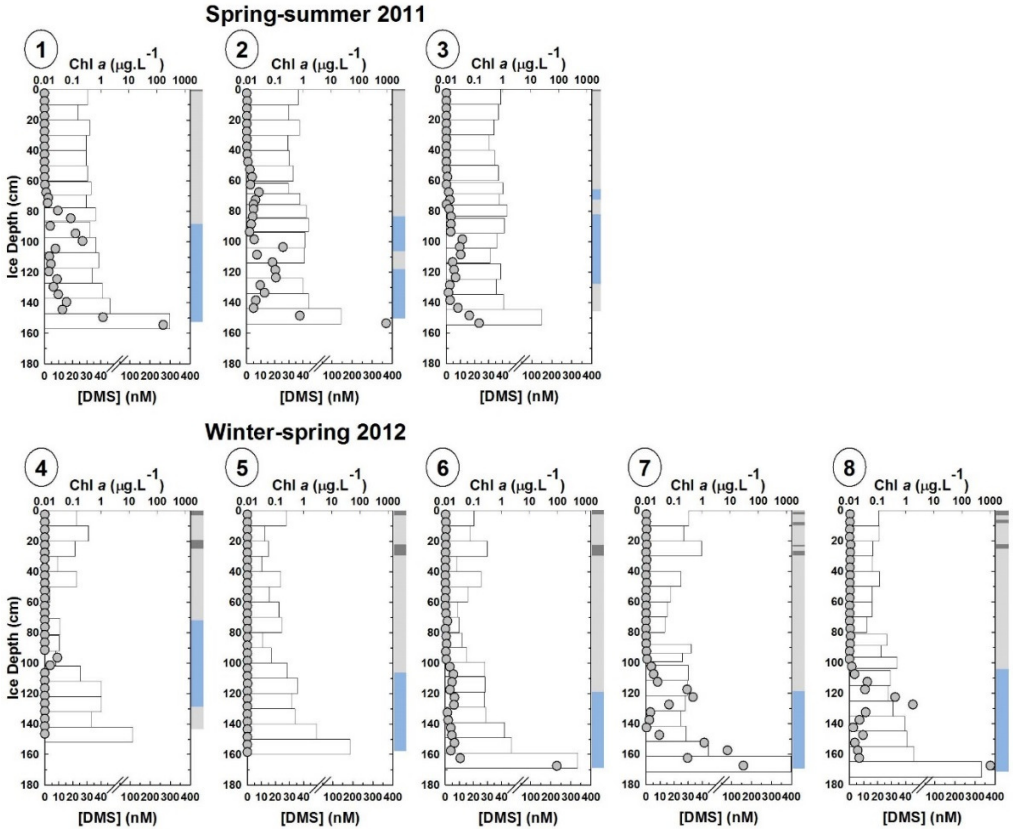

Similar changes were observed in the DMSP profiles, although the increase was less marked at 30 m depth. DMS further increased from station 2 to station 3, while the DMSP profile remained stable. DMS at 30 m depth became remarkably high (19 nM), even substantially higher than DMSP.

Figure 4.9: Vertical profiles of DMSP concentrations (grey dots) in the ice during the spring-summer transition in 2011 (upper panel) and winter-spring transition in 2012 (lower panel). For comparison purposes, chl *a* concentrations in ice are reported as horizontal bars. Ice texture is reported as vertical colored bars next to the right y-axis, using the same color code as in Figure 4.3. Dark grey is granular ice, light grey is columnar ice, and light blue is mixed columnar/platelet ice.

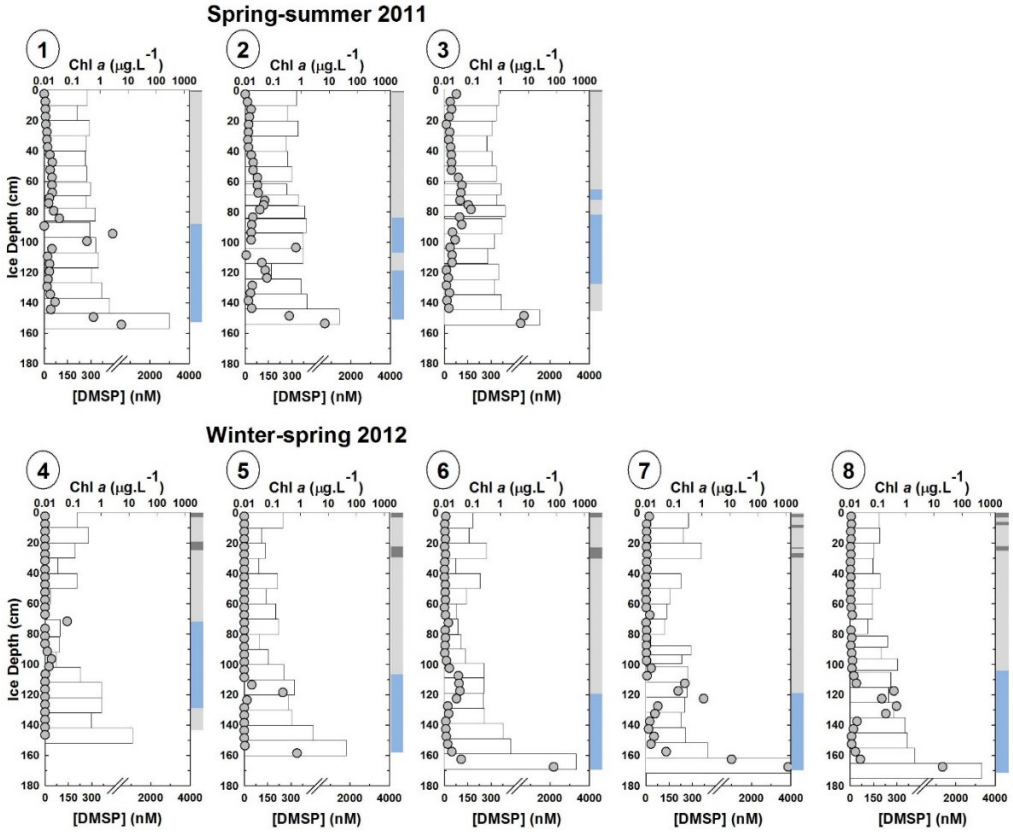

4.4. Discussion

4.4.1. Importance of DMS,P production in sea ice at Cape Evans

The bulk sea ice DMS and DMSP concentrations presented in this study are in line with previously reported concentrations in the literature (Table 4.3), and confirm that sea ice is a biome favorable to substantial production of dimethylated sulfur compounds. The maximum DMSP concentration measured in bottom ice during peak-bloom at station 7 (3865 nM) is the highest ever observed in

undeformed Antarctic first-year ice. This is not surprising given the very high biomass observed in bottom ice at station 7, with a chl *a* concentration (1440.7 $\mu g.L^{-1}$) 1 to 2 orders of magnitude higher than the maximum chl *a* concentrations reported in other studies (e.g. 28.4 $\mu g.L^{-1}$ in Tison et al. [2010] and 155.7 $\mu g.L^{-1}$ in Kirst et al. [1991]). Despite the important difference in biomass between studies, the difference between the peak-bloom DMSP production at Cape Evans and the bloom/post-bloom DMSP production in e.g. the Weddell Sea (2627 nM in Tison et al. [2010] and 1663 nM in Kirst et al. [1991]) is relatively small. This may be because our bottom ice assemblage at the time of the bloom was largely dominated by diatoms (71%, Figure 4.7) – usually acknowledged as low individual producers of DMSP [Keller et al., 1989], while high individual producers of DMSP such as haptophytes (not detected in our samples) were reported in other studies.

With the exception of the bottom ice maximum and a very localized peak in interior ice (Figure 4.9) (which we will discuss in the next section), DMSP concentrations are generally small during both seasonal episodes compared to other studies conducted at the same time of the year in other Antarctic locations (Table 4.3). As a result, the mean DMSP concentration measured during the winter-spring transition in 2012 (76 nM) and spring-summer transition in 2011 (87 nM) fall within the lower portion of the range of reported values. This is understandable given the low chl *a* concentrations (< 2.5 $\mu g.L^{-1}$) (Figure 4.6), and low percentages of acknowledged high individual DMSP producers (Figure 4.7) observed in most of Cape Evans sea ice layers, while important surface and interior ice communities were observed in other studies.

Table 4.3: Overview of available Antarctic sea ice DMS,P data sets. Note that the resolution of vertical sampling found in the different studies (0.05, 0.10, and 0.20 m) can affect the reported DMS,P concentrations. Because DMS,P is found in discrete bands within sea ice, the signal can be obscured in case of coarse ice core sectioning. In this study, we report values based on a high vertical sampling resolution (0.05 m). If we had chosen a 0.10 to 0.20 m vertical sampling resolution, our maximum DMS,P would have been 20 to 55% lower. Note also that means should not be compared between studies with different sampling strategies. For instance, in DiTullio et al. [1998], only the bottom 5 to 20 cm of ice cores with visible discoloration (and hence important algal biomass) were analyzed, whereas in the other studies referenced in this table, full ice cores were analyzed.

Location	Ice Type	Ice Texture[a]	Season	DMSP[b] (nM)	DMS[b] (nM)	Chl*a*[c] (μg/L)	DMS,P[f] sampling resolution (m)	Reference
Weddell Sea	Pack ice	F+C	Spring	**408.9** (4.1-1663.8)	NA	**24.8** (3.4-155.7)	0.10 (F.C.)	Kirst et al. (1991)
Western Weddell Sea	Pack ice	F+SU+C	Summer	**171** (5-2627)	**58** (0.5-1430)	**5.3**(0.1-28.4)	0.05 (F.C.)	Tison et al. (2010)
Bellingshausen Sea	Pack ice	Frozen snow+C	Spring/Summer	**200** (17-546)	NA	**4.6** (0.2-24)	0.15/0.20 (F.C.)	Turner et al. (1995)
Prydz Bay	Pack ice	NA	Spring	**144** (8-725)	NA	NA	0.10/0.20 (F.C.)	Curran and Jones (2000)
Offshore Prydz Bay	Pack ice	NA	Spring	**107** (6-787)	NA	**4.9** (0.1-41.5)	0.10 (F.C.)	Trevena et al. (2000)
Dumont D'Urville Sea	Pack ice	NA	Winter	**40** (nd-193)	NA	NA	0.10/0.20 (F.C.)	Curran et al. (1998)
Ross Sea	Pack ice	NA	Spring/Summer	**206.5** (4.4-980.0)	NA	**54.4** (1.2-243.3)	0.05/0.20 (B.S.)	DiTullio et al. (1998)
Ross Sea	Fast ice	NA	Spring	**150.0** (80.9-218.8)	NA	**103.7** (38.7-138.5)	0.05/0.20 (B.S.)	DiTullio et al. (1998)
Prydz Bay	Fast ice	F+C	Spring/Summer	**112** (9-1478)	NA	**5.6** (0.03-84.8)	0.10 (F.C.)	Trevena et al. (2003)
Gerlache inlet	Fast ice	NA	Summer	**nd** (4.4-450)	NA	(nd-160)	0.10 (F.C.)	Gambaro et al. (2004)
Indian sector of SO	Pack/Fast ice	NA	Spring	**185**[d,e] (45-796)	**12** (<0.3-75)	NA	0.10 (F.C.)	Trevena and Jones (2006)
McMurdo Sound	Fast ice	F+C+P	Spring/Summer	**87** (<0.3-683)	**12** (<0.3-369)	**7.6** (0.08-285.4)	0.05 (F.C)	This study
McMurdo Sound	Fast ice	F+C+P	Winter/Spring	**76** (<0.3-3865)	**7.5** (<0.3-377)	**28.4** (0.00-1440.7)	0.05 (F.C)	This study

[a]F, frazil ice; C, congelation ice; SU, superimposed ice; P, platelet ice; NA, not available; SO, Southern Ocean

[b,c]Mean (range); nd, not determined

[d]Calculated for ice categories with ice thickness <1.20 m

[e]Number of cores weighted average

[f]F.C., full core; B.S., bottom sample

Very few DMS measurements are available in Antarctic sea ice (Table 4.3). The mean DMS concentrations (7.5 and 12 nM for winter-spring 2012 and spring-summer 2011 transition respectively) are very close to the mean DMS concentration reported by Trevena and Jones [2006] in the spring in the Indian sector of the Southern Ocean (12 nM), but much lower (~5 times) than the value reported by Tison et al. [2010] during the late-summer in the Weddell Sea (58 nM). The large difference with the results from Tison et al. [2010] might originate from the fact that they sampled decaying summer ice whereas we sampled growing ice and ice in a steady-state condition (see sections 4.3.2 and 4.3.3). DMSP conversion to DMS may have been enhanced in the study of Tison et al. [2010] by an increase in the release of $DMSP_p$ upon melting. Melting could have triggered active exudation by decreasing the salinity of the ice as suggested by Delille et al. [2007]. Melting could also have facilitated the grazing of bottom ice assemblages by increasing the size of brine channels [Archer et al., 1996]. No evidence of melting (e.g. no major modification in sea ice thickness or bottom ice bulk salinity) was observed in this study, and the low ratios of phaeo *a* to the sum of phaeo *a* and chl *a* during the spring-summer transition in 2011 (Figure 4.6) suggested that the bottom ice assemblage was not heavily grazed at that time. On the other hand, differences in DMS concentrations might also originate from differences in processes such as bacterial consumption of DMS, or reduction of DMSO to DMS, which was shown to play a dominant role in the cycling of DMS in brine channels in summer sea ice in the Ross Sea [Asher et al., 2011].

4.4.2. Influence of platelet ice formation on DMS,P dynamics in interior ice

The most remarkable feature in the vertical high resolution DMS,P concentration profiles (Figures 4.8 and 4.9) was the occurrence of a DMS,P local maximum in interior ice, which was observed at similar depths at all stations during both seasonal episodes in 2011 and 2012. Such interior ice maxima are usually related to the development of interior ice algal assemblages [Trevena et al., 2003; Trevena and Jones, 2006; Tison et al., 2010] formed in response to various processes such as: mechanical deformation (i.e. rafting), infiltration of seawater in the ice floe (e.g. flooding events), vertical migration of surface or bottom ice algae through brine channels, and scavenging at depth following the accretion or growth of frazil crystals under an existing congelation ice cover [Garrison et al., 1983; Garrison, 1991; Lizotte and Sullivan, 1991; Kattner et al., 2004]. During both seasonal episodes, we observed a very good correspondence at each station between the depth of the DMSP maxima and the depth at which the ice texture changes from columnar ice to mixed columnar/platelet ice (Figure 4.9), suggesting that the development of the interior ice DMSP maxima was related to that of platelet crystals. This is further supported by the fact that some or our observations were incompatible with the development of an interior ice assemblage via the processes described above. The ice showed no signs of deformation (no rafting) (Figure 4.3), the snow cover was low at all stations (no flooding), and the maximum in DMSP was present at station 4, when the ice was very cold and hence the brine inclusions not connected (no vertical movement of algae) (Figure 4.5).

Interestingly, the DMS,P local maxima in interior ice were always associated with relatively low chl *a* (high DMSP-to-chl *a* ratios, between 101 and

440 nmol.µg^{-1}) (Figures 4.8 and 4.9), which echoes earlier observations from interior ice communities [Kirst et al., 1991; Trevena et al., 2003; Tison et al., 2010]. High DMSP-to-chl *a* ratios in sea ice studies are generally attributed to the presence of strong DMSP producers in the community considered and/or to important environmental stresses these communities are exposed to [Lizotte and Sullivan, 1991]. We investigate here if the depth and timing of platelet crystals formation corresponded to a specific community composition, and/or to specific environmental stresses.

The local DMSP maxima during the winter-spring transition in 2012 (stations 5 and 7) corresponded to the depth of appearance of dinoflagellates in the ice cover (Figure 4.7). During the spring-summer transition in 2011, the maxima corresponded to the depth where dinoflagellates largely (94%) dominated the biomass composition (Figure 4.7). Dinoflagellates are usually recognized as one of the strongest DMSP producing algal groups [Keller et al., 1989; Stefels et al., 2007], with a mean DMSP-to-chl *a* ratios in the marine environment of 111 nmol.µg^{-1} (in contrast to diatoms, 4 nmol. µg^{-1}). This value typically lies in the range of ratios measured in our interior ice assemblages (101 and 440 nmol.µg^{-1}). Dinoflagellates have been widely reported in fast ice interior layers in the McMurdo Sound [Stoecker et al., 1997; Montresor et al., 1999], including in locations very close to Cape Evans [Remy et al., 2008]. These dinoflagellates are typically incorporated during the autumnal bloom [Stoecker et al., 1997;1998; Remy et al., 2008], the timing of which corresponded with the formation of platelet crystals in 2011 and 2012 (around May, estimated using a FDD model, see Figure 4.2 caption for details). Platelet crystals could have incorporated algae via two mechanisms. First, algae could have become trapped at the base of the ice cover by platelet crystals

freezing at the ice-ocean interface by turbulent heat transfer to supercooled McMurdo ice shelf water flowing by [Gow et al., 1998; Smith et al., 2001]. Second, algae could have been transported and incorporated by frazil and/or platelet crystals initially formed at depth in supercooled plumes leaving the McMurdo ice shelf [Daly, 1984; Holland and Jenkins, 1999; Dempsey et al., 2010]. The absence of loose platelet crystals in the water column in 2011 and 2012, as well as in previous years [McMinn et al., 2000; Ryan et al., 2006; Sutherland, 2008], is more in favor of growth at the ice-ocean interface.

The transition between columnar and mixed columnar/platelet ice also corresponded to a local increase in salinity (double C-shape) in the bulk salinity profiles of growing ice during the winter-spring transition in 2012 (Figure 4.4), increasing the osmotic stress the interior ice assemblage of dinoflagellates was exposed to. The rapid freezing of interstitial columnar crystals in the mixed columnar/platelet ice growing at the ice-ocean interface may have reduced the brine inclusions connectivity, reducing the local permeability and the release of salts through brine convection. The lower brine inclusions connectivity of the mixed columnar/platelet ice transition could also have constrained the vertical redistribution of DMS,P, leading to a local accumulation. A similar physically driven accumulation process was reported by Tison et al. [2010] in the Weddell Sea.

4.4.3. Influence of ice permeability and brine dynamics on DMS,P dynamics during the spring-summer transition

Here we focus on the permeable spring-summer stations of 2011 (stations 1 to 3), assuming that the influence of brine dynamics in the impermeable winter-spring stations of 2012 was limited. A simultaneous decrease in chl *a* and increase in DMS and DMSP was observed from station 1 to station 2 (Figures 4.8, 4.9 and

4.10). We suggest that a strong brine convection episode could have occurred between the two stations, delivering some brine with large diatom cells, DMS and DMSP to the under-ice water, and replacing the brine with seawater containing smaller but more DMSP productive cells. This is supported by both physical and biological observations in ice and under-ice water. First, the ice was permeable (Figure 4.5) and the brine salinity profile was unstable at station 1. Second, the brine salinity profile became stable at station 2, suggesting that desalination of the ice through brine convection had occurred. Third, large refrozen vertical tubular drainage structure in the thin section pictures (Figure 4.3), and inverted funnel-shaped cavities at the bottom of a freshly taken ice core at station 2 (formed by turbulent micro flows developing as outgoing brine encounter warmer inflowing water), both supportive of brine convection episodes [Martin, 1974; Lewis et al., 2011], were observed. These observations are consistent with recent time series studies of ice physical properties which showed that strong brine convection is likely to occur in warming ice at the end of the spring following the increase in brine volume fraction above the permeability threshold [Carnat et al., 2013; Jardon et al., 2013; Zhou et al., 2013]. Biological observations also supported brine convection. First, although under-ice water chl *a* remained low and stable (< 0.1 $\mu g.L^{-1}$) throughout the winter-spring transition in 2012 (no significant growth) as typically observed at Cape Evans and elsewhere in McMurdo Sound [McMinn et al., 2000; Ryan et al., 2006; Sutherland, 2008; McMinn et al., 2010], a ten-fold increase was observed over a 5 days period between station 1 and 2 during the spring-summer transition in 2011. Similarly to chl *a*, DMS and DMSP in under-ice water were always below detection limit (< 0.3 nM) during the winter-spring transition in 2012, and at station 1 during the spring-summer transition in 2011. DMS and DMSP showed a drastic increase from station 1 to station 2, reaching 6

and 39 nM, respectively, at the ice-ocean interface. Second, the decrease in bottom ice chl *a* corresponded to an increase in the percentage of small cells (0.8 to 10 µm) from < 1.8% before station 1 to 4.6% at station 2, and 8.6% at station 3 (Figure 4.6).

The transition from station 2 to station 3 showed a strong decrease in DMS (from 362 to 23 nM), a more moderate decrease in DMSP (from 689 to 513 nM), and stable chl *a* (22 to 24 $\mu g.L^{-1}$) in bottom ice (Figures 4.8 and 4.9). Given that we sampled that ice in relatively warm atmospheric conditions (Figure 4.2), it is always possible that the dramatic and sudden loss of DMS was caused by partial losses of brine and gaseous inclusions upon ice core retrieval. Great care was however exercised to minimize this loss by placing the ice cores in insulated box with cold packs frozen at -30°C right after extraction. Also, we calculated the coefficient of variation between triplicates of DMS from different bottom ice sections of station 3. Assuming it is unlikely that the losses during the sampling of two different cores are equivalent (given e.g. the randomness of brine channels distribution), the low coefficient we obtained (20%) suggested that the loss was probably more than just a sampling bias. In that regard, the decrease in bottom ice DMS was coupled with a strong increase (from 6 to 21 nM) in under-ice water DMS, suggesting that the loss of DMS recorded was the result of brine release at the ice-ocean interface. A similar coupling was observed for DMSP, although the decrease/increase in bottom ice/under-ice water was less pronounced than for DMS. This echoes the observations of Tison et al. [2010] in early-summer ice from the Weddell Sea, who attributed the difference in DMS and DMSP loss to a higher resistance of DMSP to loss via brine convection. Particular DMSP linked to algal cells would mainly remain fixed to the walls of brine channels, whereas DMS present as a solute in

the brine would be more easily transported. Indeed, algal attachment to brine inclusion walls is a well-known feature [Grossmann et al., 1996; Krembs et al., 2000].

Interestingly, very high DMS was observed throughout the water column at station 3 (up to 19 nM at 30 m depth). Whether these high concentrations at depth were the result of mixing after brine drainage or the result of another process could not be assessed. Other plausible processes were: DMSP cleavage after degradation of rapidly sinking aggregates of ice algal cells [Gambaro et al., 2004], DMSP cleavage in sinking fecal pellets after grazing [Trevena and Jones, 2006], or DMS production from benthic macroalgae and surface-associated diatoms since we sampled near the coast [Van Alstyne and Puglisi, 2007]. This last process is certainly worth more investigations considering that macro-algae and surface-associated diatoms are abundant on the Cape Evans seafloor up to 25 m depth [Schwarz et al., 2003; Sutherland, 2008]. The DMS production capacity of such communities is yet to be determined.

Finally, a strong increase in DMSP in surface ice (0 to 10 cm) was observed from station 2 to station 3 (from 0.1 to 77.6 nM) (Figure 4.9). Also the DMSP peak in interior ice, well defined at stations 1 and 2, spread out at station 3 (Figure 4.9). We suggest that both these features resulted from a vertical redistribution of DMSP and biomass across the ice due to the increase in brine volume fraction (i.e. permeability) and brine convection during the spring-summer transition. The increase in brine volume fraction may have facilitated the vertical redistribution of large productive cells to surface ice (e.g. to escape grazing in bottom ice) through the widening of brine channels. In that respect, we observed a drastic change in cell sizes in favor of large cells in the surface ice from station 2 to station 3 (Figure

4.6). An alternative option to explain the changes in surface ice are seawater flooding events [Garrison, 1991]. However, these events are not common in fast ice and were not observed during this study. Brine convection might have influenced the development of the surface and interior assemblages through nutrient replenishment [Vancoppenolle et al., 2010], and might have transported both algal cells ($DMSP_p$) and $DMSP_d$ within the interior ice layers.

Unlike DMSP, no changes in DMS in surface and interior ice were observed between station 2 and station 3, although intuitively the processes described above would also have influenced DMS profiles. This maybe because the DMS produced in surface and interior ice escaped to the atmosphere given the high brine volume fraction (i.e. permeability) of the ice at the end of the sampling season, as previously suggested by Nomura et al. [2012]. Initially, this study also aimed at detecting and measuring these sea ice-atmosphere DMS fluxes on warming using gradient flux profiles. However, because of technical difficulties, we only performed a very limited amount of measurements from which we could only conclude that the DMS present in the air above the ice varied to some extent (Table 4.4).

Table 4.4: Summary of atmospheric DMS measurements. Samples were acquired using Tenax-TA cartridges following the methodology presented in Sharma et al. [1999a].

	Sampling Height (m)	Atmospheric DMS ($nmol.m^{-3}$)
Station 1	0,05	0,25
Station 2	0,15	3,18
	0,63	3,07
	0,9	3,09
Station 3	1,1	1,68

4.4.4. Coupling between DMS,P and chl *a* during the winter-spring transition

Here we focus on the bottom ice of the winter-spring transition in 2012 and investigate the coupling between DMS,P and chl *a* (Figure 4.10). In 2012, sampling started soon after the onset of algal growth, with chl *a* reaching 13 $\mu g.L^{-1}$ at station 4. DMS,P were at that point below detection limit (< 0.3 nM) and production limited to the interior ice assemblage described in section 4.4.2. DMS,P then strongly increased from station 4 to station 5 (339 nM at station 5), despite any substantial change in biomass, while DMS remained below detection limit (< 0.3 nM). The increase in DMSP did not result from an adaptation of the cells to fluctuations of temperature and salinity since those were similar between station 4 and station 5, nor did it result from a change in biomass in favor of strong DMSP producers since bottom ice was largely dominated by diatoms at station 5 (Figure 4.7). The correspondence between the increase in irradiance (Figure 4.2) during the dark-light transition from winter to spring (stations 4 to 5) and the increase in DMSP argues for a light control of DMSP synthesis in bottom ice at that time of the year, as already hypothesized by Levasseur et al. [1994] for bottom ice diatom-dominated communities in the Arctic. Further work is needed to test this hypothesis. In an experiment with a model species in the study of diatom physiology, Spielmeyer and Pohnert [2012] showed that, although cells had the capability to produce DMSP in the dark, intracellular contents were the highest close to the start of the light period. Light may stimulate the synthesis of DMSP by providing the energy required for sulfate uptake and reduction during early-growth [Stefels, 2000; van Rijssel and Gieskes, 2002]. The fact that DMS remained below the detection limit (< 0.3 nM) during the whole initial phase of algal growth (Figure 4.10) could have had several causes. The fact that the bottom assemblages were

not heavily degraded (degradation ratios between 0.14 and 0.30 at stations 4 and 5) argues for a low availability of $DMSP_d$ for conversion to DMS. This, however, requires further confirmation since removal processes such as bacterial uptake and assimilation of $DMSP_d$ and bacterial consumption of DMS could also have lowered the DMS pool [Stefels et al., 2007].

Figure 4.10: Evolution of DMS (nM), DMSP (nM), and chl *a* ($\mu g.L^{-1}$) concentrations in bottom ice (5 cm) during the spring-summer transition in 2011 (left panel) and winter-spring transition in 2012 (right panel). Each set of dots corresponds to a sampling station, identified by its number (1 to 8).

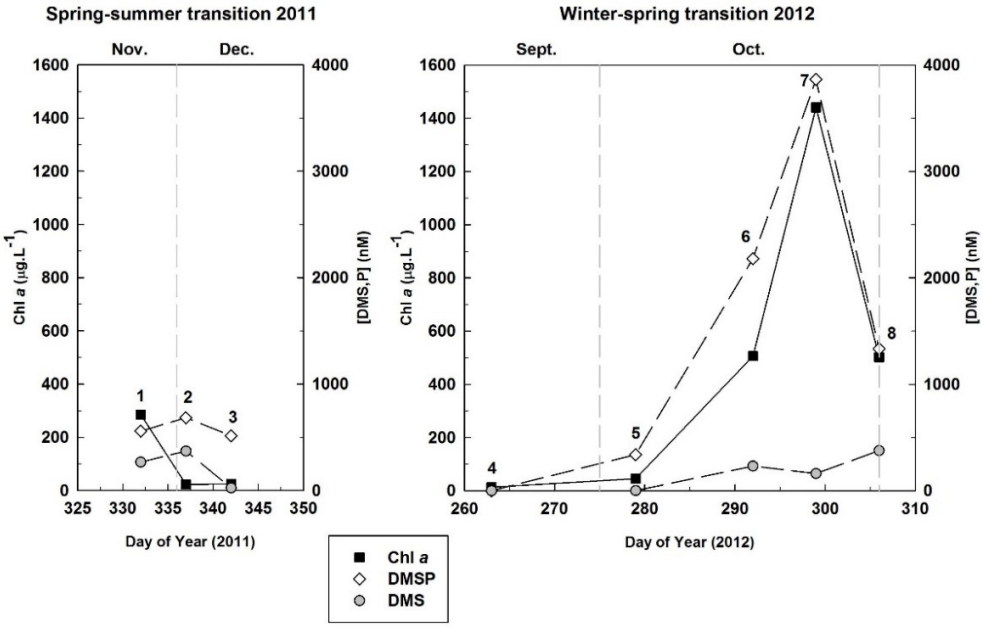

Following the initial phase of algal growth, we observed an exponential increase in chl *a* from station 5 to station 7, corresponding to the development of a bottom ice bloom dominated by diatoms (Figures 4.6 and 4.7). The development of the bloom was closely followed by an increase in DMSP, peaking at 3865 nM at station 7. This shows that DMSP may accumulate rapidly in ice during exponential algal growth and maximum biosynthesis. During the exponential growth phase, the DMSP-to-chl *a* ratio was typically very low (close to values generally measured in marine phytoplankton diatom assemblages, average = 4 $nmol.\mu g^{-1}$ [Stefels et al.,

2007]), and showed a moderate decrease from station 5 (3.7 nmol.µg^{-1}) to station 7 (1.7 nmol.µg^{-1}). These ratios support previous findings that diatoms are important DMSP producers in sea ice because of their large biomass, rather than because of intracellular adaptations of DMSP content to environmental stressors such as the low temperatures and high salinities of the brine habitat [Levasseur et al., 1994; DiTullio et al., 1998; Tison et al., 2010]. Tison et al. [2010] in the Weddell Sea observed a good linear relationship between DMS and chl *a* in bottom ice and suggested that as DMSP production is increased, the various processes leading to the cleavage of DMSP into DMS are also increased. Our data suggest that this might not always be the case. Contrary to DMSP, the evolution of DMS during the exponential algal growth was not always parallel to that of chl *a* (Figure 4.10). The initial increase in DMS from station 5 (< 0.3 nM) to 6 (231 nM) was followed by a decrease around peak-bloom (160 nM). This decoupling could have had several causes, which would again require further confirmation e.g. (1) a decrease of the $DMSP_d$ available for DMS production (2) an increase of the DMS consumption and oxidation to DMSO by bacteria [Hatton et al., 2005] due to the increase in dissolved organic carbon (3) diffusion of DMS through the ice [Loose et al., 2009; 2011a; Tison et al., 2010], and (4) a decrease of the DMS yield [Yoch, 2002; Stefels et al., 2007]. The increase of DMS loss through diffusion was a likely process since we observed an increase in DMS in the ice layers just above bottom ice, while chl *a* and DMSP remained unchanged (Figures 4.8 and 4.9).

Bottom ice chl *a* declined dramatically from station 7 to station 8 (Figure 4.10), corresponding to the collapse of the bloom. The collapse of the bloom induced a decrease in DMSP (1334 nM). Similar DMSP-to-chl *a* ratio at station 7 (1.7 nmol.µg^{-1}) and 8 (2.6 nmol.µg^{-1}) suggested close degradation rates for both

DMSP and chl *a*. The decline in chl *a* and DMSP was accompanied by an increase in DMS (377 nM). This is to be expected since cell senescence is associated with the release of $DMSP_d$ [Stefels, 2000], which becomes available for degradation into DMS. The observed increase in DMS was however small compared to the amount of DMSP lost from station 7 to station 8 (DMS-to-DMSP ratio = 0.22 at station 8). Several explanations are plausible. First, the DMS produced could have been: lost by diffusion, oxidized, or consumed. Diffusion of DMS from bottom ice to the upper ice layers was still likely to occur given the increase in brine volume fraction from station 7 to station 8 (Figure 4.5), although it was not supported this time by an increase in DMS in the ice layers just above bottom ice (Figure 4.8). Of course, DMS might always have diffused higher up on warming, and hence the signal of diffusion might have been obscured in the profile. Second, the DMS yield might have been small. In that respect, high C and S bacterial demand during the collapse of phytoplankton blooms was shown to favor the demethylation/demethiolation pathway of DMSP degradation [Kiene et al., 2000; Merzouk et al., 2008].

4.5. Conclusions and perspectives

We reported high-resolution DMS and DMSP profiles in ice shelf influenced fast ice from Cape Evans, McMurdo Sound (Antarctica) from two contrasting seasonal episodes: the winter-spring transition in 2012 and the spring-summer transition in 2011. We examined the relationships between these concentrations and ancillary physical (ice texture, ice temperature and bulk salinity) and biological (chl *a*, phaeopigments, biomass composition) properties of sea ice.

We found that the ice DMS,P cycle at Cape Evans during the winter-spring transition in 2012 was initially driven by ice formation processes. Mixed columnar/platelet ice formation in early May through interactions with ice shelf waters favored the development of strong local DMS,P maxima in interior ice. First, the formation of platelet crystals incorporated dinoflagellates, usually recognized as strong DMSP producers. This strong halo and cryo-tolerant group could have survived the winter by encysting, and moving into the winter-spring transition, could have produced significant amounts of DMSP to survive the hypersaline and cold conditions of the interior ice. Second, the formation of platelet ice provided favorable conditions for the production of DMSP by increasing the environmental stresses the interior ice assemblage was exposed to. The transition between columnar and mixed columnar/platelet ice could have represented a decrease in ice permeability reducing the release of salts through brine convection (i.e. higher osmotic stress). This is to our knowledge the first evidence of the influence of platelet ice on the DMS,P cycle in ice. The processes described above might be important regionally given the fact that platelet ice and interior ice assemblages of dinoflagellates have been widely reported in the McMurdo Sound [Stoecker et al., 1998; Montresor et al., 1999; Remy et al., 2008], but also in the Weddell and Scotia Seas [Buck et al., 1992; Garrison and Buck, 1989], in Terra Nova Bay [Andreoli et al. 1995], and near Davis station in East-Antarctica [Thomson et al., 2004].

Following the increase in solar radiation during the winter-spring transition in 2012, we found that the DMS,P profiles became strongly influenced by the development and decline of a diatom-dominated bloom in bottom ice. We therefore investigated the coupling between chl *a* and DMS,P in bottom ice. A time lag between algal growth and DMSP production was initially observed in this layer.

Since this time lag directly followed the dark-light transition from winter to spring, we suggested that the increase in solar radiation stimulated the synthesis of DMSP by providing the energy required for sulfate uptake and reduction. Further work is needed to test this hypothesis. DMSP then nicely followed the development and collapse of the bloom. At peak-bloom, very high DMSP (3865 nM) was measured, confirming the key role of bottom ice diatom assemblages in the sea ice DMSP production. Regionally, this role could be even more important. Indeed, we observed mixed platelet/columnar ice at Cape Evans whereas loose accumulations of platelet crystals have been widely reported throughout the McMurdo Sound. These loose accumulations host some of the densest diatom assemblages of the polar marine environment (up to 6500 $\mu g.L^{-1}$) [Arrigo et al.,1995]. The DMSP production of these assemblages needs to be assessed in the future.

During the spring-summer transition in 2011, DMSP was not coupled to chl *a*. We showed that this trend could be attributed to drastic changes in permeability and brine dynamics on warming. This hypothesis was supported by physical and biological observations in ice and under-ice water. Brine convection events were shown to release DMS to the under-ice water and to redistribute DMSP in interior and surface ice. We tried to quantify this DMS release by looking at the DMS burden in ice at the two last spring-summer stations, following the method described in Tison et al. [2010]. The DMS burden decreased from 29.1 to 6.1 $\mu mol.m^{-2}$ between station 2 and station 3 (5 days), corresponding to a flux of 4.6 $\mu mol.m^{-2}.day^{-1}$. Of course, this burden calculated flux did not indicate if the release was directed towards the atmosphere or the under-ice water. Given the drastic increase in under-ice DMS observed from station 2 to station 3 without any

significant increase in chl *a*, and given the fact that DMS was predominantly located in bottom ice, we believe that a larger proportion of the flux was indeed directed towards the under-ice water. It would be interesting in the future to assess the fate of this DMS in under-ice water. Indeed the strong release of DMS through brine convection would occur before melting when the ice cover is still impeding ocean-atmosphere exchanges. Whether this DMS is quickly lost through transportation to depth and bacterial consumption, or advected to open water at the retreating ice edge (only a few kilometers north of the sampling site in this study), will determine the exact impact of strong DMSP production in ice shelf influenced fast ice on the regional sulfur atmospheric budget.

Chapter 5

General conclusions and perspectives

The three main objectives of this thesis were to:

1. Characterize the seasonal evolution of brine dynamics in natural ice, with a specific focus on gravity drainage events during the spring-summer transition.

2. Document DMS,P,O concentrations in seasonal sea ice, and show how the concentrations of the respective sulfur compounds vary within sea ice at a location, with time over the seasonal transition, and spatially between polar regions.

3. Assess the influence of biological factors (biomass and community composition), sea ice growth, and brine dynamics, on this spatial and temporal variability.

The motivation of these objectives was to improve the understanding of the cycling of DMS in sea ice in order to better assess the contribution of the sea ice biome to regional DMS emissions, and hence to potential regional climate regulation. This was a particularly important task to achieve given the strong modifications of the sea ice biome observed in recent years due to climate change.

The first objective was tackled in chapter 2 of this thesis. The seasonal evolution of brine dynamics was characterized during a cycle of ice growth and melt from winter to summer in natural sea ice. The study presented in chapter 2 took advantage of the overwintering of the CCGS Amundsen icebreaker in the Amundsen Gulf, Canadian Arctic, in 2007-2008 during the international and multidisciplinary IPY-CFL study. The seasonal evolution of brine dynamics was characterized using a proxy of ice permeability (brine volume fraction) and a proxy of the potential for gravity drainage to occur (Rayleigh number), and looking at their effects on bulk sea ice salinity. It appeared that, from winter to early-spring, brine

dynamics are dominated by the drainage of salts at the ice-ocean interface. Brine density profiles are unstable but the potential for full-depth gravity drainage is low given the fact that the ice is cold and impermeable (brine inclusions are not connected). During that seasonal episode, full-depth gravity drainage is limited to recently refrozen leads. The mean salinity slightly decreases with time since the efficiency of drainage at the ice-ocean interface increases as the ice grows thicker. Warming in late-spring restores the connectivity of brine inclusions, leading to a strong desalination phase over a small time window through full-depth gravity drainage episodes. Thereafter, desalination stabilizes the brine density profiles, decreasing the potential for full-depth gravity drainage. Sea ice eventually continues to freshen through the infiltration of meltwater at the ice surface in early summer.

The study presented in chapter 2 was the first study to characterize the seasonal evolution of brine dynamics in natural Arctic sea ice using the brine volume fraction and Rayleigh number. In this study, these two proxies of permeability and gravity drainage were shown to be successful at explaining seasonal bulk ice salinity trends. However, it was also shown that the thresholds for permeability and gravity drainage calculated in theoretical and controlled experiments should be reconsidered when the proxies are calculated from field measurements of salinity and temperature obtained via destructive ice coring. This was particularly striking for the critical Rayleigh number (i.e. gravity drainage occurring for $Ra > 10$ in laboratory studies). It appeared that a Rayleigh number as small as 0.1 to 1.9 in bottom ice could be indicative of the drainage of salts at the ice-ocean interface, and a mean Rayleigh numbers of 3 (and a maximum Rayleigh number of 6) could be indicative of full-depth gravity drainage.

These findings are very important for past, current, and future interpretation of the vertical and temporal variability of biogeochemical variables (including DMS,P,O) in natural sea ice, and have already stimulated some discussions in the sea ice modelling community on the applicability of the Rayleigh number in field studies [Vancoppenolle et al., submitted to The Cryosphere]. These discussions, as well as future modelling of sea ice brine dynamics, will definitely benefit from the extensive data set of physical properties provided in this thesis. The characterization of seasonal brine dynamics described in this thesis has already proved to be useful for biogeochemical studies conducted during the IPY-CFL study, such as the vertical distribution of sympagic meiofauna [Marquardt et al., 2011], and the dynamics of carbon dioxide in spring sea ice [Geilfus et al., 2012; Fransson et al., 2013]. This characterization also served as a strong base of discussion for the two time series of DMS,P,O dynamics in Arctic and Antarctic sea ice presented in this thesis. Regarding future research, the characterization of brine dynamics in natural sea ice could be definitely improved by non-destructive measurements of sea ice temperature and bulk salinity using instruments such as thermistors and capacitance probes [Backstrom and Eicken, 2006]. The deployment of these instruments in sea ice remains however challenging, especially during transect studies or when the ice is not sampled from the early stages of growth.

The second and third objectives were tackled in chapters 3 and 4 of this thesis. The study presented in chapter 3 documented the concentrations of DMS, DMSP and DMSO in Arctic sea ice from late-autumn to summer during the IPY-CFL study in 2007-2008 in the Amundsen Gulf (Canadian Arctic), and the study presented in chapter 4 documented the concentrations of DMS and DMSP in

Antarctic sea ice during the spring-summer transition of 2011 and winter-spring transition of 2012 during the YROSIAE study in the McMurdo Sound. The Arctic study was the first simultaneous report of DMS, DMSP and DMSO concentrations in Arctic sea ice, the first report of DMS in Arctic sea ice, and the first report of DMSP in late-autumn and early spring Arctic sea ice. The Antarctic study was the first report of DMS and DMSP in winter-early spring Antarctic sea ice. In the absence of a sea ice DMS climatology, these studies present the most comprehensive sea ice DMS data base available to the scientific community, and a significant source of information for sea ice DMS modelling work which is still in its infancy.

The results presented in chapters 3 and 4 confirmed that sea ice in both hemispheres is a biome favorable to substantial DMS,P,O production with maximum concentrations 2 to 4 orders of magnitude higher than typical oceanic water concentrations. The results also confirmed the very high regional, seasonal, and vertical variability of the concentrations, spanning a range from below detection limit of traditional GC-FPD systems (<0.3 nM) to a few thousands of nM in some very productive bottom ice layers. Comparison of the results to other studies remains difficult given difference in methodology (e.g. melting vs dry-crushing) and non-standard vertical resolution of sea ice sampling. This thesis shows that, because DMS,P,O are typically found in very discrete bands in sea ice, and concentrations show strong gradients over very short distances, especially at the ice-ocean interface where maximum values are typically observed, mean concentrations are strongly influenced by the resolution of vertical sampling. The use of a common vertical sampling resolution is therefore recommended for future

sea ice DMS studies. Ideally, alongside concentrations, studies should always report DMS,P,O burdens calculated on the whole ice thickness.

In chapters 3 and 4, the influence of various physical and biological factors on DMS,P,O dynamics was investigated. Biomass and community composition, sea ice growth processes, and brine dynamics were all shown to have discernable effects on the variability of DMS,P,O concentrations.

The seasonal evolution of sympagic biomass and the seasonal succession of different algal groups with different cytosolic levels of DMSP were shown to explain much of the seasonal variability in bottom ice DMSP concentrations. In both the Arctic and Antarctic studies presented in this thesis, DMSP concentrations were observed to increase with chl *a* from late-autumn/winter through the spring, peaking during the spring-bloom, and decreasing towards the summer with the collapsing of the bloom. A great majority of DMSP production in these studies occurred during blooms largely dominated by sea ice diatoms. Very low DMSP-to-chl *a* ratios (2 to 4 nmol.μg^{-1}, comparable to oceanic diatoms ratios) suggested that DMSP production of these assemblages is driven by biomass rather than by intracellular adaptations of DMSP content to environmental stressors. The results from the Arctic study in chapter 3 suggested that this is also the case for bottom ice assemblages dominated by other algal groups during other seasons. In cases where much of the primary production occurs in bottom ice (e.g. vast majority of first-year Arctic sea ice), the bulk DMSP production of the sea ice biome could be estimated by biomass and community composition parameters only, which are relatively well constrained in models. Biomass and community composition failed on the other hand to explain all the vertical variability of sea ice DMSP concentrations. This vertical variability was important in the Antarctic study

presented in chapter 4, with strong DMS and DMSP local maxima found in interior ice. More surprisingly, vertical variability would also be relatively important in Arctic sea ice as suggested by the small and moderate local maxima in surface and interior ice described in chapter 3. These local maxima would only typically represent less than one-tenth of bottom ice concentrations during the spring season, but could amount to one half of bottom ice concentrations during the autumn and in late-spring/early-summer post-bloom conditions. Hence, targeting only bottom ice when sampling Arctic sea ice, a very usual practice, may lead to underestimates of DMSP production by the sea ice biome in some seasons.

Sea ice growth processes (approached through textural analyses) were shown to influence the vertical variability of DMS,P concentrations during both the Arctic and Antarctic studies presented in this thesis. During the Arctic study, a decrease in DMSP concentrations from surface ice to sub-surface ice was shown to correspond to a textural transition from frazil to congelation ice. Local DMSP maxima in late-autumn ice were also found in sandwiched frazil ice layers. Several processes could explain these trends. Frazil ice could incorporate higher concentrations of solutes (e.g. algae and DMSP) from the water column than congelation ice during sea ice growth. Also, scavenging by frazil ice crystals, leading to a random and non-selective entrapment of algae while congelation ice favors large organisms, could potentially lead to contrasting community composition and DMSP production. Both processes should be confirmed by further work. It was also shown in chapter 3 that the development of impermeable superimposed ice (through the melting and refreezing of snow in surface ice layers), could favor the accumulation of DMS in surface ice, thereby decreasing the exchanges of DMS between the ice surface and the atmosphere. The influence

of sea ice growth processes on the vertical variability of the concentrations was more striking during the Antarctic study. Isolated interior ice maxima in DMS and DMSP corresponded to a transition between columnar and mixed columnar/platelet ice. Results of this thesis suggest that the occurrence of incorporated platelet crystals in the ice texture, through interactions with ice shelf waters, could have three different impacts. First, the formation of platelet crystals could favor the incorporation of strong DMSP producers. Platelet crystals formation corresponded in time and depth to the incorporation of dinoflagellates in the ice cover. Second, the formation of platelet crystals could increase the environmental stresses (osmotic stress) the interior ice assemblage are exposed to. Platelet crystals formation represented a decrease in ice permeability reducing the release of salts through brine drainage. Third, the decrease in permeability could constrain the vertical redistribution of DMS,P, leading to a local accumulation of compounds. These processes might be of major importance for vast coastal regions of the Antarctic, since ice shelves exist around 44% of the Antarctic coastline. These processes should on the other hand be of minor importance for most of the Arctic where ice shelves are relatively scarce. This difference should definitely be considered in future modelling work.

Brine dynamics were also shown to considerably impact the vertical variability of DMS,P concentrations during both the Arctic and Antarctic studies presented in this thesis. Warming in the spring was shown to lead to an important redistribution of DMS,P within the ice cover through brine convection events triggered by the restored connectivity of the brine network. Brine dynamics were also shown to strongly influence the exchange of dimethylated sulfur compounds with the ocean. It appeared that full-depth gravity drainage can lead to strong

releases of the sea ice DMS pool in late-spring. This was supported by drastic increases in under-ice water concentrations observed in conjunction with drastic decreases in bottom ice concentrations, at a time of the year when the potential for gravity drainage is the highest (fully permeable sea ice and unstable brine density profiles, high Rayleigh numbers). An important difference in the magnitude of this release to the ocean could be observed between DMS and DMSP probably due to a higher resistance of DMSP to brine drainage. Particular DMSP linked to algal cells would mainly remain fixed to the walls of brine channels, whereas DMS present as a solute in the brine would be more easily transported.

These results indicate that the contribution of the sea ice biome to the regional oceanic DMS budget is not limited to the summer melting period and ice break-up as it was generally admitted in the literature. Future research should aim at determining the fate of this important fraction of the sea ice DMS pool released by brine drainage. Indeed, full-depth gravity drainage would occur before ice break-up, when the ice cover is still partially impeding the exchanges between the ocean and the atmosphere. Whether this DMS is quickly lost through transportation to depth and bacterial consumption, or advected to open water at the retreating ice edge will determine the exact impact of brine drainage on regional DMS emissions.

Finally, the most stimulating finding of this thesis concerns the difference in the magnitude and timing of ice-atmosphere DMS exchanges between the Arctic and Antarctic. On the whole, the results and discussions presented in this thesis tend to indicate that Antarctic sea ice could release a significantly higher amount of DMS to the atmosphere than Arctic sea ice through the ice surface. This difference could primarily be driven by the differences in the snow cover between the two polar regions, highlighting this parameter as a key parameter for future sea

ice modelling. First, differences in the snow cover (generally thicker in the Antarctic) can lead to stronger losses of DMS in Arctic surface ice through photo-chemical oxidation to DMSO. This was supported by observations in the Arctic study showing strong relationships between the relative proportion of DMSO (much higher than in Antarctic sea ice) and depth-attenuated spectral irradiance in surface ice. Second, heavy snow loading in Antarctic sea ice, promoting the development of surface communities through flooding, can further increase the difference in surface ice DMS pool available for exchange with the atmosphere. Third, more intense surface melt and lower snow insulation of the ice cover in the Arctic can lead to important differences in the time window during which direct DMS emissions from surface ice can occur. As indicated by the Arctic study, the time window between the moment the surface ice becomes permeable to gas exchange and the moment impermeable superimposed ice starts to form at the ice surface could be very small. These hypotheses could definitely be confirmed in the future by sea ice-atmosphere DMS fluxes measurements, which unfortunately only exist in the Antarctic at the present time.

References

Aagaard, K. (1981). On the deep circulation in the Arctic Ocean. *Deep-Sea Research*, 28, 3, 251-268

Ackley, S.F. (1982). Ice scavenging and nucleation: two mechanisms for the incorporation of algae into newly forming sea ice. *EOS: Transactions of the American Geophysical Union*, 63, 65

Ackley, S.F., and Sullivan, C. (1994). Physical controls on the development and characteristics of Antarctic sea ice biological communities: a review and synthesis. *Deep-sea Research I*, 41(10), 1583-1604

Alou-Font, E., Mundy, C.J., Roy, S., Gosselin, M., and Agusti, S. (2013). Snow cover affects ice algal pigment composition in the coastal Arctic Ocean during spring. *Marine Ecology Progress Series*, 474, 89-104

Anderson, L.G. (2001). Chemical oceanography in polar oceans. In: Leppäranta, M. (Ed.), Physics of ice covered seas, Volume 2, Helsinki University Press, Helsinki, Finland, pp. 787-810

Andreae, M.O. (1990). Ocean-atmosphere interactions in the global biogeochemical sulfur cycle. *Marine Chemistry*, 30, 1-29

Andreae, M.O., and Barnard, W.R. (1983). Determination of trace quantities of dimethylsulfide in aqueous solutions. *Analytical Chemistry*, 55, 608-612

Andreae, M.O., Elbert, W., and De Mora, S.J. (1995). Biogenic sulfur emissions over the tropical South Pacific: 3. Atmospheric dimethylsulfide, aerosols and cloud condensation nuclei. *Journal of Geophysical Research*, 100, 11335-11356

Andreas, E.L., and Ackley, S.F. (1981). On the differences in ablation seasons of the Arctic and Antarctic sea ice. *Journal of Atmospheric Sciences*, 39, 440-447

Andreoli, C., Tolomio, C., Moro, I., Radice, M., Moschin, E., and Bellato, S. (1995). Diatoms and dinoflagellates in Terra Nova Bay (Ross Sea-Antarctica) during austral summer 1990. *Polar Biology*, 15, 465-475, doi: 10.1007/BF00237460

Archer, S.D., Leakey, R.J.G., Burkill, P., Sleigh, M.A., and Appleby, C.J. (1996). Microbial ecology of sea ice at a coastal Antarctic site: community composition, biomass and temporal change. *Marine Ecology Progress Series*, 135, 179-195

Archer, S.D., Stelfox-Widdicombe, C.E., Burkill, P.H., and Malin, G. (2001). A dilution approach to quantify the production of dissolved dimethylsulphoniopropionate and dimethyl sulphide due to microzooplankton herbivory. *Aquatic Microbial Ecology*, 23, 131-145

Archer, S.D., Smith, G.C, Nightingale, P.D., Widdicombe, C.E., Tarran, G.A., Ress, A.P., and Burkill, P.H. (2002). Dynamics of particulate dimethylsulphoniopropionate during a Lagrangian experiment in the northern North Sea. *Deep-Sea Research Part II*, 49, 2979-2999

Archer, S.D., Kimmance, S.A., Stephens, J.A., Hopkins, F.E., Bellerby, R.G.J., Schulz, K.G., Piontek, J., and Engel, A. (2013). Contrasting responses of DMS and DMSP to ocean acidification in Arctic waters. *Biogeosciences*, 10, 1893-1908

Arrigo, K.R. (2003). Primary production in sea ice. In: Thomas, D.N., and Dieckmann, G.S. (Ed.), Sea ice: An introduction to its physics, biology, chemistry, and geology, Blackwell Science, Oxford, pp. 143-183

Arrigo, K.R., Dieckmann, G., Gosselin, M., Robinson, D.H., Fritsen, C.H., and Sullivan, C.W. (1995). A high resolution study of the platelet ice ecosystem in McMurdo Sound, Antarctica: biomass, nutrient, and production profiles within a dense microalgal bloom. *Marine Ecology Progress Series*, 127, 255-268

Arrigo, K.R., van Dijken, G., and Pabi, S. (2008). Impact of a shrinking Arctic ice cover on marine primary production. *Geophysical Research Letters*, 35, L19603

Asher, E.C., Dacey, J.W.H., Mills, M.M., Arrigo, K.R., and Tortell, P.D. (2011). High concentrations and turnover rates of DMS, DMSP and DMSO in Antarctic sea ice. *Geophysical Research Letters*, 38, L23609, doi: 10.1029/2011GL049712

Assur, A. (1958). Composition of sea ice and its tensile strength. In: Arctic sea ice. Proceedings of the Conference held 24-27 February 1958, Easton, Maryland, USA. (National Research Council Publication 598) US National Academy of Sciences, Washington, DC, pp. 106-138

Ayers, G.P., and Caney, J.M. (2007). The CLAW hypothesis: a review of the major developments. *Environmental Chemistry*, 4, 366-374

Backstrom, L.G.E., and Eicken, H. (2006). Capacitance probe measurements of brine volume and bulk salinity in first-year sea ice. *Cold Regions Science and Technology*, 46, 167-180

Bandy, A.R., Thornton, D.C., Blomquist, B.W., Chen, S., Wade, T.P., Ianni, J.C., Mitchell, G.M., and Nadler, W. (1996). Chemistry of dimethyl sulfide in the equatorial Pacific atmosphere. *Geophysical Research Letters*, 23, 741-744

Barber, D.G., and Hanesiak, J.M. (2004). Meteorological forcing of sea ice concentrations in the southern Beaufort Sea over the period 1979 to 2000. *Journal of Geophysical Research*, 109, C6, C06014

Barber, D.G., and Massom, R.A. (2007). The role of sea ice in Arctic and Antarctic polynyas. In: Smith, W.O.J., and Barber, D.G. (Ed.), Polynyas: windows to the world. Elsevier Oceanography Series, 74, Elsevier, Amsterdam, pp. 1-54

Barber, D.G., Asplin, M.G., Gratton, Y., Lukovich, J.V., Galley, R.J., Raddatz, R.L., and Leitch, D. (2010). The International Polar Year (IPY) circumpolar flaw lead (CFL) system study: overview and the physical system: overview and the physical system. *Atmosphere-Ocean*, 48, 4, 225-243

Bates, T.S., Cline, J.D., Gammon, R.H., and Kelly-Hansen, S.R. (1987). Regional and seasonal variations in the flux of oceanic dimethylsulfide to the atmosphere. *Journal of Geophysical Research*, 92, 2930-2938

Bates, T.S., Lamb, B.K., Guenther, A., Dignon, J., and Stoiber, R.E. (1992). Sulfur emissions to the atmosphere from natural sources. *Journal of Atmospheric Chemistry*,14, 315-337

Bell, W., and Mitchell, R. (1972). Chemotactic and growth responses of marine bacteria to algal extracellular products. *The Biological Bulletin*, 143, 265-277

Belzile, C., Johannessen, S.C., Gosselin, M., Demers, S., and Miller, W.L. (2000). Ultraviolet attenuation by dissolved and particulate constituents of first-year ice during late spring in an Arctic polynya. *Limnology and Oceanography*, 45, 1265-1273

Bigg, E.K. (2007). Sources, nature, and influence on climate of marine airborne particulates. *Environmental Chemistry*, 4, 155-161

Blunden, J., and Arndt, D.S. (2013). State of the Climate in 2012. *Bulletin of American Meteorological Society*, 94, S1-S258

Bopp, L., Boucher, O., Aumont, O., Belviso, S., Dufresne, J.L., Pham, M., and Monfray, P. (2004). Will marine dimethylsulfide emissions amplify or alleviate global warming? A model study. Canadian *Journal of Fisheries and Aquatic Science*, 61, 826-835

Boucher, O., Moulin, C., Belviso, S., Aumont, O., Bopp, L., Cosme, E., von Kuhlmann, R., Lawrence, M.G., Pham, M., Reddy, M.S., Sciare, J., and Venkataraman, C. (2003). DMS atmospheric concentrations and sulphate aerosol indirect radiative forcing: a sensitivity study to the DMS source representation and oxidation. *Atmospheric Chemistry and Physics*, 3, 49-65

Bouillon, R.C., and Miller, W.L. (2005). Photodegradation of dimethyl sulfide (DMS) in natural waters: Laboratory assessment of the nitrate-photolysis-induced DMS oxidation. *Environmental Science Technology*, 39, 9471-9477

Bouillon, R.-C., Lee, P.A., de Mora, S.J., Levasseur, M., and Lovejoy, C. (2002). Vernal distribution of dimethylsulphide, dimethylsulphoniopropionate, and dimethylsulphoxide in the North Water in 1998. *Deep-Sea Research II*, 49, 5171-5189

Brabant, F., El Amri, S., and Tison, J.-L. (2011). A robust approach for the determination of dimethylsulfoxide in sea ice. *Limnology and Oceanography: methods*, 9, 261-274

Brabant, F., Carnat, G., Dumont, I., Becquevort, S., Vancoppenolle, M., Ackley, S.F., Fritsen, C., and Tison, J.-L. (in prep).Thermally forced DMS, DMSP, DMSO and biogeochemical cycling in spring sea ice : a contrasting study.

Bratbak, G., Levasseur, M., Michaud, S., Cantin, G., Fernandez, E., Heimdal, B.R., and Heldal, M. (1995). Viral activity in relation to Emiliania huxleyi blooms: A mechanism of DMPS release?. *Marine Ecological Progress Series*, 128, 133-142

Breckels, M.N., Boakes, D.E., Codling, E.A., Malin, G., Archer, S.D., and Steinke, M. (2010). Modelling the concentration of exuded dimethylsulfoniopropionate (DMSP) in the boundary layer surrounding phytoplankton cells. *Journal of Plankton Research*, 32, 253-257

Breckels, M.N., Bode, N.W.F., Steinke, M., and Codling, E. (2013). Effect of dimethyl sulfide (DMS) production on the swimming behavior of the copepod Calanus helgolandicus. *Marine Drugs*, 11, 2486-250

Brimblecombe, P., and Shooter, D. (1986). Photo-oxidation of dimethylsulfide in aqueous solution. *Marine Chemistry*, 19, 343-353

Brinkley, J.C. (2008). Quantification of dimethylsulfoxide in seawater through its reduction to dimethylsulfide: A method comparison. M.Sc. thesis. State University of New York, College of Environmental Science and Forestry

Brugger, A., Slezak, D., Obernosterer, I., and Herndl, G.J. (1998). Photolysis of dimethylsulfide in the northern Adriatic Sea: Dependence on substrate concentration, irradiance and DOC concentration. *Marine Chemistry*, 59, 321-331

Bucciarelli, E., and Sunda, W.G. (2003). Influence of CO_2,nitrate, phosphate, and silicate limitation on intracellular dimethylsulfoniopropionate in batch cultures of the coastal diatom Thalassiosira pseudonana. *Limnology and Oceanography*, 48, 2256-2265

Bucciarelli, E., Ridame, C., Sunda, W.G., Dimier-Hugueney, C., Cheize, M., and Belviso, S. (2013). Increased intracellular concentrations of DMSP and DMSO in iron-limited oceanic phytoplankton Thalassiosira oceanica and Trichodesmium erythraeum. *Limnology and Oceanography*, 58(5),1667-1679

Buck, K.R., Bolt, P.A., Bentham, W.N., and Garrison, D.L. (1992). A dinoflagellate cyst from Antarctic sea ice. *Journal of Phycology*, 28, 15-18

Bunt, J.S., and Lee, C.C. (1970). Seasonal primary production in Antarctic sea ice at McMurdo Sound in 1967. *Journal of Marine Research*, 28, 304-320

Cantoni, G.L., and Anderson, D.G. (1956). Enzymatic cleavage of dimethylpropiothetin by *Polysiphonia lanosa*. *Journal of biological chemistry*, 222, 171-177

Carnat, G., Papakyriakou, T., Geilfus, N.-X., Brabant, F., Delille, B., Vancoppenolle, M., Gilson, G., Zhou, J., and Tison, J.-L. (2013). Investigations on physical and textural properties of Arctic first-year sea ice in the Amundsen Gulf, Canada, November 2007-June 2008 (IPY-CFL system study). *Journal of Glaciology*, 59, 217, doi: 10.3189/2013JoG12J148

Cavalieri, D.J., and Parkinson, C.L. (2012). Arctic sea ice variability and trends, 1979-2010. *The Cryosphere*, 6, 881-889

Challenger, F. (1951). Biological methylation. *Advanced Enzymology*, 12, 429-491

Chang, R.Y-W, Sjostedt, S.J., Pierce, J.R., Papakyriakou, T.N., Scarratt, M.G., Michaud, S., Levasseur, M., Leaitch, W.R., and Abbatt, J.P.D. (2011). Relating atmospheric and oceanic DMS levels to particle nucleation events in the Canadian Arctic. *Journal of Geophysical Research: Atmospheres*, 116, D17, doi: 10.1029/2011JD015926

Charlson, R.J., and Rodhe, H. (1982). Factors controlling the acidity of rainwater. *Nature*, 295, 683-685

Charlson, R.J., Lovelock, J.E., Andreae, M.O., and Warren, S.G. (1987). Oceanic phytoplankton, atmospheric sulphur, cloud albedo and climate. *Nature*, 326, 655-661

Chaulk, A., Stern, G.A., Armstrong, D., Barber, D.G., and Wang, F. (2011). Mercury distribution and transport across the ocean-sea-ice-atmosphere interface in the Arctic Ocean. *Environmental Science and Technology*, 45, 5, 1866-1872

Chierici, M., Fransson, A., Lansard, B., Miller, L.A., Mucci, A., Shadwick, E., Thomas, H., Tremblay, J.-E., and Papakyriakou, T. (2011). Impact of biogeochemical processes and environmental factors on the calcium carbonate saturation state in the circumpolar flaw lead in the Amundsen Gulf, Arctic Ocean. *Journal of Geophysical Research*, 116, C9, C00G09

Cottier, F., Eicken, H., and Wadhams, P. (1999). Linkages between salinity and brine channel distribution in young sea ice. *Journal of Geophysical Research*, 104, C7, 15859-15871

Cox, G.F.N., and Weeks, W.F. (1975). Brine drainage and initial salt entrapment in sodium chloride ice. *CRREL Research Report*, 345

Cox, G.F.N., and Weeks, W.F. (1983). Equations for determining the gas and brine volumes in sea-ice samples. *Journal of Glaciology*, 29, 306-316

Cox, G.F.N., and Weeks, W.F. (1986). Changes in the salinity and porosity of sea-ice samples during shipping and storage. *Journal of Glaciology*, 32, 371-375

Cox, G.F.N., and Weeks, W.F. (1988). Numerical simulations of the profile properties of undeformed first-year sea ice during the growth season. *Journal of Geophysical Research*, 93, 12449-12460, doi: 10.1029/JC093iC10p12449

Curran, M.A.J., and Jones, G.B. (2000). Dimethyl sulfide in the Southern Ocean: seasonality and flux. *Journal of Geophysical Research*, 105, D16, 20451-20459

Curran, M.A.J., Jones G.B., and Burton, H. (1998). Spatial distribution of dimethylsulfide and dimethylsulfoniopropionate in the Australasian sector of the Southern Ocean. *Journal of Geophysical Research*, 103, D13, 16677-16689

Curry, J.A., Schramm, J.L., and Ebert, E.E. (1995). Sea-ice-albedo climate feedback mechanism. *Journal of Climate*, 8, 2, 240-247

Dacey, J.W.H., and Blough, N. (1987). Hydroxide decomposition of dimethylsulfoniopropionate to form dimethylsulfide. *Geophysical Research Letters*, 14, 1246-1249

Daly, S.F. (1984). Frazil Ice Dynamics. CRREL Monograph 84-1, US Cold Regions Research and Engineering Laboratory, Hanover, N. H.

Daly, K.L., and DiTullio, G.R. (1996). Particulate dimethylsulfoniopropionate removal and dimethylsulfide production by zooplankton in the Southern Ocean. In: Kiene, R.P., Visscher, P.T., Keller, M.D., and Kirst, G.O. (Ed.), Biological and Environmental Chemistry of DMSP and Related Sulfonium Compounds. Plenum Press, New-York, pp. 223-238

Delille, B., Jourdain, B., Borges, A.V., Tison, J.-L., Delille, D. (2007). Biogas (CO_2, O_2, dimethylsulfide) dynamics in spring Antarctic fast ice. *Limnology and Oceanography*, 52(4), 1367-1379

Del Valle, D.A., Kieber, D.J., and Kiene, R.P. (2007a). Depth-dependent fate of biologically-consumed dimethylsulfide in the Sargasso Sea. *Marine Chemistry*, 103, 197-208

Del Valle, D.A., Kieber, D.J., Bisgrove, J., and Kiene, R.P. (2007b). Light-stimulated production of dissolved DMSO by a particle-associated process in the Ross Sea, Antarctica. *Limnology and Oceanography*, 52, 2456-2466

Del Valle, D.A., Kieber, D.J., Toole, D.A., Bisgrove, J., and Kiene, R.P. (2009). Dissolved DMSO production via biological and photochemical oxidation of dissolved DMS in the Ross Sea, Antarctica. *Deep-Sea Research I*, 56, 166-177

Dempsey, D.E., Langhorne, P.J., Robinson, N.J., Williams, M.J.M., Haskell, T.G., and Frew, R.D. (2010). Observation and modeling of platelet ice fabric in McMurdo Sound, Antarctica. *Journal of Geophysical Research*, 115, C01007, doi: 10.1029/2008JC005264

Diaz, M.R., Visscher, P.T., and Taylor, B.F. (1992). Metabolism of dimethylsulfoniopropionate and glycine betaine by a marine bacterium. *FEMS Microbiological Letters*, 96, 61-66

Dickson, D.M.J., and Kirst, G.O. (1986). The role of betadimethylsulphoniopropionate, glycine betaine and homarine in the osmoacclimation of *Platymonas Subcordiformis*. *Planta*, 167(4), 536-543

Dieckmann, G.S, and Hellmer, H.H. (2003). The importance of sea ice: An overview. In: Thomas, D.N., and Dieckmann, G.S. (Ed.), Sea ice: An introduction to its physics, biology, chemistry, and geology, Blackwell Science, Oxford, pp. 1-21

Dieckmann, G.S., Mock, T., and Thomas, D.T. (2005). Low temperature stress in sea ice algae. *Phycologia*, 44(4), 27-28

DiTullio, G.R., Garrison, D.L., and Mathot, S. (1998). Dimethylsulfoniopropionate in sea ice algae from the Ross Sea polynya. *Antarctic Sea Ice Biological Processes*, *Interactions*, *and Variability*, *Antarctic Research Series*, 73, 139-146

DiTullio, G.R., Jones, D.R., and Geesey, M. (2003). Dimethylsulfide dynamics in the Ross Sea during austral summer. In: DiTullio, G.R., and Dunbar, R.B. (Ed.), Biogeochemistry of the Ross Sea. AGU Antarctic Research Series, 78, 279-294

Drewry, D.J., Jordan, S.R., and Jankowski, E. (1982). Measured properties of the Antarctic ice sheet: Surface configuration, ice thickness, volume and bedrock characteristics. *Annals of Glaciology*, 3, 83-91

Eicken, H. (1992). Salinity profiles of Antarctic sea ice: field data and model results. *Journal of Geophysical Research*, 97, C10, 15545-15557

Eicken, H. (1994). Structure of under-ice melt ponds in the central Arctic and their effect on the sea-ice cover. *Limnology and Oceanography*, 39, 3, 682-694

Eicken, H. (2003). From the Microscopic, to the Macroscopic, to the Regional Scale: Growth, Microstructure and Properties of Sea ice. In: Thomas, D.N., and Dieckmann, G.S. (Ed.), Sea ice: An introduction to its physics, biology, chemistry, and geology, Blackwell Science, Oxford, pp. 22-81

Eicken, H., and Lange, M.A. (1989). Development and properties of sea ice in the coastal regime of the southeastern Weddell Sea. *Journal of Geophysical Research*, 94, C6, 8193-8206

Eicken, H. and Lange, M.A. (1991). Image analysis of sea-ice thin sections: a step towards automated texture classification. *Annals of Glaciology*, 15, 204-209

Eicken, H., Lange, M.A., and Dieckmann, G.S. (1991). Spatial variability of sea-ice properties in the northwestern Weddell Sea. *Journal of Geophysical Research*, 96, C6, 10603-10615

Eicken, H., Krouse, H.R., Kadko, D., and Perovich, D.K. (2002). Tracer studies of pathways and rates of meltwater transport through Arctic summer sea ice. *Journal of Geophysical Research*, 107, doi: 10.1029/2000JC000583

Eicken, H., Grenfell, T.C., Perovich, D.K., Richter-Menge, J.A., and Frey, K. (2004). Hydraulic controls of summer Arctic pack ice albedo. *Journal of Geophysical Research*, 109, C8, C08007

Eide, L.I. and Martin, S. (1975). The formation of brine drainage features in young sea ice. *Journal of Glaciology*, 14, 70, 137-154

Evans, C., Kadner, S.V., Darroch, L.J., Wilson, W.H., Liss, P.S., and Malin, G. (2007). The relative significance of viral lysis and microzooplankton grazing as pathways of dimethylsulfoniopropionate (DMSP) cleavage: An Emiliania huxleyi culture study. *Limnology and Oceanography*, 52, 3, 1036-1045

Fanning, K.A., and Torres, L.M. (1991). 222Rn and 226Ra: Indicators of sea-ice effects on air-sea gas exchange. *Polar Research*, 10 (1), 51-58

Fofonoff, N.P. (1985). Physical properties of seawater: a new salinity scale and equation of state for seawater. *Journal of Geophysical Research*, 90, C2, 3332-3342

Forest, A., Galindo, V., Darnis, G., Pineault, S., Lalande, C., Tremblay, J.-E., and Fortier, L. (2011). Carbon biomass, elemental ratios (C:N) and stable isotopic composition (δ13C, δ15N) of dominant calanoid copepods during the winter-to-summer transition in the Amundsen Gulf (Arctic Ocean). Journal of Plankton Research, 33, 1, 161-178

Franklin, D.J., Steinke, M., Young, J., Probert, I., and Malin, G. (2010). Dimethylsulfoniopropionate (DMSP), DMSP-lyase activity (DLA) and dimethylsulfide (DMS) in 10 species of coccolithophore. *Marine Ecological Progress Series*, 410, 13-23

Fransson, A., Chierici, M., Miller, L.A., Carnat, G., Shadwick, E., Thomas, H., Pineault, S., and Papakyriakou, T. (2013). Impact of sea-ice processes on the carbonate system and ocean acidification at the ice-water interface of the Amundsen Gulf, Arctic Ocean. *Journal of Geophysical Research: Oceans*, 118, 1-23

Fredrickson, K.A., and Strom, S.L. (2009). The algal osmolyte DMSP as a microzooplankton grazing deterrent in laboratory and field studies. *Journal of Plankton Research*, 31, 135-152

Freitag, J. (1999). Untersuchungen zur Hydrologie des arktischen Meereises – Konsequenzen für den kleinskaligen Stofftransport. *Ber. Polarforsch/Rep. Pol. Res.*, 325

Freitag, J., and Eicken, H. (2003). Meltwater circulation and permeability of Arctic summer sea ice derived from hydrological field experiments. *Journal of Glaciology*, 49, 166, 349-358

Fritsen, C.H., Lytle, V.I., Ackley, S.F., and Sullivan, C.W. (1994). Autumn bloom of Antarctic pack-ice algae. *Science*, 266, 5186, 782-784

Fuse, H., Takimura, O., Murakami, K., Yamoaka, Y., and Omori, T. (2000). Utilization of dimethyl sulfide as a sulfur source with the aid of light by Marinobacterium sp. Strain DMS-S1. *Applied and Environmental Microbiology*, 66, 5527-5532

Gabric, A.J., Qu, B., Matrai, P., and Hirst, A. (2005). The simulated response of dimethylsulfide production in the Arctic Ocean to global warming. *Tellus*, 57B, 391-403

Gage,D.A., Rhodes, D., Nolte, K.D., Hicks, W.A., Leustek, T., Cooper, A.J.L., and Hanson, A.D. (1997). A new route for synthesis of dimethylsulphoniopropionate in marine algae. *Nature*, 387, 891-894

Galí, M., and Simó, R. (2010). Occurrence and cycling of dimethylated sulfur compounds in the Arctic during summer receding ice edge. *Marine Chemistry*, 122, 105-117

Galley, R.J., Key, E., Barber, D.G., Hwang, B.J., and Ehn, J.K. (2008). Spatial and temporal variability of sea ice in the southern Beaufort Sea and Amundsen Gulf: 1980-2004. *Journal of Geophysical Research*, 113, C5, C05S95

Gambaro, A., Moret, I., Piazza, R., Andreoli, C., Da Rin, E., Capodaglio, G., Barbante, C., and Cescon, P. (2004). Temporal evolution of DMS and DMSP in Antarctic Coastal Sea water. *International Journal of Environmental Analytical Chemistry*, 84, 401-412

Garrison, D.L. (1991). Antarctic sea ice biota. *American Zoologist*, 31, 17-33

Garrison, D.L., and Buck, K.R. (1986). Organism losses during ice melting – a serious bias in sea ice community studies. *Polar Biology*, 6, 4, 237-239

Garrison, D.L., and Buck, K.R. (1989). The biota of Antarctic pack ice in the Weddell Sea and Antarctic Peninsula Regions. *Polar Biology*, 10, 211-219

Garrison, D.L., Ackley, S.F., and Buck, K.R. (1983). A physical mechanism for establishing algal populations in frazil ice. *Nature*, 306, 363-365

Garrison, D.L., Close, A.R., and Reimnitz, E. (1990). Microorganisms concentrated by frazil ice: evidence from laboratory experiments and field measurements. In: Ackley, S.F.,and Weeks, W.F. (Ed.), Sea Ice Properties and Processes, U.S. Army Corps of Engineers, Cold Regions Research and Engineering Laboratory, pp. 92-96

Geilfus, N.X., Carnat, G., Papakyriakou, T., Tison, J.-L., Else, B., Thomas, H., Shadwick, E., and Delille, B. (2012). Dynamics of pCO_2 and related air-ice CO_2 fluxes in the Arctic coastal zone (Amundsen Gulf, Beaufort Sea). *Journal of Geophysical Research*, 117, C9, C00G10

Gleitz, M.A., Bartsch, A., Dieckmann, G., and Eicken, H. (1998). Composition and succession of sea ice diatom assemblages in the eastern and southern Weddell Sea, Antarctica. In: Lizotte, M.P., and Arrigo, K. (Ed.), Sea Ice: Biological Processes, Interactions and Variability, Antarctic Research Series, American Geophysical Union, Washington D.C., pp. 107-120

Golden, K.M., Ackley, S.F., and Lytle, V.I. (1998). The percolation phase transition in sea ice. *Science*, 282, 2238-2241, doi: 10.1126/science.282.5397.2238

Golden, K.M., Heicken, H., Heaton, A.L., Miner, J., Pringle, D.J., and Zhu, J. (2007). Thermal evolution of permeability and microstructure in sea ice. *Geophysical Research Letters*, 34, L16501, doi: 10.1029/2007GL030447

Gosink, T.A., Pearson, J.G., and Kelley, J.J. (1976). Gas movement through sea ice. *Nature*, 263, 41-42

Gosselin, M., Legendre, L., Therriault, J.-C., and Demers, S. (1990). Light and nutrient limitation of sea-ice microalgae (Hudson Bay, Canadian Arctic). *Journal of Phycology*, 20, 220-232

Gough, A.J., Mahoney, A.R., Langhorne, P.J., Williams, M.J.M., and Haskell, T.G. (2012). Sea ice salinity and structure: A winter time series of salinity and its distribution. *Journal of Geophysical Research*, 117, C03008, doi: 10.1029/2011JC007527

Gow, A.J., and Tucker, W.B. III (1990). Sea ice in the polar regions. In: Smith, W.O.J. (Ed.), Polar Oceanography. Part A: physical science. Academic Press, San Diego, CA, pp. 47-122

Gow, A.J., Ackley, S.F., Govoni, J.W., and Weeks, W.F. (1998). Physical and structural properties of land-fast sea ice in McMurdo Sound, Antarctica. *Antarctic Sea Ice*: *Physical Processes*, *Interactions and Variability*, *Antarctic Research Series*, 74, 355-374

Gradinger, R., Meiners, K., Plumley, G., Zhang, Q., and Bluhm, B.A. (2005). Abundance and composition of the sea-ice meiofauna in off-shore pack ice of the Beaufort Gyre in summer 2002 and 2003. *Polar Biology*, 28, 171-181

Grenfell, T.C., and Maykut, G.A. (1977). The optical properties of ice and snow in the Arctic Basin. *Journal of Glaciology*, 18, 445-463

Grossi, S.M., Kotmeier, S.T., Moe, R.L., Taylor, G.T., and Sullivan, C.W. (1987). Sea ice microbial communities. VI. Growth and primary production in bottom ice under graded snow cover. *Marine Ecological Progress Series*, 35, 153-164

Grossmann, S., Lochte, K., and Scharek, R. (1996). Algal and bacterial processes in platelet ice during late summer. *Polar Biology*, 16, 623-633

Gunson, J.R., Spall, S.A., Anderson, T.R., Jones, A., Totterdell, I.J., and Woodage, M.J. (2006). Climate sensitivity to ocean dimethylsulphide emissions. *Geophysical Research Letters*, 33, L07701, doi: 10.1029/2005GL024982

Haas, C. (2003). Dynamics versus thermodynamics: the sea ice thickness distribution. In: Thomas, D.N., and Dieckmann, G.S. (Ed.), Sea ice: An introduction to its physics, biology, chemistry, and geology, Blackwell Science, Oxford, pp. 82-111

Haas, C., Thomas, D.N., and Bareiss, J. (2001). Surface properties and processes of perennial Antarctic sea ice in summer. *Journal of Glaciology*, 47, 159, 613-625

Hatton, A.D. (2002). Influence of photochemistry on the marine biogeochemical cycle of dimethylsulphide in the northern North Sea. *Deep-Sea Research Part II*, 49, 3039-3052

Hatton, A.D., and Wilson, S.T. (2007). Particulate dimethylsulphoxide and dimethylsulphoniopropionate in phytoplankton cultures and Scottish coastal waters. *Aquatic Sciences*, 69, 330-340

Hatton, A.D., Darroch, L., and Malin, G. (2004). The role of dimethylsulphoxide in the marine biogeochemical cycle of dimethylsulphide. *Oceanography and Marine Biology*, 42, 29-56

Hatton, A.D., Darroch, L., and Malin, G. (2005). The role of dimethylsulphoxide in the marine biogeochemical cycle of dimethylsulphide. *Oceanography and Marine Biology*, 42, 29-56

Hegseth, E.N., and Sundfjord, A. (2008). Intrusion and blooming of Atlantic phytoplankton species in the high Arctic. *Journal of Marine System*, 74, 108-119

Hellmer, H.H. (2004). Impact of Antarctic ice shelf basal melting on sea ice and deep ocean properties. *Geophysical Research Letters*, 31, L10307, doi: 10.1029/2004GL019506

Hill, R.W., White, B., Cottrell, M., and Dacey, J.W.H. (1998). Virus-mediated release of dimethylsulfoniopropionate from marine phytoplankton. *Aquatic Microbiology and Ecology*, 14, 1-6

Holland, D.M., and Jenkins, J.A. (1999). Modelling thermodynamic ice-ocean interactions at the base of an ice shelf. *Journal of Physical Oceanography*, 29, 1787-1800

Hopkins, M.A. (1994). On the ridging of intact lead ice. *Journal of Geophysical Research*, 99, 351-360

Horner, R.A., Ackley, S.F., Dieckmann, G.S., Gulliksen, B., Hoshiai, T., Legendre, L., Melnikov, I.A., Reeburgh, W.S., Spindler, M., and Sullivan, C.W. (1992). Ecology of sea ice biota. 1. Habita, terminology, and methodology. *Polar Biology*, 12, 417-427

Huebert, B.J., Blomquist, B.W., Hare, J.E., Fairall, C.W., Johnson, J.E., and Bates, T.S. (2004). Measurement of the sea-air DMS flux and transfer velocity using eddy correlation. *Geophysical Research Letters*, 31, L23113, doi: 10.1029/2004GL021567

Hynes, A.J., Wine, P.H., and Semmes, D.H. (1986). Kinetics and mechanisms of OH reactions with organic sulfides. *Journal of Physical Chemistry*, 90, 4148-4156

Jardon, F.P., Vivier, F., Vancoppenolle, M., Lourenço, A., Bouruet-Aubertot, P., and Cuypers, Y. (2013). Full-depth desalination of warm sea ice. *Journal of Geophysical Research*, 118, 435-447, doi: 10.1029/2012JC007962

Jeffrey, S.W., Mantoura, R.F.C., and Wright, S.W. (1997). Phytoplankton Pigments in Oceanography. SCOR, UNESCO Publishing

Jeffries, M.O., Weeks, W.F., Shaw, R., and Morris, K. (1993). Structural characteristics of congelation and platelet ice and their role in the development of Antarctic land-fast sea ice. *Journal of Glaciology*, 39, 132, 223-238

Jeffries, M.O., Shaw, R.A., Morris, K., Veazey, A.L., and Krouse, H.R. (1994). Crystal structure, stable isotopes ($\delta^{18}O$) and development of sea ice in the Ross, Amundsen and Bellingshausen seas, Antarctica. *Journal of Geophysical Research*, 99, C1, 985-995

Jeffries, M.O., Schwartz, K., Morris, K., Veazey, A.D., Krouse, H.R., and Cushing, S. (1995). Evidence for platelet ice accretion in Arctic sea ice development. *Journal of Geophysical Research*, 100, C6, 10905-10914

Juhl, A.R., and Krembs, C. (2010). Effects of snow removal and algal photoacclimation on growth and export of ice algae. *Polar Biology*, 33, 1057-1065

Karsten, U., Kück, K., Vogt, C., and Kirst, G.O. (1996). Dimethylsulfoniopropionate production in phototrophic organisms and its physiological function as a cryoprotectant. In: Kiene, R.P. (Ed.), Biological and environmental chemistry of DMSP and related sulfonium compounds, Plenum Press, New-York, pp. 143-153

Kattner, G., Thomas, D.N., Haas, C., Kennedy, H., and Dieckmann, G.S. (2004). Surface ice and gap layers in Antarctic sea ice: highly productive habitats. *Marine Ecology Progress Series*, 277, 1-12

Keller, M.D., Bellows, W.K., and Guillard, R.R.L. (1989). Dimethylsulfide production in marine phytoplankton. In: Saltzman, E.S., and Cooper, W.J. (Ed.), Biogenic sulfur in the environment, American Chemical Society, Washington DC, pp. 167-182

Kettle, A.J. et al. (1999). A global database of sea surface dimethylsulfide (DMS) measurements and a procedure to predict sea surface DMS as a function of latitude, longitude, and month. *Global Biogeochemical Cycles*, 13(2), 399-444

Kieber, D.J., Jiao, J.F., Kiene, R.P., and Bates, T.S. (1996). Impact of dimethylsulfide photochemistry on methyl sulfur cycling in the equatorial Pacific Ocean. *Journal of Geophysical Research: Oceans*, 101 (C2), 3715-3722

Kiene, R.P. (1992). Dynamics of dimethyl sulphide and dimethylsulfoniopropionate in oceanic waters. *Marine Chemistry*, 37, 29-52

Kiene, R.P. (1996). Turnover of dissolved DMSP in estuarine and shelf waters of the northern Gulf of Mexico. *Biological and environmental Chemistry of DMSP and related compounds*

Kiene, R.P., and Bates, T.S. (1990). Biological removal of dimethyl sulfide from sea water. *Nature*, 345, 702-705

Kiene, R.P. and Linn, L.J. (2000). The fate of dissolved dimethylsulfoniopropionate (DMSP) in seawater: tracer studies using ^{35}S-DMSP. *Geochimica and Cosmochimica Acta*, 64, 2797-2810

Kiene, R.P., and Slezak, D. (2006). Low dissolved DMSP concentrations in seawater revealed by small-volume gravity filtration and dialysis sampling. *Limnology and Oceanography Methods*, 4, 80-95

Kiene, R.P., Hoffmann Williams, L.P., and Walker, J.E. (1998). Sea water microorganisms have a high affinity glycine betaine uptake system which also recognizes dimethylsulfoniopropionate. *Aquatic Microbial Ecology*, 15, 39-51

Kiene, R.P., Linn, L.J., Gonzalez, J., Moran, M.A., and Bruton, J.A. (1999). Dimethylsulfoniopropionate and methanethiol are important precursors of methionine and protein-sulfur in marine bacterioplankton. *Applied and Environmental Microbiology*, 65, 4549-4558

Kiene, R.P., Linn, L.J., and Bruton, J.A. (2000). New and important roles for DMSP in marine microbial communities. *Journal of Sea Research*, 43, 209-224

Kipfstuhl, J. (1991). On the formation of underwater ice and the growth and energy budget of the sea ice in Atka Bay, Antarctica. *Berichte Zur Polarforschung*, 85, 1-89

Kirst, G.O., Thiel, C., Wolff, H., Nothnagel, J., Wanzek, M., and Ulmke, R. (1991). Dimethylsulfoniopropionate (DMSP) in ice-algae and its possible biological role. *Marine Chemistry*, 35, 381-388

Kloster, S., Feichter, J., Maier-Reimer, E., Six, K.D., Stier, P., and Wetzel, P. (2006). DMS cycle in the marine ocean-atmosphere system – a global model study. *Biogeosciences*, 3(1), 29-51

Koga, S., and Tanaka, H. (1993). Numerical study of the oxidation processes of DMS in the marine atmosphere. *Journal of Atmospheric Chemistry*, 17, 201-228

Krembs, C., and Engel, A. (2001). Abundance and variability of microorganisms and transparent exopolymer particles across the ice-water interface of melting first-year sea ice in the Laptev Sea (Arctic). *Marine Biology*, 138, 173-185

Krembs, C., Gradinger, R., and Spindler, M. (2000). Implications of brine channel geometry and surface area for the interaction of the sympagic organisms in Arctic sea ice. *Journal of Experimental Marine Biology and Ecology*, 243, 55-80

Krüger, O., and Grassl, H. (2011). Southern Ocean phytoplankton increases cloud albedo and reduces precipitation. *Geophysical Research Letters*, 38, L08809, doi: 10.1029/2011GL047116

Kwint, R.L.J., and Kramer, K.J.M. (1996). The annual cycle of the production and fate of DMS and DMSP in a marine coastal system. *Marine Ecological Progress Series*, 134, 217-224

Kwok, R., Cunningham, G.F., Wensnahan, M., Rigor, I., Zwally, H.J., and Yi, D. (2009). Thinning and volume loss of the Arctic Ocean sea ice cover: 2003-2008. *Journal of Geophysical Research*, 114, C7, C07005

Lana, A., Bell, T.G., Simò, R., Vallina, S.M., Ballabrera-Poy, J., Kettle, A.J., Dachs, J., Bopp, L., Saltzman, E.S., Stefels, J., Johnson, J.E., and Liss, P.S. (2011). An updated climatology of surface dimethylsulfide concentrations and emission fluxes in the global ocean. *Global Biogeochemical Cycles*, 25, doi: 10.1029/2010GB003850

Lana, A., Simó, R., Vallina, S.M., and Dachs, J. (2012). Potential for a biogenic influence on cloud microphysics over the ocean: a correlation study with satellite-derived data. *Atmospheric Chemistry and Physics*, 12, 7977-7993

Lange, M.A., Ackley, S.F., Wadhams, P., Dieckmann, G.S., and Eicken, H. (1989). Development of sea ice in the Weddell Sea. *Annals of Glaciology*, 12, 92-96

Lange, M.A., and Eicken, H. (1991). Textural characteristics of sea ice and the major mechanisms of ice growth in the Weddell Sea. *Annals of Glaciology*, 15, 210-215

Lange, M.A., Schlosser, P., Ackley, S.F., Wadhams, P., and Dieckmann, G.S. (1990). O-18 concentrations in sea ice of the Weddell Sea, Antarctica. *Journal of Glaciology*, 36, 124, 315-323

Langway, C.C. (1958), Ice fabrics and the universal stage. SIPRE Tech. Rep., 62

Lannuzel, D., Schoemann, V., de Jong, J., Tison, J.-L., and Chou, L. (2006). Distribution and biogeochemical behavior of iron in the East Antarctic sea ice. *Marine Chemistry*, 106, 18-32

Laroche, D., Vezina, A.F., Levasseur, M., Gosselin, M., Stefels, J., Keller, M.D., Matrai, P.A., and Kwint, R.L.J. (1999). DMSP synthesis and exudation in phytoplankton: a modeling approach. *Marine Ecological Progress Series*, 180, 37-49

Larose, C., Dommergue, A., De Angelis, M., Cossa, D., Averty, B., Marusczak, N., Soumis, D., Schneider, D., and Ferrari, C. (2010). Springtime changes in snow chemistry lead to new insights into mercury methylation in the Arctic. *Geochimica and Cosmochimica Acta*, 74, 6263-6275

Leck, C., and Persson, C. (1996). The central Arctic Ocean as a source of dimethyl sulphide: Seasonal variability in relation to biological activity. *Journal of Geophysical Research*, 95, 3353-3364

Leck, C., Norman, M., Bigg, E.K., and Hillamo, R. (2002). Chemical composition and sources of the high Arctic aerosol relevant for cloud formation. *Journal of Geophysical Research*, 107, 1-17

Lee, P.A., and de Mora, S.J. (1999). Intracellular dimethylsulfoxide (DMSO) in unicellular marine algae: speculations on its origin and possible biological role. *Journal of Phycology*, 35 (1), 8-18

Lee, P.A., de Mora, S.J., Gosselin, M., Levasseur, M., Bouillon, R.-C., Nozais, C., and Michel, C. (2001). Particulate dimethylsulfoxide in Arctic sea-ice algal communities: the cryoprotectant hypothesis revisited. *Journal of Phycology*, 37, 488-499

Lepparänta, M., and Manninen, T. (1988). The brine and gas content of sea ice, with attention to low salinities and high temperatures. Internal Report, 88-2, Finnish Institute of Marine Research, Helsinki

Levasseur, M. (2013). Impact of Arctic meltdown on the microbial cycling of sulphur. *Nature Geoscience*, 6, 691-698

Levasseur, M., Gosselin, M., and Michaud, S. (1994). A new source of dimethylsulfide (DMS) for the arctic atmosphere: ice diatoms. *Marine Biology*, 121, 381-387

Levy, H.I. (1971). Normal Atmosphere: Large Radical and Formaldehyde Concentrations Predicted. *Science*, 173, 141-143

Lewis, M.J., Tison, J.-L., Weissling, B., Delille, B., Ackley, S.F., Brabant, F., and Xie, H. (2011). Sea ice and snow cover characteristics during the winter-spring transition in the Bellingshausen Sea: An overview of SIMBA 2007. *Deep-Sea Research II*, 58, 101-1038

Lewis, E.L., and Perkin, R.G. (1983). Supercooling and energy exchange near the Arctic Ocean surface. *Journal of Geophysical Research*, 88, C12, 7681-7685

Liss, P.S., and Slater, P.G. (1974). Flux of gasses across the air-sea interface. *Nature*, 247, 181-184

Liss, P.S., and Merlivat, L. (1986). Air-sea gas exchange rates: introduction and synthesis. In: Buat-Ménard, P., and Reidel, D. (Ed.), The role of air-sea exchange in geochemical cycling. Boston, Mass., 113-129

Lizotte, M.P. (2003). The Microbiology of Sea Ice. In: Thomas, D.N., and Dieckmann, G.S. (Ed.), Sea ice: An introduction to its physics, biology, chemistry, and geology, Blackwell Science, Oxford, pp. 184-210

Lizotte, M.P., and Sullivan, C.W. (1991). Photosynthesis-irradiance relationships in microalgae associated with Antarctic pack ice: evidence for *in situ* activity. *Marine Ecology Progress Series*, 71, 175-184

Loose, B., McGillis, W.R., Schlosser, P., Perovich, D., and Takahashi, T. (2009). Effects of freezing, growth, and ice cover on gas transport processes in laboratory seawater experiments. *Geophysical Research Letters*, 36, L05603, doi: 10.1029/2008GL036318

Loose, B., Schlosser, P., Perovich, D., Ringelberg, D., Ho, D.T., Takahashi, T., Richter-Menge, J., Reynolds, C.M., Mcgillis, W.R., and Tison, J.-L. (2011a). Gas diffusion through columnar laboratory sea ice: Implications for mixed-layer ventilation of CO_2 in the seasonal ice zone. *Tellus B*, 63 (1), 23-39

Loose, B., Miller, L.A., Elliott, S., and Papakyriakou, T. (2011b). Sea ice biogeochemistry and material transport across the frozen interface. *Oceanography*, 24(3), 202-218

Lovelock, J.E., Maggs, R.J., and Rasmussen, R.A. (1972). Atmospheric dimethyl sulphide and the natural sulphur cycle. *Nature*, 237, 452-453

Lyon, B.R., Lee, P.A., Bennett, J.M., DiTullio, G.R., and Janech, M.G. (2011). Proteomic Analysis of a Sea-Ice Diatom: Salinity Acclimation Provides New Insight into the Dimethylsulfoniopropionate Production Pathway. *Plant Physiology*, 157, 1926-1941

Malin, G. (1997). Biological oceanography: Sulphur, climate and the microbial maze. *Nature*, 387, 857-859

Malin, G.,and Kirst, G.O. (1997). Algal production of dimethyl sulfide and its atmospheric role. *Journal of Phycology*, 33, 889-896

Malin, G., Wilson, W.H., Bratbak, G., Liss, P.S., and Mann, N.H. (1998). Elevated production of dimethylsulfide resulting from viral infection of cultures of Phaeocystis pouchetii. *Limnology and Oceanography*, 43, 1389-1393

Malmgren, F. (1927). On the properties of sea ice. In: Sverdrup, H.U. (Ed.), The Norwegian North Polar Expedition with the "Maud" 1918-1925. John Griegs, Bergen, Norway, pp. 1-67

Marquardt, M., Kramer, M., Carnat, G., and Werner, I. (2011). Vertical distribution of sympagic meiofauna in sea ice in the Canadian Beaufort Sea. *Polar Biology*, 34, 1887-1900

Martin, S. (1974). Ice stalactites: comparison of a laminar flow theory with experiment. *Journal of Fluid Mechanics*, 63, 1, 51-79

Martin, S. (1981). Frazil ice in rivers and oceans. *Annual Review of Fluid Mechanisms*, 13, 379-397

Martinez, J.M., Schroeder, D.C., Larsen, A., Bratback, G., and Wilson, W.H. (2007). Molecular dynamics of Emiliania huxleyi and co-occurring viruses during two separate mesocosm studies. *Applied Environmental Biology*, 73, 554-562

Massom, R.A., Lytle, V.I., Worby, A.P., and Allison, I. (1998). Winter snow cover variability on East Antarctic sea ice. *Journal of Geophysical Research*, 103, C11, 24837-24855

Massom, R.A., Eicken, H., Haas, C., Jeffries, M.O., Drinkwater, M.R., Sturm, M., Worby, A.P., Wu, X., Lytle, V.I., Ushio, S., Morris, K., Reid, P.A., Warren, S.G., and Allison, I. (2001). Snow on Antarctic sea ice. *Reviews of Geophysics*, 39, 3, 413-445

Maykut, G.A. (1982). Large-scale heat exchange and ice production in the central Arctic. *Journal of Geophysical Research*, 87, C10, 7971-7984

Maykut, G.A. (1985). An introduction to ice in the polar oceans. *Technical Report 8510*. University of Washington, Seattle, WA

Maykut, G.A. (1986). The Surface Heat and Mass Balance. In: Untersteiner, N. (Ed.), Geophysics of Sea Ice, Series B: Physics, Plenum Press, 146, pp. 395-463

McGillis, W.R., Dacey, J.W.H., Frew, N.M., Bock, E.J., and Nelson, R.K. (2000). Water-air flux of dimethylsulfide. *Journal of Geophysical Research*, 105, 1187-1193

McMinn, A., Ashworth, C., and Ryan, K.G. (2000). In situ net primary productivity of an Antarctic fast ice bottom algal community. *Aquatic Microbial Ecology*, 21, 177-185

McMinn, A., Pankowski, A., and Delfatti, T. (2005). Effect of hyperoxia on the growth and photosynthesis of polar sea ice microalgae. *Journal of Phycology*, 41, 732-741

McMinn, A., Martin, A., and Ryan, K. (2010). Phytoplankton and sea ice algal biomass and physiology during the transition between winter and spring (McMurdo Sound, Antarctica). *Polar Biology*, 33, 1547-1556, doi: 10.1007/s00300-010-0844-6

Meddlin, L.K., and Priddle, J. (1990). Polar Marine Diatoms. British Antarctic Survey, Natural Environment Research Council, Science, 214 pp.

Meese, D.A. (1989). The chemical and structural properties of sea ice in the southern Beaufort Sea. *CRREL Report*, 89-25

Melling, H., Topham, D.R., and Riedel, D. (1993). Topography of the upper and lower surfaces of 10 hectares of deformed sea ice. *Cold Regions Science and Technology*, 21, 4, 349-369

Merico, A., Tyrrell, T., Brown, C.W., Groom, S.B., and Miller, P.I. (2003). Analysis of satellite imagery for *Emiliania huxleyi* blooms in the Bering Sea before 1997. *Geophysical Research Letters*, 30, 6, 1337

Merzouk, A., Levasseur, M., Scarratt, M., Michaud, S., Lizotte, M., Rivkin, R.B., and Kiene, R.P. (2008). Bacterial DMSP metabolism during the senescence of the spring diatom bloom in the Northwest Atlantic. *Marine Ecological Progress Series*, 369, 1-11, doi: 10.3354/meps07664

Miller, T.R., Hnilicka, K., Dziedzic, A., Desplats, P., and Belas, R. (2004). Chemotaxis of Silicibacter sp. Strain TM1040 toward dinoflagellate products. *Applied Environmental Microbiology*, 70(8), 4692-4701

Mock, T., and Thomas, D.N. (2005). Recent advances in sea-ice microbiology. *Environmental Microbiology*, 7(5), 605-619

Monks, P.S. (2005). Gas-phase radical chemistry in the troposphere. *Chemical Society Reviews*, 34, 376-395

Montresor, M., Procaccini, G., and Stoecker, D.K. (1999). Polarella glacialis, gen. nov., sp. Nov. (Dinophyceae): Suessiaceae are still alive!. *Journal of Phycology*, 35, 186-197

Montresor, M.G., Lovejoy, C., Orsini, L., Procaccini, G., and Roy, S. (2003). Bipolar distribution of the cyst-forming dinoflagellate *Polarella glacialis*. *Polar Biology*, 26, 186-194

Moran, M.A., Reisch, C.R., R.P. Kiene, and Whitman, W.B. (2012). Genomic Insights into Bacterial DMSP Transformations. *Annual Review of Marine Science*, 4, 523-542

Mundy, C.J., Barber, D.G., and Michel, C. (2005). Variability of snow and ice thermal, physical and optical properties pertinent to sea ice algae biomass during spring. *Journal of Marine Systems*, 58, 107-120

Mundy, C.J., Gosselin, M., Ehn, J.K., Belzile, C., Poulin, M., Alou, E., Roy, S., Hop, H., Lessard, S., and Papakyriakou, T. (2011). Characteristics of two distinct high-light acclimated algal communities during advanced stages of sea ice melt. *Polar Biology*, 34, 12, 1869-1886

Nakawo, M. and Sinha, N.K. (1981). Growth rate and salinity profile of first-year sea ice in the High Arctic. *Journal of Glaciology*, 27, 96, 315-330

Nguyen, B.C., Belviso, S., Mihalopoulos, N., Gostan, J., and Nival, P. (1988). Dimethyl Sulfide Production During Natural Phytoplanktonic Blooms. *Marine Chemistry*, 24, 133-141

Nicolaus, M., Katlein, C., Maslanik, J., and Hendricks, S. (2012). Changes in Arctic sea ice result in increasing light transmittance and absorption. *Geophysical Research Letters*, 39, 24, doi: 10.1029/2012GL053738

Niemi, A., Michel, C., Hille, K., and Poulin, M. (2011). Protist assemblages in winter sea ice : setting the stage for the spring ice algal bloom. *Polar Biology*, 34, 1803-1817

Nightingale, P.D., Malin, G., Law, C.S., Watson, A.J., Liss, P.S., Liddicoat, M.I., Boutin, J., and Upstill-Goddard, R.C. (2000). In situ evalutation of air-sea gas exchange parameterizations using novel conservative and volatile tracers. *Global Biogeochemical Cycles*, 14, 373-387

Niki, T., Kunugi, M., and Otsuki, A. (2000). DMSP-lyase activity infive phytoplankton species: its potential importance in DMS production. *Marine Biology*, 136, 759-764

Nilsson, E.D., Rannik, U., Swietlicki, E., Leck, C., Aalto, P.P., Zhou, J., and Norman, M. (2001). Turbulent aerosol fluxes over the Arctic Ocean 2. Wind-driven sources from the sea. *Journal of Geophysical Research*, 106, 32139-32154

Nomura, D., Koga, S., Kasamatsu, N., Shinagawa, H., Simizu, D., Wada, M., and Fukuchi, M. (2012). Direct measurements of DMS flux from Antarctic fast sea ice to the atmosphere by a chamber technique. *Journal of Geophysical Research*, 117, doi: 10.1029/2010JC006755

Noordkamp, D.J.B., Gieskes, W.W.C., Gottschal, J.C., Forney, L.J., and van Rijssel, M. (2000). High acrylate concentrations in the mucus of Phaeocystis globosa colonies. *Aquatic Microbial Ecology*, 16, 45-52

Notz, D. (2005). Thermodynamic and fluid-dynamical processes in sea ice. *PhD Thesis*. University of Cambridge

Notz, D., and Worster, M.G. (2008). In situ measurements of the evolution of young sea ice. *Journal of Geophysical Research*, 113, C3, C03001

Notz, D., and Worster, M.G. (2009). Desalination processes of sea ice revisited. *Journal of Geophysical Research*, 114, C5, C05006

Notz, D., Wettlaufer, J.S., and Worster, M.G. (2005). A non-destructive method for measuring the salinity and solid fraction of growing sea ice in situ. *Journal of Glaciology*, 51, 172, 159-166

Perovich, D.K. (1996). The optical properties of sea ice. *CRREL Monograph*, 96-1, Hanover, N.H., USA

Perovich, D.K. (2001). UV radiation and optical properties of sea ice and snow. In: Hessen, D. (Ed.), UV-Radiation and Arctic Ecosystems, Springer-Verlag, Heidelberg, pp. 73-89

Perovich, D.K., and Elder, B.C. (2001). Temporal evolution of Arctic sea-ice temperature. *Annals of Glaciology*, 33, 207-211

Perovich, D.K., and Govoni, J.W. (1991). Absorption coefficients of sea ice from 250 to 400 nm. *Geophysical Research Letters*, 18, 7, 1233-1235

Perovich, D.K., and Richter-Menge, J.A. (1994). Surface characteristics of lead ice. *Journal of Geophysical Research*, 99, C8, 16341-16350

Perovich, D.K., Roesler, C.S., and Pegau, W.S. (1998). Variability in Arctic sea ice optical properties. *Journal of Geophysical Research*, 103, C1, 1193-1208

Petrich, C., and Eicken, H. (2010). Growth, structure and properties of sea ice. In: Thomas, D.N., and Dieckmann, G.S. (Ed.), Sea ice. Wiley-Blackwell, Oxford, pp. 23-77

Pfirman, S.L., Eicken, H., Bauch, D., and Weeks, W.F. (1995). The potential transport of pollutants by Arctic sea ice. *Science of the Total Environment*, 159, 2-3, 129-146

Poulin, M., Daugbjerg, N., Gradinger, R., Ilyash, L., Ratkova, T., and von Quillfeldt, C. (2011). Pan-Arctic biodiversity of marine pelagic and sea-ice unicellular eukaryotes: a first-attempt assessment. *Marine Biodiversity*, 41, 13-28

Proshutinsky, A., Bourke, R.H., and McLaughlin, F.A. (2002). The role of the Beaufort Gyre in Arctic climate variability: seasonal to decadal climate scales. *Geophysical Research Letters*, 29, 23, 2100

Qu, B., and Gabric, A. (2010). Using genetic algorithm to calibrate a dimethylsulfide production model in the Arctic Ocean. *Chinese Journal of Oceanology and Limnology*, 28, 573-582

Quinn, P.K., and Bates, T.S. (2011). The case against climate regulation via oceanic phytoplankton sulphur emissions. *Nature*, 480, 51-56

Read, K.A., Mahajan, A.S., Carpenter, L.J., Evans, M.J., Fari, B.V.E., Heard, D.E., Hopkins, J.R., Lee, J.D., Moller, S.J., Lewis, A.C., Mendes, L., McQuaid, J.B., Oetjen, H., Saiz-Lopez, A., Pilling, M.J., and Plane, J.M.C. (2008). Extensive halogen-mediated ozone destruction over the tropical Atlantic Ocean. *Nature*, 453, 1232-1235

Reimnitz, E., Kempema, E.W., and Barnes, P.W. (1987). Anchor ice, seabed freezing and sediment dynamics in shallow Arctic seas. *Journal of Geophysical Research*, 92, C13, 14671-14678

Rempillo, O., Seguin, A.M., Norman, A.-L., Scarratt, M., Michaud, S., Chang, R., Sjostedt, S., Abbatt, J., Else, B., Papakyriakou, T., Sharma, S., Grasby, S., and Levasseur, M. (2011). Dimethyl sulfide air-sea fluxes and biogenic sulfur as a source of new aerosols in the Arctic fall. *Journal of Geophysical Research*, 116, D00S04, doi: 10.1029/2011JD016336

Remy, J.-P., Becquevort, S., Haskell, T.G., and Tison, J.-L. (2008). Impact of the B-15 iceberg “stranding event” on the physical and biological properties of sea ice in McMurdo Sound, Ross Sea, Antarctica. *Antarctic Science*, 20, 593-604, doi: 10.1017/S0954102008001284

Riseman, S.F., and DiTullio, G.R. (2004). Particulate dimethylsulfoniopropionate and dimethylsulfoxide in relation to iron availability and algal community structure in the Peru Upwelling System. *Canadian Journal of Fisheries and Aquatic Science*, 61, 721-735

Różańska, M., Poulin, M., Gosselin, M. (2008). Protist entrapment in newly formed sea ice in the coastal Arctic Ocean. *Journal of Marine System*, 74, 887-901

Różańska, M., Gosselin, M., Poulin, M., Wiktor, J.M., and Michel, C. (2009). Influence of environmental factors on the development of bottom ice protist communities during the winter-spring transition. *Marine Ecology Progress Series*, 386, 43-59

Ryan, K.G., Hegseth, E.N., Martin, A., Davy, S.K., O'Toole, R., Ralph, P.J., McMinn, A., and Thorn, C.J. (2006). Comparison of the microalgal community within fast ice at two sites along the Ross Sea coast, Antarctica. *Antarctic Science*, 18(4), 583-594, doi: 10.1017/S0954102006000629

Rysgaard, S., and Glud, R.N. (2004). Anaerobic N_2 production in Arctic sea ice. *Limnology and Oceanography*, 49, 1, 86-94

Rysgaard, S., Kuhl, M., Glud, R.N., and Hansen, J.W. (2001). Biomass, production and horizontal patchiness of sea ice algae ina high-Arctic fjord (Young Sound, NE Greenland). *Marine Ecology Progress Series*, 223, 15-26

Savoie, D.L., and Prospero, J.M. (1989). Comparison of oceanic and continental sources of non-seasalt sulphate over the Pacific Ocean. *Nature*, 339, 685-687

Scarratt, M.G., Levasseur, M., Michaud, S., Cantin, G., Gosselin, M., and de Mora, S.J. (2002). Influence of phytoplankton taxonomic profile on the distribution of dimethylsulfide and dimethylsulfoniopropionate in the northwest Atlantic. *Marine Ecological Progress Series*, 244, 49-61

Schäfer, H., Myronova, N., and Boden, R. (2010). Microbial degradation of dimethylsulphide and related C_1-sulphur compounds: organisms and pathways controlling fluxes of sulphur in the biosphere. *Journal of Experimental Botany*, 61, 2, 315-334

Schwarz, A.-M., Hawes, I., Andrew, N., Norkko, A., Cummings, V., and Thrush, S. (2003). Macroalgal photosynthesis near the southern global limit for growth; Cape Evans, Ross Sea, Antarctica. *Polar Biology*, 26, 789-799

Scott, F.J., and Marchant, H.J. (2005). Antarctic marine protists. ABRS Canberra, Australia, 563 pp.

Seinfeld, J.H., and Pandis, S.N. (2006). Atmospheric Chemistry and Physics: From Air Pollution to Climate Change, 2nd Edition, J. Wiley, New-York

Sharma, S., Barrie, L.A., Hastie, D.R., and Kelly, C. (1999a). Dimethyl sulfide emissions to the atmosphere from lakes of the Canadian boreal region. *Journal of Geophysical Research*, 104, 11585-11592

Sharma, S., Barrie, L.A., Plummer, D., McConnell, J.C., Brickell, P.C., Levasseur, M., Gosselin, M., and Bates, T.S. (1999b). Flux estimation of oceanic dimethyl sulfide around North America. *Journal of Geophysical Research*, 104, D17, 21327-21342

Simó, R. (2004). From cells to globe: approaching the dynamics of DMS(P) in the ocean at multiple scales. *Canadian Journal of Fisheries and Aquatic Sciences*, 61, 673-684

Simó, R., and Pedros-Alio, C. (1999). Role of vertical mixing in controlling the oceanic production of dimethyl sulphide. *Nature*, 402, 396-399

Simó, R., and Vila-Costa, M. (2006). Ubiquity of algal dimethylsulfoxide in the surface ocean: Geographic and temporal distribution patterns. *Marine Chemistry*, 100, 136-146

Simó, R., Hatton, A.D., Malin, G., and Liss, P.S. (1998). Particulate dimethyl sulphoxide in seawater: production by microplankton. *Marine Ecological Progress Series*, 167, 291-296

Simó, R., Pedros-Alio, C., Malin, G., and Grimalt, J.O. (2000). Biological turnover of DMS, DMSP and DMSO in contrasting open-sea waters. *Marine Ecological Progress Series*, 203, 1-11

Simó, R., Archer, S.D., Pedros-Alio, C., Gilpin, L., Stelfox-Widdicombe, C.E. (2002). Coupled dynamics of dimethylsulfoniopropionate and dimethylsulfide cycling and the microbial food web in surface waters of the North Atlantic. *Limnology and Oceanography*, 47, 53-61

Small, J.D., Chuang, P.Y., Feingold, G., and Jiang, H.L. (2009). Can aerosol decrease cloud lifetime?. *Geophysical Research Letters*, 36, L16806

Smith, I.J., Langhorne, P.J., Trodahl, H.J., Haskell, T.G., Frew, R., and Vennell, R. (2001). Platelet ice and the land-fast sea ice of McMurdo Sound, Antarctica. *Annals of Glaciology*, 33, 21-27

Song, G., Xie, H., Aubry, C., Zhang, Y., Gosselin, M., Mundy, C.J., Philippe, B., and Papakyriakou, T.N. (2011). Spatiotemporal variations of dissolved organic carbon and carbon monoxide in first-year sea ice in the western Canadian Arctic. Journal of Geophysical Research, 116, C00G05, doi: 10.1029/2010JC006867

Spielmeyer, A., and Pohnert, G. (2012). Daytime, growth phase and nitrate availability dependent variations of dimethylsulfoniopropionate in batch cultures of the diatom Skeletonema marinoi. *Journal of Experimental Marine Biology and Ecology*, 413, 121-130, doi: 10.1016/j.jembe.2011.12.004

Spiese, C.E., Kieber, D.J., and Nomura, C.T. (2009). Reduction of dimethylsulfoxide to dimethylsulfide by marine phytoplankton. *Limnology and Oceanography*, 54 (2), 560-570

Stedmon, C.A., Amon, R.M.W., Rinehart, A.J., and Walker, S.A. (2011). The supply and characteristics of colored dissolved organic matter (CDOM) in the Arctic Ocean: Pan Arctic trends and differences. *Marine Chemistry*, 124, 108-118

Steele, M., and Flato, G.M. (2000). Sea ice growth, melt and modeling: a survey. In: Lewis, E.L., Jones, E.P., Lemke, P., Prowse, T.D., and Wadhams, P. (Ed.), The freshwater budget of the Arctic Ocean. NATO Science Series 2, Kluwer Academic Publishers, Dordrecht, pp. 549-587

Stefels, J. (2000). Physiological aspects of the production and conversion of DMSP in marine algae and higher plants. *Journal of Sea Research*, 43, 183-197

Stefels, J. (2009). Determination of DMS, DMSP and DMSO in seawater. In: Wurl, O. (Ed.), Practical Guidelines for the Analysis of Seawater, CRC Press, Taylor and Francis Group, Boca Raton, US, pp. 223-235

Stefels, J., and van Boekel, W.H.M. (1993). Production of DMS from dissolved DMSP in axenic cultures of the marine phytoplankton species *Phaeocystis sp.*. *Marine Ecological Progress Series*, 97, 11-18

Stefels, J., and van Leeuwe, M.A. (1998). Effects or iron and light stress on the biochemical composition of Antarctic Phaeocystis sp.(Prymnesiophyceae). I. Intracellular DMSP concentrations. *Journal of Phycology*, 34, 486-495

Stefels, J., Steinke, M., Turner, S., Malin, G., and Belviso, S. (2007). Environmental constraints on the production and removal of the climatically active gas dimethylsulphide (DMS) and implications for ecosystem modeling. *Biogeochemistry*, 83, 245-275, DOI 10.1007/s10533-007-9091-5

Stefels, J., Carnat, G., Dacey, J.W.H., Goossens, T., Elzenga, J.T.M., and Tison, J.-L. (2012). The analysis of dimethylsulfide and dimethylsulfoniopropionate in sea ice: Dry-crushing and melting using stable isotope additions. *Marine Chemistry*, 128-129, 34-43

Steinke, M., Daniel, C., and Kirst, G.O. (1996). DMSP lyase in marine micro- and macroalgae: intraspecific differences in cleavage activity. In: Kiene, R.P., Visscher, P.T., Keller, M.D., and Kirst, G.O. (Ed.), Biological and Environmental Chemistry of DMSP and Related Sulfonium Compounds, Plenum Press, New-York, pp. 317-324

Steinke, M., Wolfe, G.V., and Kirst, G.O. (1998). Partial characterization of dimethylsulfoniopropionate (DMSP) lyase isozymes in 6 strains of Emiliania huxleyi. *Marine Ecological Progress Series*, 175, 215-255

Steinke, M., Malin, G., Archer, S.D., Burkill, P.H., and Liss, P.S. (2002). DMS production in a coccolithophorid bloom: evidence for the importance of dinoflagellate DMSP lyases. *Aquatic Microbial Ecology*, 26, 259-270

Steinke, M., Stefels, J., and Stamhuis, E. (2006). Dimethyl sulfide triggers search behavior in copepods. *Limnology and Oceanography*, 51, 1925-1930

Stigebrandt, A. (1981). On the rate of ice formation in water cooled by a more saline sublayer. *Tellus*, 33, 6, 604-609

Stoecker, D.K., Gustafson, D.E., Merrell, J.R., Black, M.M.D., and Baier, C.T. (1997). Excystment and growth of chrysophytes and dinoflagellates at low temperatures and high salinities in Antarctic sea-ice. *Journal of Phycology*, 33, 585-595

Stoecker, D.K., Gustafson, D.E., Black, M.M.D., and Baier, C.T. (1998). Population dynamics of microalgae in the upper land-fast sea ice at a snow-free location. *Journal of Phycology*, 34, 60-69

Sturm, M., Holmgren, J., König, M., and Morris, K. (1997). The thermal conductivity of seasonal snow. *Journal of Glaciology*, 43, 143, 26-41

Sturm, M., Holmgren, J., and Perovich, D.K. (2002).Winter snow cover on the sea ice of the Arctic Ocean at the Surface Heat Budget of the Arctic Ocean (SHEBA): temporal evolution and spatial variability. *Journal of Geophysical Research*, 107, C10, 8047

Sunda, W., Kieber, D.J., Kiene, R.P., and Huntsman, S. (2002). An antioxidant function for DMSP and DMS in marine algae. *Nature*, 418, 317-320, doi: 10.1038/nature00851

Sunda, W.G., Hardison, R., Kiene, R., Bucciarelli, E., and Harada, H. (2007). The effect of nitrogen limitation on cellular DMSP and DMS release in marine phytoplankton: Climate feedback implications. *Aquatic Sciences*, 69, 341-351

Sutherland, D.L. (2008). Surface-associated diatoms from marine habitats at Cape Evans, Antarctica, including the first record of living Eunotogramma marginopunctatum (2008). *Polar Biology*, 31, 879-888

Taalba, A., Xie, H., Scarratt, M.G., Bélanger, S., and Levasseur, M. (2013). Photooxidation of dimethylsulfide (DMS) in the Canadian Arctic. *Biogeosciences Discussion*, 10, 2093-2126

Tang, K.W., Dam, H.G., Visscher, P.T., and Fenn, T.D. (1999). Dimethylsulfoniopropionate (DMSP) in marine copepods and its relation with diets and salinity. *Marine Ecological Progress Series*, 179, 71-79

Tang, K.W., and Simó, R. (2003). Trophic uptake and transfer of DMSP in simple planktonic food chains. *Aquatic Microbial Ecology*, 31, 193-202

Thomas, C.R. (1997). Identifying marine phytoplankton. Academic Press, San Diego, 858 pp.

Thomas, D.N., and Dieckmann, G.S. (2010). Sea Ice: Second Edition. Wiley-Blackwell Publishing Ltd, Oxford

Thomas, D.N., Lara, R.J., Haas, C., Schnack-Schiel, S.B., Dieckmann, G.S., Kattner, G., Nöthig, E.-M., and Mizdalski, E. (1998). Biological soup within decaying summer sea ice in the Amundsen sea, Antarctica. In: Lizotte, M.P., and Arrigo, K. (Ed.), Sea Ice: Biological Processes, Interactions and Variability, Antarctic Research Series, American Geophysical Union, Washington D.C., pp. 161-171

Thomas, D.N., Engbrodt, R., Gianelli, V., Kattner, G., Kennedy, H., Haas, C., and Dieckmann, G.S. (2001). Dissolved organic matter in Antarctic sea ice. *Annals of Glaciology*, 33, 297-303

Thomas, D.N., Papadimitriou, S., and Michel, C. (2010). Biogeochemistry of sea ice. In: Thomas, D.N., and Dieckmann, G.S. (Ed.), Sea ice. Wiley-Blackwell, Oxford, pp. 425-466

Thomson, P.G., Wright, S.W., Bolch, C.J.S., Nichols, P.D., Skerratt, J.H., and McMinn, A. (2004). Antarctic distribution, pigment and lipid composition, and molecular identification of the brine dinoflagellate *Polarella glacialis* (Dinophyceae). *Journal of Phycology*, 40, 867-873

Timco, G.W., and Frederking, R.M.W. (1990). Compressive strength of sea ice sheets. *Cold Regions Science and Technology*, 17, 3, 227-240

Tison, J.-L., Lorrain, R.D., Bouzette, A., Dini, M., Bondesan, A., and Stiévenard, M. (1998). Linking landfast sea ice variability to marine ice accretion at Hells Gate Ice Shelf, Ross Sea. In: Jeffries, M.O. (Ed.), Antarctic sea ice: physical processes,

interactions and variability, Antarctic Research Series, 74, American Geophysical Union, Washington, DC, pp. 375-407

Tison, J.-L., Haas, C., Gowing, M.M., Sleewaegen, S., and Bernard, A. (2002). Tank study of physico-chemical controls on gas content and composition during growth of young sea ice. *Journal of Glaciology*, 48, 161, 177-191

Tison, J.-L., Worby, A., Delille, B., Brabant, F., Papadimitriou, S., Thomas, D., de Jong, J., Lannuzel, D., and Haas, C. (2008). Temporal evolution of decaying summer first-year sea ice in the Western Weddell Sea, Antarctica. *Deep-Sea Research II*, 55, 975-987

Tison, J.-L., Brabant, F., Dumont, I., and Stefels, J. (2010). High-resolution dimethyl sulfide and dimethylsulfoniopropionate time series profiles in decaying summer first-year sea ice at Ice Station Polarstern, western Weddell Sea, Antarctica. *Journal of Geophysical Research*, 115, doi: 10.1029/2010JG001427

Todd, J.D., Rogers, R., Li, Y.G., Wexler, M., Bond, P.L., Sun, L., Curson, A.R.J., Malin, G., Steinke, M., and Johnston, A.W.B. (2007). Structural and regulatory genes required to make the gas dimethyl sulfide in bacteria. *Science*, 315(5812), 666-669

Todd, J., Kirkwood, M., Newton-Payne, S., and Johnston, A. (2012). DddW, a third DMSP lyase in a model Roseobacter marine bacterium, Ruegeria pomeroyi DSS-3. *The ISME Journal*, 6, 223-226

Toole, D.A., Kieber, D.J., Kiene, R.P., Siegel, D.A., and Nelson, N.B. (2003). Photolysis and the dimethylsulfide (DMS) summer paradox in the Sargasso Sea. *Limnology and Oceanography*, 48, 1088-1100

Toole, D.A., Kieber, D.J., Kiene, R.P., White, E.M., Bisgrove, J., del Valle, D.A., and Slezak, D. (2004). High dimethylsulfide photolysis rates in nitrate-rich Antarctic waters. *Geophysical Research Letters*, 31, L11307

Tréguer, P., and Pondaven, P. (2002). Climatic changes and the carbon cycle in the Southern Ocean: A step forward. *Deep-Sea Research II*, 49, 1597-1600

Trevena, A.J., Jones, G.B., Wright, S.W., and van den Enden, R.L. (2000). Profiles of DMSP, algal pigments, nutrients and salinity in pack ice from eastern Antarctica. *Journal of Sea Research*, 43, 265-273

Trevena, A.J., Jones, G.B., Wright, S.W., and van den Enden, R.L. (2003). Profiles of dimethylsulphoniopropionate (DMSP), algal pigments, nutrients, and salinity in the fast ice of Prydz Bay, Antarctica. *Journal of Geophysical Research*, 108, doi: 10.1029/2002JC001369

Trevena, A.J., and Jones, G.B. (2006). Dimethylsulphide and dimethylsulphoniopropionate in Antarctic sea ice and their release during sea ice melting. *Marine Chemistry*, 98, 210-222

Tucker, W.B. III, Gow, A.J., and Weeks, W.F. (1987). Physical properties of summer sea ice in the Fram Strait. *Journal of Geophysical Research*, 92, C7, 6787-6803

Tunved, P., Ström, J., and Krejci, R. (2013). Arctic aerosol life cycle: linking aerosol size distribution observed between 2000 and 2010 with air mass transport and

precipitation at Zeppelin station, Ny-Alesund, Svalbard. *Atmospheric Chemistry and Physics*, 13, 3643-3660

Turner, S.M., Nightingale, P.D., Broadgate, W., and Liss, P.S. (1995). The distribution of dimethyl sulphide and dimethylsulphoniopropionate in Antarctic waters and sea ice. *Deep-Sea Research II*, 42, 1059-1080

Turner, S.M., Malin, G., Liss, P.S., Harbour, D.S., and Holligan, P.M. (1998). The seasonal variation of dimethyl sulfide and dimethylsulfoniopropionate concentrations in nearshore waters. *Limnology and Oceanography*, 33, 364-375

Turnipseed, A.A., and Ravishankara, A.R. (1992). The atmospheric oxidation of dimethyl sulfide: elementary steps in a complex mechanism. In: Restelli, G., and Angeletti, G. (Ed.), Dimethylsulphide: Oceans, Atmosphere, and Climate. Proceedings of the International Symposium, Commission of the European Communities, pp. 185-195

Twohy, C.H., and Anderson, J.R. (2008). Droplet nuclei in non-precipitating clouds: composition and size matter. *Environmental Research Letters*, 3, 045002, 1-9

Untersteiner, N. (1961). On the mass and heat budget of Arctic sea ice. *Archiv fur Meteorologie, Geophysik und Bioklimatologie*, 12, 2, 151-182

Untersteiner, N. (1968). Natural desalination and equilibrium salinity profile of perennial sea ice. *Journal of Geophysical Research*, 73, 4, 1251-1257

Ütermöhl, H. (1958). Zur Vervollkommnung der quantitativen Phytoplankton-Methodik. Mitt. Int. Verein. Theor. Angew.. *Limnology*, 9, 1-38

Uzuka, N. (2003). A Time Series Observation of DMSP Production in the Fast Ice Zone Near Barrow. *Tôhoku Geophysical Journal*, 36, 439-442

Vairavamurthy, A., Andreae, M.O., and Iverson, R.L. (1985). Biosynthesis of dimethylsulfide and dimethylpropiothetin by Hymenomonas carterae in relation to sulfur source and salinity variations. *Limnology and Oceanography*, 30, 59-70

Vallina, S.M., Simó, R., and Manizza, M. (2007). Weak response of oceanic dimethylsulfide to upper mixing shoaling induced by global warming. *Proceedings of The National Academy of Sciences of The United States of America*, 104, 16004-16009

Van Alstyne, K.L., and Puglisi, M.P. (2007). DMSP in marine macroalgae and macroinvertebrates: distribution, function, and ecological impacts. *Aquatic Sciences*, 69, 394-402, doi: 10.1017/s00027-007-0888-z

Van Duyl, F.C., Gieskes, W.W.C., Kop, A.J., and Lewis, W.E. (1998). Biological control of short-term variations in the concentration of DMSP and DMS during a Phaeocystis spring bloom. *Journal of Sea Research*, 40, 221-231

Van Rijssel, M., and Buma, A.G.J. (2002). UV radiation induced stress does not affect DMSP synthesis in the marine prymnesiophyte Emiliania huxleyi. *Aquatic Microbial Ecology*, 28, 167-174

Van Rijssel, M., and Gieskes, W.W.C (2002). Temperature, light, and the dimethylsulfoniopropionate (DMSP) contentof Emiliania huxleyi (Prymnesiophyceae). *Journal of Sea Research*, 48, 17-27

Vancoppenolle, M., Fichefet, T., and Bitz, C.M. (2006). Modeling the salinity profile of undeformed Arctic sea ice. *Geophysical Research Letters*, 33, 21, L31501

Vancoppenolle, M., Goosse, H., de Montety, A., Fichefet, T., Tremblay, B., and Tison, J.-L. (2010). Modeling brine and nutrient dynamics in Antarctic sea ice: The case of dissolved silica. *Journal of Geophysical Research*, 115, C02005, doi: 10.1029/2009JC005369

Vancoppenolle, M., Notz, D., Vivier, F., Tison, J.-L., Delille, B., Carnat, G., Zhou, J., Jardon, F., Griewank, P., Lourenço, A., and Haskell, T. (submitted to The Cryosphere). Technical Note: On the useof the mushy-layer Rayleigh number for the interpretation of sea-ice core data.

Vila-Costa, M., del Valle, D.A., Gonzalez, J.M., Slezak, D., Kiene, R.P., Sanchez, O., and Simó, R. (2006a). Phylogenetic identification and metabolism of marine dimethylsulfide-consuming bacteria. *Environmental Microbiology*, 8(12), 2189-2200

Vila-Costa, M., Simó, R., Harada, H., Gasol, J.M., Slezak, D., and Kiene, R.P. (2006b). Dimethylsulfoniopropionate uptake by marine phytoplankton. *Science*, 314, 652-654

Von Glasow, R., and Crutzen, P.J. (2004). Model study of multiphase DMS oxidation with a focus on halogens. *Atmospheric Chemistry and Physics*, 4, 589-608

Wadhams, P. (2000). Ice in the Ocean. Gordon and Breach Science Publishers, Amsterdam

Wanninkhof, R. (1992). Relationship between wind speed and gas exchange over the ocean. *Journal of Geophysical Research*, 97, 7373-7382

Weaver, J.C. (1951). The ice of sea in the North American Arctic. In: Vilhjalmur, S. (Ed.), Encyclopedia Arctica, volume 7, The Stefansson library, New-York

Weeks, W.F., and Ackley, S.F. (1982). The growth, structure and properties of sea ice. *CRREL Monograph*, 82-1

Weeks, W.F., and Ackley, S.F. (1986). The growth, structure and properties of sea ice. In: Untersteiner, N. (Ed.), Geophysics of sea ice, NATO ASI Series B: Physics, 146, Plenum Press, London

Weeks, W.F., and Gow, A.J. (1978). Preferred crystal orientations in the fast ice along the margins of the Arctic Ocean. *Journal of Geophysical Research*, 83, C10, 5105-5121

Wettlaufer, J.S., Worster, M.G., and Huppert, H.E. (1997). Natural convection during solidification of an alloy from above with application to the evolution of sea ice. *Journal of Fluid Mechanics*, 344, 291-316

Wettlaufer, J.S., Worster, M.G., and Huppert, H.E. (2000). Solidifications of leads: theory, experiment and field observations. *Journal of Geophysical Research*, 105, C1, 1123-1134

Weyprecht, K. (1875). Die2. Österr.-Hungarische Nordpolar-Expedition unter Weyprecht und Payer. *Petermanns Geographische Mitt*, 21: 65-72

Wine, P.H., Thompson, R.J., Ravishankara, A.R., Semmes, D.H., Gump, T.A., and Nicovich, J.M. (1984). Kinetics of the reaction $OH+SO_2+M$ -> $HOSO_2+M$ – temperature and pressure dependence in the fall off region. *Journal of Physical Chemistry*, 88, 2095-2104

Williams, P.J. (1981). Incorporation of microheterotrophic processes into the classical paradigm of the planktonic food web. *Kieler Meeresforsch. Sonderh.*, 5, 1-28

Wilson, W.H., Tarran, G., and Zubkov, M.V. (2002). Virus dynamics in a coccolithophore-dominated bloom in the North Sea. *Deep-Sea Research Part II*, 49, 2951-2963

World Meteorological Organization (1985). WMO, Sea ice nomenclature, terminology, codes, and illustrated glossary. WMO/DMM/BMO 259-TP-145, Secretariat of the World Meteorological Organization, Geneva

Wolfe, G.V., and Steinke, M. (1996). Grazing-activated production of dimethyl sulfide (DMS) by two clones of *Emiliania huxleyi*. *Limnology and Oceanography*, 41, 1151-1160

Wolfe, G.V., Steinke, M., and Kirst, G.O. (1997). Grazing-activated chemical defense in a unicellular marine alga. *Nature*, 387, 894-897

Wood, R. (2007). Cancellation of aerosol indirect effects in marine stratocumulus through cloud thinning. *Journal of The Atmospheric Sciences*, 64, 7, 2657-2669

Woodhouse, M.T., Carslaw, K.S., Mann, G.W., Vallina, S.M., Vogt, M., Halloran, P.R., and Boucher, O. (2010). Low sensitivity of cloud condensation nuclei to changes in the sea-air flux of dimethyl-sulphide. *Atmospheric Chemistry and Physics*, 10, 7545-7559, doi: 10.5194/acp-10-7545-2010

Woodhouse, M.T., Mann, G.W., Carslaw, K.S., and Boucher, O. (2013). Sensitivity of cloud condensation nuclei to regional changes in the dimethyl-sulfide emissions. *Atmospheric Chemistry and Physics*, 13, 2723-2733

Worster, M.G. (1992). Instabilities of the liquid and mushy regions during solidification of alloys. *Journal of Fluid Mechanics*, 237, 649-669

Yentsch, C.S., and Menzel, D.W. (1963). A method for the determination of phytoplankton chlorophyll and phaeophytin by fluorescence. *Deep-Sea Research*, 10, 221-231

Yoch, D.C. (2002). Dimethylsulfoniopropionate: Its Sources, Role in the Marine Food Web, and Biological Degradation to Dimethylsulfide. *Applied and Environmental Microbiology*, 68, 5804-5815

Zemmelink, H.J., Dacey, J.W.H., and Hintsa, E.J. (2004). Direct measurements of biogenic dimethylsulphide fluxes from the oceans: a synthesis. *Canadian Journal of Fisheries and Aquatic Science*, 61, 836-844

Zemmelink, H.J., Houghton, L., Frew, N.M., and Dacey, J.W.H. (2005). Gradients in dimethylsulfide, dimethylsulfoniopropionate, dimethylsulfoxide, and bacteria near the sea surface. *Marine Ecology Progress Series*, 295, 33-42

Zemmelink, H.J., Delille, B., Tison, J.-L., Hintsa, E.J., Houghton, L., and Dacey, J.W.H. (2006). CO_2 deposition over the multi-year ice of the western Weddell Sea. *Geophysical Research Letters*, 33, doi: 10.1029/2006GL026320

Zemmelink, H., Dacey, J.W.H., Houghton, L., Hintsa, E.J., and Liss, P.S. (2008a). Dimethylsulfide emissions over the multi-year ice of the Western Weddell Sea. *Geophysical Research Letters*, 35, L06603, doi: 10.1029/2007GL031847

Zemmelink, H.J., Houghton, L., Dacey, J.W.H., Stefels, J., Koch, B.P., Schröder, M., Wisotzki, A., Scheltz, A., Thomas, D.N., Papadimitriou, S., Kennedy, H., Kuosa, H., and Dittmar, T. (2008b). Stratification and the distribution of phytoplankton, nutrients, inorganic carbon, and sulfur in the surface waters of Weddell Sea leads. *Deep-Sea Research II*, 55, 8-9, 988-999

Zeyer, J., Eicher, P., Wakeham, S.G., and Schwarzenbach, R.P. (1987). Oxidation of dimethyl sulfide to dimethyl sulfoxide by phototrophic bacteria. *Applied and Environmental Microbiology*, 53, 2026-2032

Zhou, J., Delille, B., Eicken, H., Vancoppenolle, M., Brabant, F., Carnat, G., Geilfus, N.-X., Papakyriakou, T., Heinesch, B., and Tison, J.-L. (2013). Physical and biogeochemical properties in landfast sea ice (Barrow, Alaska): Insights on brine and gas dynamics across seasons. *Journal of Geophysical Research*, 118, 1-18, doi: 10.1002/jgrc.20232.2013

Zhou, J., Delille, B., Brabant, F., and Tison, J.-L. (submitted to Biogeosciences). Insights into oxygen transport and net community production in sea ice from oxygen, nitrogen and argon concentrations.